

TA7

ER-86/87-8

C. E. - R. N. COPY

COPY 2

LNG VAPOR BARRIER AND OBSTACLE EVALUATION:
WIND-TUNNEL PRE-FIELD TEST RESULTS

FINAL REPORT

(January 1986 - September 1986)

Prepared by

D. E. Neff and R. N. Meroney



**FLUID MECHANICS AND
WIND ENGINEERING PROGRAM**

COLLEGE OF ENGINEERING

COLORADO STATE UNIVERSITY
FORT COLLINS, COLORADO

ER86-87 DEN-RNM 8

LNG VAPOR BARRIER AND OBSTACLE EVALUATION:
WIND-TUNNEL PRE-FIELD TEST RESULTS

FINAL REPORT

(January 1986 - September 1986)

Prepared by

D. E. Neff and R. N. Meroney

Fluid Mechanics and Wind Engineering Program
Department of Civil Engineering
Colorado State University
Fort Collins, Colorado 80523

For

Lawrence Livermore Laboratory

Contract No. 8432705

LLL Project Manager

Dr. Ronald P. Koopman

LGF Program Leader

September 1986

RESEARCH SUMMARY

Title LNG Vapor Barrier and Obstacle Evaluation:
Wind-Tunnel Pre-field Test Results

Contractor Civil Engineering Department
Colorado State University
Fort Collins, Colorado 80523
Contract Number: 8432705

Principal Investigators D. E. Neff and R. N. Meroney

Report Period January 1986 - September 1986
Final Report

Objective The objective of this task was to simulate in a wind tunnel the dispersion behavior of several planned LNG spill configurations to be performed at field scales. The data from these reduced scale tests will assist in the planning and execution of the field tests.

Technical Perspective When liquefied natural gas (LNG) spills from a storage vessel or transportation container, the LNG vaporizes and a potentially flammable cloud is formed. Techniques to predict the extent of the flammable zone are needed to assist in developing siting criteria and plant layout design.

Results Visual and concentration data were obtained on seventeen different LNG spill configurations. These included variations in wind speed, spill volume, spill rate, vortex generator height and with or without an enclosure.

Technical Approach An LNG vapor plume at boiloff conditions is heavier than air. Although the plume will eventually become positively buoyant due to heat absorbed from the surroundings, much of the dispersion will occur while the plume density is greater than the that of air. The dispersion during the heavier-than-air phase may be approximated in a wind tunnel by means of isothermal-model plumes produced by high-molecular-weight gases. In laboratory tests, heavy gases were introduced into the wind tunnel via an area source mounted flush on the wind-tunnel floor. This area source was in most tests surrounded by an enclosure designed to detain the plume. The floor was level and smooth for all tests. Concentration sensors downwind of this source were used to measure the structure of the different model plumes tested.

TABLE OF CONTENTS

<u>Section</u>	<u>Page</u>
RESEARCH SUMMARY	ii
LIST OF TABLES	iv
LIST OF FIGURES	v
LIST OF SYMBOLS	vii
1.0 INTRODUCTION	1
2.0 MODELING OF PLUME DISPERSION	3
2.1 PHYSICAL MODELING OF THE ATMOSPHERIC BOUNDARY LAYER	4
2.1.1 Partial Simulation of the Atmospheric Boundary Layer	5
2.2 PHYSICAL MODELING OF LNG PLUME MOTION	7
2.2.1 Partial Simulation of Plume Motion.	8
2.3 MODELING OF PLUME DISPERSION FOR PRESENT STUDY	13
2.3.1 Physical Modeling of the Field Site Atmospheric Surface Layer	13
2.3.2 Physical Modeling of the Field Site LNG Spill Plume	14
3.0 DATA AQUISITION AND ANALYSIS	17
3.1 WIND-TUNNEL FACILITIES	17
3.2 MODEL	17
3.3 FLOW VISUALIZATION TECHNIQUES	18
3.4 WIND PROFILE AND TURBULENCE MEASUREMENTS	18
3.5 CONCENTRATION MEASUREMENTS	19
3.5.1 Hot-Wire Aspirating Probe	20
3.5.2 Error in Concentration Measurements	21
4.0 TEST PROGRAM AND DATA	22
REFERENCES	25
TABLES	28
FIGURES	31
APPENDIX - REDUCED CONCENTRATION DATA LISTINGS	110

LIST OF TABLES

<u>Table</u>		<u>Page</u>
1	Field Test Conditions	28
2	Model Test Conditions	29
3	Concentration Data File Description	30

LIST OF FIGURES

<u>Figure</u>		<u>Page</u>
1	Specific Gravity of LNG Vapor - Humid Atmospheric Mixtures	31
2	Specific Gravity of Gas-Air Mixtures	32
3	Variation of Isothermal Plume Behavior from Equivalent Cold Methane Plume Behavior	32
4	Environmental Wind Tunnel	33
5	Field Test Facility	34
6	Velocity Probes and Velocity Standard	35
7	Velocity Data Reduction Flow Chart	36
8	Hot-Wire Katharometer Probes	37
9	Block Diagram Katharometer Array	38
10	Concentration Sampling Locations	39
11	Model Velocity Profiles	40
12	Prototype Velocity Profiles	41
13	2.0 M/S Prototype Velocity Profile with Regressions	42
14	2.0 M/S Prototype Turbulent Intensity Profile	43
15	3.5 M/S Prototype Velocity Profile with Regressions	44
16	3.5 M/S Prototype Turbulent Intensity Profile	45
17	5.0 M/S Prototype Velocity Profile with Regressions	46
18	5.0 M/S Prototype Turbulent Intensity Profile	47
19-25	Selected Concentration Time Series Plots for Run No. 1	48
26-34	Concentration Contour Plots at X = 15 meters for Run Numbers 1-9	55
35-46	Concentration Contour Plots at Y = 0 meters for Run Numbers 1-11, 16	64
47-56	Concentration Contour Plots at Y = -18 meters for Run Numbers 1-10	76

<u>Figure</u>		<u>Page</u>
57-71	Concentration Contour Plots at $Z = 0$ meters for Run Numbers 1-13, 16, 17	86
72-80	Concentration Contour Plots at $Z = 18.2$ meters for Run Numbers 1-9	101

LIST OF SYMBOLS

Dimensions are given in terms of mass (m), length (L), time (t), moles (n), and temperature (T).

<u>Symbol</u>	<u>Definition</u>	
A	Area	$[L^2]$
C_p	Specific heat capacity at constant pressure	$[L^2 t^{-2} T^{-1}]$
C_p^*	Molar specific heat capacity at constant pressure	$[L^2 m t^{-2} T^{-1} n^{-1}]$
D	Source diameter	$[L]$
g	Gravitational acceleration	$[L t^{-2}]$
h	Local plume depth	$[L]$
k	Thermal conductivity	$[m L T^{-1} t^{-3}]$
L	Length	$[L]$
M	Molecular weight	$[m n^{-1}]$
n	Mole	$[n]$
p	Velocity power law exponent	-
Q	Volumetric rate of gas flow	$[L^3 t^{-1}]$
T	Temperature	$[T]$
ΔT	Temperature difference across some reference layer	$[T]$
t	Time	$[t]$
u_x	Friction velocity	$[L t^{-1}]$
U	Velocity	$[L t^{-1}]$
V	Volume	$[L^3]$
W	Plume vertical velocity	$[L t^{-1}]$
x	General downwind coordinate	$[L]$
y	General lateral coordinate	$[L]$
z	General vertical coordinate	$[L]$
z_0	Surface roughness parameter	$[L]$

LIST OF SYMBOLS (continued)

<u>Symbol</u>	<u>Definition</u>	
δ	Boundary layer thickness	[L]
Λ	Integral length scale of turbulence	[L]
ρ	Density	[mL ⁻³]
σ	Standard deviation	
χ	Mole fraction of gas component	
Ω	Angular velocity of earth = 0.726×10^{-4} (radians/sec)	[t ⁻¹]
λ_p	Peak wavelength	[L]
ν	Kinematic viscosity	[L ² t ⁻¹]
<u>Subscripts</u>		
a	Air	
Ar	Argon	
b.o.	Boiloff	
g	Gas	
i	Cartesian index	
LNG	Liquefied Natural Gas	
m	Model	
NG	Natural gas	
o	Reference conditions	
p	Prototype	
s	Source gas	

1.0 INTRODUCTION

Natural gas is a highly desirable form of energy for consumption in the United States. A sophisticated distribution network already services a major part of the country. Recent efforts to expand this nation's natural gas supply include the transport of natural gas in a liquid state from distant gas fields and the temporary storage of surplus capacity in peak shaving facilities. To transport and store liquefied natural gas (LNG) it is cooled to a temperature of -162°C . At this temperature if a storage tank on a ship or land were to rupture and the contents spill out onto the earth's surface, rapid boiling of the LNG would ensue and the liberation of a flammable vapor would result [1,2]. Past studies [3,4] have demonstrated that the cold LNG vapor plume will remain negatively buoyant for a majority of its flammable lifetime. This hazard will extend downwind until the atmosphere has diluted the LNG vapor below the lower flammability limit (a local concentration for methane below 5 percent by volume).

The ability to predict the dispersion of heavy gases associated with an LNG spill is an important requirement in the assessment of the hazards of such flammable gases to the atmosphere. Field experiments on the dispersion of heavy gases started around 1970, but have included a very limited set of data on the mitigating effects of vapor barrier fences, obstacles, and water or steam spray curtains. As observed by Wiersma [5] this means the focus of most field experiments has been on "idealized release scenarios, especially with no obstacle or terrain effects." These data do not address the need for "real life" scenarios where such complexities and mitigating dispersion effects exist. New field experiments as planned by LLNL and financed by GRI and DOE will

soon attempt to provide additional field data on the diluting and holdup effects of vapor barrier fences.

McQuaid [6] advised that a limiting characteristic of large-scale field experiments that demand particular attention is the "inability to control the flow conditions..." Hence, he concludes careful pre-planning is necessary, and recommends "...Wind tunnel and computer modeling and preliminary tests to try out the engineering of the experimental design...to maximize the probability of success." He further notes "such measures are assuredly cost effective in relation to the cost of an abortive effort in the field."

The intent of the present wind-tunnel tests was to provide data that would better define the relative influence of wind velocity, vortex inducers, spill rate, spill volume, and impoundment volume on dispersion distances in the upcoming field test program. These data should assist in the design of the field experiments in the following ways:

- i) Advantageous placement of field instruments,
- ii) Reformulation as necessary of the test plan to maximize sensitivity to barrier height and spill area size, and
- iii) Preparation of safety plans which are realistic.

Scaling methods employed during physical modeling of atmospheric and plume motion are discussed in Chapter 2. The details of the experimental measurements are described in Chapter 3. Chapter 4 discusses the laboratory tests and the data obtained.

2.0 MODELING OF PLUME DISPERSION

To obtain a predictive model for a specific plume dispersion problem one must quantify the pertinent physical variables and parameters into a logical expression that determines their interrelationships. This task is achieved implicitly for processes occurring in the atmospheric boundary layer by the formulation of the equations for conservation of mass, momentum, and energy. These equations together with site and source conditions and associated constitutive relations are highly descriptive of the actual physical interrelationship of the various independent (space and time) and dependent (velocity, temperature, pressure, density, etc.) variables.

These generalized conservation statements subjected to the typical boundary conditions of atmospheric flow are too complex to be solved by present analytical or numerical techniques. It is also unlikely that one could create a physical model for which exact similarity exists for all the dependent variables over all the scales of motion present in the atmosphere at a reduced geometric scale. Thus, one must resort to various degrees of approximation to obtain a predictive model. At present purely analytical or numerical solutions of plume dispersion are unavailable because of the classical problem of turbulent closure [7]. Such techniques rely heavily upon empirical input from observed or physically modeled data. The combined empirical-analytical-numerical solutions have been combined into several different predictive approaches by Pasquill [8] and others. The estimates of dispersion by these approaches are often crude; hence, they should only be used when the approach and site terrain are uniform and without obstacles. Boundary layer wind tunnels are capable of physically modeling plume

processes in the atmosphere under certain restrictions. These restrictions are discussed in the next few sections.

2.1 PHYSICAL MODELING OF THE ATMOSPHERIC BOUNDARY LAYER

The atmospheric boundary layer is that portion of the atmosphere extending from ground level to a height of approximately 1000 meters within which the major exchanges of mass, momentum, and heat occur. This region of the atmosphere is described mathematically by statements of conservation of mass, momentum, and energy [11]. The general requirements for laboratory-atmospheric-flow similarity may be obtained by fractional analysis of these governing equations [12]. This methodology is accomplished by scaling the pertinent dependent and independent variables and then casting the equations into dimensionless form by dividing by one of the coefficients (the inertial terms in this case). Performing these operations on such dimensional equations yields dimensionless parameters commonly known as:

Reynolds number	$Re = U_0 L_0 / \nu_0$	$= \frac{\text{Inertial Force}}{\text{Viscous Force}}$
Bulk Richardson number	$Ri = [(\Delta T)_0 / T_0] (L_0 / U_0^2) g_0$	$= \frac{\text{Gravitational Force}}{\text{Inertial Force}}$
Rossby number	$Ro = U_0 / L_0 \Omega_0$	$= \frac{\text{Inertial Force}}{\text{Coriolis Force}}$
Prandtl number	$Pr = \nu_0 / (k_0 / \rho_0 C_{p_0})$	$= \frac{\text{Viscous Diffusivity}}{\text{Thermal Diffusivity}}$
Eckert number	$Ec = U_0^2 / C_{p_0} (\Delta \bar{T})_0$	

For exact similarity between different flows which are described by the same set of equations, each of these dimensionless parameters must be equal for both flow systems. In addition to this requirement, there must be similarity between the surface-boundary conditions.

Surface-boundary condition similarity requires equivalence of the following features:

- a. surface-roughness distributions,
- b. topographic relief, and
- c. surface-temperature distribution.

If all the foregoing requirements are met simultaneously, all atmospheric scales of motion ranging from micro to mesoscale could be simulated within the same flow field for a given set of boundary conditions [11]. However, all of the requirements cannot be satisfied simultaneously by existing laboratory facilities; thus, a partial or approximate simulation must be used. This limitation requires that atmospheric simulation for a particular wind-engineering application be designed to simulate most accurately those scales of motion which are of greatest significance for the given application.

2.1.1 Partial Simulation of the Atmospheric Boundary Layer

A partial simulation is practically realizable only because the kinematics and dynamics of flow systems above a certain minimum Reynolds number are independent of the magnitude of this number [12,13]. The magnitude of the minimum Reynolds number will depend upon the geometry of the flow system being studied. Halitsky [14] reported that for concentration measurements on a cube placed in a near uniform flow field the Reynolds number required for invariance of the concentration distribution over the cube surface and downwind must exceed 11,000. Because of this invariance exact similarity of Reynolds parameter is neglected when physically modeling the atmosphere.

When the flow scale being modeled is small enough such that the turning of the mean wind directions with height is unimportant, similarity of the Rossby number may be relaxed. For the case of dispersion of

LNG or a neutral plume near the ground level the Coriolis effect on the plume motion would be extremely small.

The Eckert number for air is equivalent to $0.4 \text{ Ma}^2 (T_o/\Delta T_o)$ where Ma is the Mach number [7]. For the wind velocities and temperature differences which occur in either the atmosphere or the laboratory flow the Eckert number is very small; thus, the effects of energy dissipation with respect to the convection of energy is negligible for both model and prototype. Eckert number equality is relaxed.

Prandtl number equality is easily obtained since it is dependent on the molecular properties of the working fluid which is air for both model and prototype.

Bulk Richardson number equality may be obtained in special laboratory facilities such as the Meteorological Wind Tunnel at Colorado State University [15].

Quite often during the modeling of a specific flow phenomenon it is sufficient to model only a portion of a boundary layer or a portion of the spectral energy distribution. This relaxation allows more flexibility in the choice of the length scale that is to be used in a model study. When this technique is employed it is common to scale the flow by any combination of the following length scales, δ , the portion of the boundary layer to be simulated; z_o , the aerodynamic roughness; Λ_i , the integral length scale of the velocity fluctuations, or λ_p , the wavelength at which the peak spectral energy is observed.

Unfortunately many of the scaling parameters and characteristic profiles are difficult to obtain in the atmosphere. They are infrequently known for many of the sites at which a model study is to be performed. To help alleviate this problem Counihan [16] has summarized

measured values of some of these different parametric descriptions for the atmospheric flow at many different sites and flow conditions.

2.2 PHYSICAL MODEL OF PLUME MOTION

In addition to modeling the turbulent structure of the atmosphere in the vicinity of a test site it is necessary to scale the LNG plume source conditions properly. One approach would be to follow the methodology used in Section 2.1, i.e., writing the conservation statements for the combined flow system followed by fractional analysis to find the governing parameters. An alternative approach, the one which will be used here, is that of similitude [14]. The method of similitude obtains scaling parameters by reasoning that the mass ratios, force ratios, energy ratios, and property ratios should be equal for both model and prototype. When one considers the dynamics of gaseous LNG plume behavior the following nondimensional parameters of importance are identified [14,19,20,21,22].^{1,2}

$$\begin{aligned} \text{Mass Ratio} &= \frac{\text{mass flow of LNG plume}}{\text{effective mass flow of air}} \\ &= \frac{\rho_s W_s A_s}{\rho_a U_a A_a} = \frac{\rho_s Q}{\rho_a U_a L^2} \end{aligned}$$

¹It has been assumed that the dominant transfer mechanism is that of turbulent entrainment. Thus the transfer processes of heat conduction, convection, and radiation are negligible.

²The scaling of plume Reynolds number is also a significant parameter. Its effects are invariant over a large range thus making it possible to scale the distribution of mean and turbulent velocities and relax exact parameter equality.

$$\begin{aligned}
 \text{Momentum Ratio} &= \frac{\text{inertia of LNG plume}}{\text{effective inertia of air}} \\
 &= \frac{\rho_s W_s^2 A_s}{\rho_a U_a^2 A_a} = \frac{\rho_s Q^2}{\rho_a U_a^2 L^4} \\
 \\
 \text{Densimetric Froude No. (Fr)} &= \frac{\text{effective inertia of air}}{\text{buoyancy of LNG plume}} \\
 &= \frac{\rho_a U_a^2 A_a}{g(\rho_g - \rho_a) V_s} = \frac{U_a^2}{g \left(\frac{\rho_s - \rho_a}{\rho_a} \right) L} \\
 \\
 \text{Volume Flux Ratio} &= \frac{\text{Volume flow of LNG plume}}{\text{effective volume flow of air}} \\
 &= \frac{Q}{UL^2}
 \end{aligned}$$

To obtain simultaneous simulation of these four parameters at a reduced geometric scale it is necessary to maintain equality of the plume specific gravity ratio ρ_s/ρ_a .

2.2.1 Partial Simulation of Plume Motion

The restriction to an exact variation of the density ratio for the entire life of a plume is difficult to meet for LNG plumes which simultaneously vary in molecular weight and temperature. To emphasize this point more clearly, consider the mixing of two volumes of gas, one being the source gas, V_s , the other being ambient air, V_a . Consideration of the conservation of mass and energy for this system yields [18]¹:

$$\frac{\rho_g}{\rho_a} = \frac{\frac{\rho_s}{\rho_a} V_s + V_s}{\left(\frac{T_a}{T_s} V_s + V_a \right) \left(\frac{C_{p_s} M_s}{C_{p_a} M_a} V_s + V_a \right) / \left(\frac{C_{p_s} M_s T_a}{C_{p_a} M_a T_s} V_s + V_a \right)}$$

¹The pertinent assumption in this derivation is that the gases are ideal and properties are constant.

If the temperature of the air, T_a , equals the temperature of the source gases, T_s , or if the product, $C_p M$, is equal for both source gas and air then the equation reduces to:

$$\frac{\rho_g}{\rho_a} = \frac{\frac{\rho_s}{\rho_a} V_s + V_a}{V_s + V_a} .$$

Thus for two prototype cases: 1) an isothermal plume and 2) a thermal plume which is mostly composed of air; it does not matter how one models the density ratio as long as the initial density ratio value is equal for both model and prototype.

For a plume where temperature, molecular weight, and specific heat are all different from that of the ambient air, e.g., a cold natural gas plume, equality in the variation of the density ratio upon mixing must be relaxed slightly if one is to model utilizing a gas different from that of the prototype.¹ In most situations this deviation from exact similarity is small (see discussion Section 2.3.2).

Scaling of the effects of heat transfer by conduction, convection, or radiation cannot be reproduced when the model source gas and environment are isothermal. Fortunately in a large majority of industrial plumes the effects of heat transfer by conduction, convection, and radiation from the environment are small enough that the plume buoyancy essentially remains unchanged. In the specific case of a cryogenic liquid spill the influence of heat transfer on cold dense gas dispersion can be divided into two phases. First the temperature (and hence specific gravity) of the plume as exit from a containment tank and

¹If one were to use a gas whose temperature is different from that of the ambient air then consideration of similarity in the scaling of the energy ratios must be considered.

surrounding dike area is dependent on the thermal diffusivity of the tank-dike-spill surface materials, the volume of the tank-dike structure, the actual boiloff rate, and details of the spill surface geometry. A second plume phase involves the heat transfer from the ground surface beyond the spill area which lowers plume density.

It is tempting to try to simulate the entire transient spill phenomenon in the laboratory including spill of cryogenic fluid into the dike, heat transfer from the tank and dike materials to the cryogenic fluid, phase change of the liquid and subsequent dispersal of cold gas downwind. Unfortunately, the different scaling laws for the conduction and convection suggest that markedly different time scales occur for these various processes as the length scale changes. Since the volume of dike material storing sensible heat scales with the cube of the length scale whereas the pertinent surface area scales as the square of the length scale one perceives that heat is transferred to a model cold plume much too rapidly within the model containment structures. This effect is apparently unavoidable since a material having a thermal diffusivity low enough to compensate for this effect does not appear to exist. Calculations for the full-scale situation suggest minimal heating of a cold gas plume by the tank-dike structure; thus it may suffice to cool the model tank-dike walls to reduce the heat transfer to a cold model vapor and study the resultant cold plume.

Boyle and Kneebone [20] released under equivalent conditions room temperature propane and LNG onto a water surface. The density of propane at ambient temperatures and methane at -161°C relative to air are the same. Using the modified Froude number as a model law they concluded

that the dispersion characteristics were equivalent within experimental error.

A mixture of 50 percent helium and 50 percent nitrogen pre-cooled to 115°K was released from model tank-dike systems by Meroney et al. [21], to simulate equivalent LNG spill behavior. There was no guarantee that these experiments reproduced quantitatively similar situations in the field. Rather it was expected that the gross influences of different heat transfer conditions could be determined. Since the turbulence characteristics of the flow are dominated by roughness, upstream wind profile shape, and stratification one expects the Stanton number in the field will equal that in the model, and heat transfer rates in the two cases should be in proper relation to plume entrainment rates. On the other hand, if temperature differences are such that free convection heat transfer conditions dominate, scaling inequalities may exist; nonetheless, model dispersion rates would be conservative.

Visualization experiments performed with equivalent dense isothermal and dense cold plumes revealed no apparent change in plume geometry. Concentration data followed similar trends in both situations. No significant differentiation appeared between insulated versus heat conducting ground surfaces or neutral versus stratified approach flows.

The influence of latent heat release by moisture upon the buoyancy of a plume is a function of the quantity of water vapor present in the plume and the humidity of the ambient atmosphere. Such phase change effects on plume buoyancy can be very pronounced in some prototype situations. Figure 1 displays the variation of specific gravity from a spill of liquefied natural gas in atmospheres of different humidities.

For a LNG vapor plume humidity effects are thus shown to reduce the extent in space and time of plume buoyancy dominance on plume motion. Hence a dry adiabatic model condition should be conservative.

A reasonably complete simulation may be obtained in some situations even when a modified density ratio ρ_s/ρ_a is stipulated. The advantage of such a procedure is demonstrated most clearly by the statement of equality of Froude numbers.

$$\left(\frac{U_a^2}{\left(\frac{\rho_s}{\rho_a} - 1\right)Lg} \right)_m = \left(\frac{U_a^2}{\left(\frac{\rho_s}{\rho_a} - 1\right)Lg} \right)_p$$

Solving this equation to find the relationship between model velocity and prototype velocity yields:

$$(U_a)_m = \left(\frac{S.G._m - 1}{S.G._p - 1} \right)^{1/2} \left(\frac{1}{L.S.} \right)^{1/2} (U_a)_p$$

where S.G. is the specific gravity, (ρ_s/ρ_a) , and L.S. is the length scale, (L_p/L_m) . By increasing the specific gravity of the model gas compared to that of the prototype gas, for a given length scale, one increases the reference velocity used in the model. It is difficult to generate a flow which is similar to that of the atmospheric boundary layer in a wind tunnel run at very low wind speeds. Thus the effect of modifying the model specific gravity extends the range of flow situations which can be modeled accurately. But unfortunately during such adjustment of the specific gravity of the model gases at least two of the four similarity parameters listed must be neglected. The options as to which two of these parameters to retain, if any, depends upon the physical situation being modeled. Two of the three possible options are listed below.

- (1) Froude No. Equality
Momentum Ratio Equality
Mass Ratio Inequality
Velocity Ratio Inequality¹
- (2) Froude No. Equality
Momentum Ratio Inequality
Mass Ratio Inequality
Velocity Ratio Equality

Both of these schemes have been used to model plume dispersion downwind of an electric power plant complex by Isyumov [18] and Meroney [22] respectively.

The modeling of the plume Reynolds number is relaxed in all physical model studies. This parameter is thought to be of small importance since the plume character will be dominated by background atmospheric turbulence soon after its emission. But, if one was interested in plume behavior near the source, then steps should be taken to assure that the plume in the model is fully turbulent.

2.3 MODELING OF PLUME DISPERSION FOR PRESENT STUDY

In the sections above a review of the extent to which wind tunnels can model plume dispersion in the atmospheric boundary layer has been presented. In this section these arguments will be applied to the specific case of an LNG spill at the Department of Energy spill site in Nevada.

2.3.1 Physical Modeling of the Field Site Atmospheric Surface Layer

In order to obtain a proper wind-tunnel scaling of the Field Site surface layer winds the approach flow characteristics must be similar. To achieve these upstream flow conditions, the wind tunnel must be modified through the introduction of surface roughness elements and

¹When this technique is employed distortion in velocity scales or similarly volume flow rates requires that a correction be applied to the measured concentration field.

boundary layer trip devices in such a way that similarity is obtained in both the mean velocity variation with height and the characteristic length scales of turbulence. A convenient parameter which characterizes the mean velocity variation with height is z_0 , the aerodynamic roughness height [12], as defined by log-linear description of velocity variation in a boundary layer. A convenient parameter which characterizes the scales of turbulent velocity fluctuations is Λ_i , the integral scale of turbulence [7].

The conditions in the wind tunnel were adjusted until both of these length scales were in the same proportion to their atmospheric equivalents (obtained from Counihan [16]) as the geometric length scale chosen for the model terrain construction. This optimal geometric length scale was chosen to be 1:100.

2.3.2 Physical Modeling of the Field Site LNG Spill Plume

The buoyancy of a plume resulting from an LNG spill is a function of both the mole fraction of methane and temperature. If the plume entrains air adiabatically, then the plume would remain negatively buoyant for its entire lifetime. If the humidity of the atmosphere were high then the state of buoyancy of the plume will vary from negative to weakly positive. These conclusions are born out in Figure 1, which illustrates the specific gravity of a mixture of methane at boiloff temperature with ambient air and water vapor.

Since the adiabatic plume assumption will yield the most conservative downwind dispersion estimates this situation was simulated. (Conservative is defined here to be highest peak concentrations furthest downwind.) Several investigators have confirmed that the Froude number is the parameter which governs plume spread rate, trajectory, plume size

and entrainment during initial dense plume dilution [17,20,24,25]. The modeling of momentum is not a critical importance for a ground source released over a fairly large area. The strict equality of model and prototype specific gravity was relaxed so that pure Argon gas (specific gravity at 1.38) could be used for the model source gas. The Froude number was maintained at equal values by adjusting reference wind speed.

Argon provides almost eight times the detection sensitivity for instantaneous concentration measurements as the carbon dioxide used in previous studies [21]. The variation of specific gravity with equivalent observed mole fraction of methane for these different gases is plotted in Figure 2. The use of an isothermal dense model gas such as Argon in place of cold methane vapor also results in a slight distortion of the local dynamic forces acting on equivalent plume volumes as the gas mixes. Unfortunately this distortion is not conservative. The thermal capacitance properties of methane result in plumes which are more dense than the model equivalent. This results in less rapid prototype mixing. Analytical approximations based on the integral entrainment box model of Fay [25] suggest that buoyancy forces are more at equivalent time and space positions during adiabatic mixing of methane. Let $Fr = [U(h)^2]/g(\Delta\rho/\rho_a)h$ be a local Froude number, where h is local plume depth, $U(h)$ is wind speed at plume depth, h , and $\Delta\rho/\rho_a$ is a local density difference ratio. Then given a power law wind profile $U(h) \sim h^p$ one finds

$$\frac{Fr_{\text{isothermal gas}}}{Fr_{\text{LNG vapor}}} = \frac{(1+\chi S)(\beta+(1-\beta)\theta)}{(\beta(1+\chi S)+(1+S)(1-\beta)\theta)} \left[\frac{(1+\chi S+\chi(1+S)\theta)}{(1-\chi\theta)(1+\chi S)} \right]^{2p} \left[\frac{R_{\text{LNG}}}{R_{\text{iso}}} \right]^{2-4p}$$

where χ = mole fraction methane vapor

R = local plume spread

$$\beta = 1 - M_a/M_s \cong -0.81$$

$$\theta = 1 - T_s/T_a \cong 0.6$$

$$S = (Cp_s^*/Cp_a^* - 1) \cong 0.2$$

$$p = \text{velocity power law exponent} \cong 0.5.$$

The variation of this Froude number ratio with equivalent mole fraction methane is plotted in Figure 3. Over most of the concentration range where buoyancy forces are dominant the variation of Froude number is reasonably simulated by the isothermal model gas. Indeed, integral-model calculations predict equal or slightly higher concentration values at equivalent times.

The actual source condition, boiloff rate per unit area over the time duration of the spill, for a spill of LNG on land is highly unpredictable. There were no data on the variable area and variable volume nature of the different LNG tests to be conducted at the Field Site thus the source conditions were approximated by assuming a steady boiloff rate for the duration of the spill over a constant area.

Since the thermally variable prototype gas was simulated by an isothermal simulation gas, the concentration measurements observed in the model must be adjusted to equivalent concentrations that would be measured in the field. This relationship is:

$$x = \frac{x_m}{x_m + (1 - x_m) \frac{T_s}{T_a}}$$

where

x_m = volume or mole fraction measured during the model tests,

T_s = source temperature of LNG during field conditions,

T_a = ambient air temperature during field conditions, and

x_p = volume or mole fraction in the field.

3.0 DATA ACQUISITION AND ANALYSIS

The methods used to make laboratory measurements and the techniques used to convert these measured quantities to meaningful field equivalent quantities are discussed in this section. Attention has been drawn to the limitations in the techniques in an attempt to prevent misinterpretation or misunderstanding of the results presented in the next section. Some of the methods used are conventional and need little elaboration.

3.1 WIND-TUNNEL FACILITIES

The Environmental Wind Tunnel (EWT) shown in Figure 4 was used for all tests performed. This wind tunnel, specially designed to study atmospheric flow phenomena, incorporates special features such as adjustable ceiling, rotating turntables, transparent boundary walls, and a long test section to permit reproduction of micrometeorological behavior at much smaller length scales. Mean wind speeds of 0.10 to 12 m/s can be obtained in the EWT. A boundary layer depth of 1 m thickness at 6 m downstream of the test entrance can be obtained with the use of the vortex generators at the test section entrance and surface roughness on the floor. The flexible test section roof on the EWT is adjustable in height to permit the longitudinal pressure gradient to be set to zero. The vortex generators at the tunnel entrance were followed by 10 m of smooth floor approaching the 1:100 scale model of the field site.

3.2 MODEL

Based on atmospheric data over sites similar to that of the field site it was decided that the best reproduction of the surface wind characteristics would be at a model scale of 1:100. Figure 5 displays the layout of the source area, the vortex generating barrier and the

vapor fence. The field dimensions are in meters and the model dimensions are in centimeters. To insure a uniform release of source gas over the modeled evaporation pond the 38 cm x 38 cm area was sectioned into nine squares. Equal rates of source gas was released from each of these subsources. The simulant gas, Argon, stored in a pressurized cylinder was directed through a solenoid valve, a flowmeter, and into the square area source mounted in the model's vapor containment area.

3.3 FLOW VISUALIZATION TECHNIQUES

Smoke was used to define plume behavior over the China Lake site. The smoke was produced by passing the simulation gas through an oil fog generator located outside the wind tunnel. The plume was illuminated with arc-lamp beams. A visible record was obtained with a VHS video camera.

3.4 WIND PROFILE AND TURBULENCE MEASUREMENTS

Velocity profile measurements, reference wind speed conditions, and turbulence measurements were obtained with a Thermo-Systems Inc. (TSI) 1050 anemometer and a TSI model 1210 hot-film probe. Since the voltage response of these anemometers is nonlinear with respect to velocity, a multi-point calibration of system response versus velocity was utilized for data reduction.

The velocity standard utilized in the present study was that depicted in Figure 6. This consisted of a Matheson model 8116-0154 mass flowmeter, a Yellowsprings thermistor, and a profile conditioning section constructed by the Colorado State University shop. The mass flowmeter measures mass flow rate independent of temperature and pressure, the thermistor measures the temperature at the exit conditions, and the

profile conditioning section forms a flat velocity profile of very low turbulence at the position where the probe is to be located. Incorporating a measurement of the ambient atmospheric pressure and a profile correction factor permits the calibration of velocity at the measurement station from 0.1-2.0 m/s \pm 5.0 cm/s or \pm 10 percent whichever is smaller.

During calibration of the single film anemometer, the anemometer voltage response values over the velocity range of interest were fit to an expression similar to that of King's law [27] but with a variable exponent. The accuracy of this technique is approximately \pm 2 percent of the actual longitudinal velocity.

The velocity sensors were mounted on a vertical traverse and positioned over the measurement location on the model. The anemometer responses were fed to a Preston analog-to-digital converter and then directly to a HP-1000 minicomputer for immediate interpretation. The HP-1000 computer also controls probe position. A flow chart depicting the control sequence for this process is presented in Figure 7.

3.5 CONCENTRATION MEASUREMENTS

To obtain the concentration time histories at points downwind of the spill site a rack of eight hot-wire aspirating probes were designed and constructed. A layout of this design is presented in Figure 8. The films on these probes were replaced with 0.005 in. platinum wire to improve signal-to-noise characteristics. These eight instantaneous concentration sensors were connected to an eight-channel TSI hot-wire anemometer system. The output voltages from the TSI unit are conditioned for input to the analog-to-digital converter by a DC-suppression circuit, a passive low-pass filter circuit tuned to 100 Hz, and an operational amplifier of times five gain. A schedule of this process is shown in Figure 9.

3.5.1 Hot-Wire Aspirating Probes

The basic principles governing the behavior of aspirating hot-wire probes have been discussed by Blackshear and Fingerson [28], Brown and Rebollo [29], and Kuretsky [30]. A vacuum source sufficient to choke the flow through the small orifice just downwind of the sensing element was applied. This wire was operated in a constant temperature mode at a temperature above that of the ambient air temperature. A feedback amplifier maintained a constant overheat resistance through adjustment of the heating current. A change in output voltage from this sensor circuit corresponds to a change in heat transfer between the hot wire and the sampling environment.

The heat transfer rate from a hot wire to a gas flowing over it depends primarily upon the wire diameter, the temperature difference between the wire and the gas, the thermal conductivity and viscosity of the gas, and the gas velocity. For a wire in an aspirating probe with a sonic throat, the gas velocity can be expressed as a function of the ratio of the probe cross-sectional area at the wire position to the area at the throat, the specific heat ratio, and the speed of sound in the gas. The latter two parameters, as well as the thermal conductivity and viscosity of the gas mentioned earlier, are determined by the gas composition and temperature. Hence, for a fixed probe geometry and wire temperature, the heat transfer rate, or the related voltage drop across the wire is a function of only the gas composition and temperature. Since all tests performed in this study were in an isothermal flow situation the wire response was only a function of gas composition.

During probe calibration known compositions of Argon-air mixtures were passed through a pre-heat exchanger to condition the gas to the

tunnel temperature environment. These known compositions for the Argon-air calibration systems were drawn from bottles of prepared gas composition provided by Matheson Laboratories. An overheat ratio (temperature of wire/ambient temperature) of 1.65 was used to maximize signal response while maintaining acceptable noise and signal drifting levels.

3.5.2 Errors in Concentration Measurement

The effective sampling area of the probe inlet is a function of the probe aspiration rate and the distribution of approach velocities of the gases to be sampled. A calculation of the effective sampling area during all tests suggests that the effective sampling area was approximately 0.5 cm^2 . Thus the resolution of the concentration measurements as applied to the field site is 0.5 m^2 .

The travel time from the sensor to the sonic choke limits the upper frequency response of the probe. At high frequencies the correlation between concentration fluctuation and velocity fluctuations (velocity fluctuations are a result of the changes of sonic velocity with concentration) at the sensor begin to decline. The CSU aspirated probe is expected to have a 100 Hz upper frequency response, thus the signal was filtered at 100 Hz. This is well above the frequencies of concentration fluctuations that were expected to occur.

The accumulative error, due to the combined effect of calibration uncertainties and nonlinear voltage drifting during the testing time, is estimated to be approximately ± 20 percent of component value in the range of 5-15 percent equivalent methane concentrations.

4.0 TEST PROGRAM RESULTS

Seventeen different pre-field tests were simulated in the Environment Wind Tunnel at Colorado State University at a length scale ratio of 1:100. Video tape movies of all tests except run 15 were obtained and concentration data were obtained on all tests except runs 14 and 15.

Table 1 summarizes the pertinent field test conditions. The following equations were used to convert field values to model values,

$$L_m = \frac{1}{L.S.} L_p = 0.01 L_p,$$

$$U_m = \left(\frac{S.G._m^{-1}}{S.G._p^{-1}} \right)^{1/2} \left(\frac{L_m}{L_p} \right)^{1/2} U_p = 0.0872 U_p,$$

$$Q_m = \left(\frac{S.G._m^{-1}}{S.G._p^{-1}} \right)^{1/2} \left(\frac{L_m}{L_p} \right)^{5/2} Q_p = 8.72 \times 10^{-6} Q_p,$$

$$t_m = \left(\frac{S.G._p^{-1}}{S.G._m^{-1}} \right)^{1/2} \left(\frac{L_m}{L_p} \right)^{1/2} t_p = 0.115 t_p,$$

where L is length, U is wind speed, Q^\dagger is plume vapor flow rate at the source, t is time, $L.S.$ is length scale factor, and $S.G.$ is the plume specific gravity at the source. The subscripts m and p indicate model and prototype (field) conditions respectively. Table 2 summarizes the equivalent model test conditions.

Table 3 specifies measurement locations of the instrumentation rake during measurements, the number of repetitions completed for each run and the number of saves completed for each run. The six character File name indicated on the concentration data sheets (e.g. A01107) contains information about the repetition number (first character-A), and run

[†]LNG vapor at the boiloff temperature of -162°C requires 253 times the volume as LNG.

number (second and third character-01), the position code (fourth character-1), and the computer channel number (last two characters-07). Rake position is always set by rake probe number 1 (Channel 07). Figure 10 displays the spacial locations of the different measurement points.

Velocity profiles are supplied for all cases for both model and prototype scales, respectively in Figures 11 and 12. Individual profiles are provided at prototype scale of each mean wind speed and turbulent intensity profile in Figures 13 through 18. The fit lines on the mean profile plots are the best rms fit to data by power-law and log-linear regressions. These velocity profiles should compare quite well to the field site values. The average power-law exponent of 0.18 is appropriate for a prototype roughness of 1 to 2 cm. The turbulent intensity ratio at 30 m is about 0.06, which agrees with Counihan's [16] prediction of about 0.1 for equivalent surface roughness. The surface drag coefficient, $C_d = 2(u^*/U_2)^2$, equals about 0.014, which agrees with Sutton (Atmospheric Turbulence, 1960; p. 107), who predicts a value of 0.015 for surface roughness of 1 to 2 cm.

Figures 19-25 display the concentration time series plots for Run 1 at a position 15 m downwind of the fence centerline. The plots are for elevations ranging from ground level to a height of 27.3 m. Notice the increasing concentration intermittency as height increases. Indeed, at 27.3 m the average concentration is an order of magnitude less than peak values. This is not unexpected near the edge of a plume. The situation is probably aggravated for these LNG tests due to the sloshing of dense gas within the enclosure. The occasional ramp-like concentration changes noticed for the higher elevations is an artifact of the plotting

program. Small base line drifts in the measurement instrumentation can result in negative concentrations when concentrations are essentially zero. The plotter program avoids plotting these numbers until the next positive value appears; the result is the occasional ramp lines noted.

Contour plots of peak concentrations measured over the total dispersion period are included for the crosswind plane at $X = 15$ meters (Figures 26-34), the downwind vertical plane at fence centerline (Figures 35-46), the downwind vertical plane near the edge of the fence (Figures 47-56), the ground plane (Figures 57-71) and an elevated ground plane at $Z = 18.2$ meters (Figures 72-80). The plots are based on the average peak concentrations for those points where repeated realizations were obtained; otherwise the values were maximums noted during the single run. The interpolation used in these contour plots was linear in the Y and Z direction but logarithmic in the X direction.

Computer prepared tables list field positions, peak concentrations, and arrival times (i.e. 5 percent, 10 percent, and peak arrival times, and 5 percent and 10 percent departure times). In the column labeled SUM is the integral value of concentration over time for the duration of the plume passage. Assuming a constant wind speed at the probe height the SUM value is related to plume dosage, which in turn is related to mass balance. Negative values of SUM should be disregarded. They occur near zero concentration as a result of base line drift in the measurement instrumentation.

REFERENCES

1. Fay, J. A. (1973) "Unusual Fire Hazard of LNG Tanker Spills," Combustion Science and Technology, Vol. 7, pp. 47-49.
2. Burgess, D. S., Biardi, J., and Murphy, J. N. (1972) "Hazards of Spillage of LNG into Water," Bureau of Mines, MIPR No. Z-70099-9-12395.
3. American Gas Association (1974) "LNG Safety Program, Interim Report on Phase II Work," Report on American Gas Association Project IS-3-1, Battelle Columbus Laboratories.
4. Neff, D. E., Meroney, R. N., and Cermak, J. E. (1976) "Wind Tunnel Study of Negatively Buoyant Plume Due to an LNG Spill," Report prepared for R & D Associates, California, Fluid Dynamics and Diffusion Laboratory Report CER76-77DEN-RNM-JEC22, Colorado State University, Fort Collins, Colorado, 241 p.
5. Wiersma, J. (1983) "Recommendations for Research to Assess LNG Safety Hazards," AGA Transmission Conference, Seattle, Washington, 3 May 1983.
6. McQuaid, J. (1982) "Observations on the Current Status of Field Experimentation on Heavy Gas Dispersion," Symposium on Atmosphere Dispersion on Heavy Gases and Small Particles, Delft University of Technology, 29 August - 2 September 1982.
7. Hinze, J. O. (1975) Turbulence, McGraw-Hill, 790 p.
8. Pasquill, F. (1974) Atmospheric Diffusion, D. von Nostrand Co., 429 p.
9. Cermak, J. E. (1971) "Laboratory Simulation of the Atmospheric Boundary Layer," AIAA Jl., Vol. 9, No. 9, pp. 1746-1754, September.
10. Kline, S. J. (1965) Similitude and Approximation Theory, McGraw-Hill, 229 p.
11. Cermak, J. E. (1975) "Applications of Fluid Mechanics to Wind Engineering, A Freeman Scholar Lecture," J. of Fluid Engineering, Vol. 97, Ser. 1, No. 1, pp. 9-38.
12. Schlichting, H. (1968) Boundary Layer Theory, McGraw-Hill, New York.
13. Zoric, D. and Sandborn, V. A. (1972) "Similarity of Large Reynolds Number Boundary Layers," Boundary-Layer Meteorology, Vol. 2, No. 3, March, pp. 326-333.
14. Halitsky, J. (1969) "Validation of Scaling Procedures for Wind Tunnel Model Testing of Diffusion Near Buildings," Geophysical Sciences Laboratory, Report No. TR-69-8, New York University, New York.

15. Plate, E. J. and Cermak, J. E. (1963) "Micro-Meteorological Wind-Tunnel Facility: Description and Characteristics," Fluid Dynamics and Diffusion Laboratory Report CER63-ELP-JEC9, Colorado State University, Fort Collins, Colorado.
16. Counihan, J. (1975) "Adiabatic Atmospheric Boundary Layers: A Review and Analysis of Data from the Period 1880-1972," Atmospheric Environment, Vol. 9, pp. 871-905.
17. Hoot, T. G., et al. (1974) "Wind Tunnel Tests of Negatively Buoyant Plumes," Fluid Dynamics and Diffusion Laboratory Report CER73-74TGH-RNM-JAP13, Colorado State University, Fort Collins, Colorado, October.
18. Isyumov, N., Jandali, T., and Davenport, A. G., "Model Studies and the Prediction of Full Scale Levels of Stack Gas Concentrations," APCA Journal, Vol. 26, No. 10, October 1976.
19. Snyder, W. H. (1972) "Similarity Criteria for the Application of Fluid Models to the Study of Air Pollution Meteorology," Boundary Layer Meteorology, Vol. 3, No. 1, September.
20. Boyle, G. J. and Kneebone, A. (1973) "Laboratory Investigation into the Characteristics of LNG Spills on Water, Evaporation, Spreading and Vapor Dispersion," Shell Research, Ltd., Report to API, March.
21. Meroney, R. N., Neff, D. E., Cermak, J. E. and Megahed, M. (1977) "Dispersion of Vapor from LNG Spills - Simulation in a Meteorological Wind Tunnel," Report prepared for R & D Associates, California, Fluid Dynamics and Diffusion Laboratory Report CER76-77RNM-JEC-DEN-MM57, Colorado State University, Fort Collins, Colorado, 151 p.
22. Meroney, R. N., et al. (1974) "Wind Tunnel Study of Stack Gas Dispersal at the Avon Lake Power Plant," Fluid Dynamics and Diffusion Laboratory Report CER73-74RNM-JEC-BTY-SKN35, Colorado State University, Fort Collins, Colorado, April.
23. Kothari, K. M. and Meroney, R. N. (1979) "Building Effects on National Transonic Facility Exhaust Plume," A Technical Report prepared for NASA, Hampton, Virginia, also, Colorado State University Report CER79-80KMK-RNM35.
24. Bodurtha, F. T., Jr. (1961) "The Behavior of Dense Stack Gases," J. of APCA, Vol. 11, No. 9, pp. 431-437.
25. van Ulden, A. P. (1974) "On the Spreading of a Heavy Gas Released Near the Ground," Loss Prevention and Safety Promotion Seminar, Delft, Netherlands, 6 p.
26. Fay, J. A. (1980) "Gravitational Spread and Dilution of Heavy Vapor Clouds," Second International Symposium on Stratified Flows, the Norwegian Institute of Technology, Trondheim, Norway, 24-27 June.

27. Sandborn, V. A. (1972) Resistance Temperature Transducers, Metrology Press, 545 p.
28. Blackshear, P. L., Jr., and Fingerson, L. (1962) "Rapid Response Heat Flux Probe for High Temperature Gases," ARS Journal, November 1962, pp. 1709-1715.
29. Brown, G. L. and Rebollo, M. R. (1972) "A Small, Fast Response Probe to Measure Composition of a Binary Gas Mixture," AIAA Journal, Vol. 10, No. 5, pp. 649-752.
30. Kuretsky, W. H. (1967) "On the Use of an Aspirating Hot-Film Anomometer for the Instantaneous Measurement of Temperature," Thesis, Master of Mechanical Engineering, University of Minnesota, Minneapolis, Minnesota.

Table 1. Field Test Conditions

Test No.	Velocity ⁺ (m/s)	Vortex Height (m)	Spill ^o Rate (m ³ /min)	Volume ^o (m ³)	Enclosure
1	3.5	14.1	40	100	yes
2	2.0	14.1	40	100	yes
3	5.0	14.1	40	100	yes
4	3.5	9.4	40	100	yes
5	3.5	0	40	100	yes
6	3.5	14.1	20	100	yes
7	3.5	14.1	10	100	yes
8	3.5	14.1	40	70	yes
9	3.5	14.1	40	50	yes
10	3.5	0	40	100	no
11	2.0	0	20	100	no
12	3.5	14.1	20	50	yes
13	3.5	14.1	40	150	yes
14	3.5	0	20	100	yes
15	2.0	0	40	100	no
16	5.0	0	40	100	no
17	3.5	0	10	100	no

⁺At 2 meters height

^oLiquid Conditions

(S.G.)_p = 1.5

Table 2. Model Test Conditions

Test No.	Velocity (cm/s)	Vortex Height (cm)	Spill ^Δ Rate (cc/s)	Volume ^Δ (cc)	Release Time (sec)	Concentration Data	Visualization Data
1	30.5	14.1	1471	25300	17.2	x	x
2	17.5	14.1	1471	25300	17.2	x	x
3	43.5	14.1	1471	25300	17.2	x	x
4	30.5	9.4	1471	25300	17.2	x	x
5	30.5	0	1471	25300	17.2	x	x
6	30.5	14.1	735	25300	34.4	x	x
7	30.5	14.1	368	25300	68.8	x	x
8	30.5	14.1	1471	17710	12	x	x
9	30.5	14.1	1471	12650	8.6	x	x
10	30.5	0	1471	25300	17.2	x	x
11	17.5	0	735	25300	34.4	x	x
12	30.5	14.1	735	12650	17.2	x	x
13	30.5	14.1	1471	37950	25.8	x	x
14	30.5	0	735	25300	34.4		x
15	17.5	0	1471	25300	17.2		
16	43.5	0	1471	25300	17.2	x	x
17	30.5	0	368	25300	68.8	x	x

^ΔGas conditions
(S.G.)_m = 1.38

Table 3. Concentration Data File Description

Position Code	X (cm)	Y (cm)	Z (cm)	Z (H)	No. Rep.	No. Saves (files)
0	15	63	0	0		
1	15	0	0	0	3	2
2	15	0	4.55	1/2	1	1
3	15	0	9.1	1	3	2
4	15	0	13.6	3/2	1	1
5	15	0	18.2	2	3	2
6	15	0	22.7	5/2	1	1
7	15	0	27.3	3	1	1
8	75	0	0	0	3	2
N	75	0	4.55	1/2	2	2
9	75	0	9.1	1	3	2
0	75	0	13.6	3/2	2	2
A	75	0	18.2	2	3	2
B	75	0	27.3	3	1	1
C	75	-63	0	0	1	1
D	200	0	0	0	3	2
P	200	0	4.55	1/2	2	2
E	200	0	9.1	1	2	1
Q	200	0	13.6	3/2	2	2
F	200	0	18.2	2	2	1
G	200	0	27.3	3	1	1
H	200	-63	0	0	1	1
I	400	0	0	0	3	2
R	400	0	4.55	1/2	2	2
S	400	0	9.1	1	2	2
T	400	0	13.6	3/2	2	2
J	400	0	18.2	2	1	1
K	400	-63	0	0	1	1

File Name - A01107
 ↑ run no.
 ↓ position code
 channel no. (computer assigned)

Rake position set a rake probe number 1 (Channel 7)

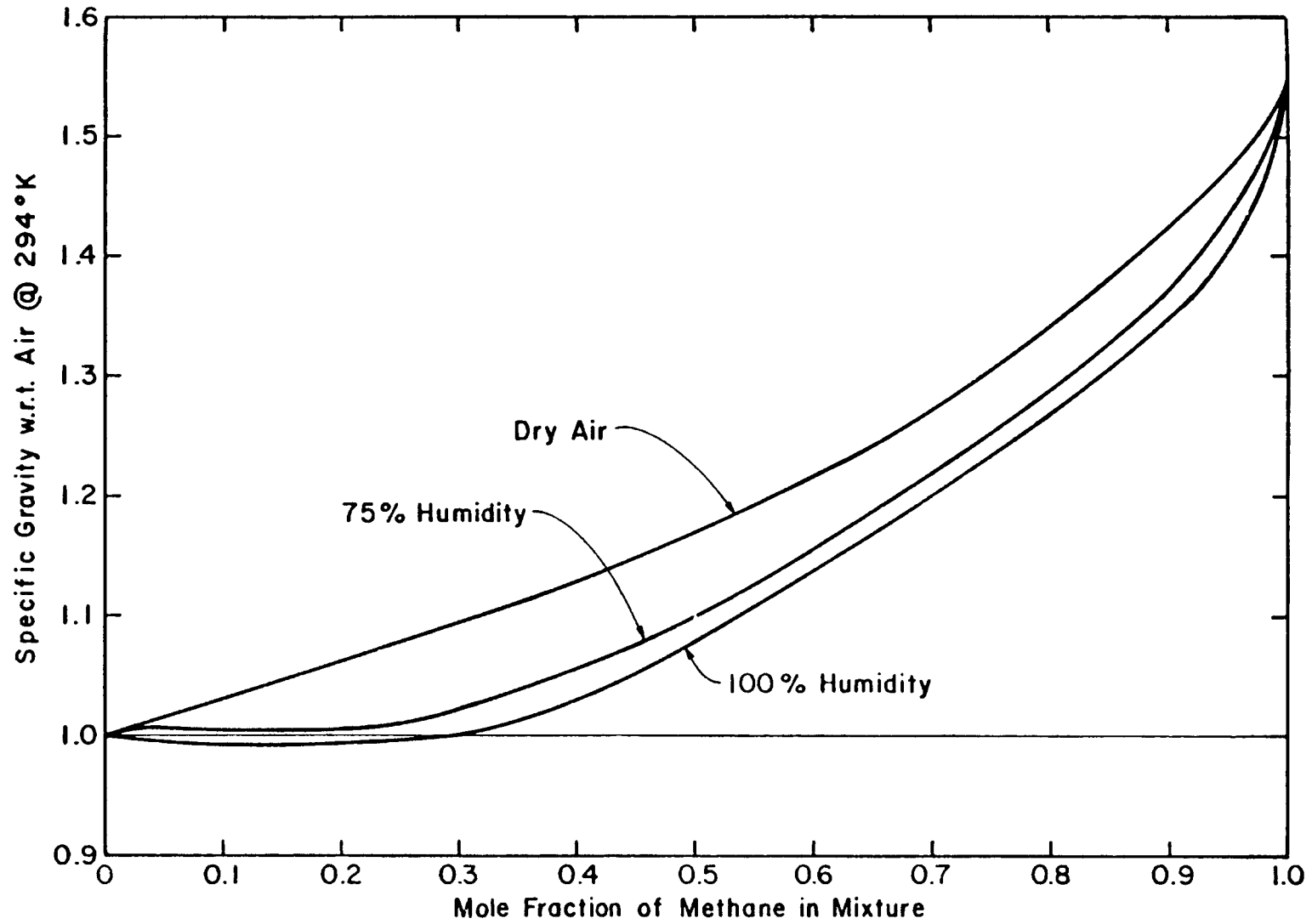


Figure 1. Specific Gravity of LNG Vapor - Humid Atmospheric Mixtures

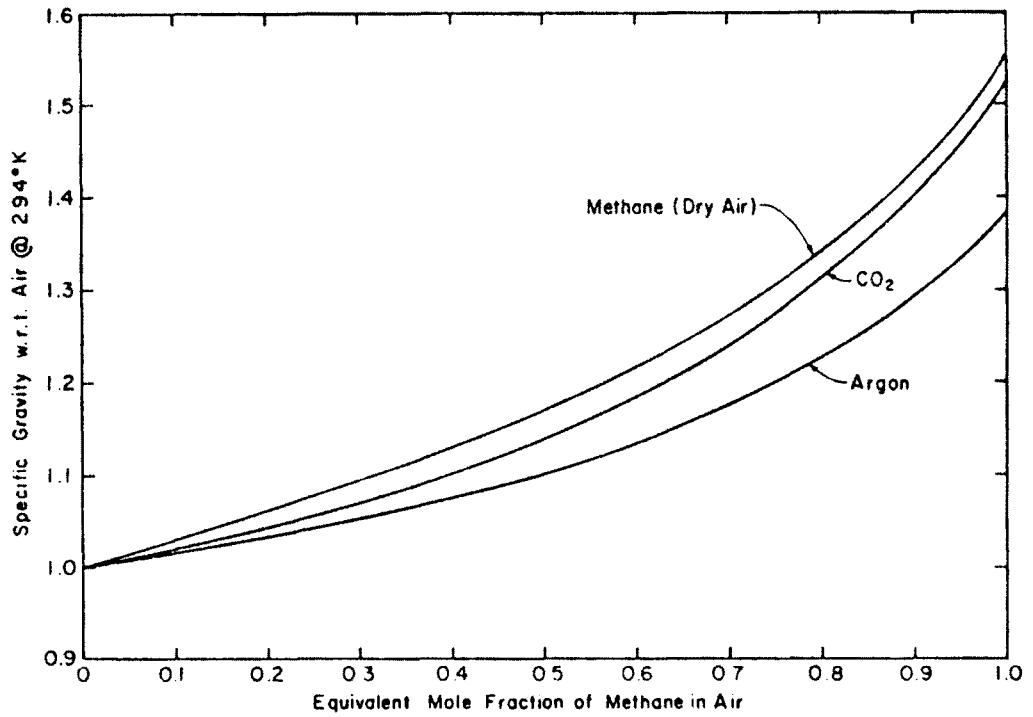


Figure 2. Specific Gravity of Gas-Air Mixtures

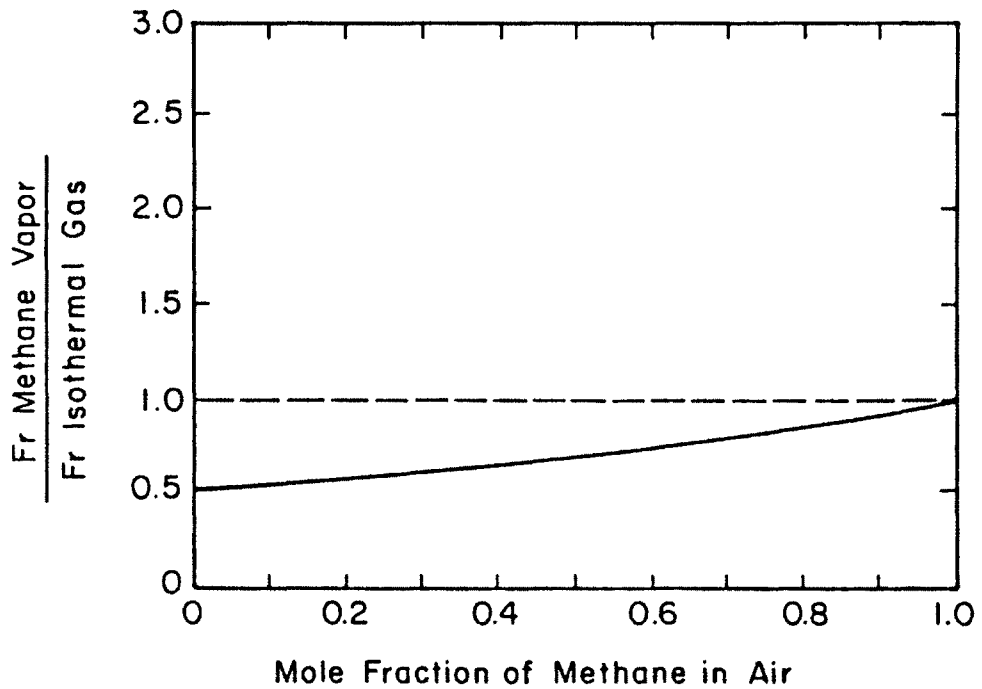
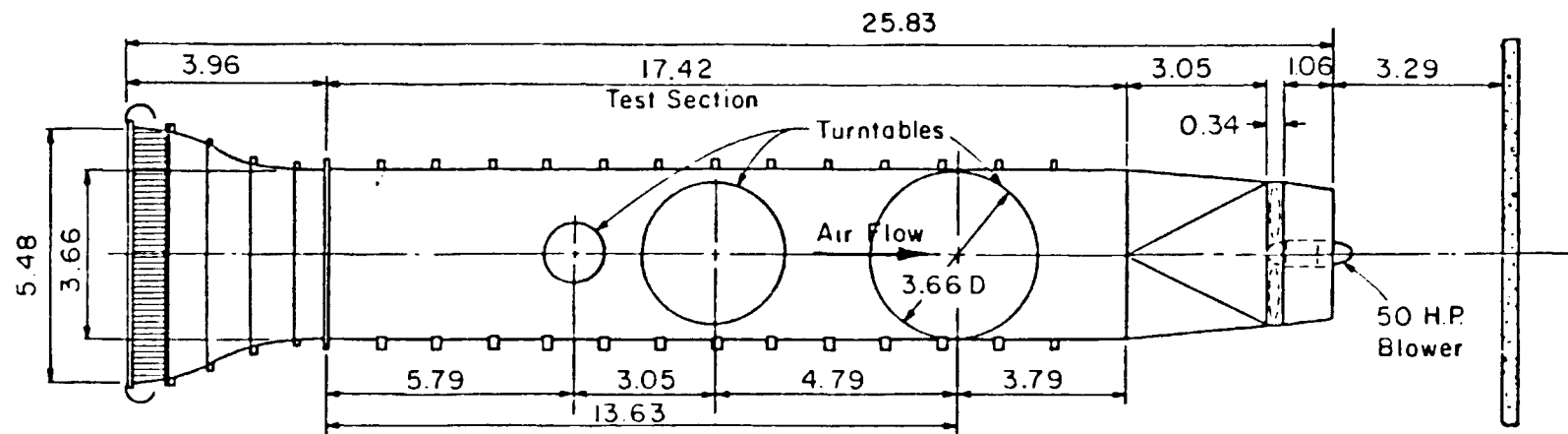
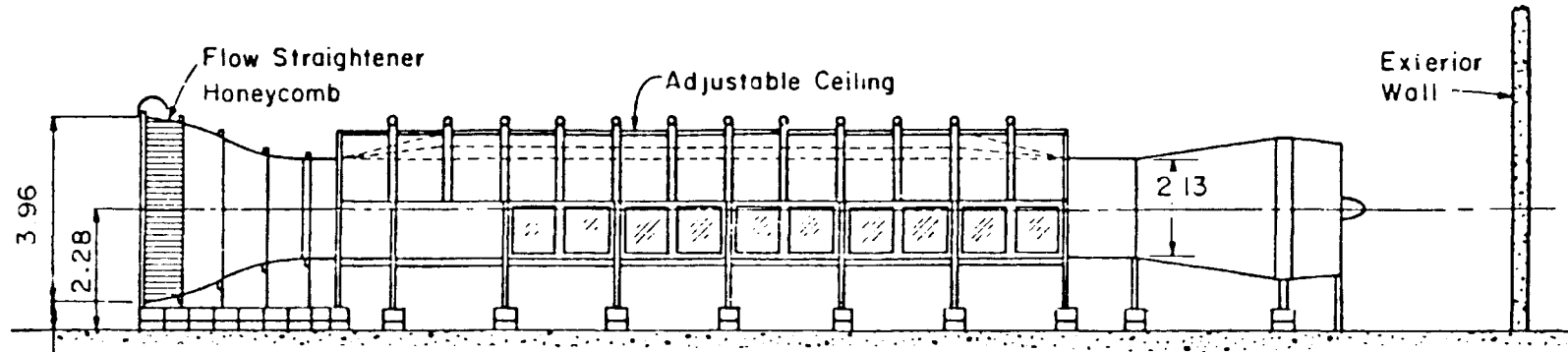


Figure 3. Variation of Isothermal Plume Behavior from Equivalent Cold Methane Plume Behavior



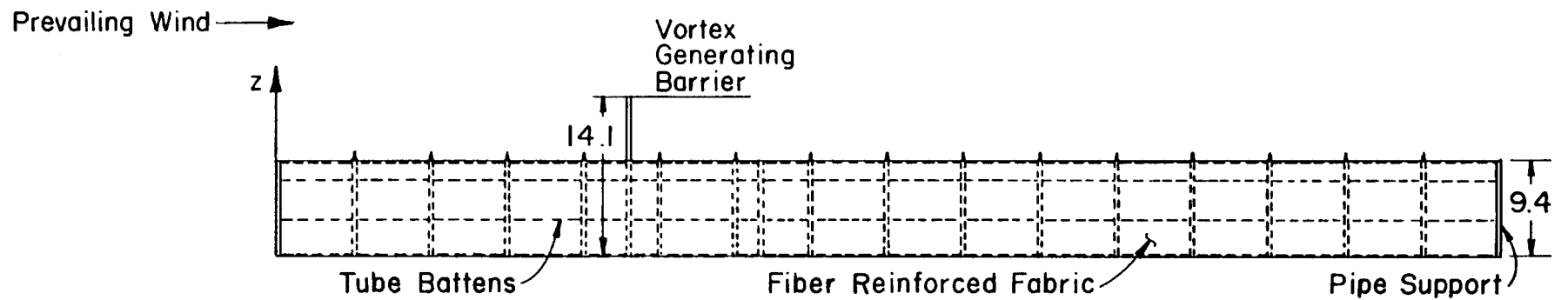
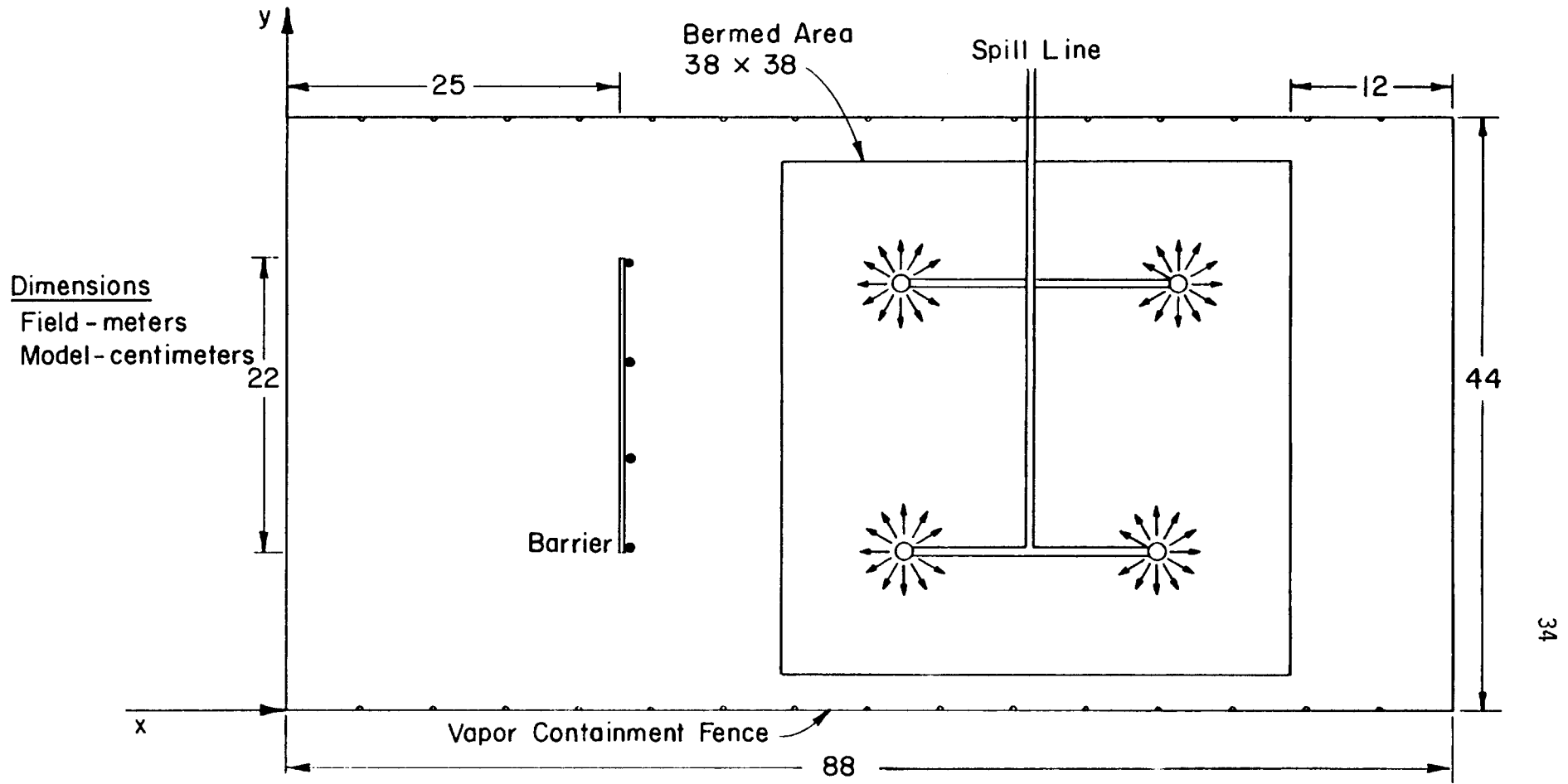
PLAN

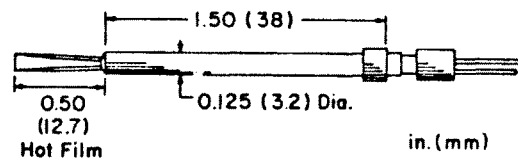
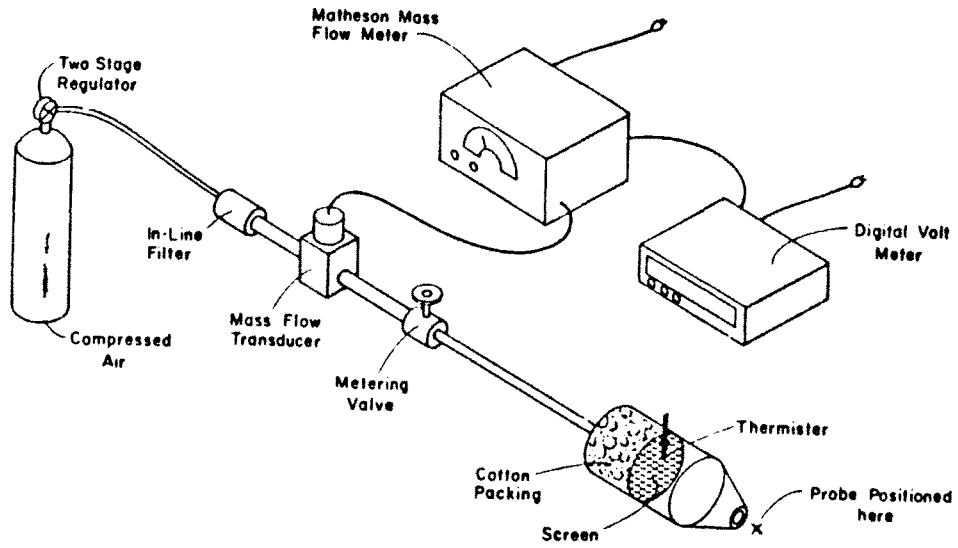


ELEVATION

All Dimensions in m

Figure 4. Environmental Wind Tunnel





TSI Single Film Sensor

Figure 6. Velocity Probes and Velocity Standard

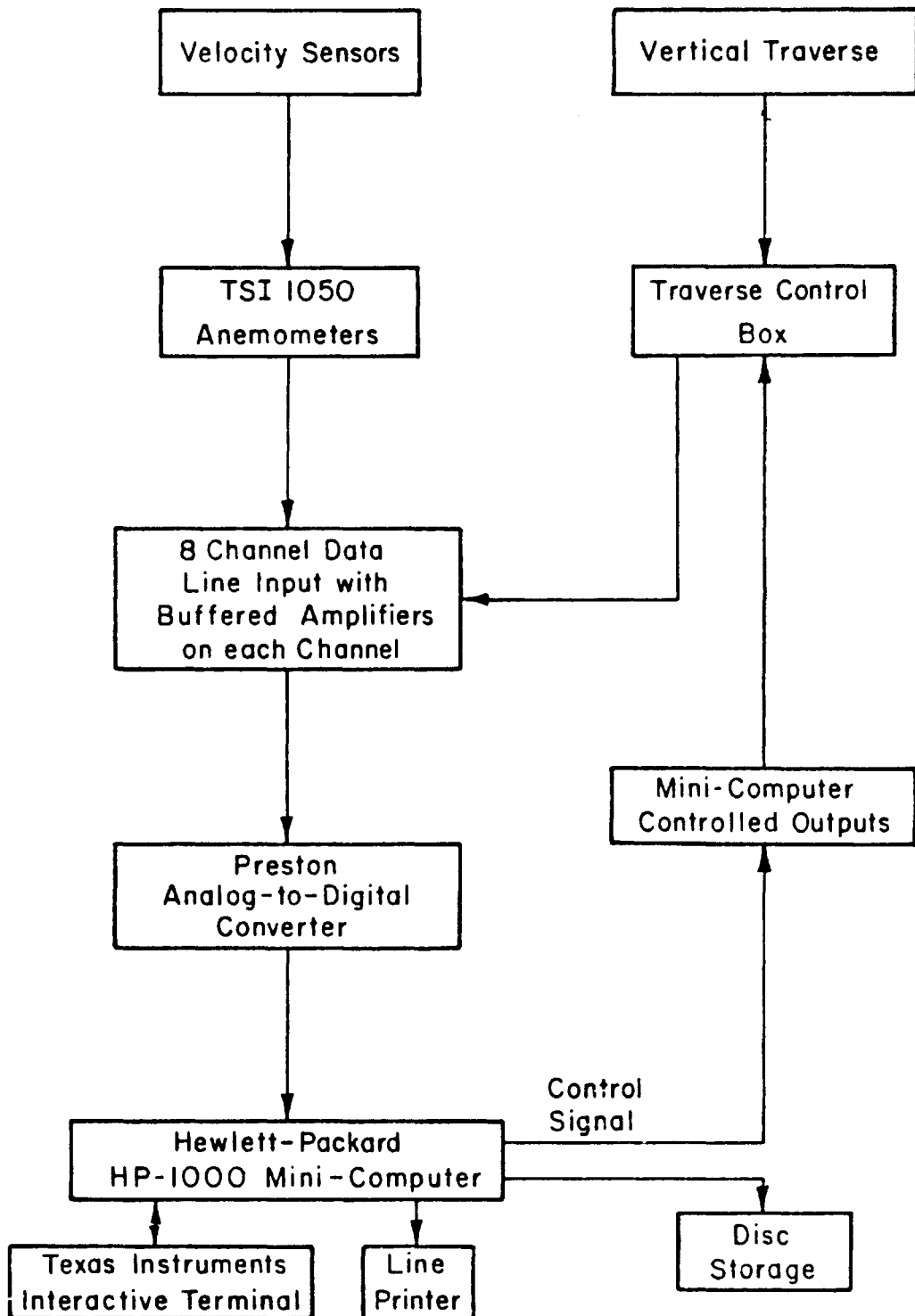


Figure 7. Velocity Data Reduction Flow Chart

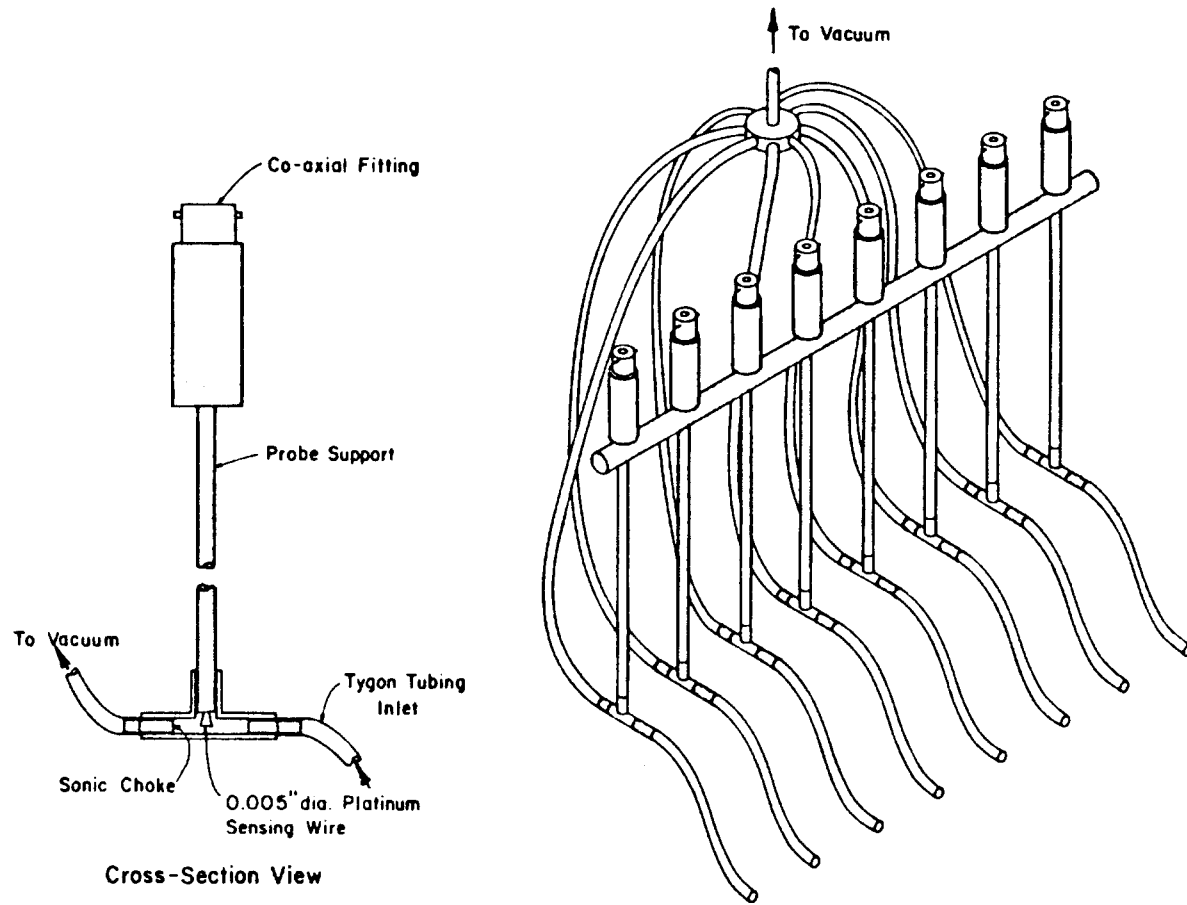


Figure 8. Hot-Wire Katharometer Probes

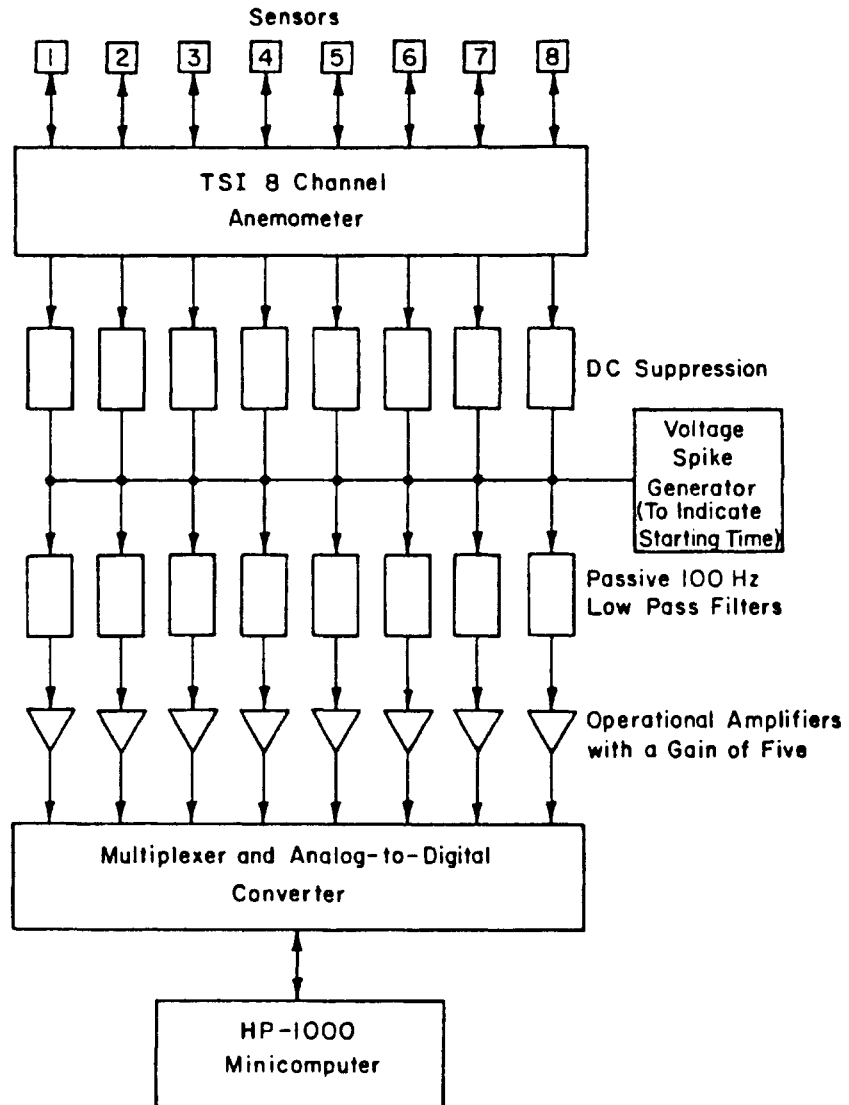


Figure 9. Block Diagram Katharometer Array

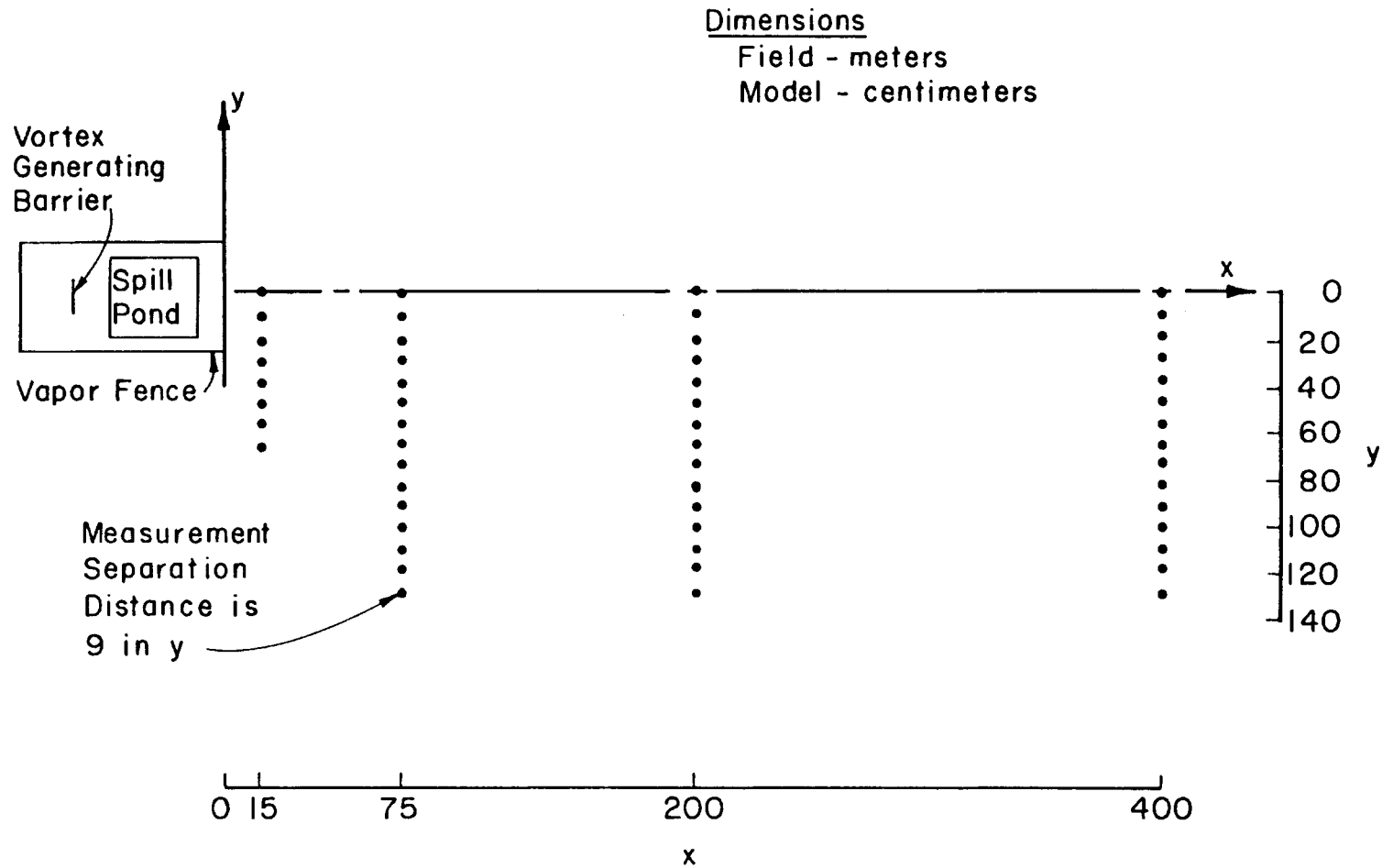
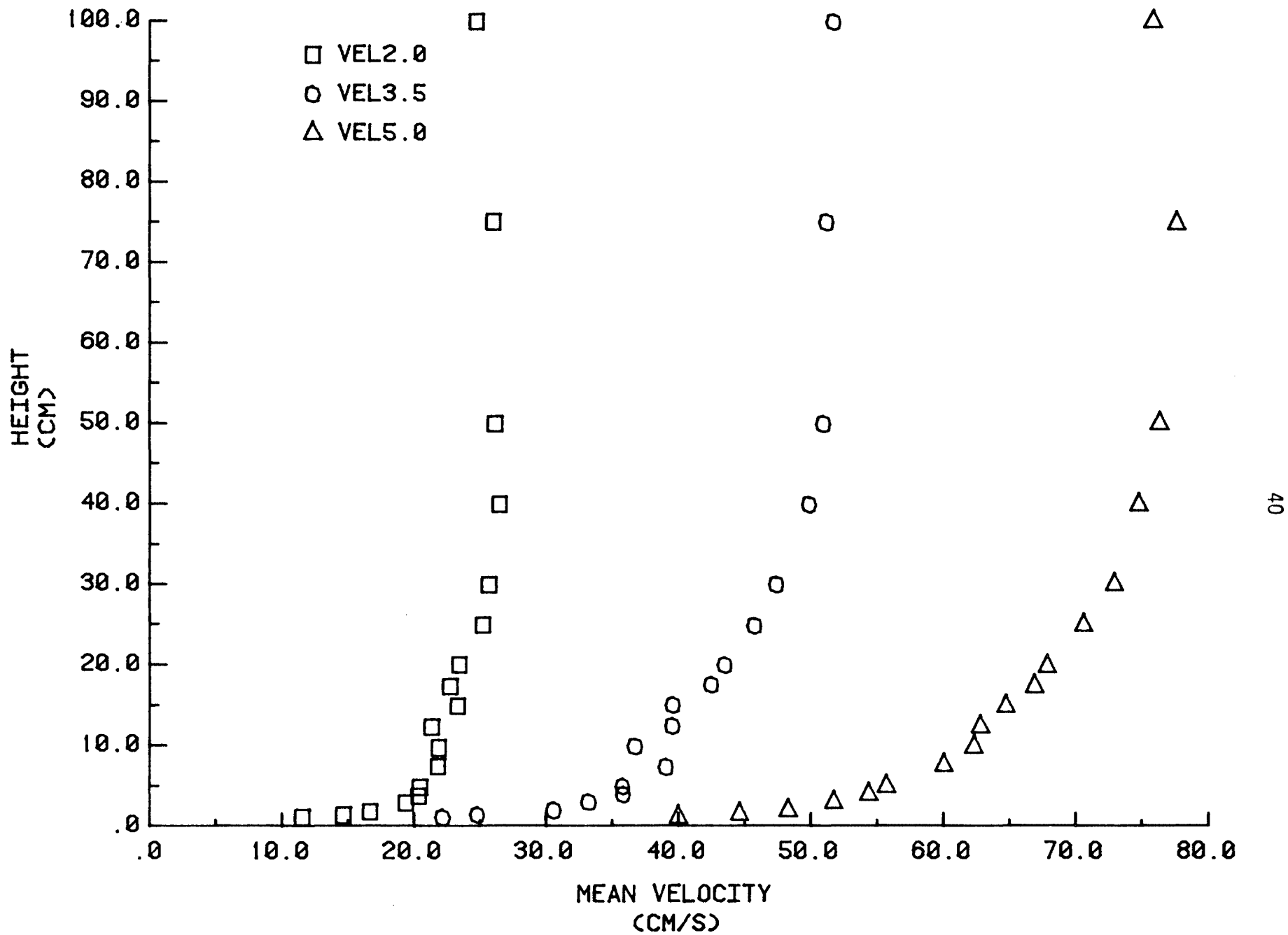


Figure 10. Concentration Sampling Locations



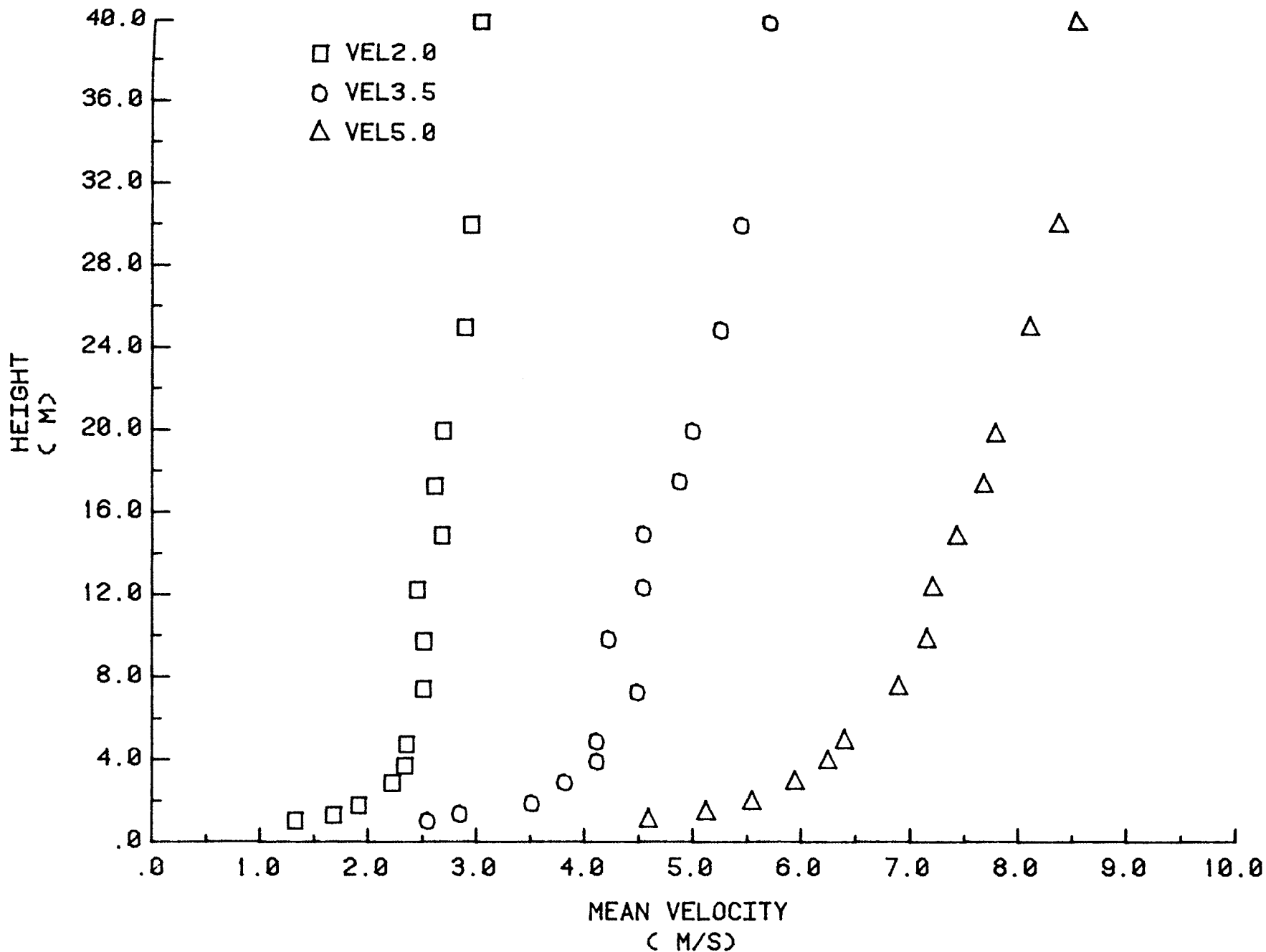


Figure 12. Prototype Velocity Profiles

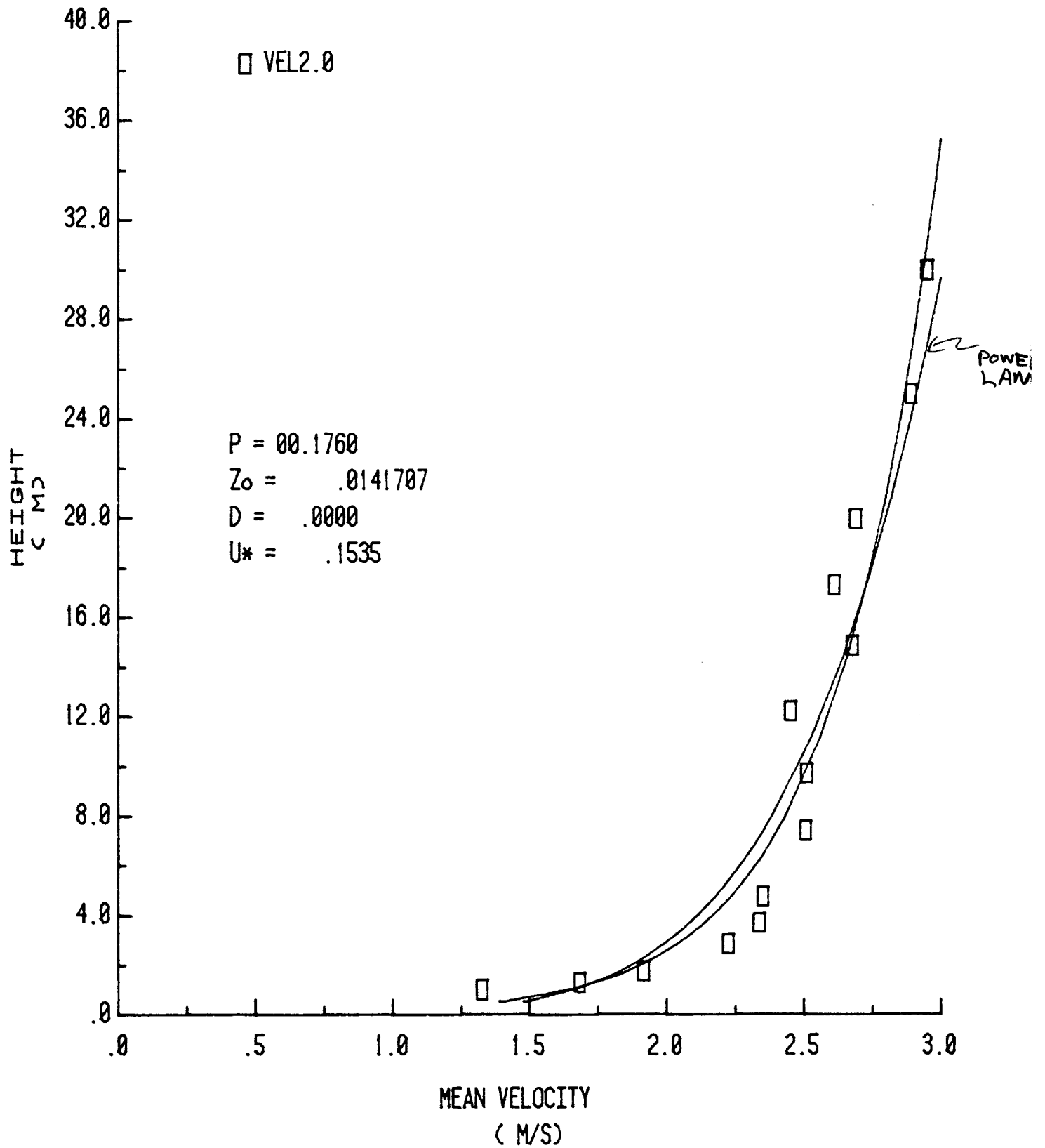


Figure 13. 2.0 M/S Prototype Velocity Profile with Regressions

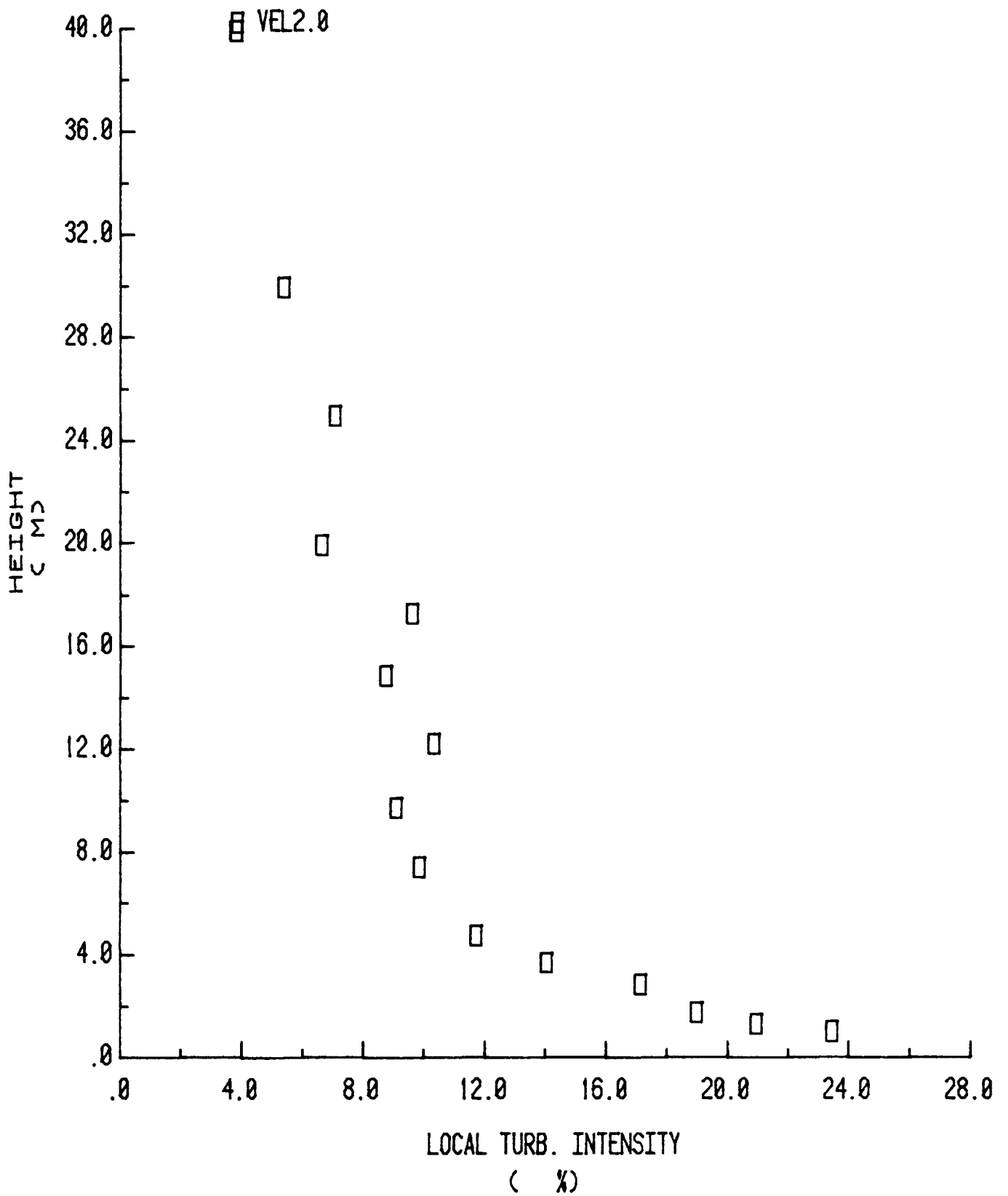


Figure 14. 2.0 M/S Prototype Turbulent Intensity Profile

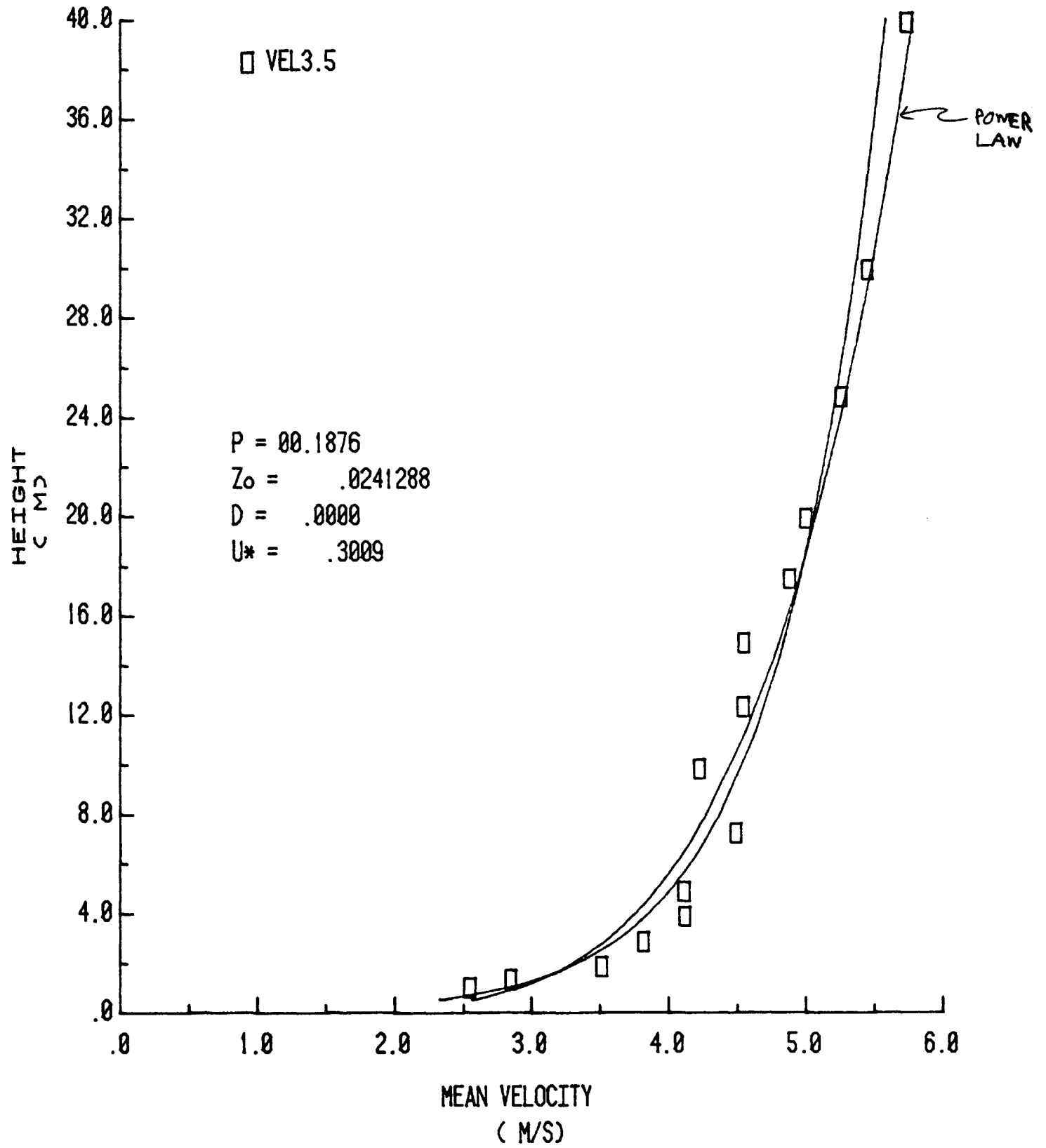


Figure 15. 3.5 M/S Prototype Velocity Profile with Regressions

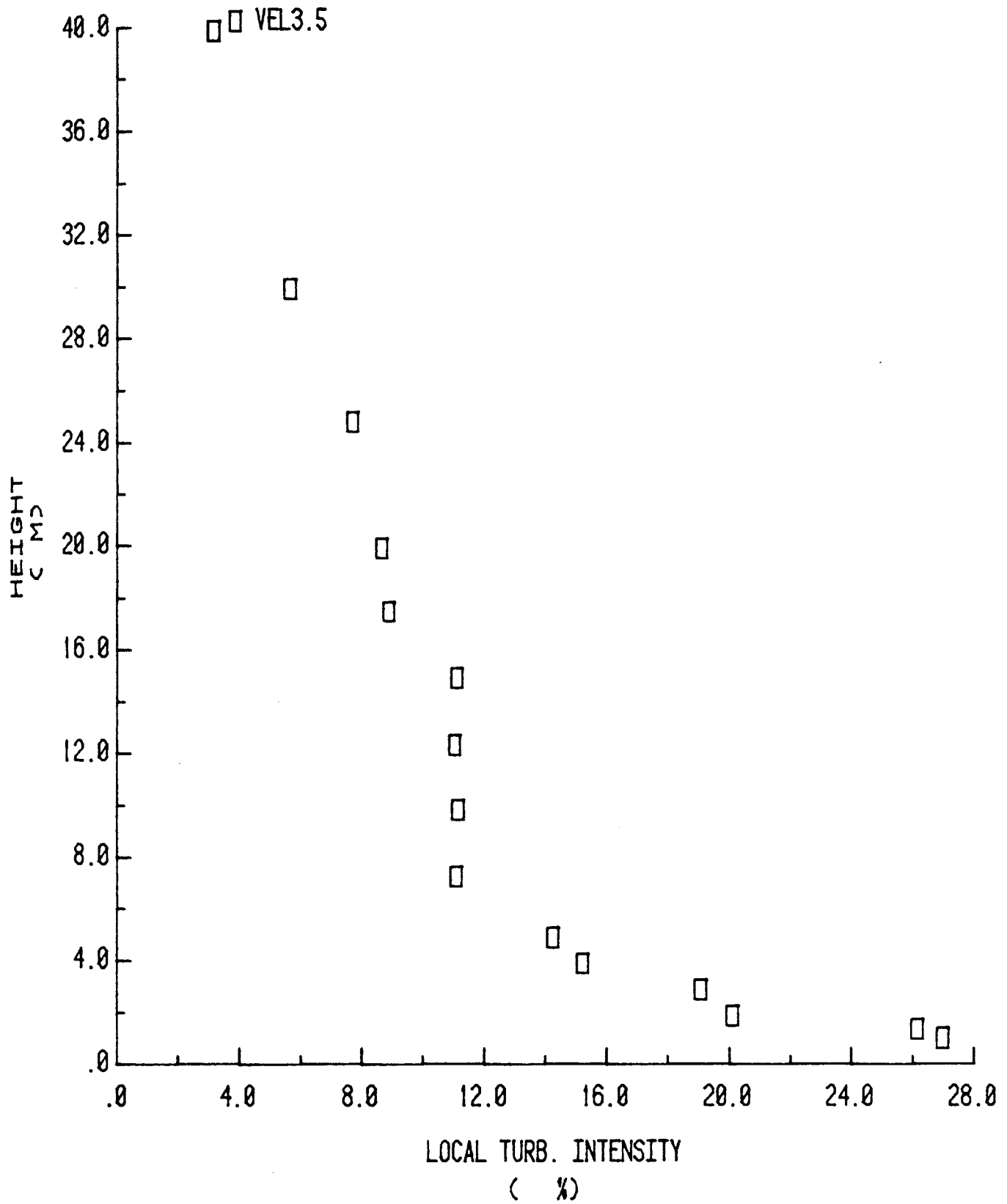


Figure 16. 3.5 M/S Prototype Turbulent Intensity Profile

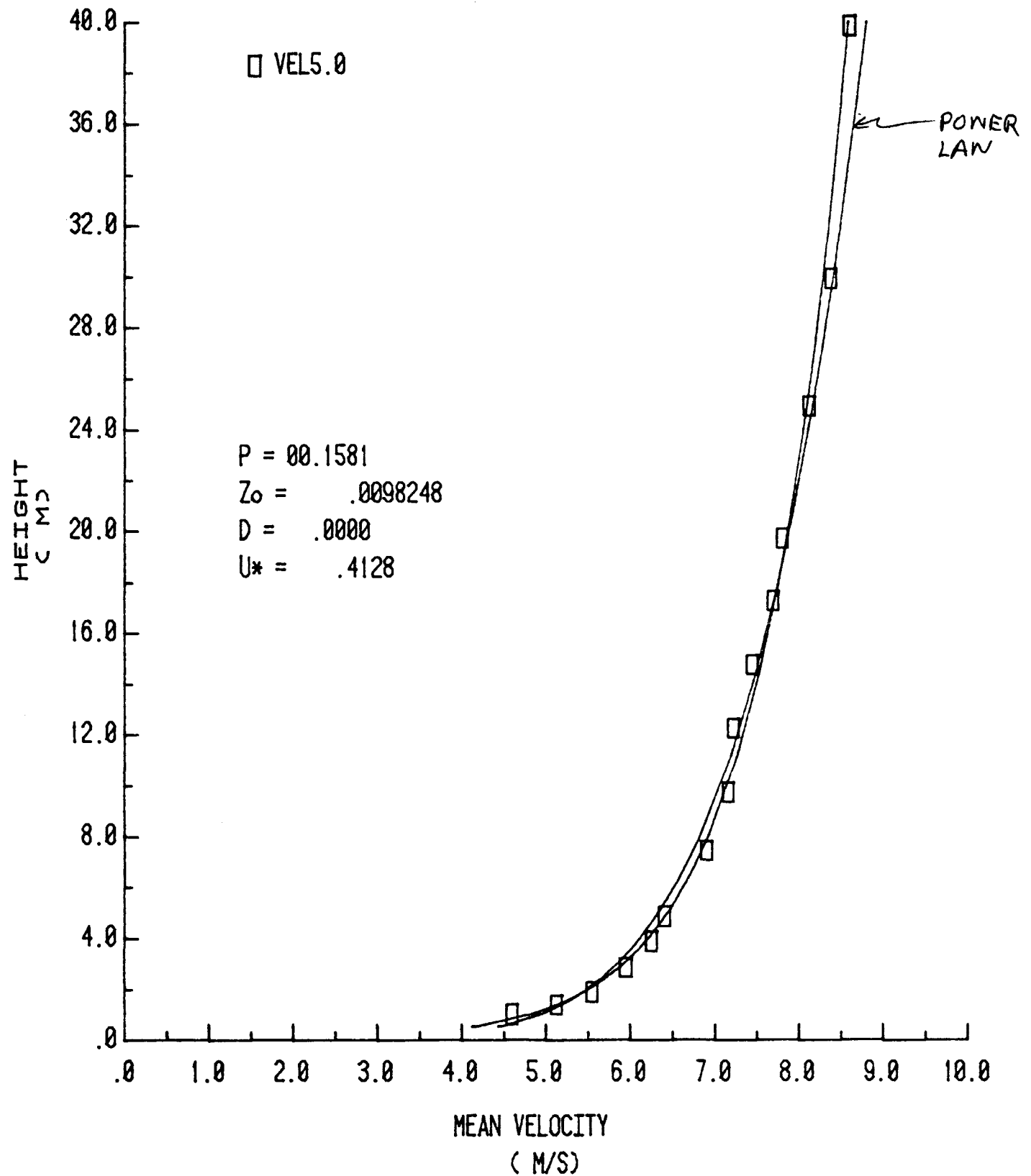


Figure 17. 5.0 M/S Prototype Velocity Profile with Regressions

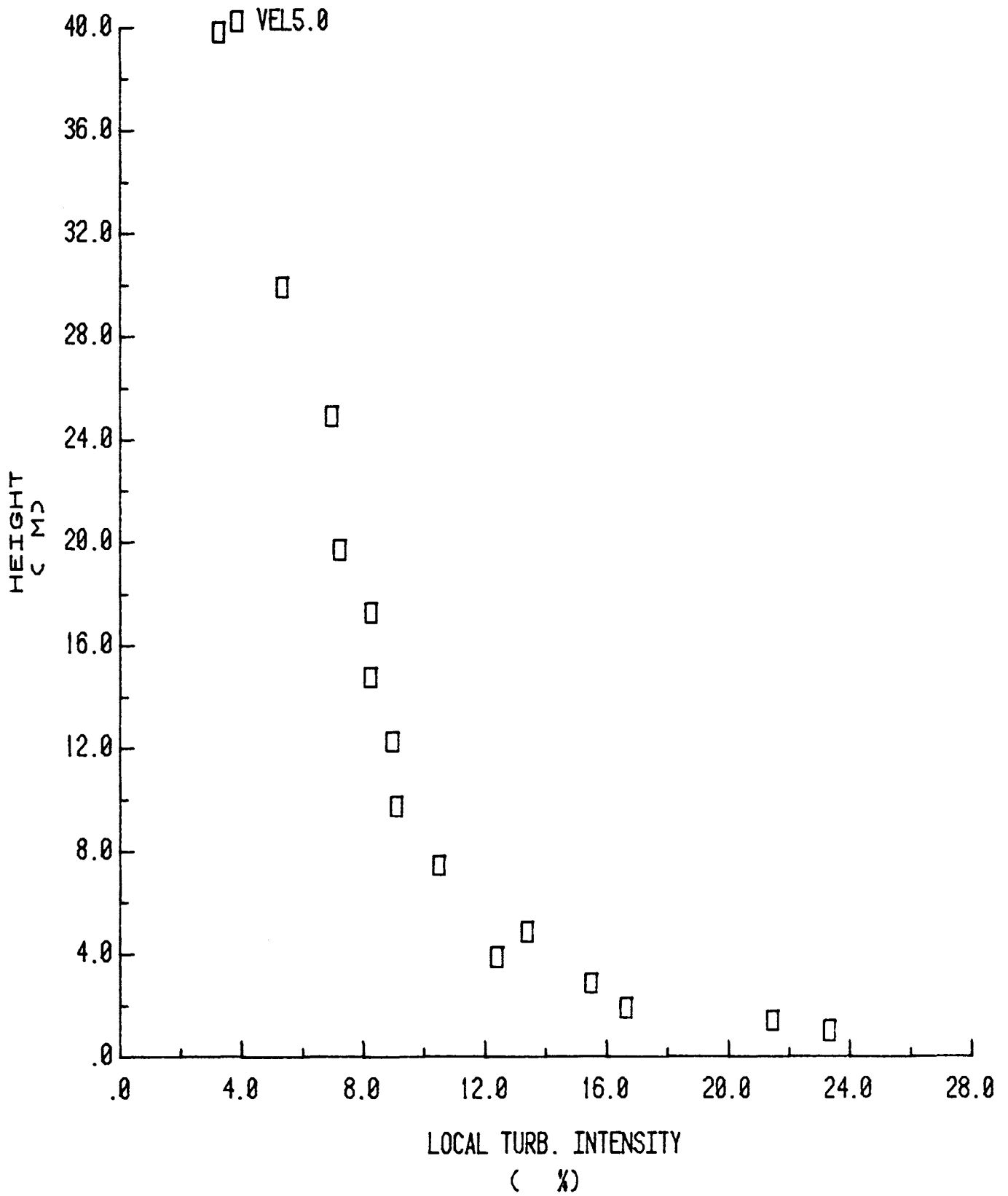


Figure 18. 5.0 M/S Prototype Turbulent Intensity Profile

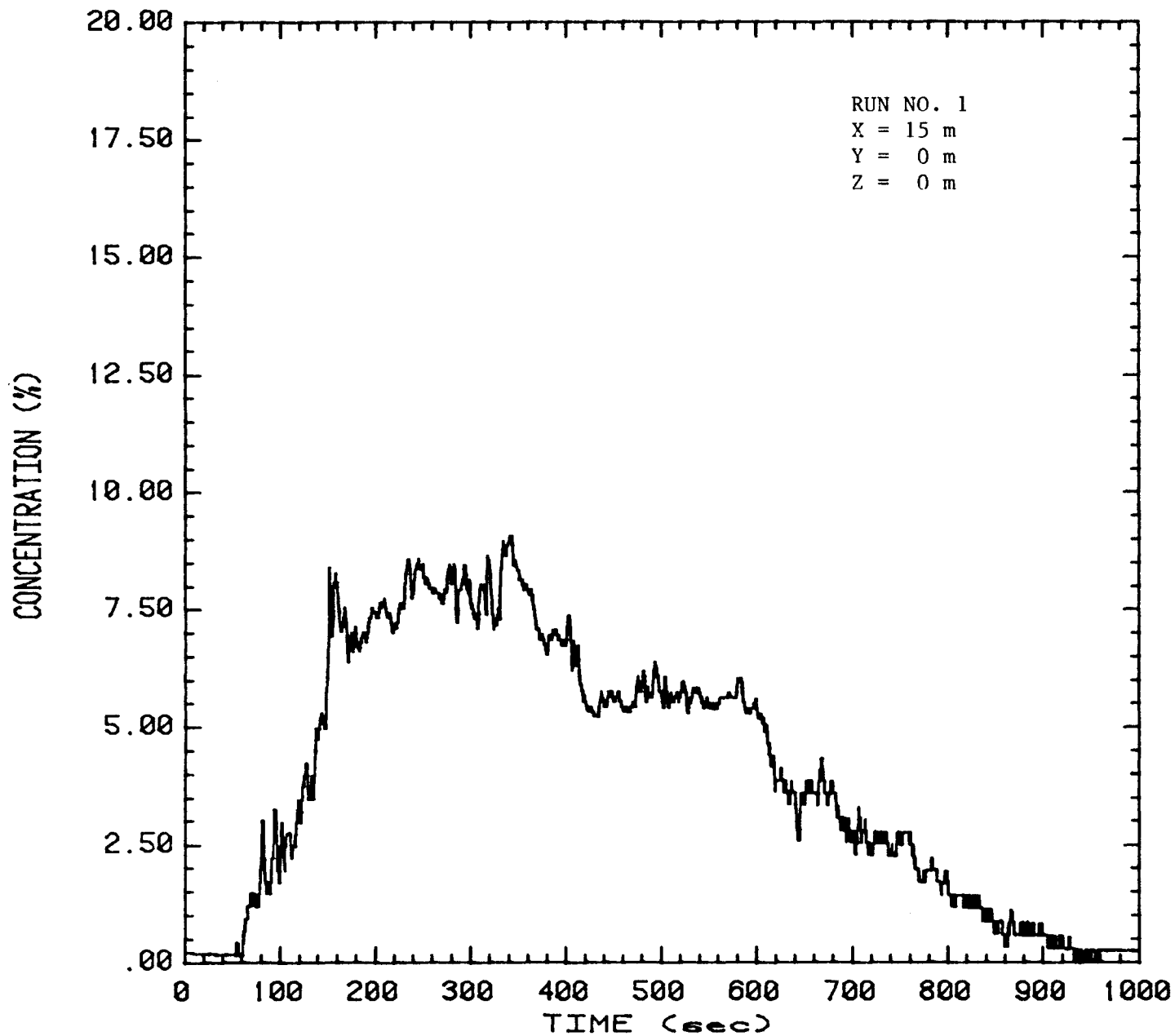


Figure 19. Concentration Time Series

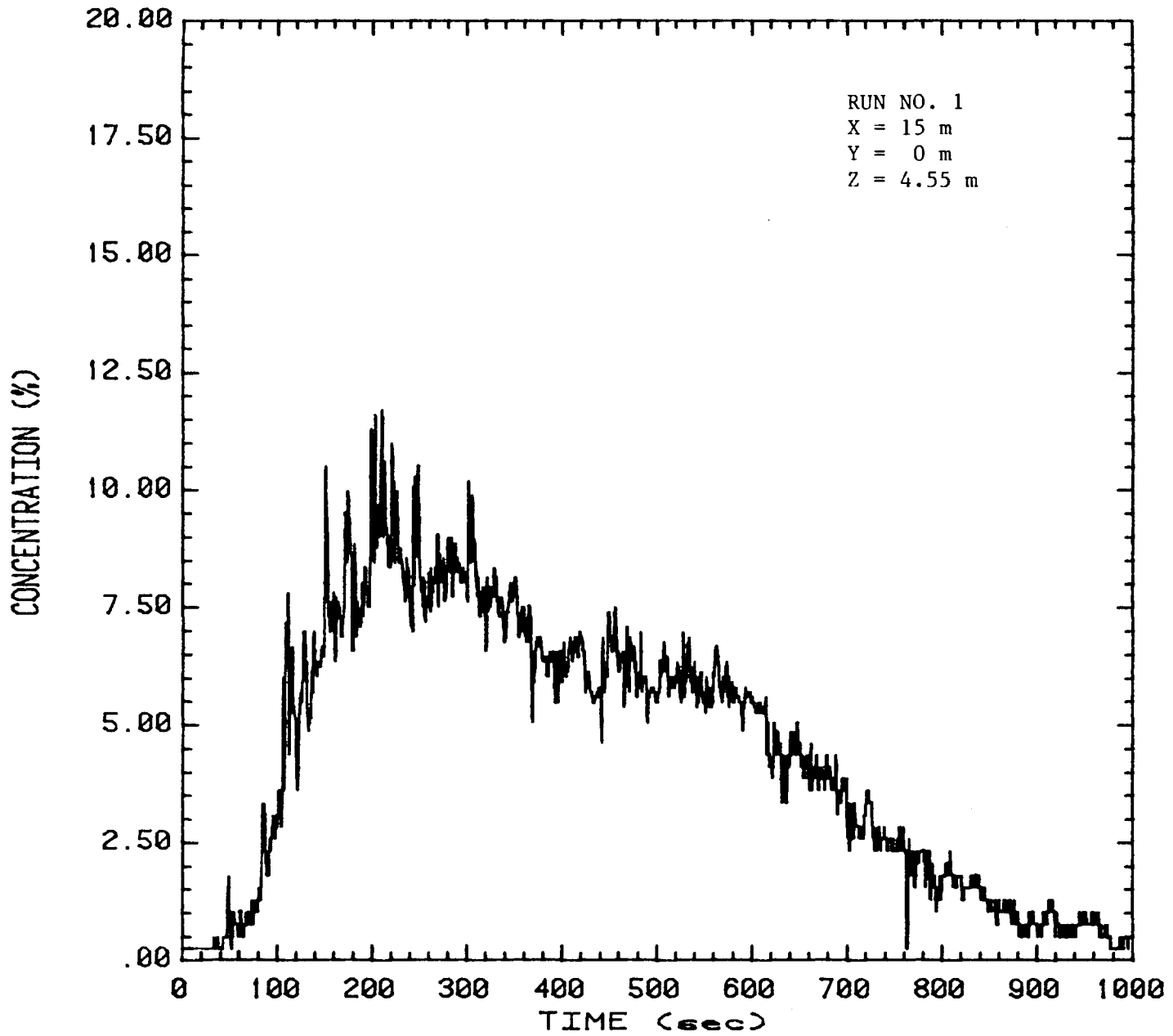


Figure 20. Concentration Time Series

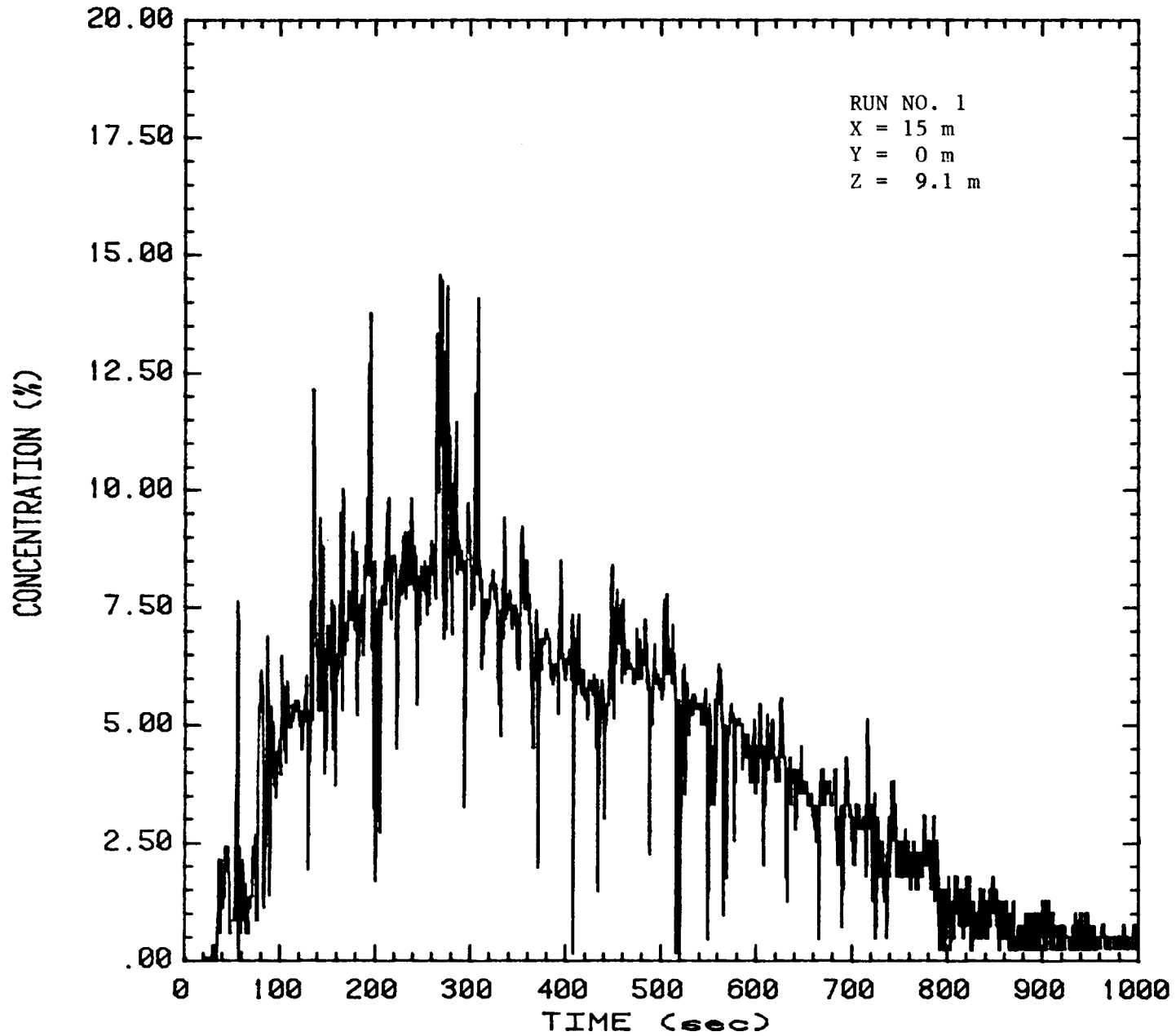


Figure 21. Concentration Time Series

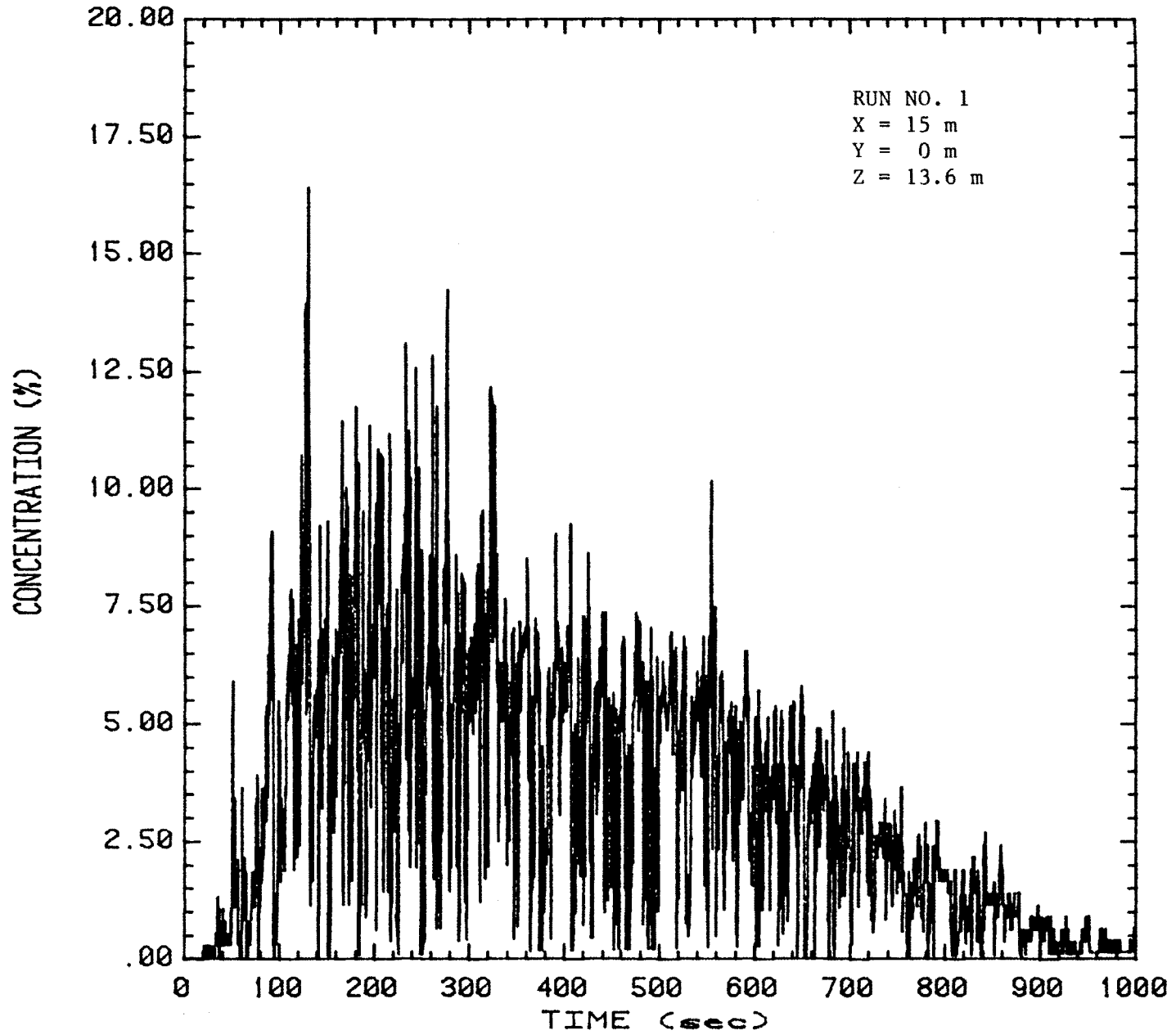


Figure 22. Concentration Time Series

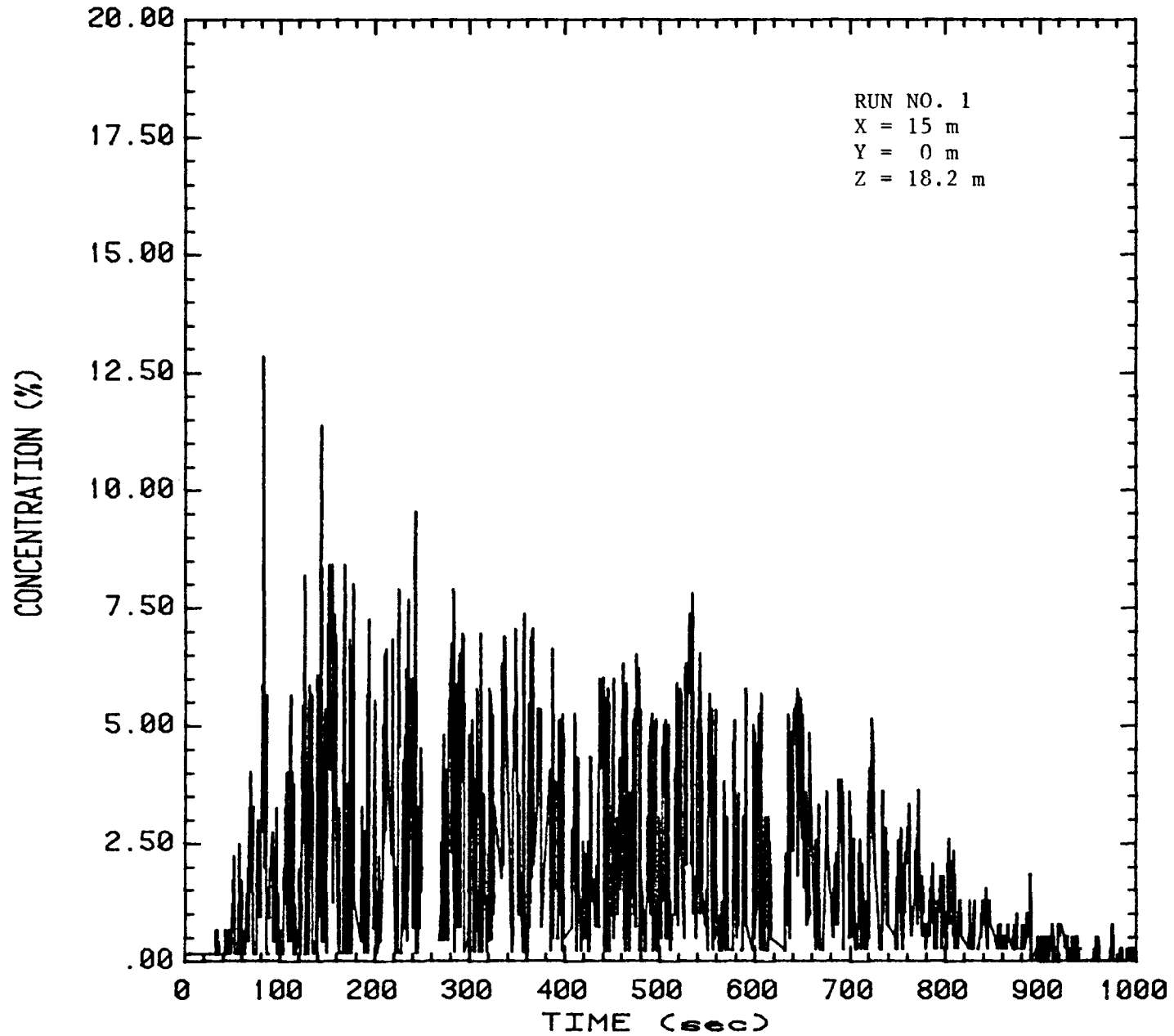


Figure 23. Concentration Time Series

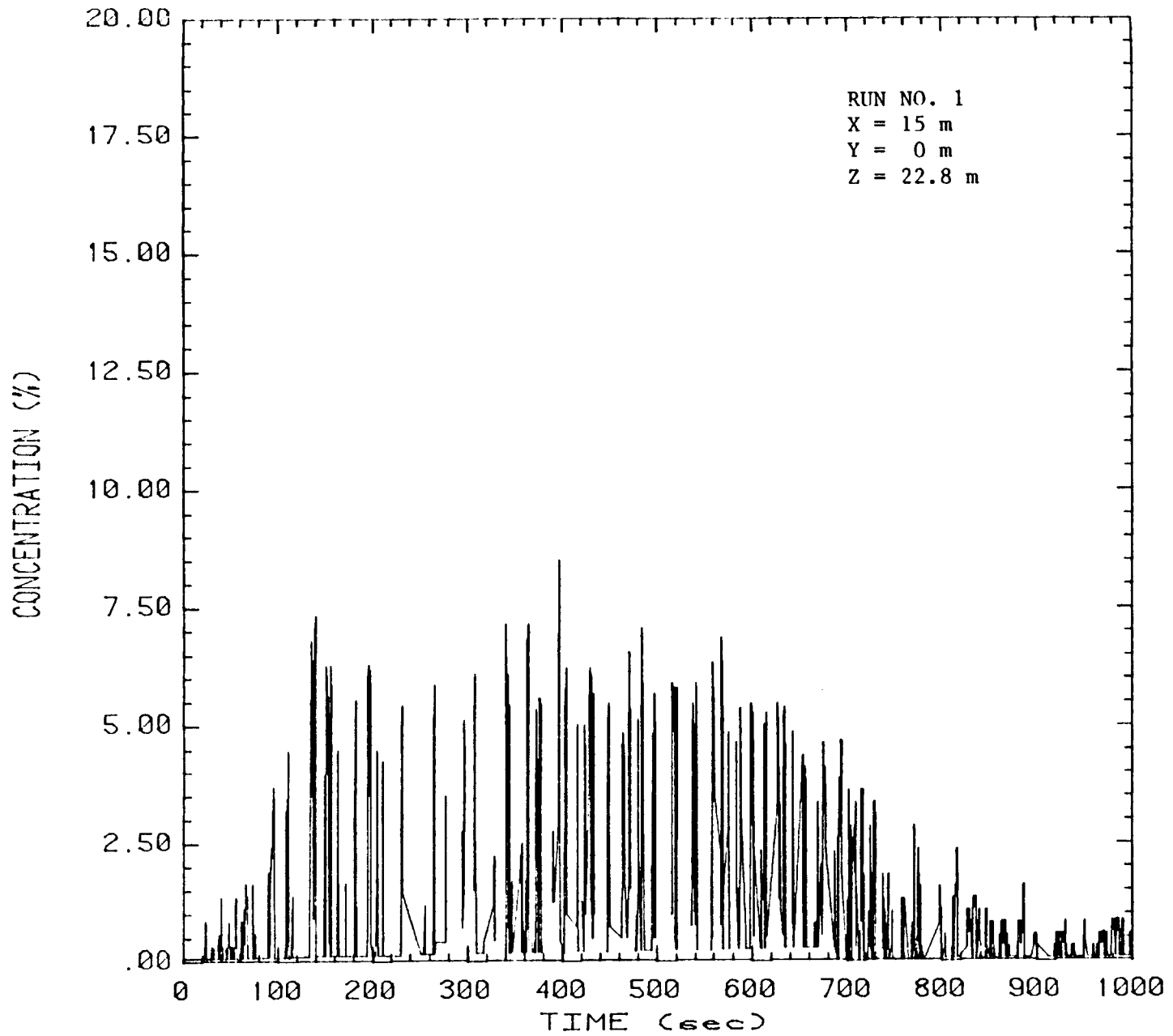


Figure 24. Concentration Time Series

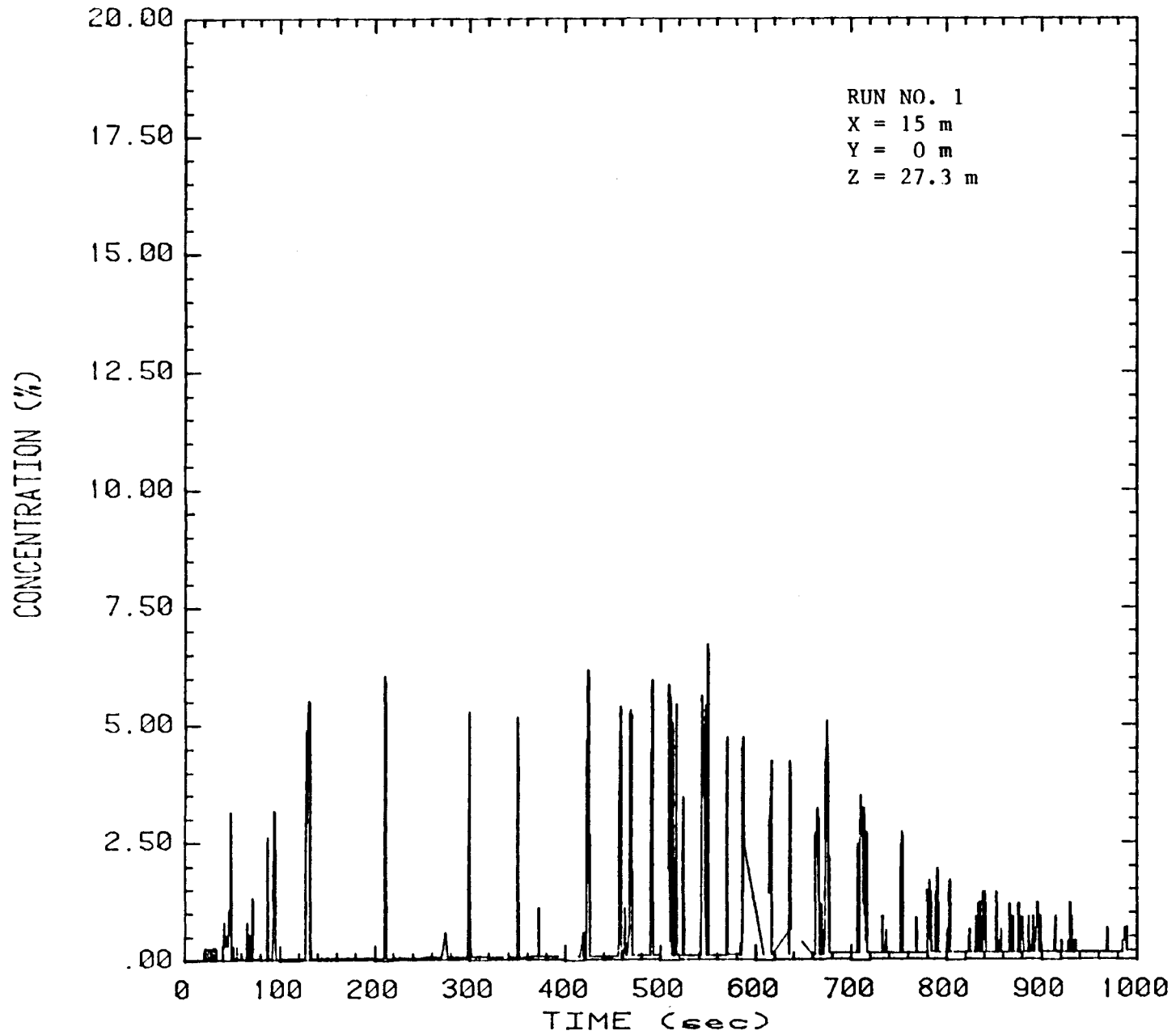


Figure 25. Concentration Time Series

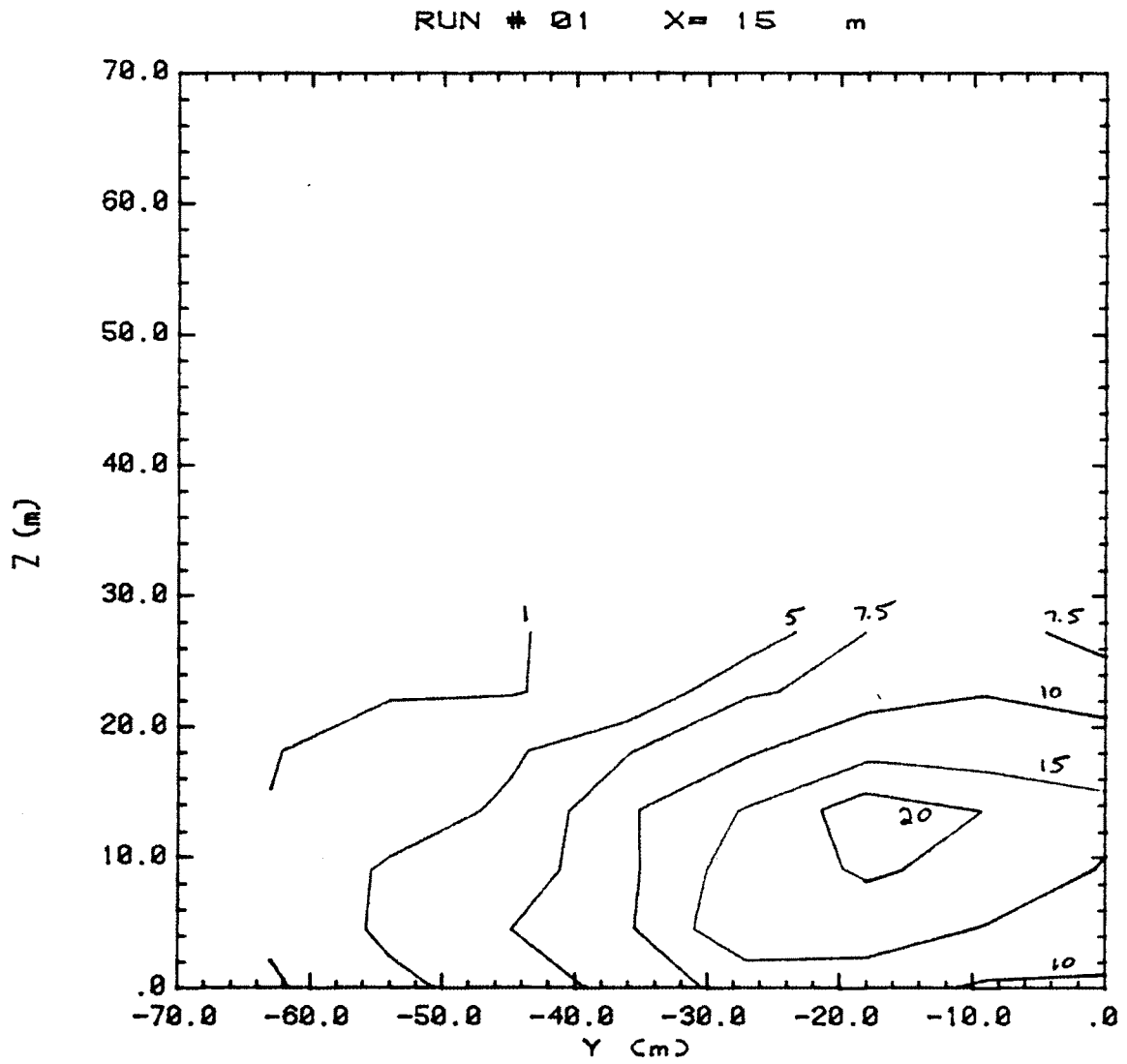


Figure 26. Concentration Contour Plot

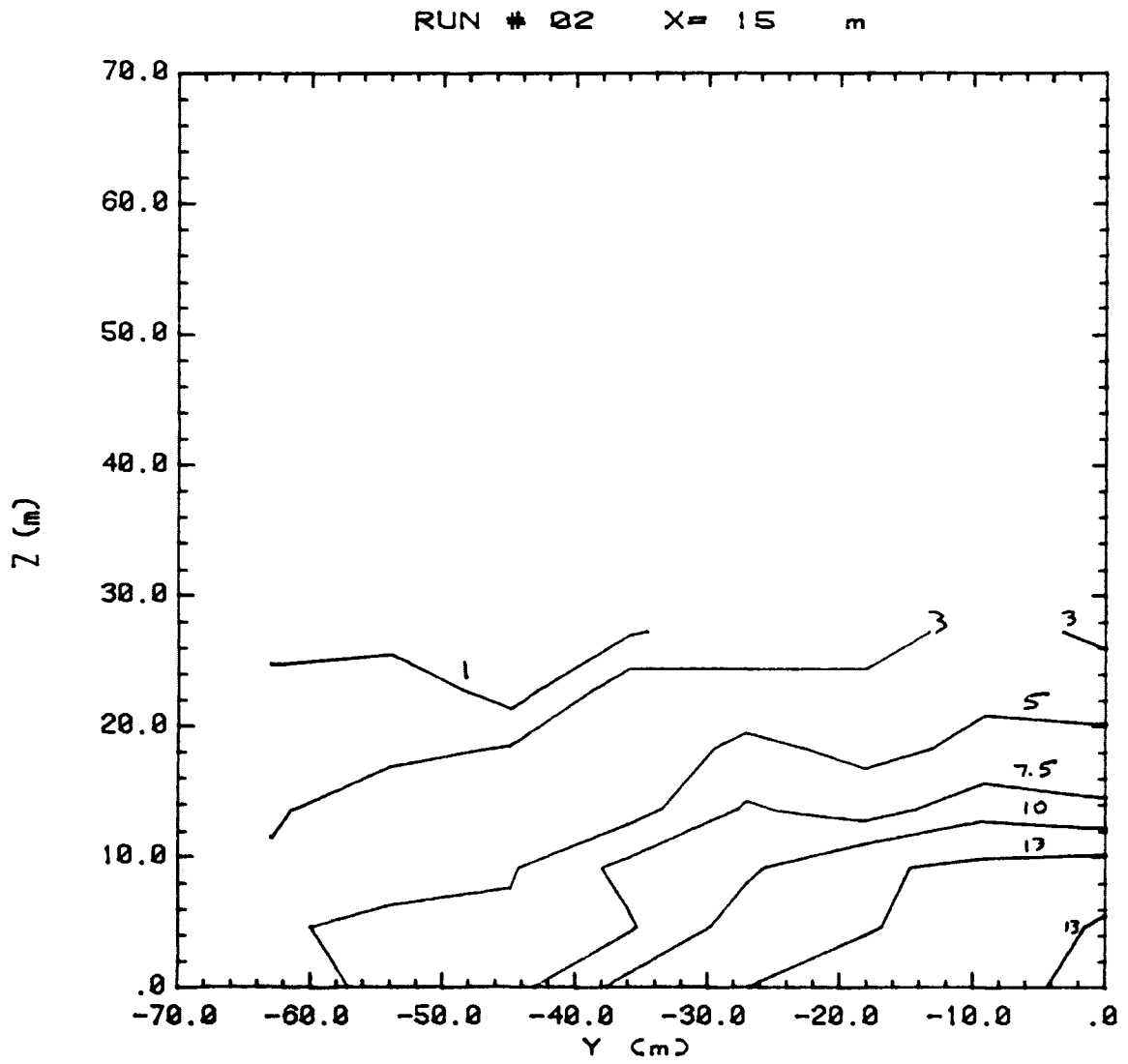


Figure 27. Concentration Contour Plot

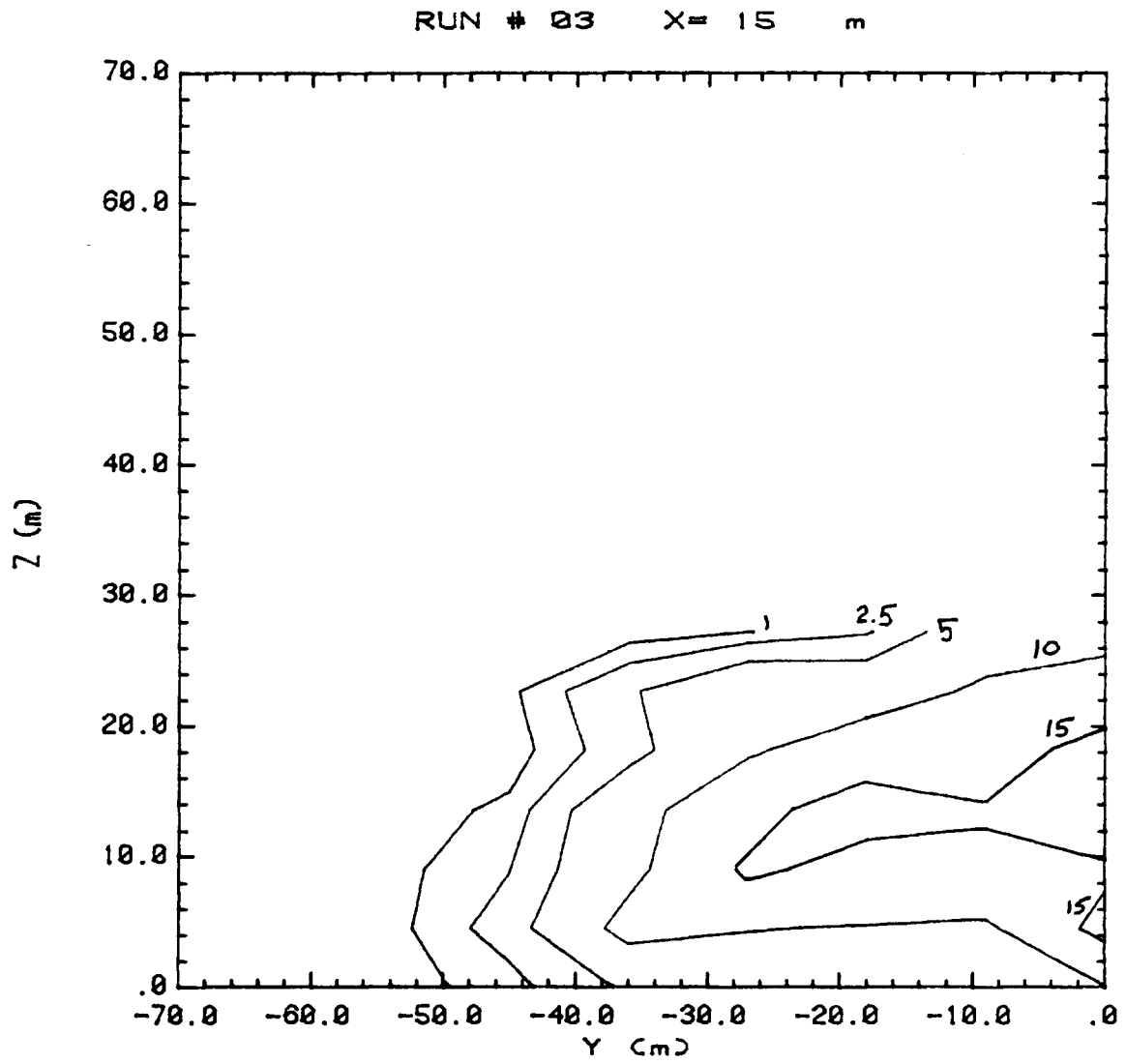


Figure 28. Concentration Contour Plot

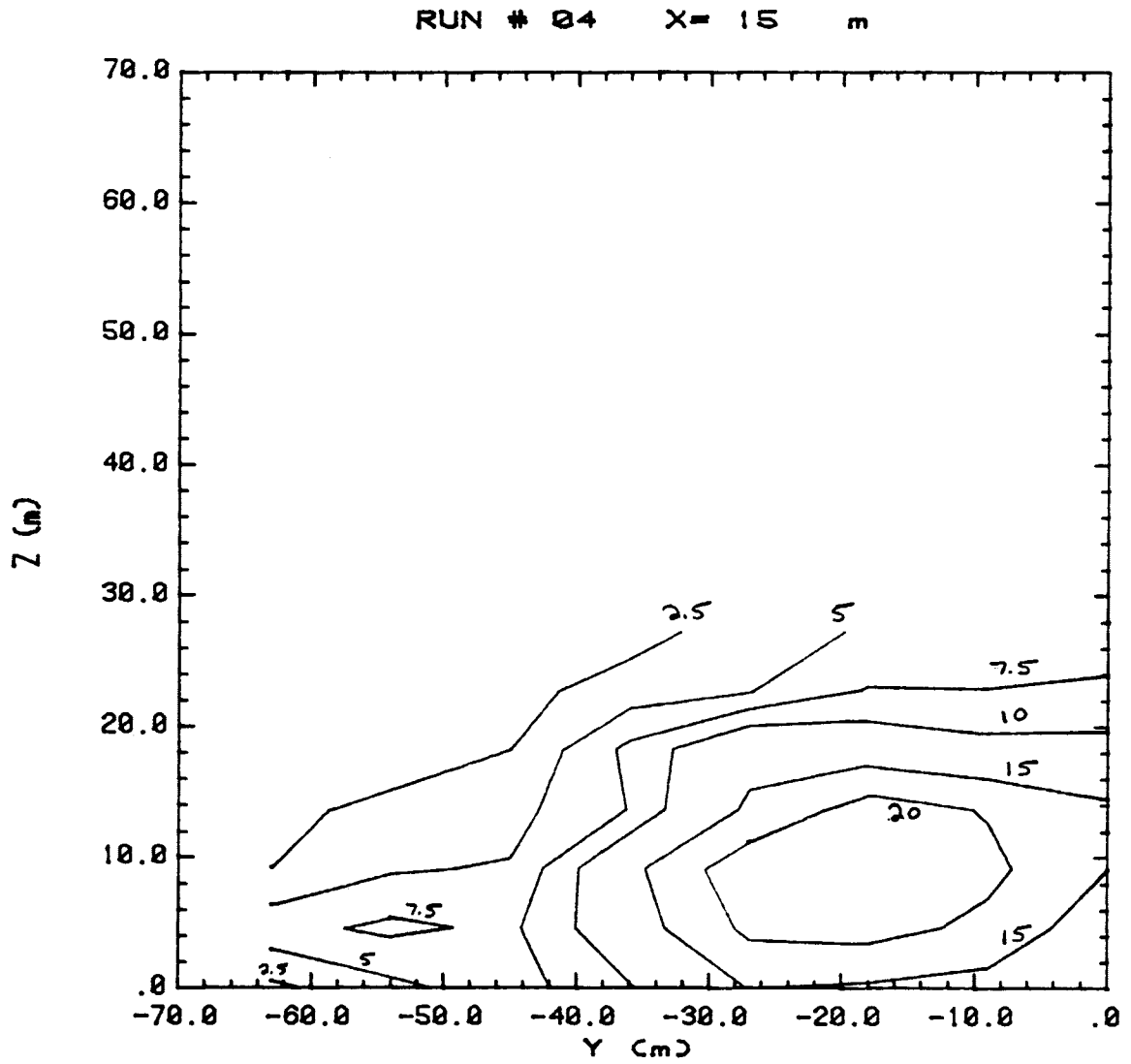


Figure 29. Concentration Contour Plot

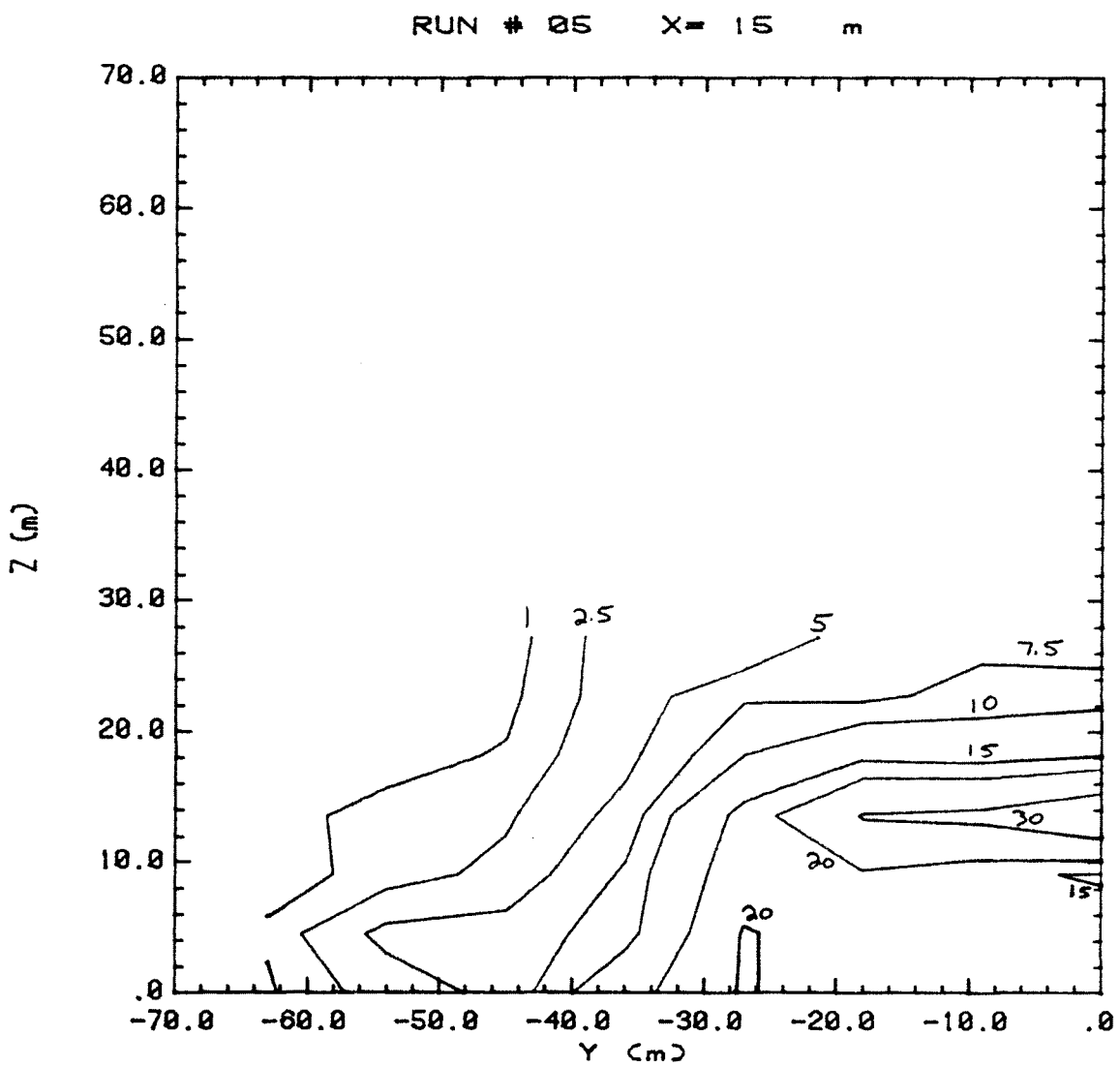


Figure 30. Concentration Contour Plot

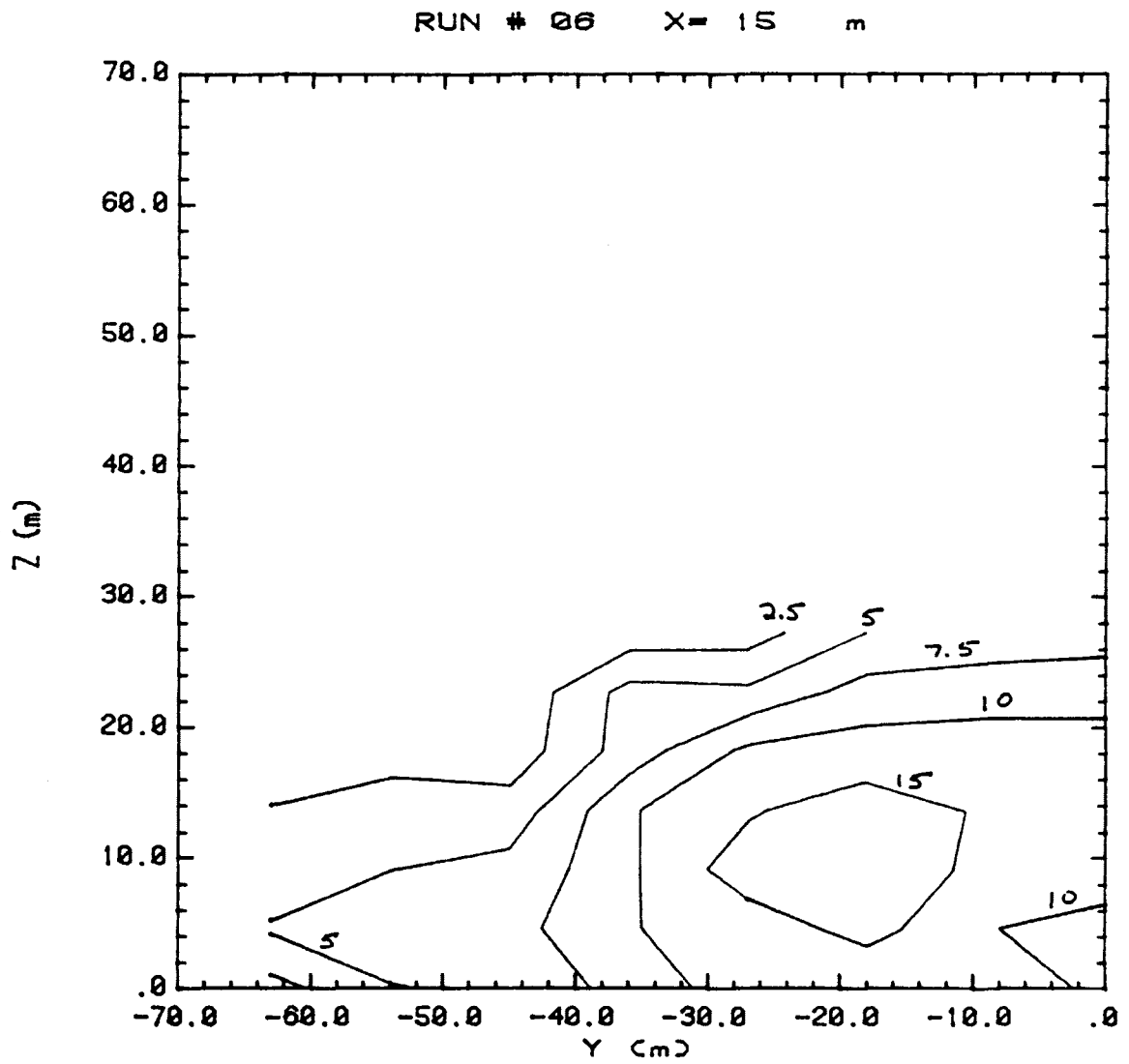


Figure 31. Concentration Contour Plot

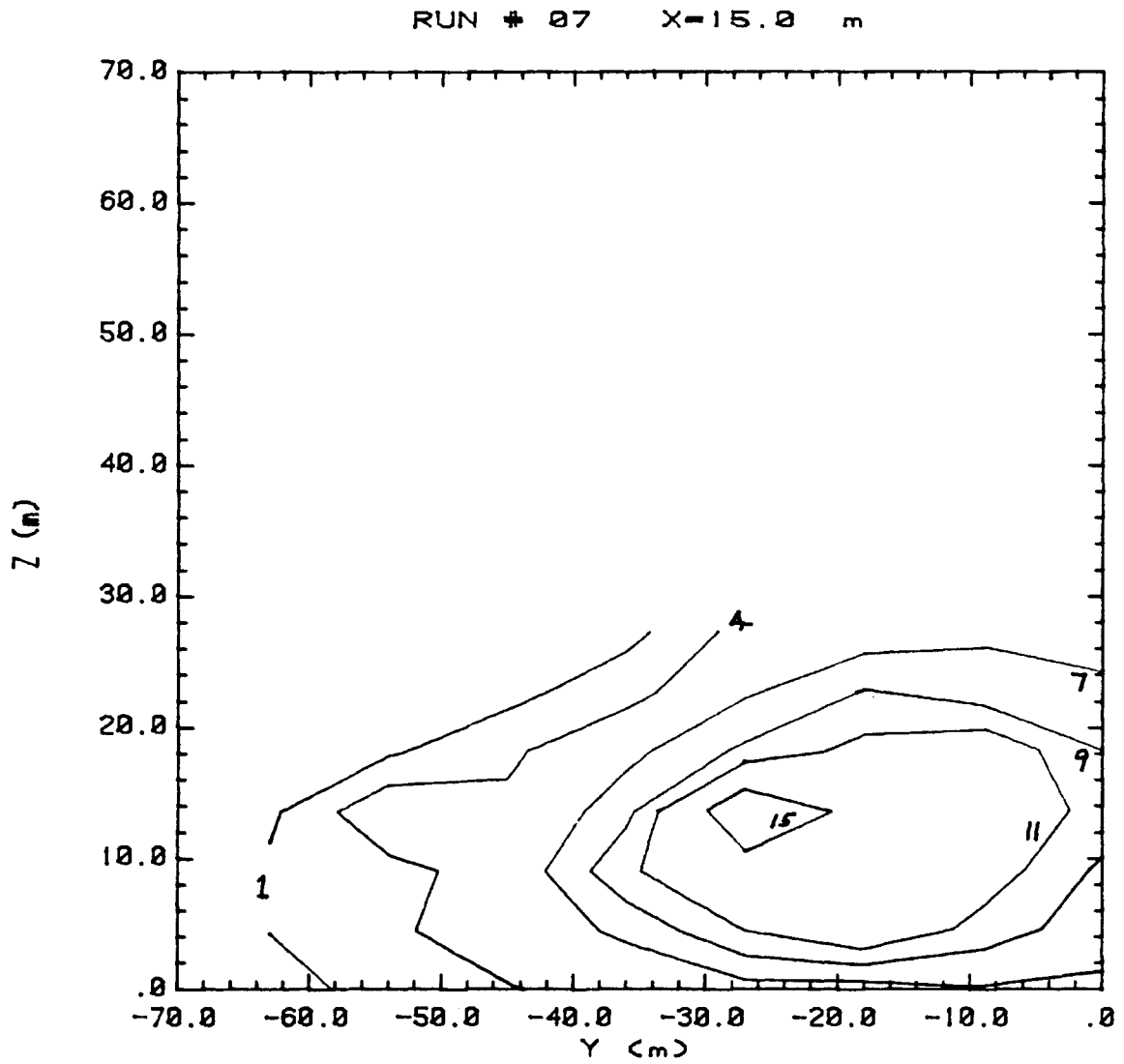


Figure 32. Concentration Contour Plot

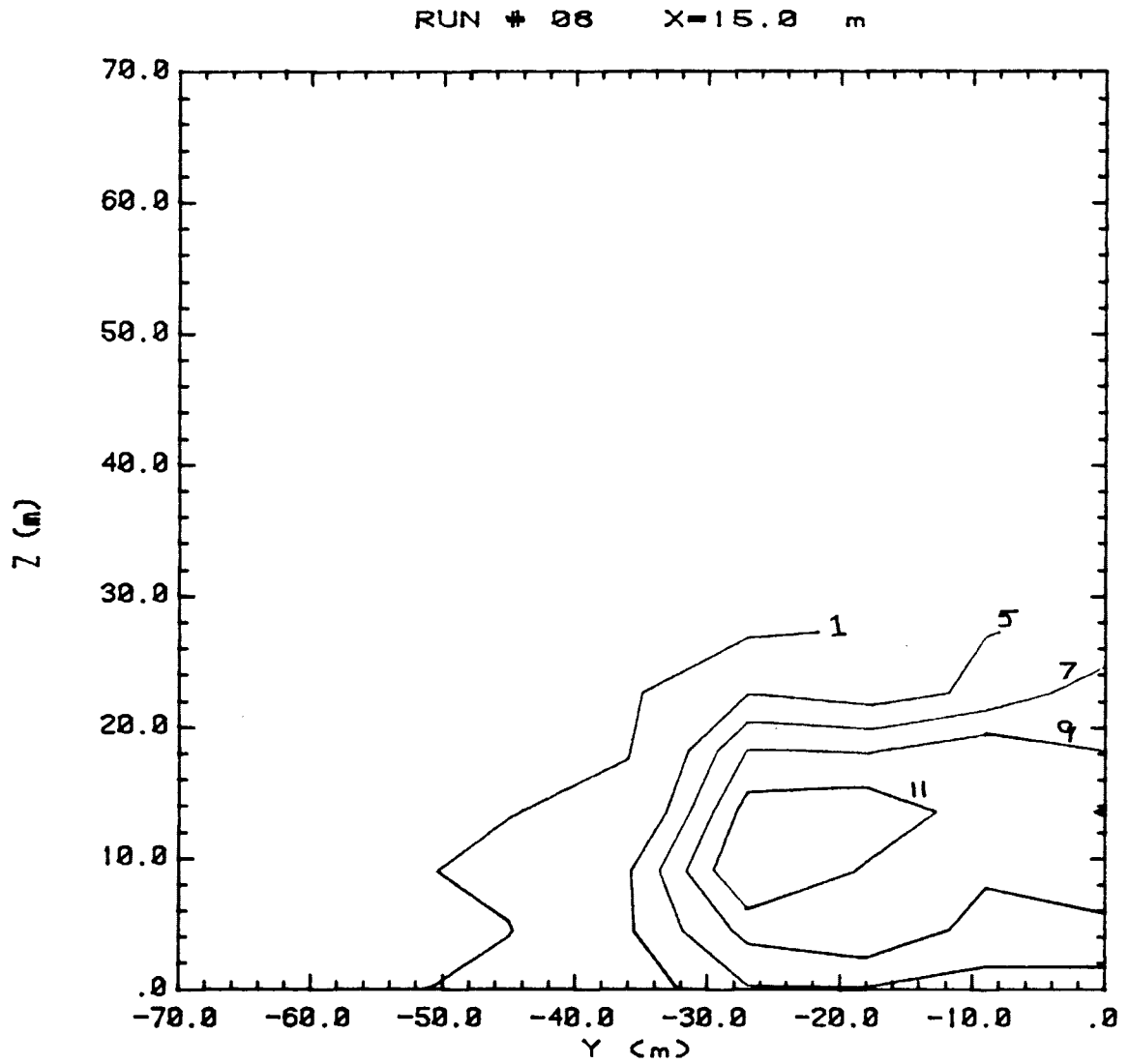


Figure 33. Concentration Contour Plot

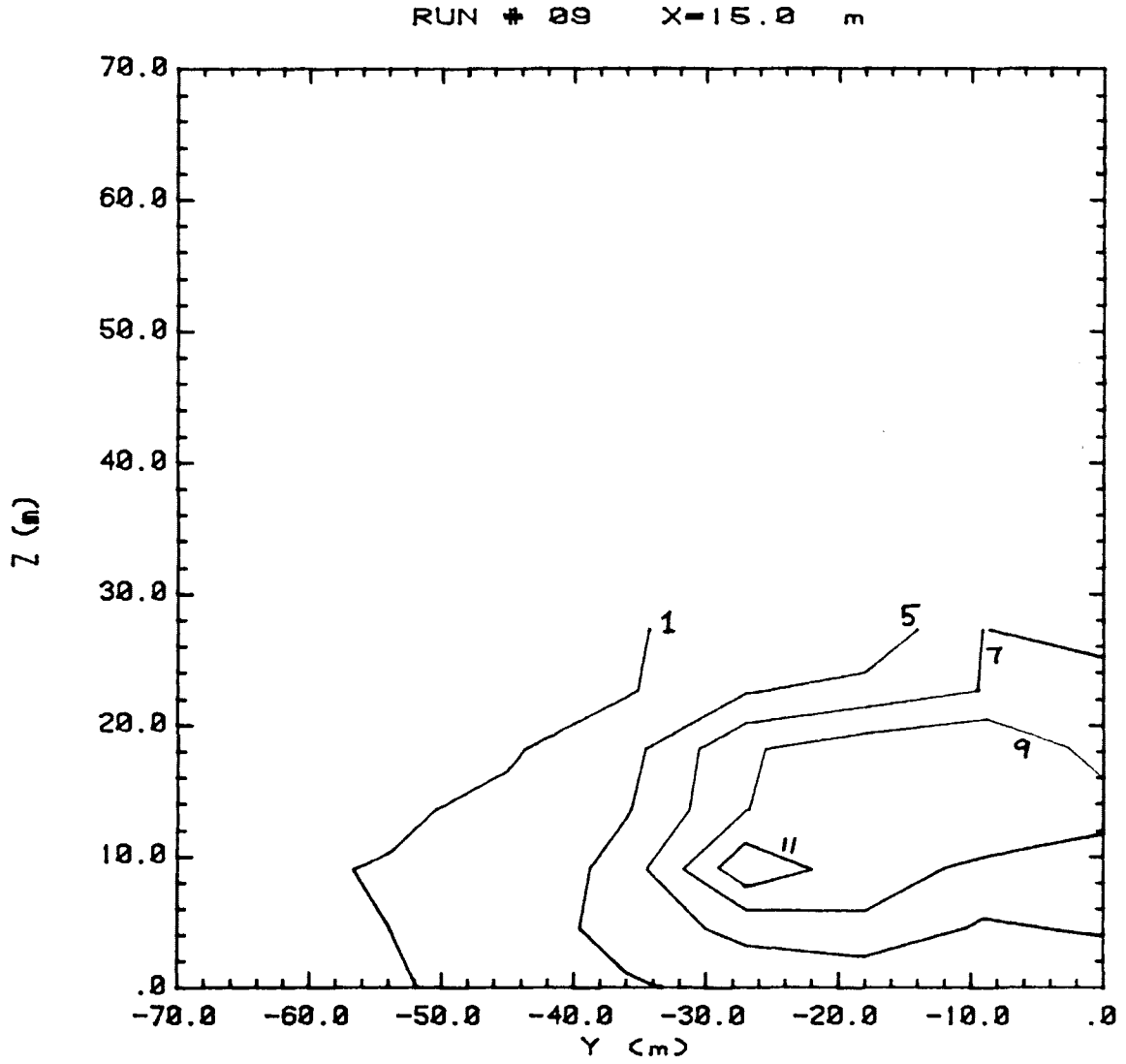


Figure 34. Concentration Contour Plot

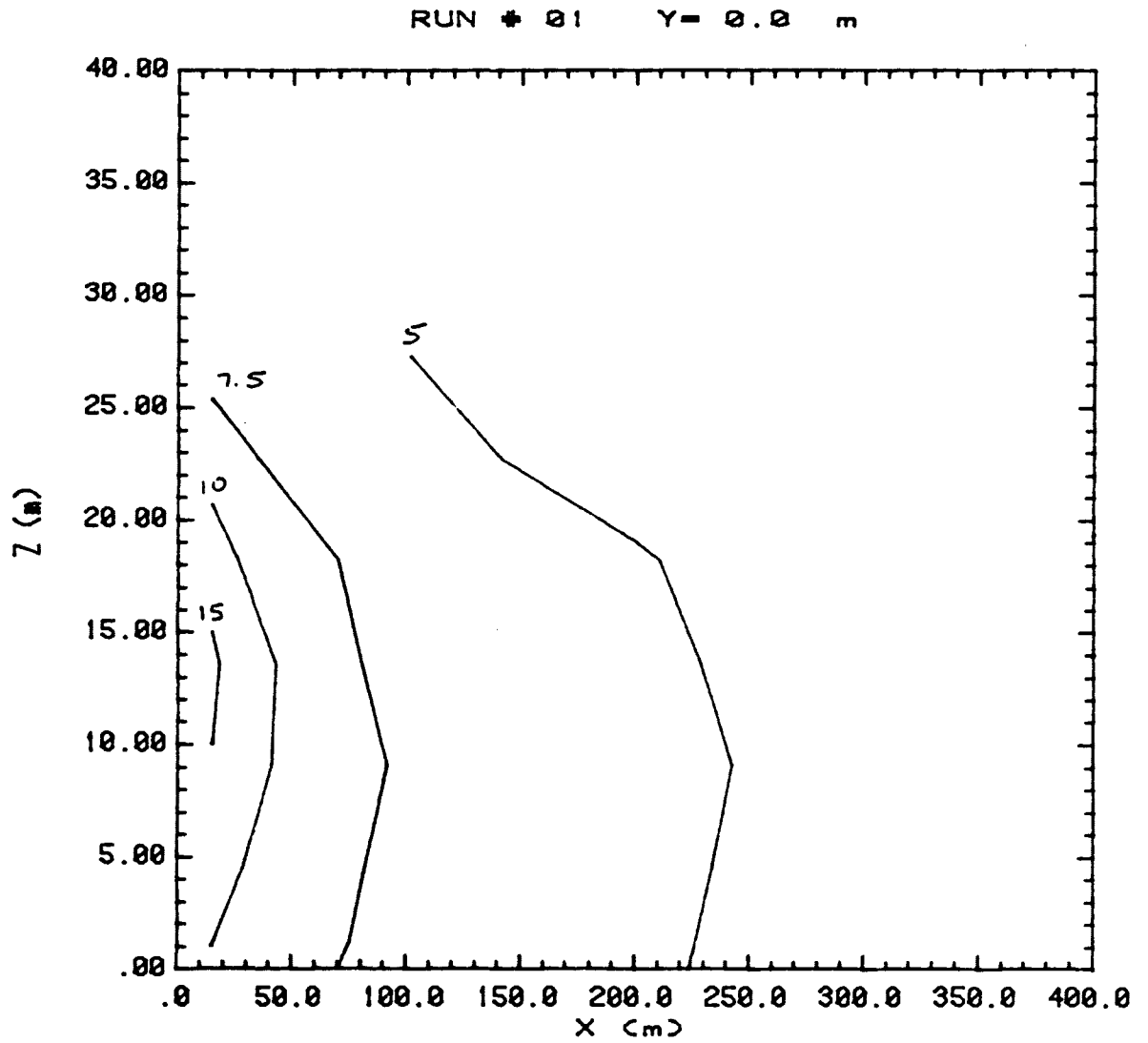


Figure 35. Concentration Contour Plot

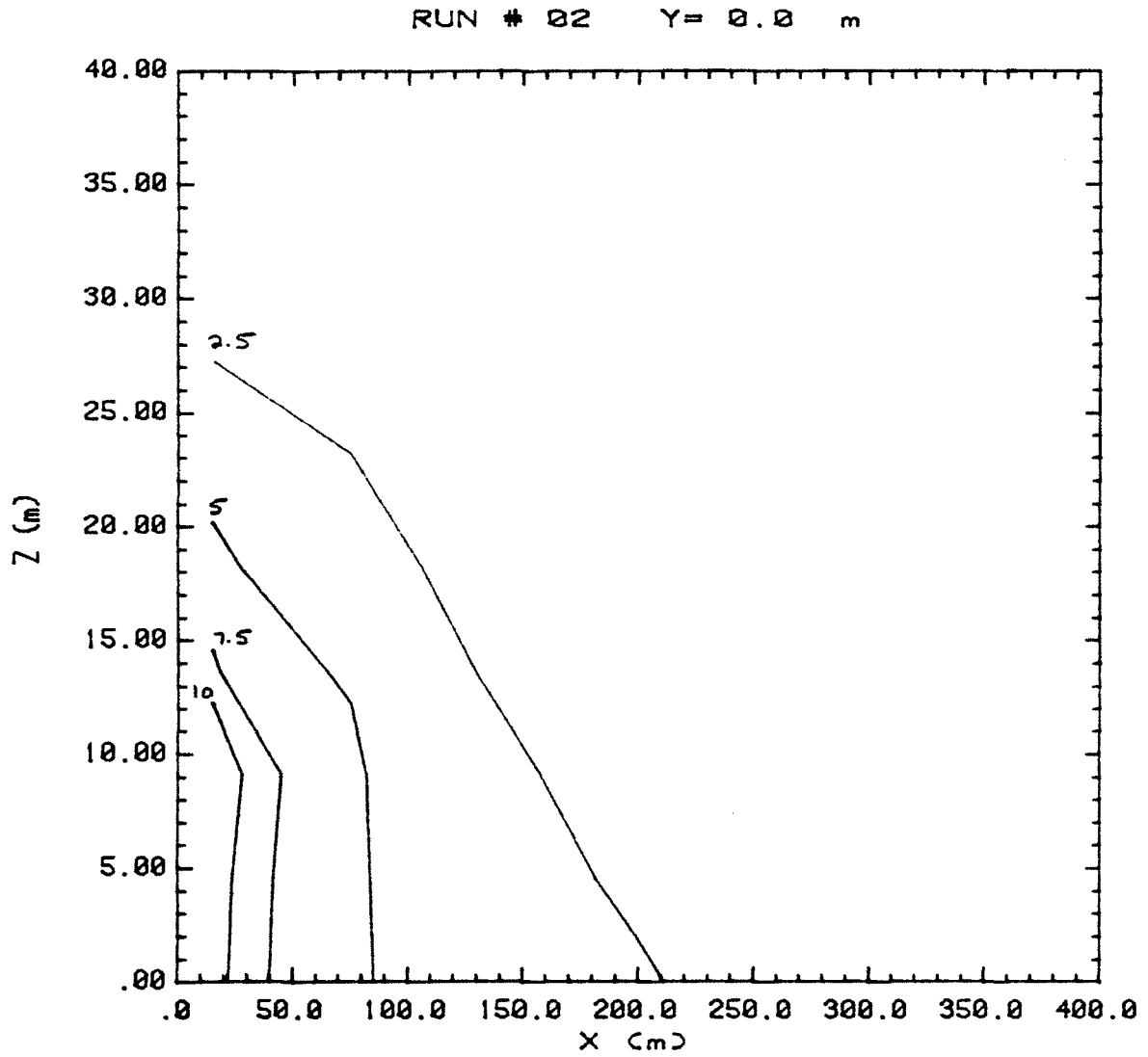


Figure 36. Concentration Contour Plot

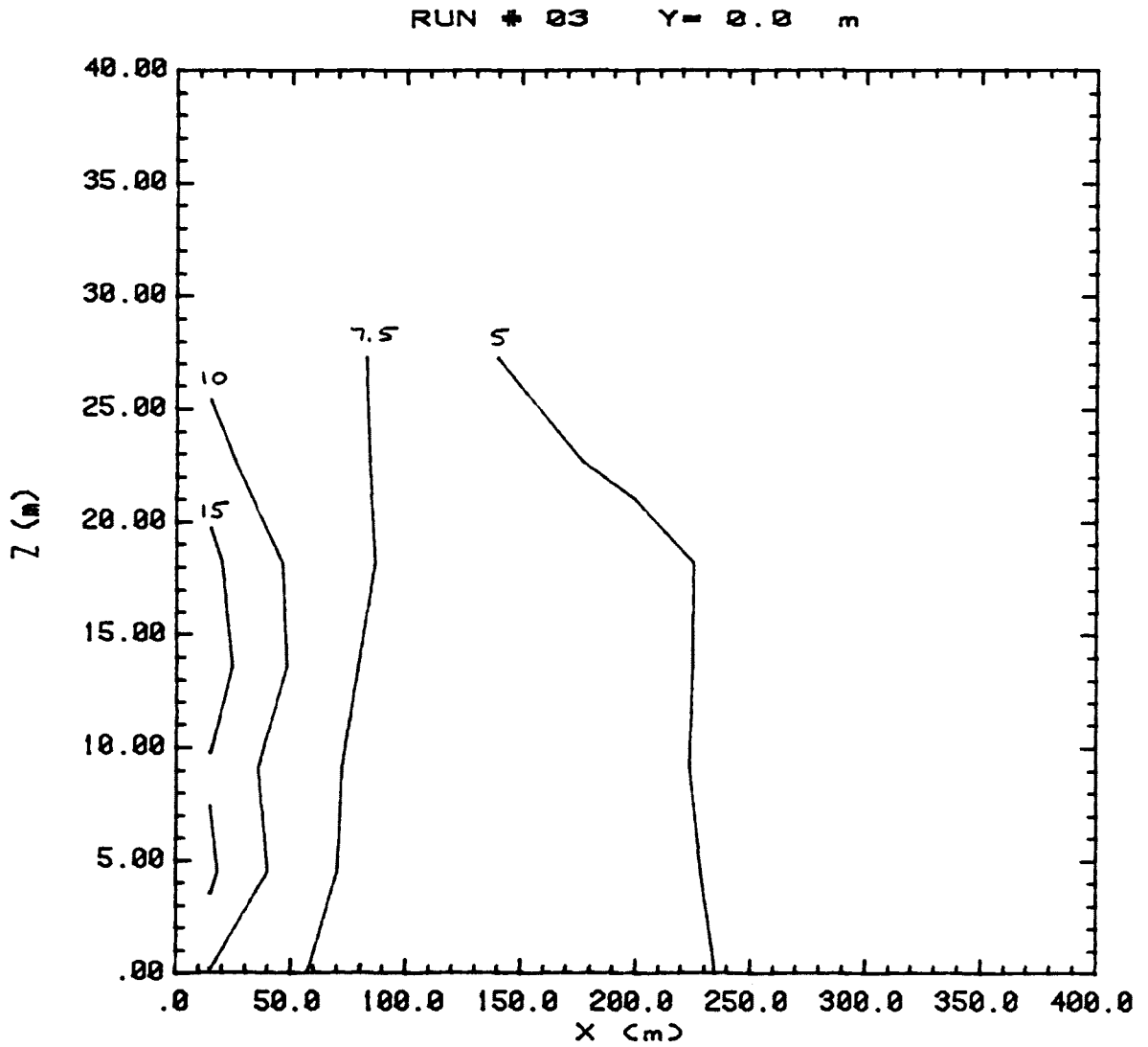


Figure 37. Concentration Contour Plot

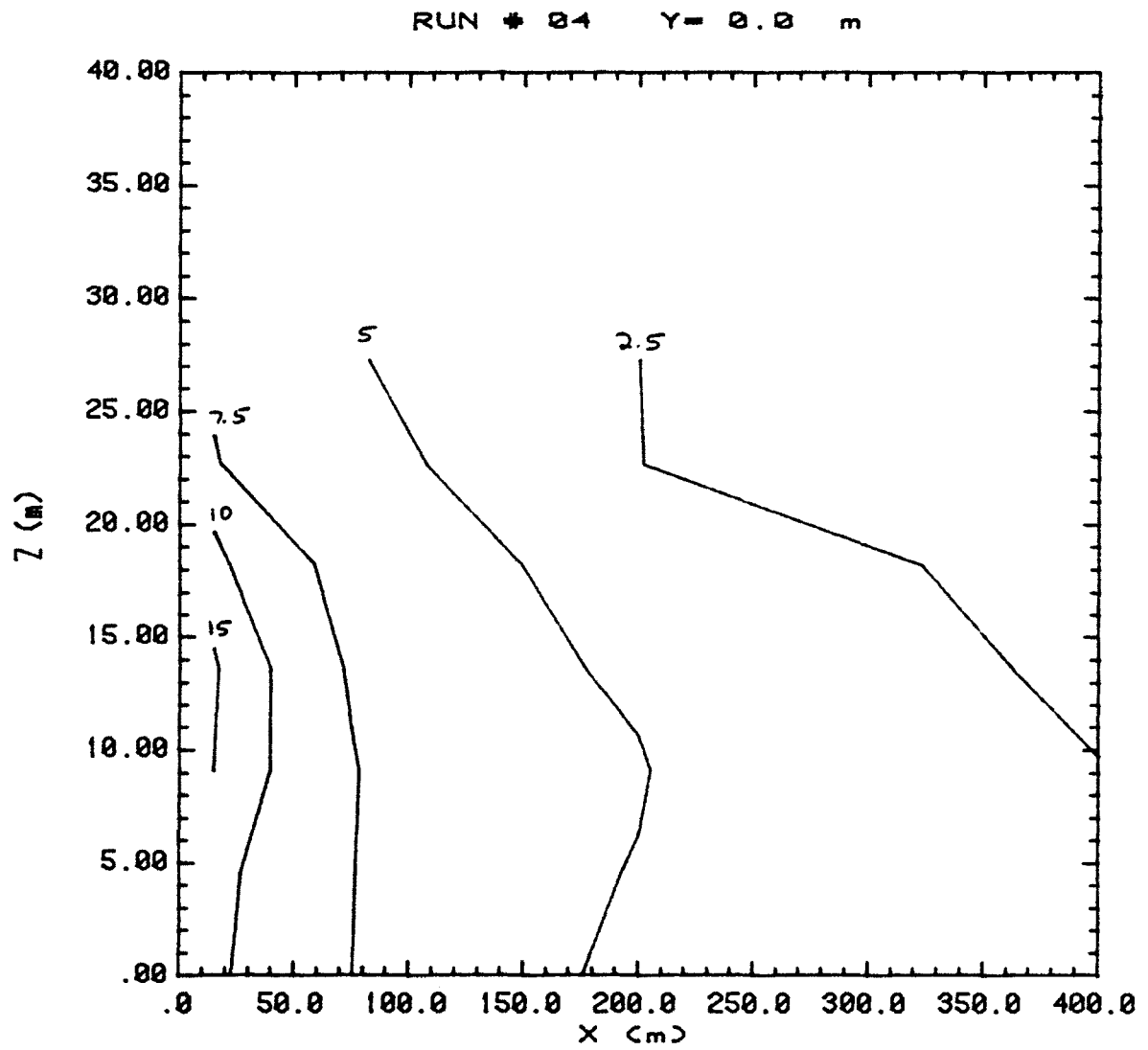


Figure 38. Concentration Contour Plot

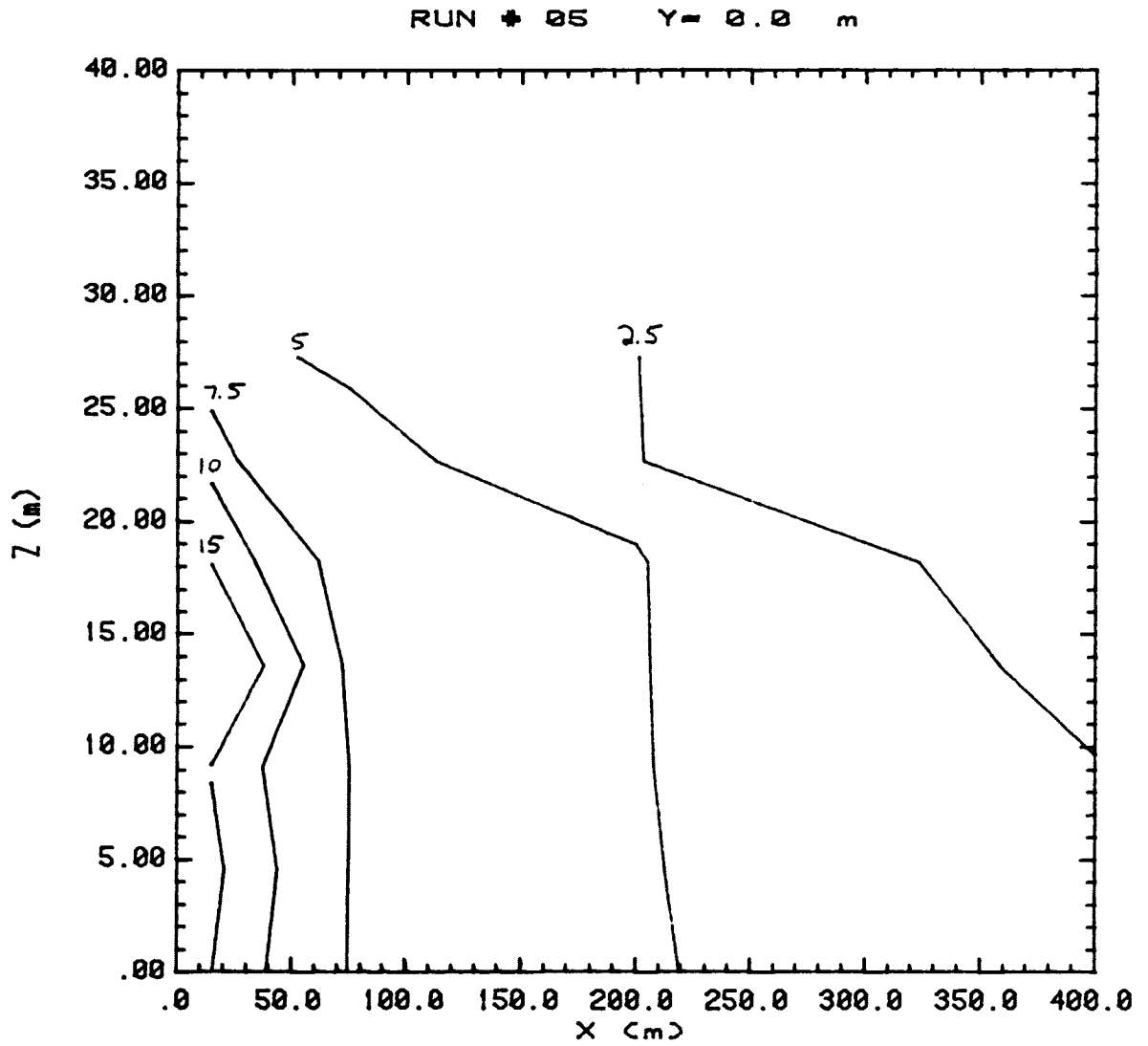


Figure 39. Concentration Contour Plot

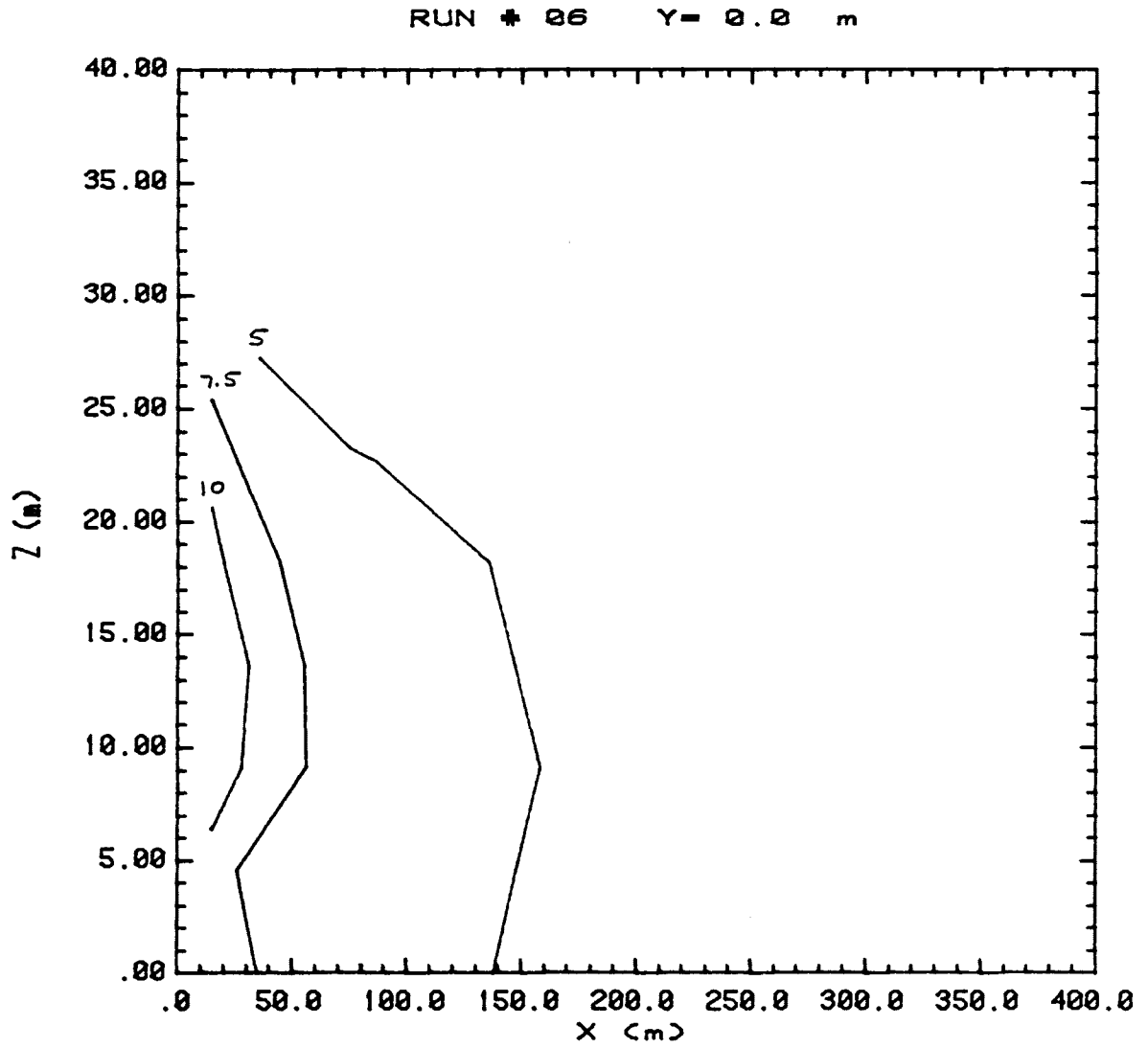


Figure 40. Concentration Contour Plot

RUN # 07 Y=0.0 m

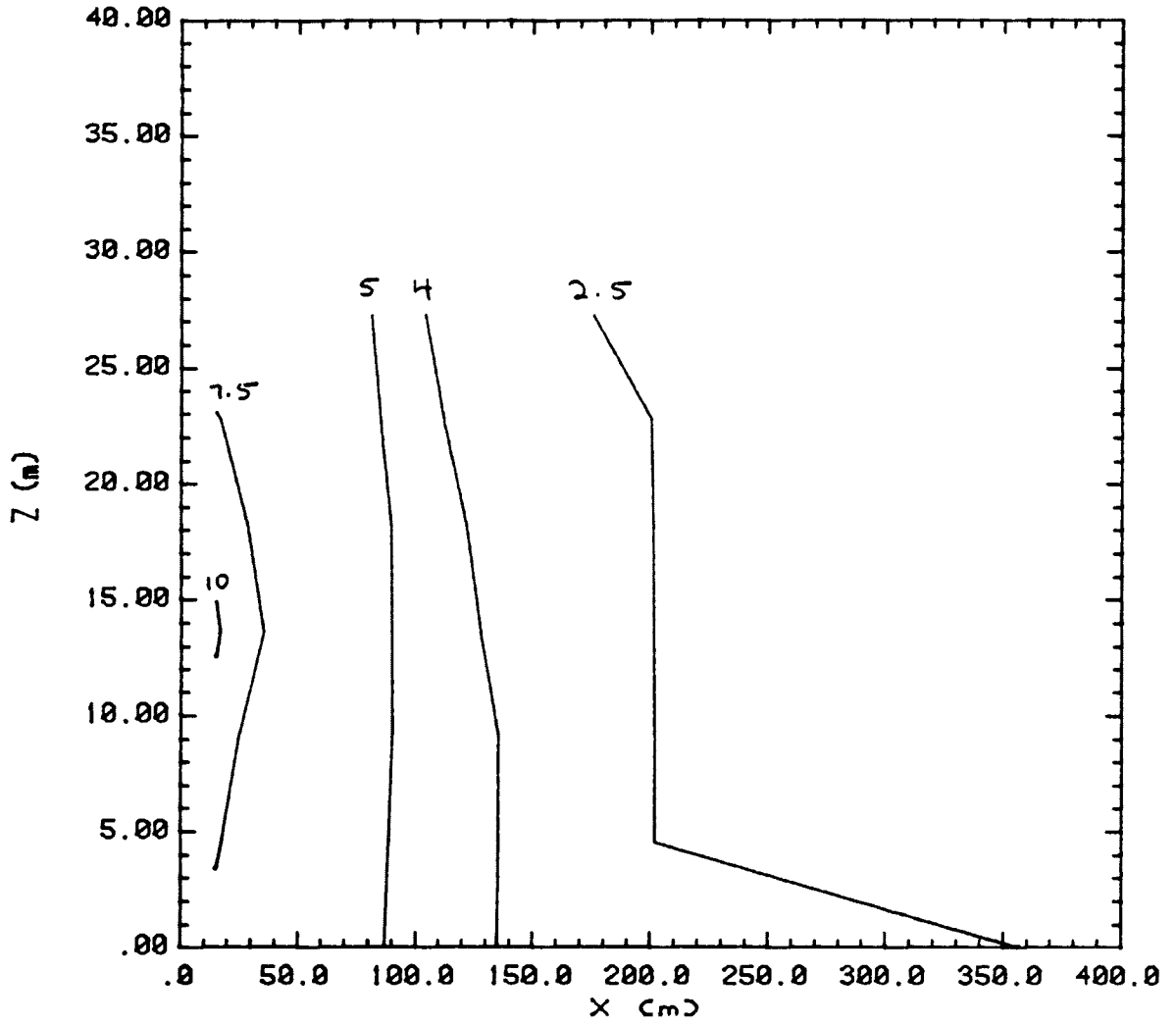


Figure 41. Concentration Contour Plot

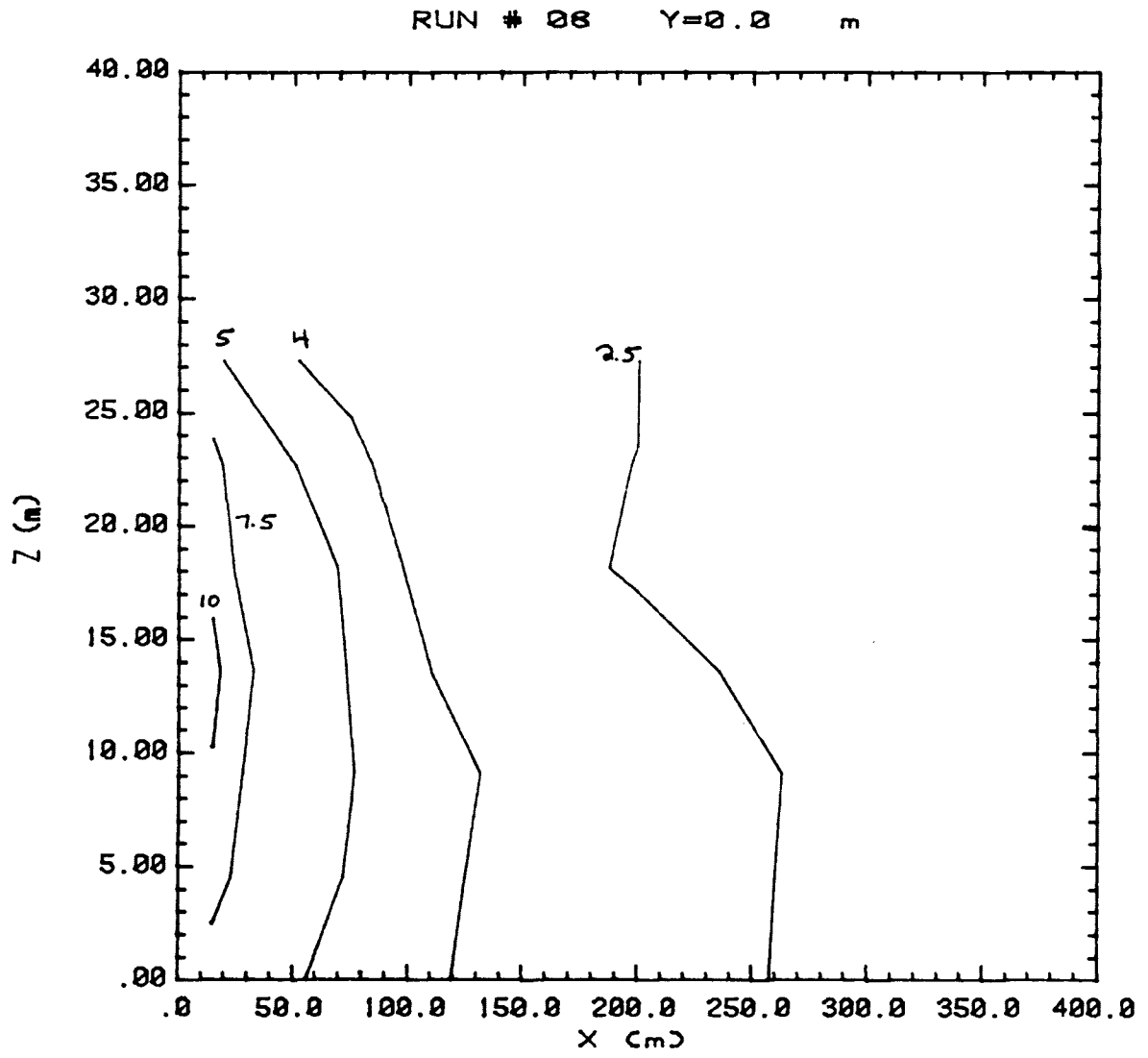


Figure 42. Concentration Contour Plot

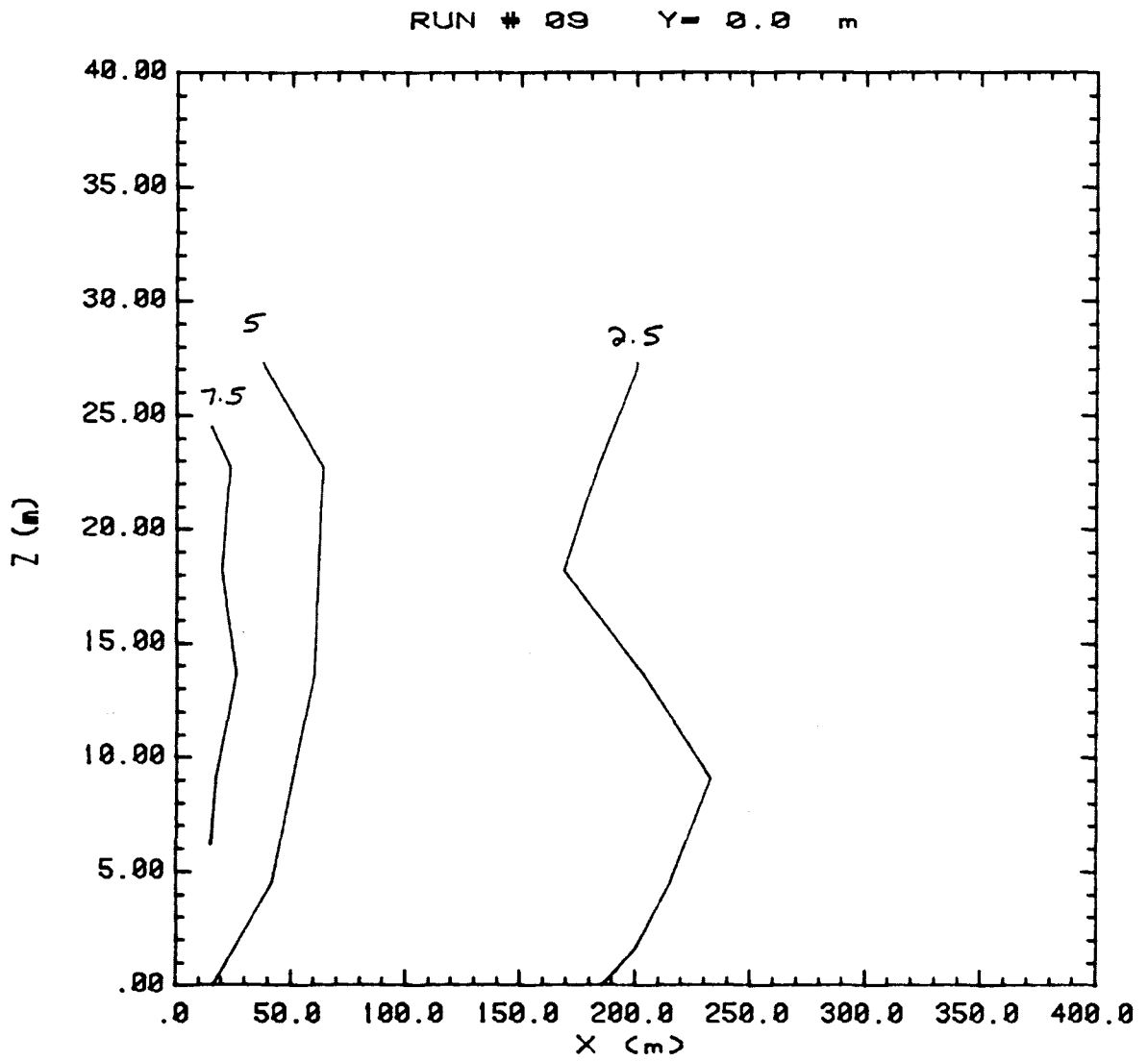


Figure 43. Concentration Contour Plot

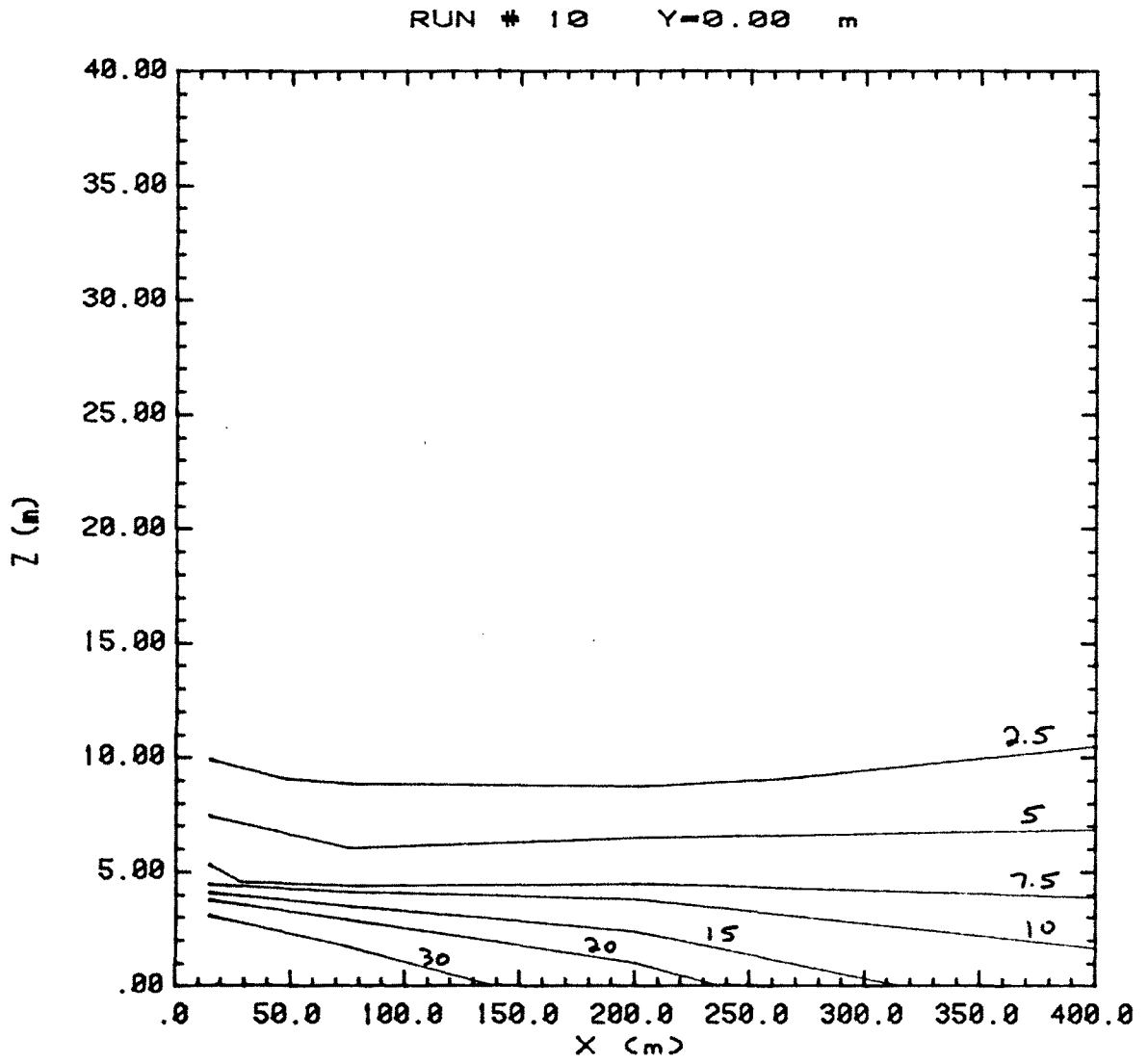


Figure 44. Concentration Contour Plot

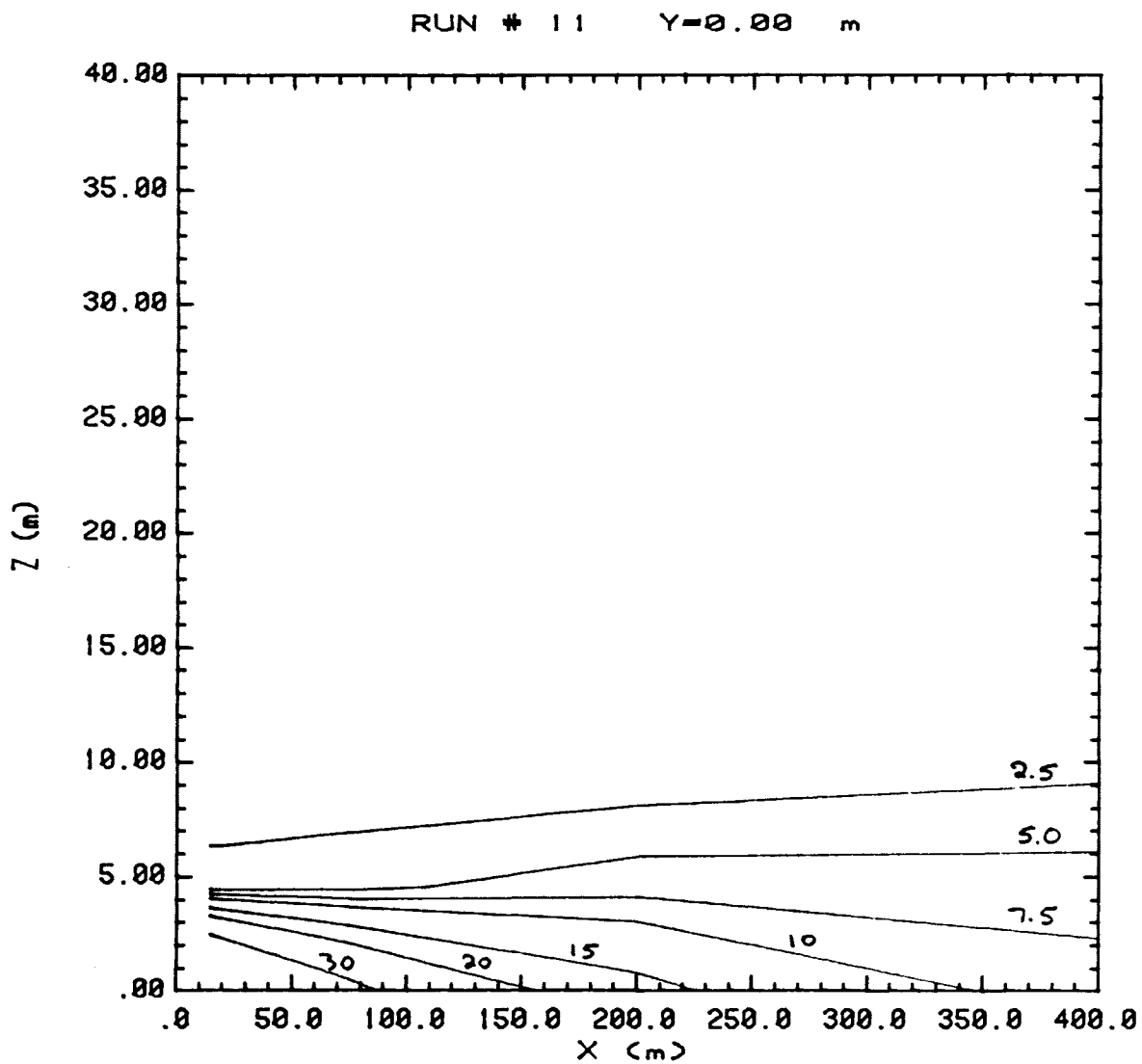


Figure 45. Concentration Contour Plot

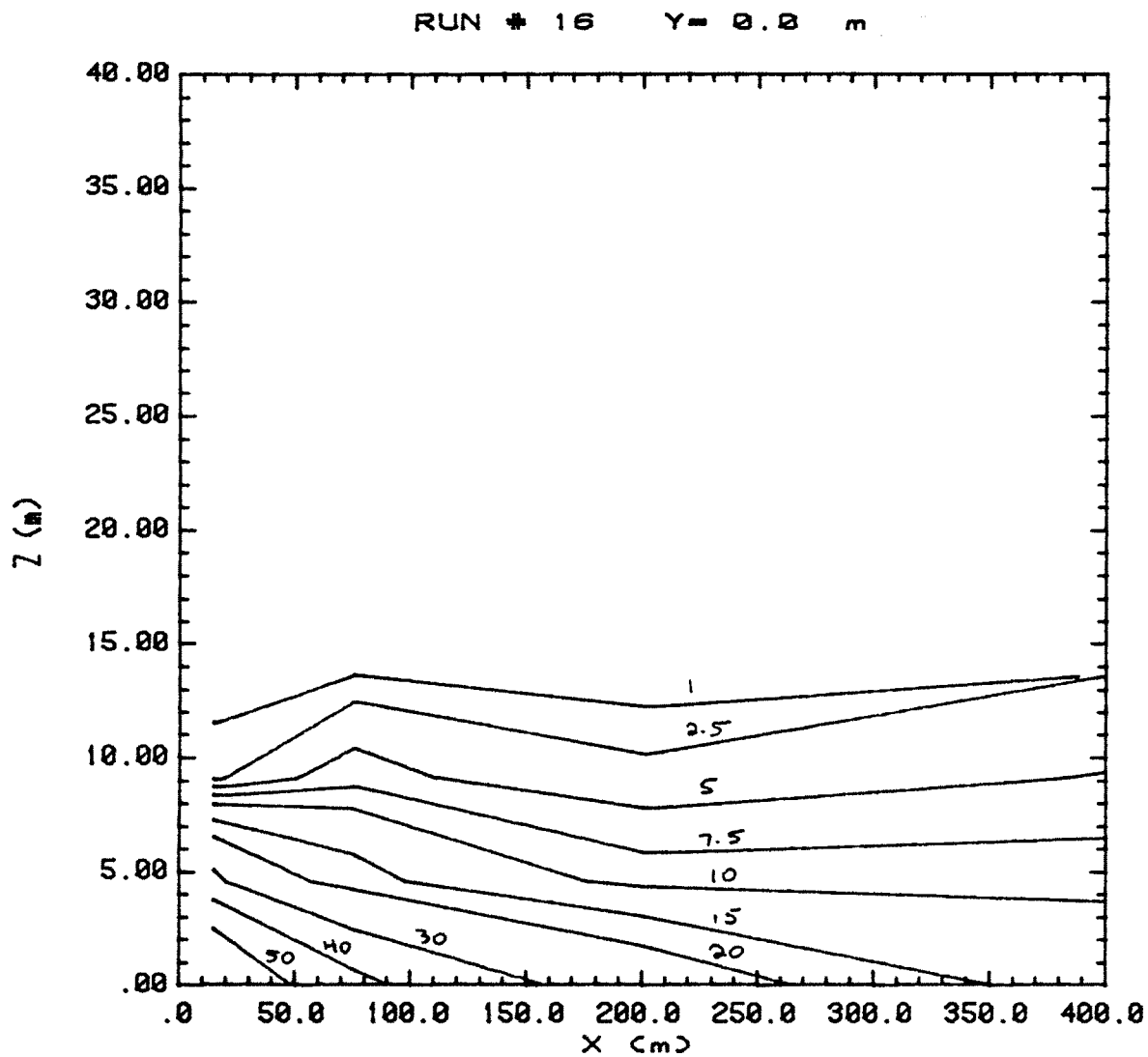


Figure 46. Concentration Contour Plot

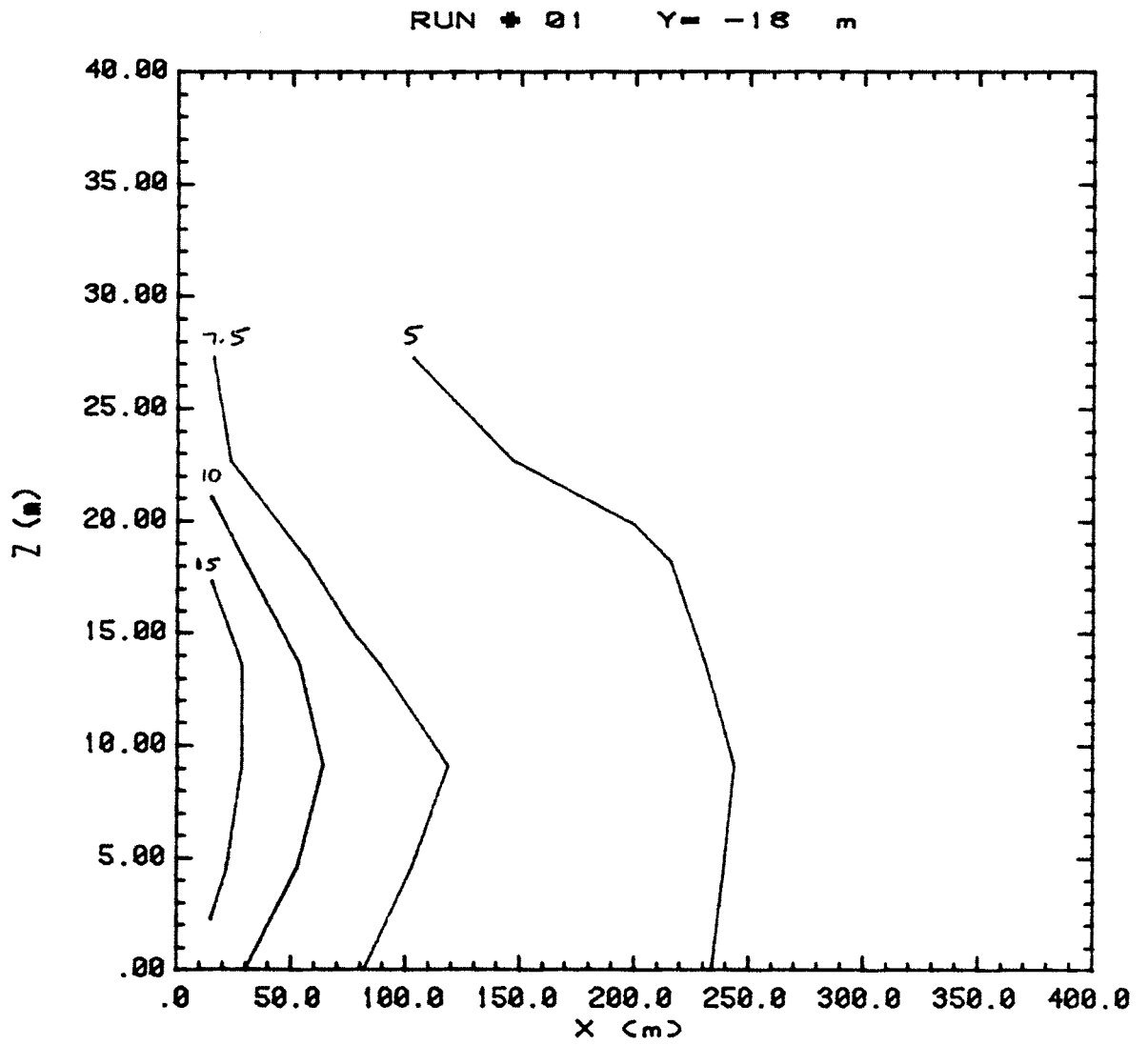


Figure 47. Concentration Contour Plot

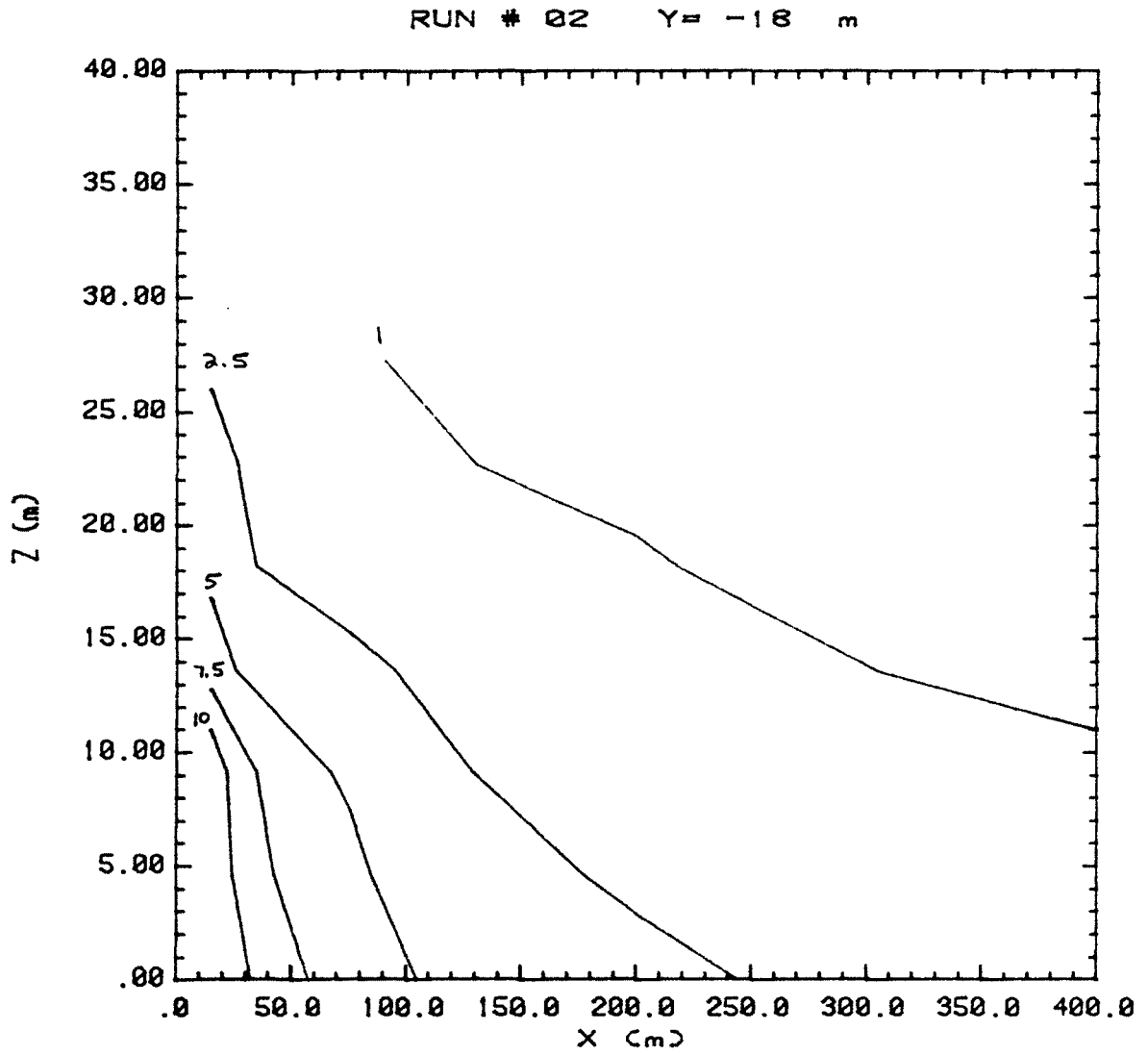


Figure 48. Concentration Contour Plot

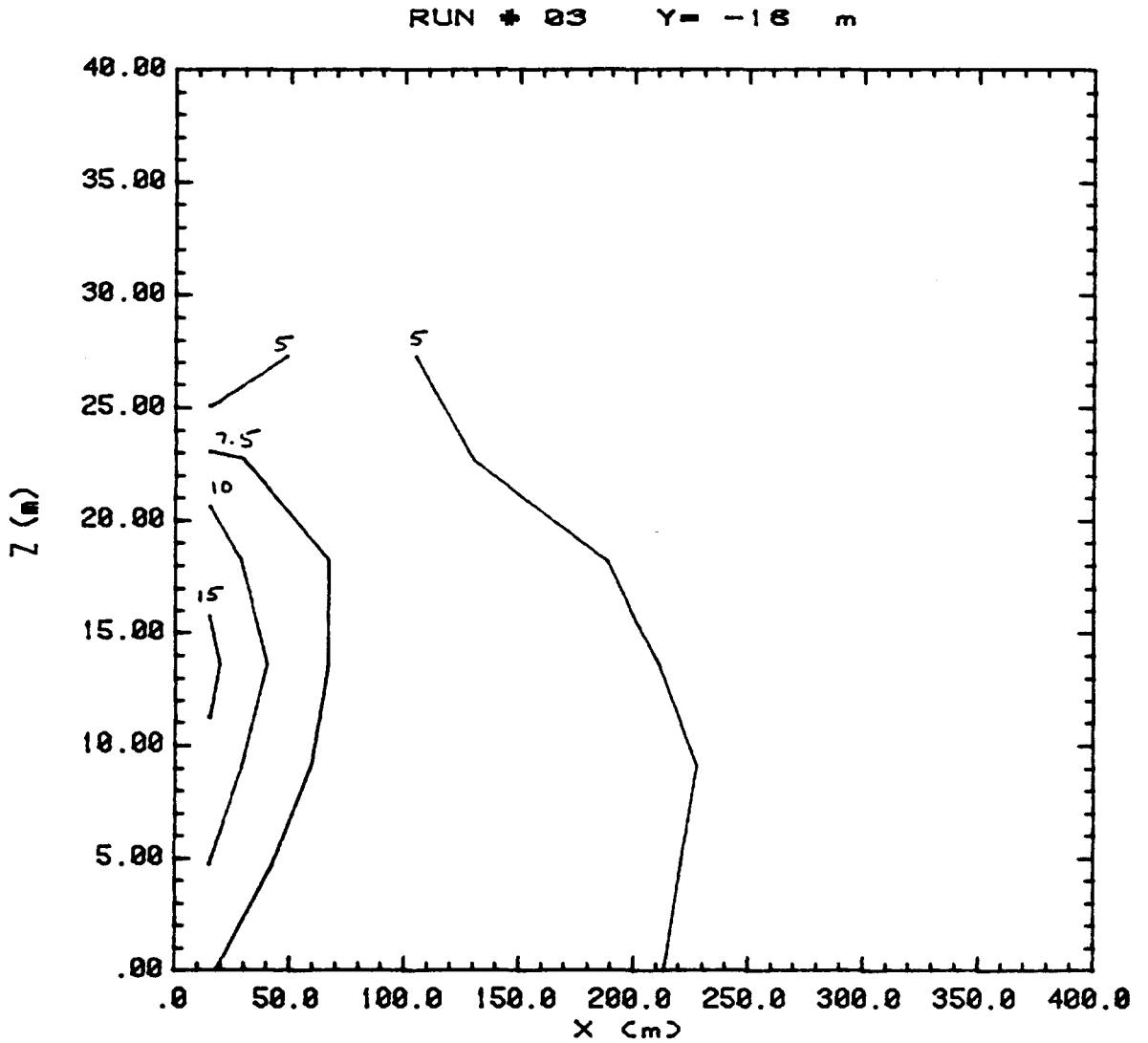


Figure 49. Concentration Contour Plot

RUN # 04 Y = -18 m

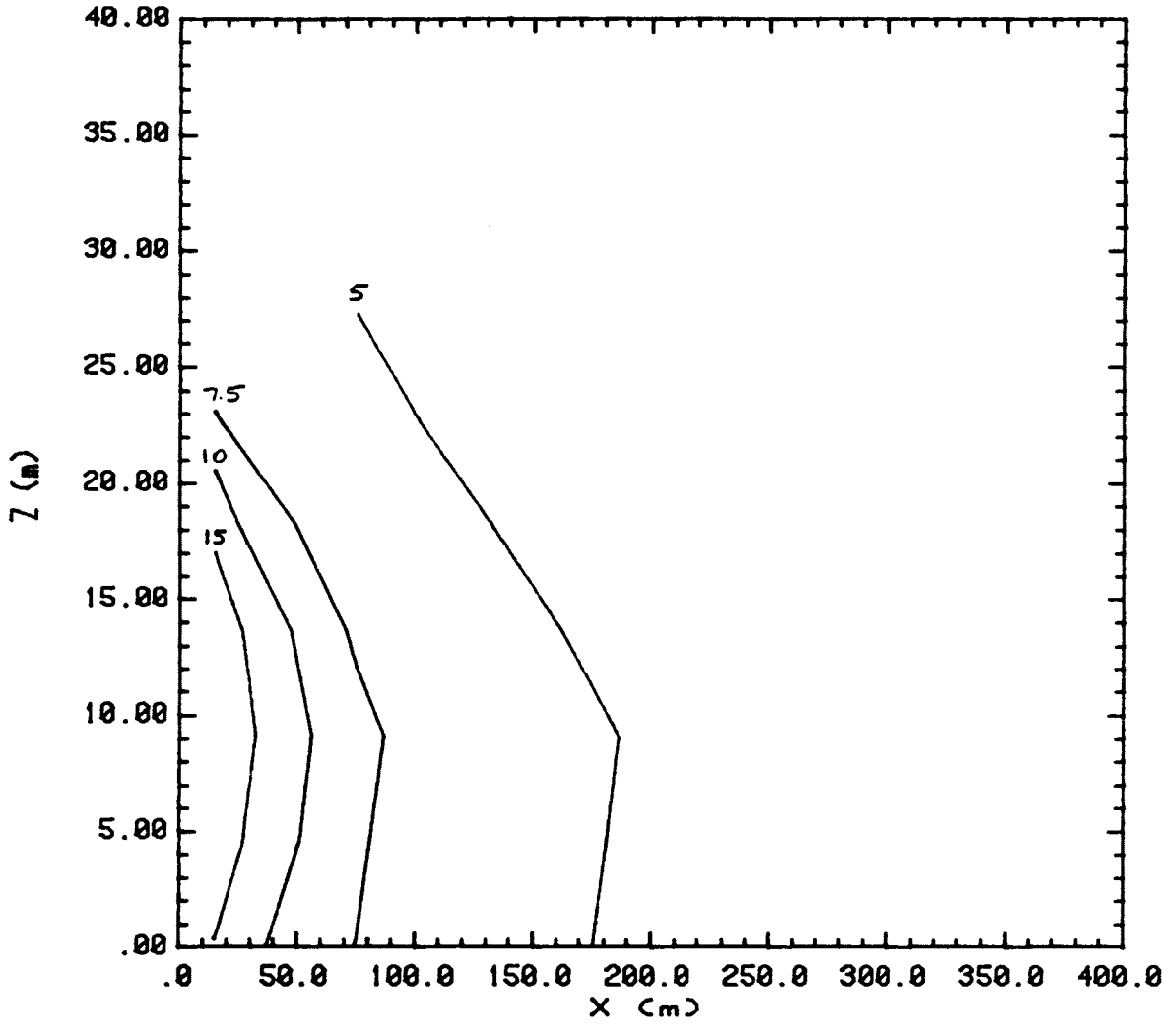


Figure 50. Concentration Contour Plot

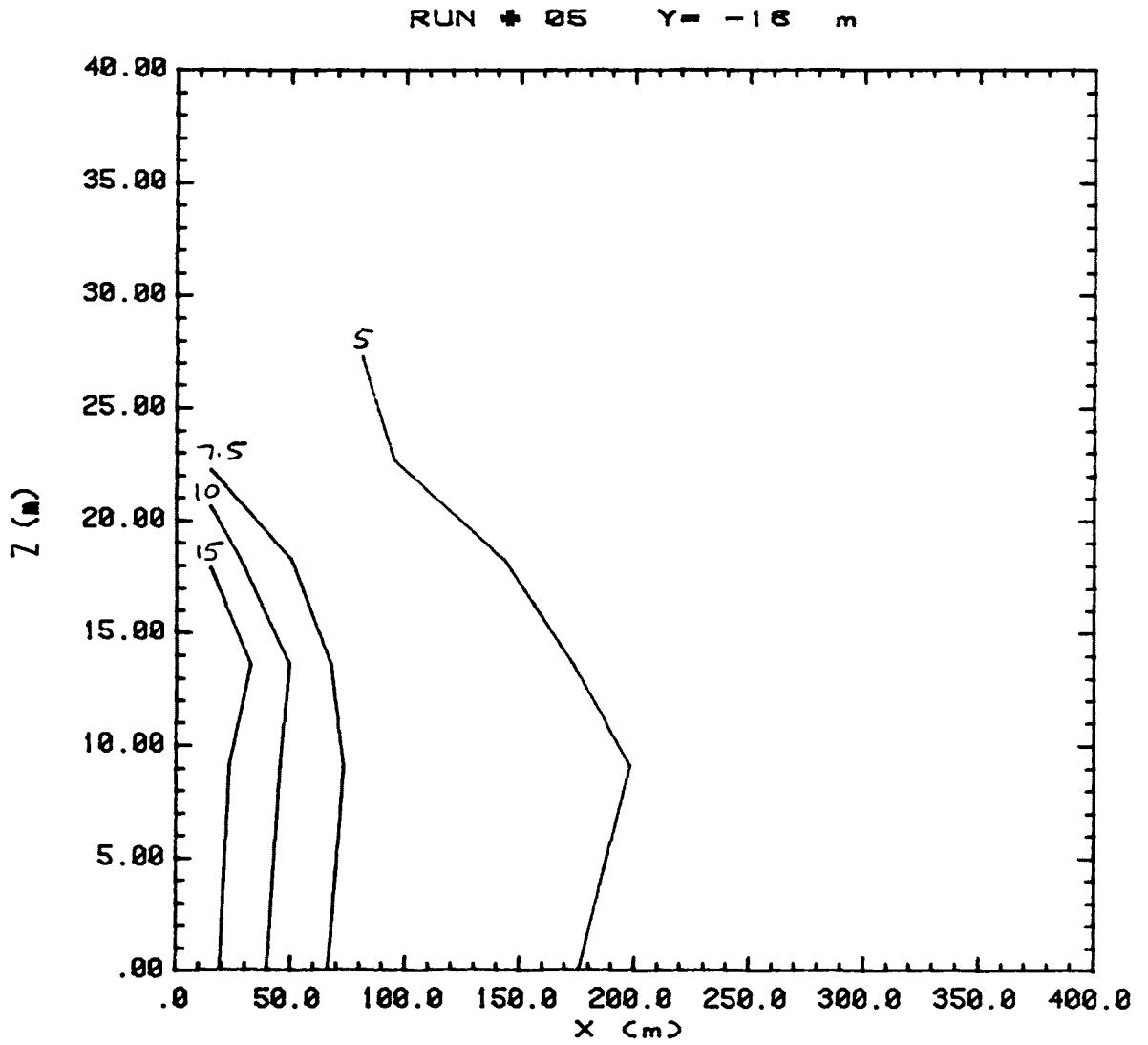


Figure 51. Concentration Contour Plot

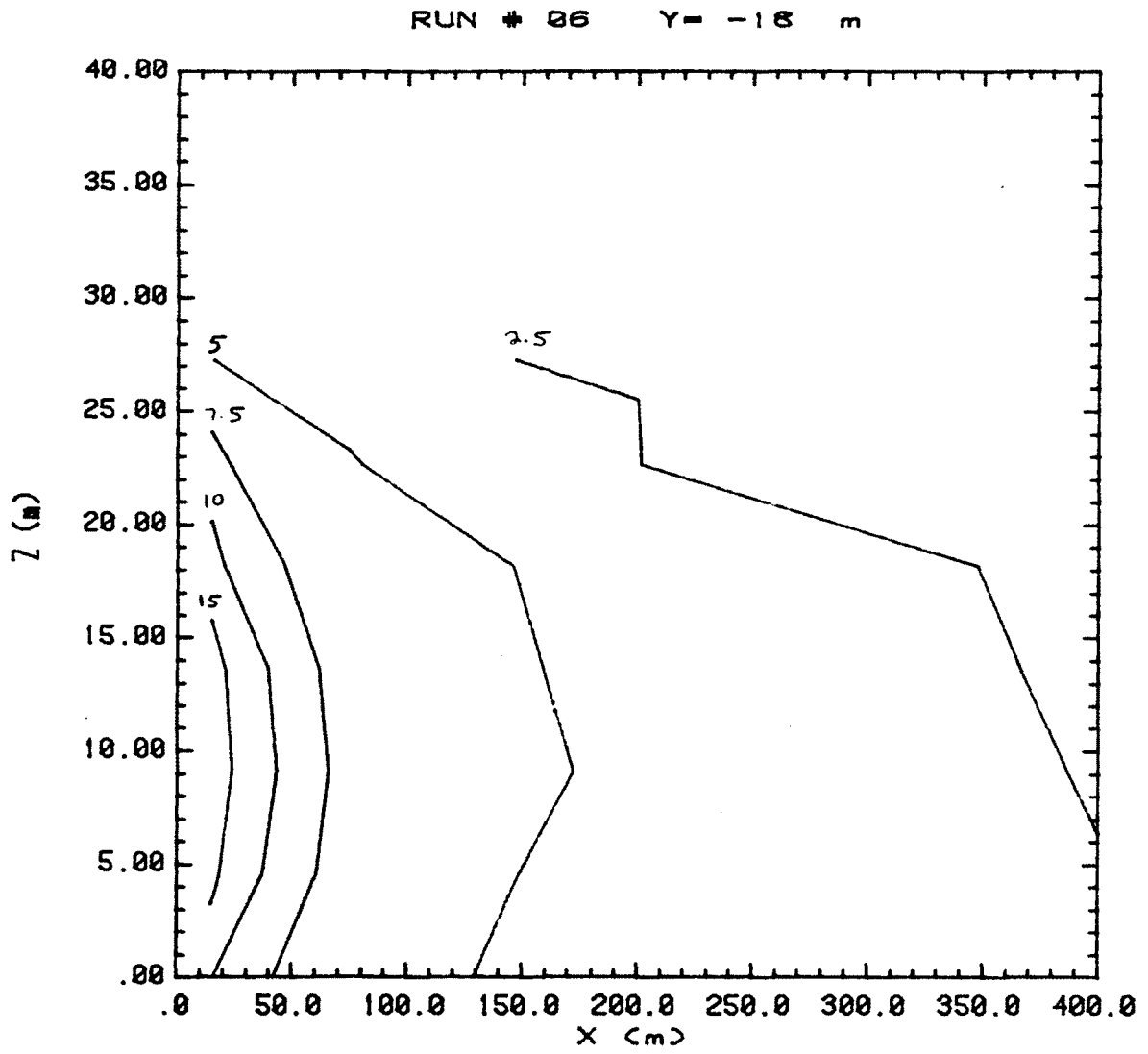


Figure 52. Concentration Contour Plot

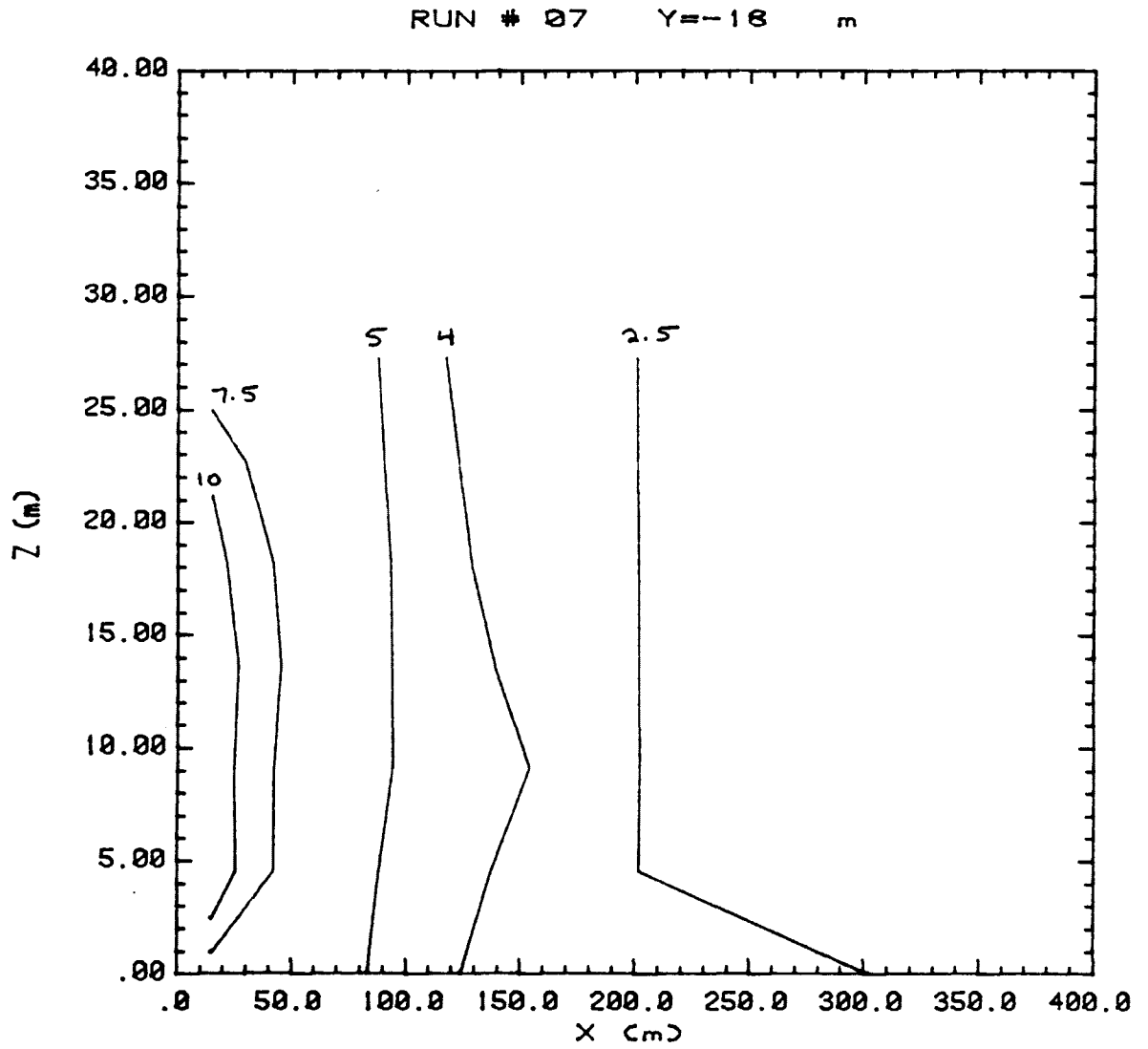


Figure 53. Concentration Contour Plot

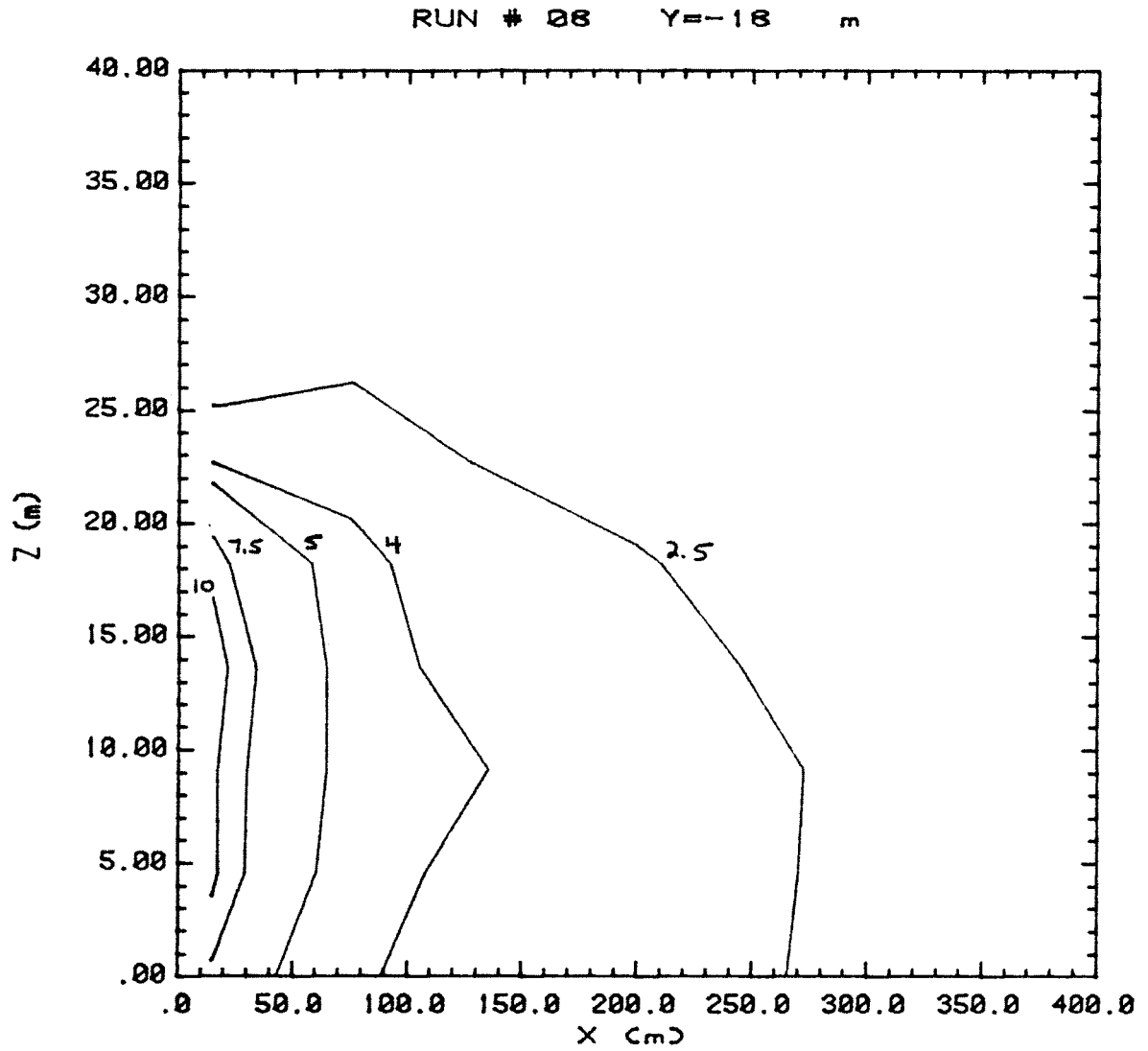


Figure 54. Concentration Contour Plot

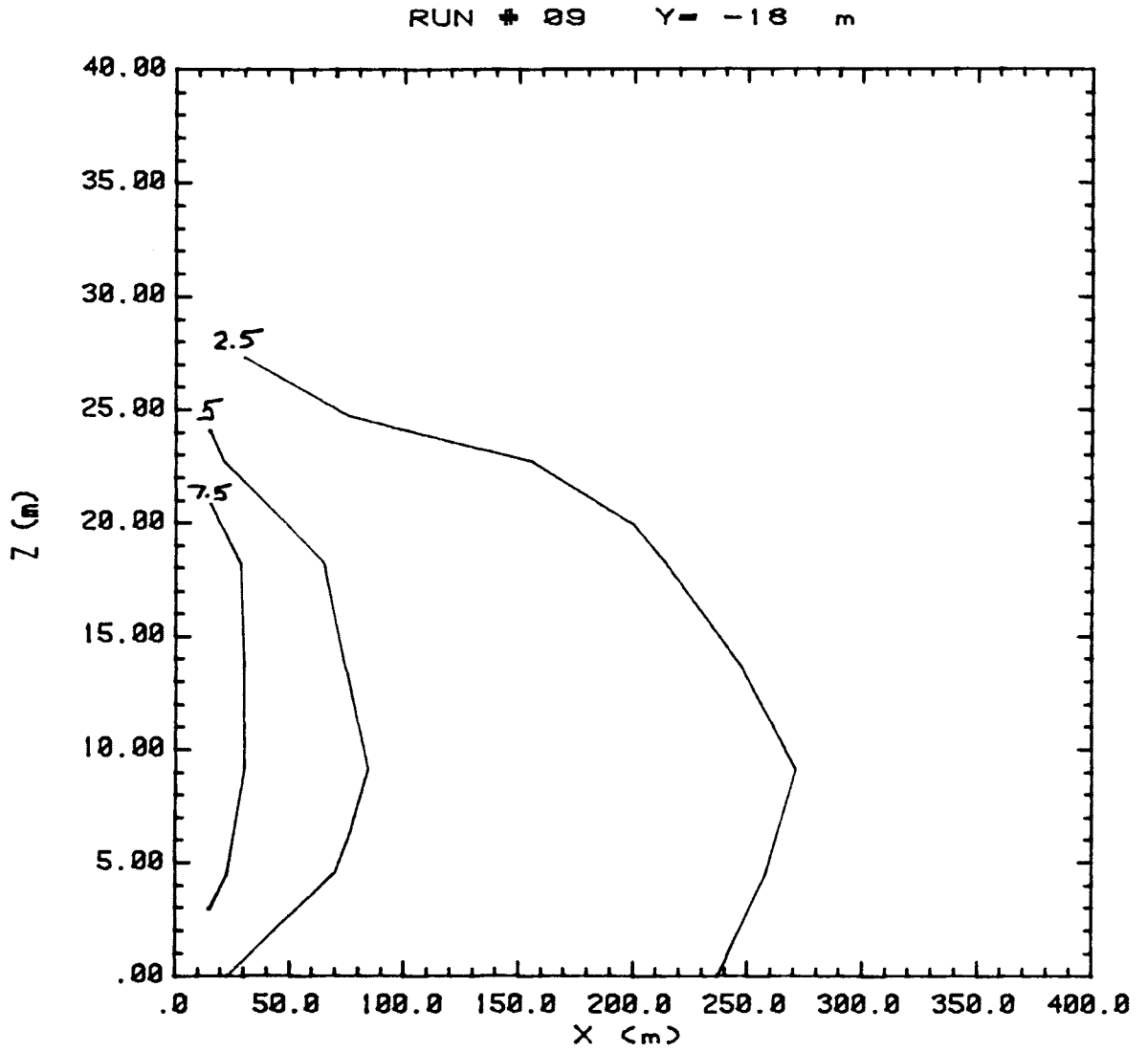


Figure 55. Concentration Contour Plot

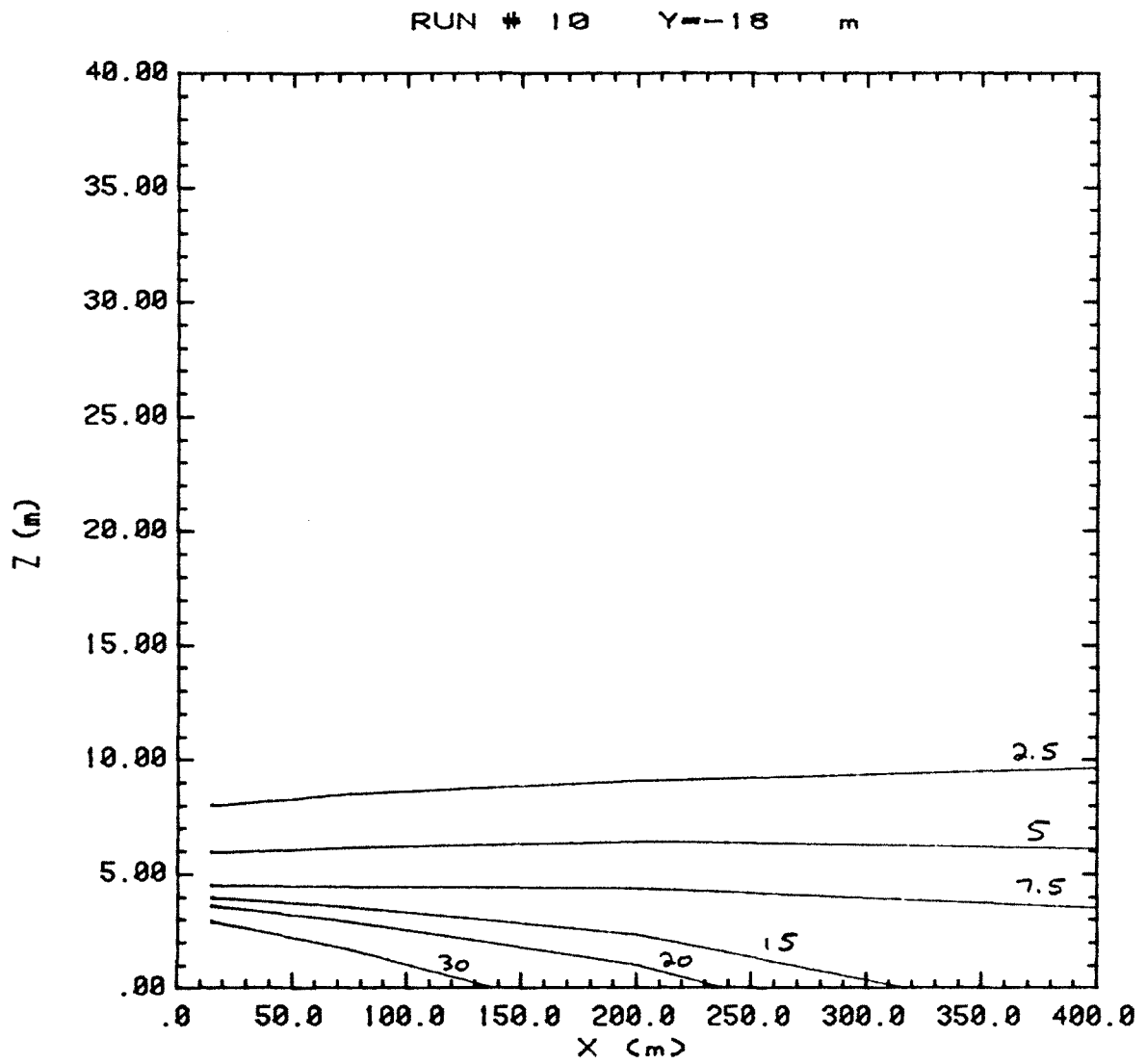


Figure 56. Concentration Contour Plot

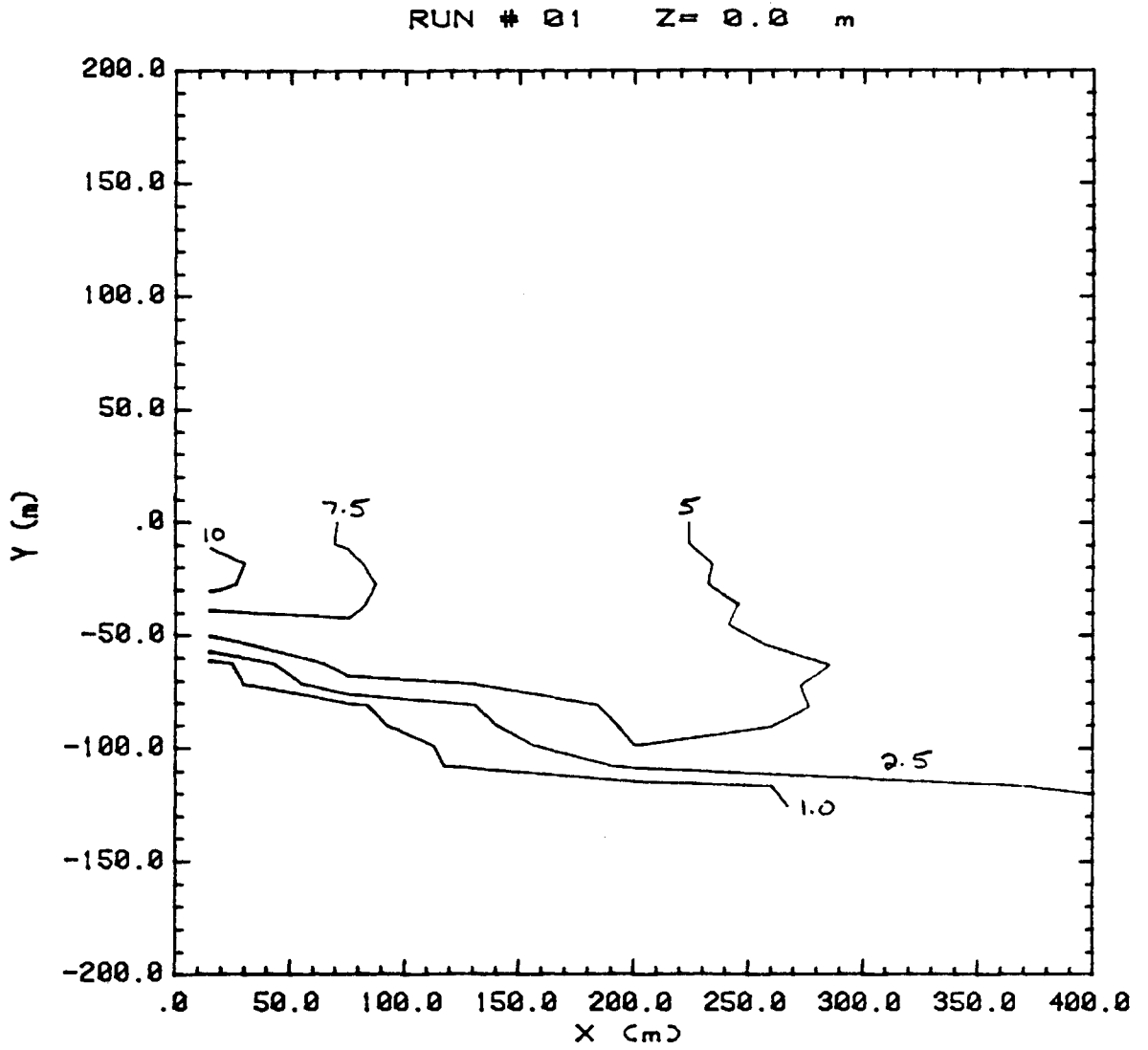


Figure 57. Concentration Contour Plot

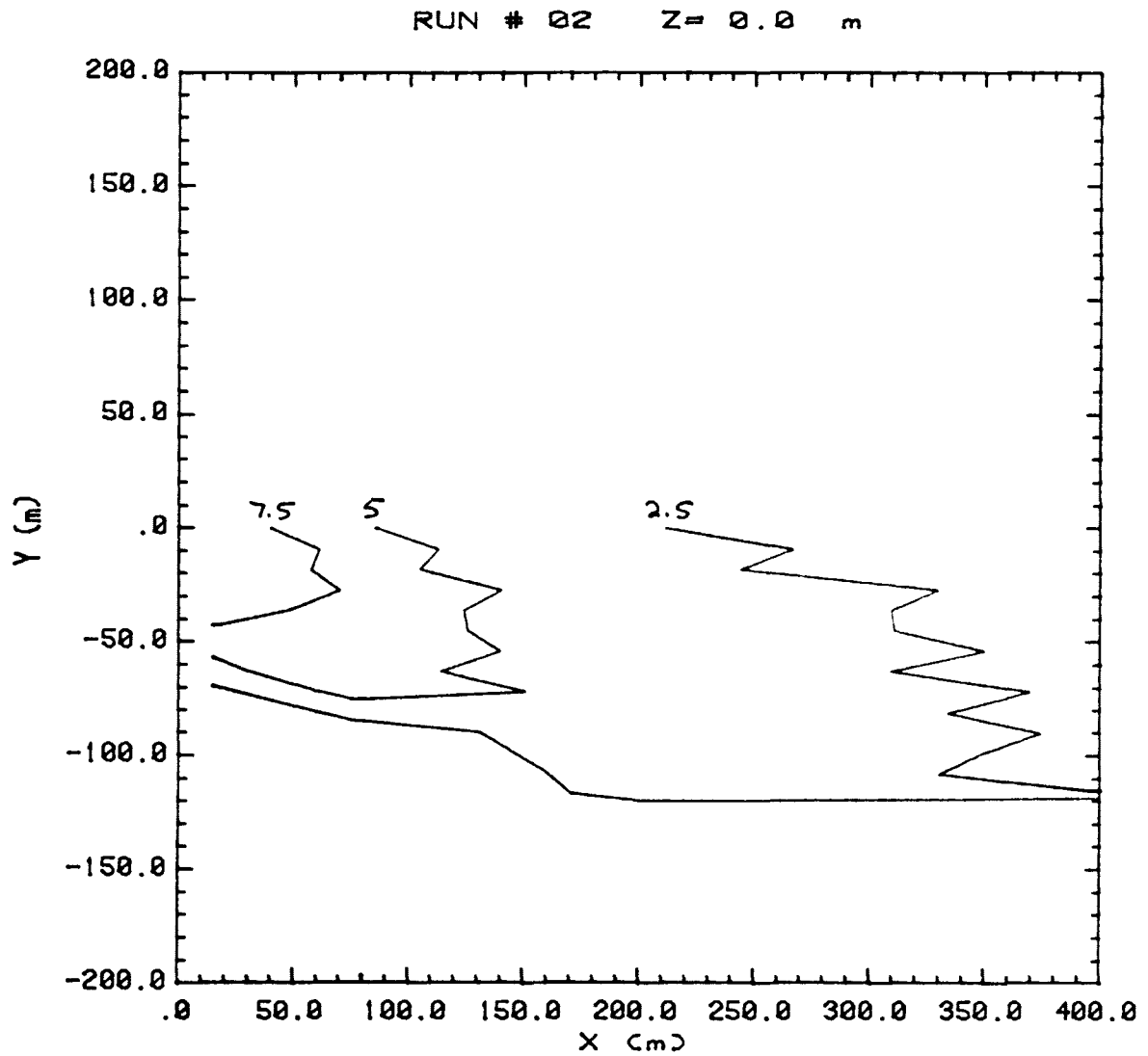


Figure 58. Concentration Contour Plot

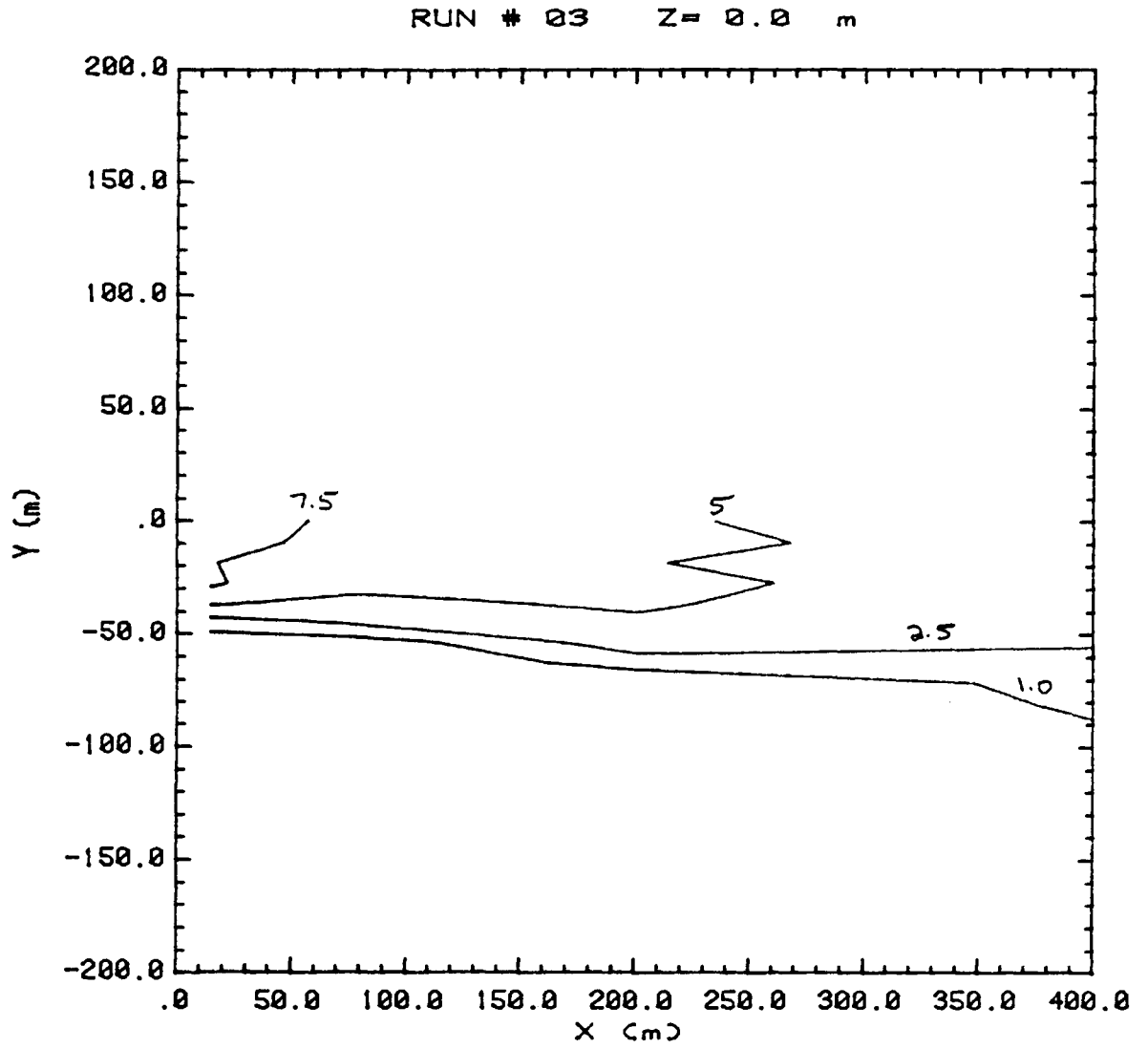


Figure 59. Concentration Contour Plot

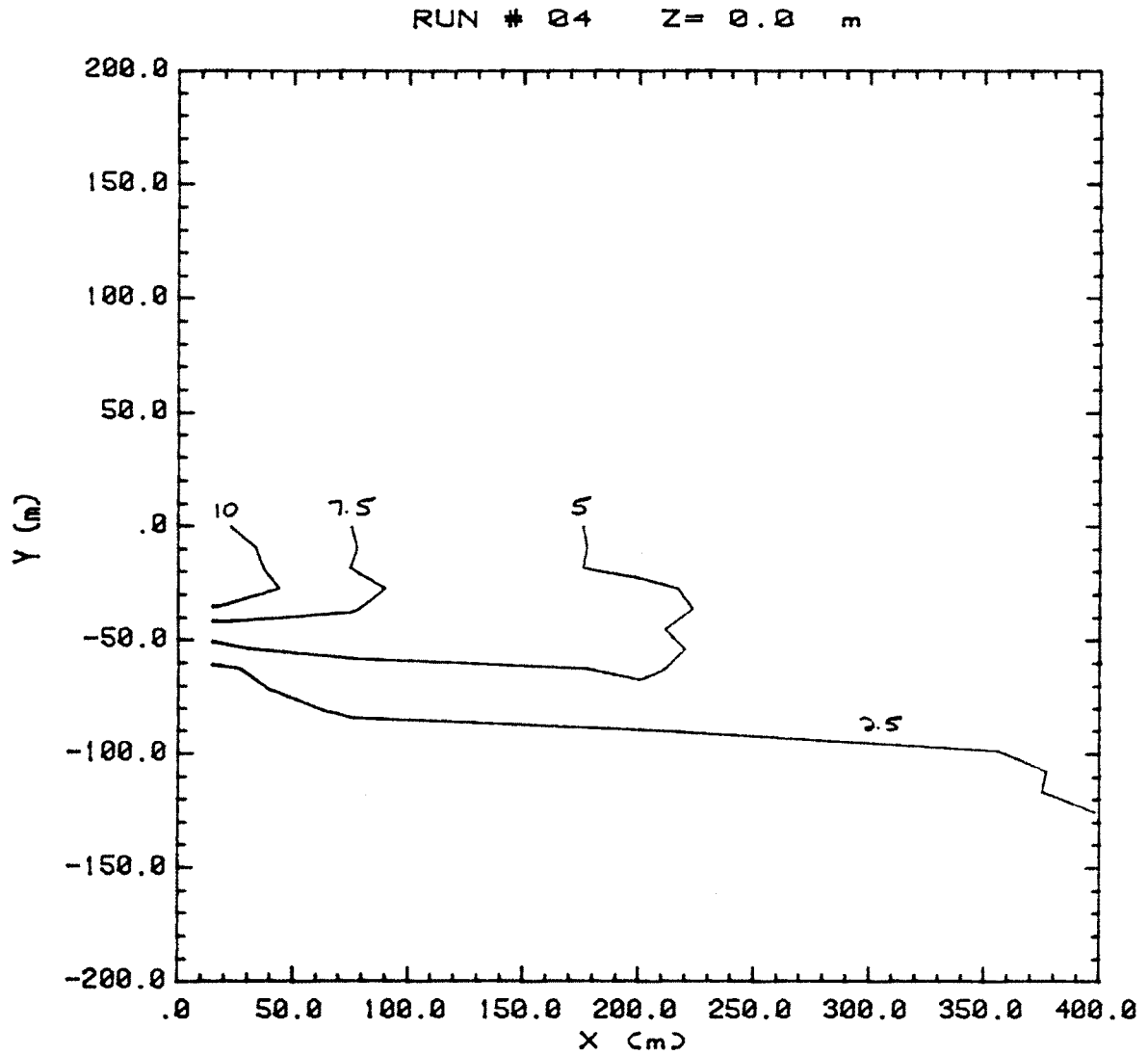


Figure 60. Concentration Contour Plot

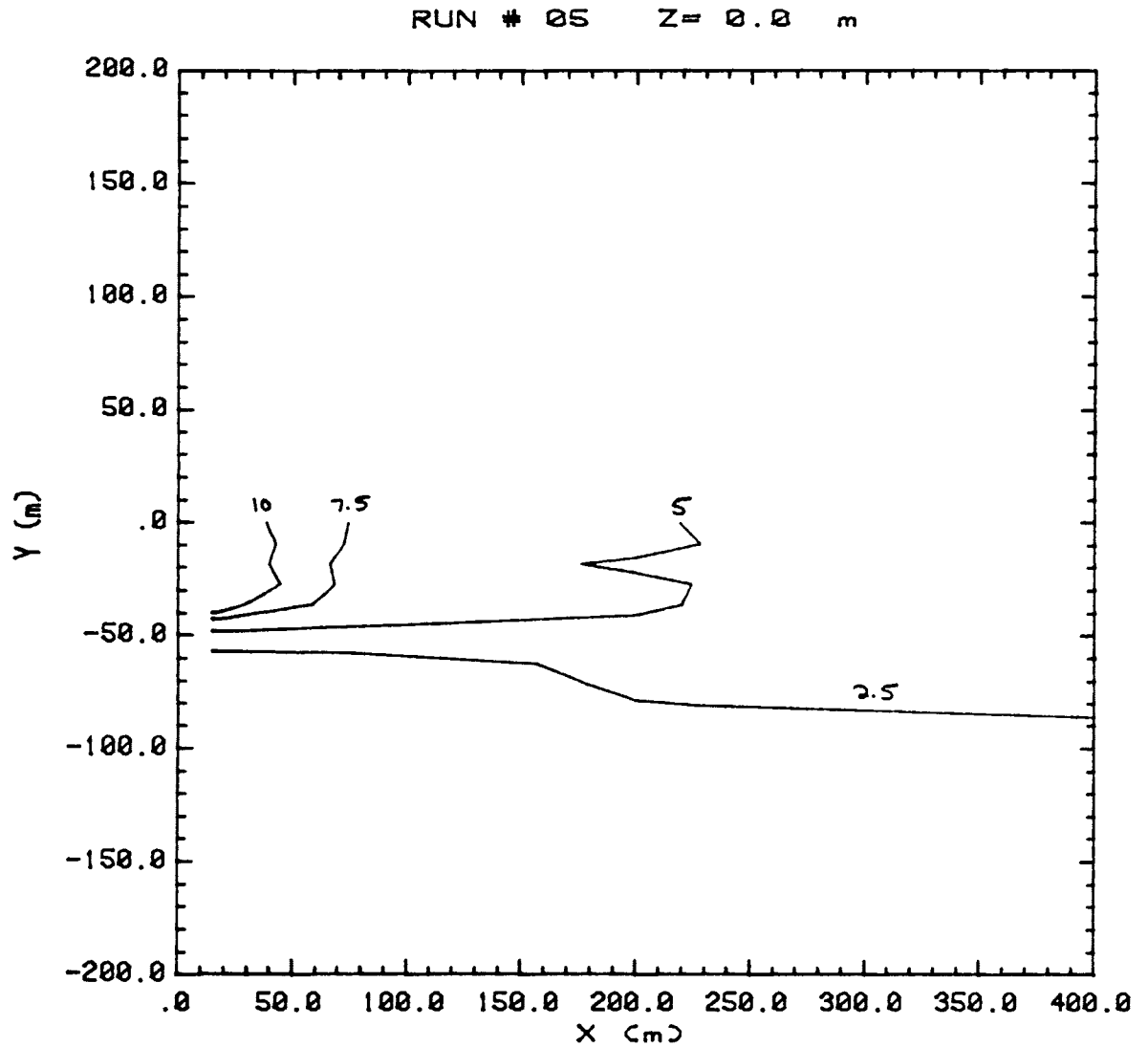


Figure 61. Concentration Contour Plot

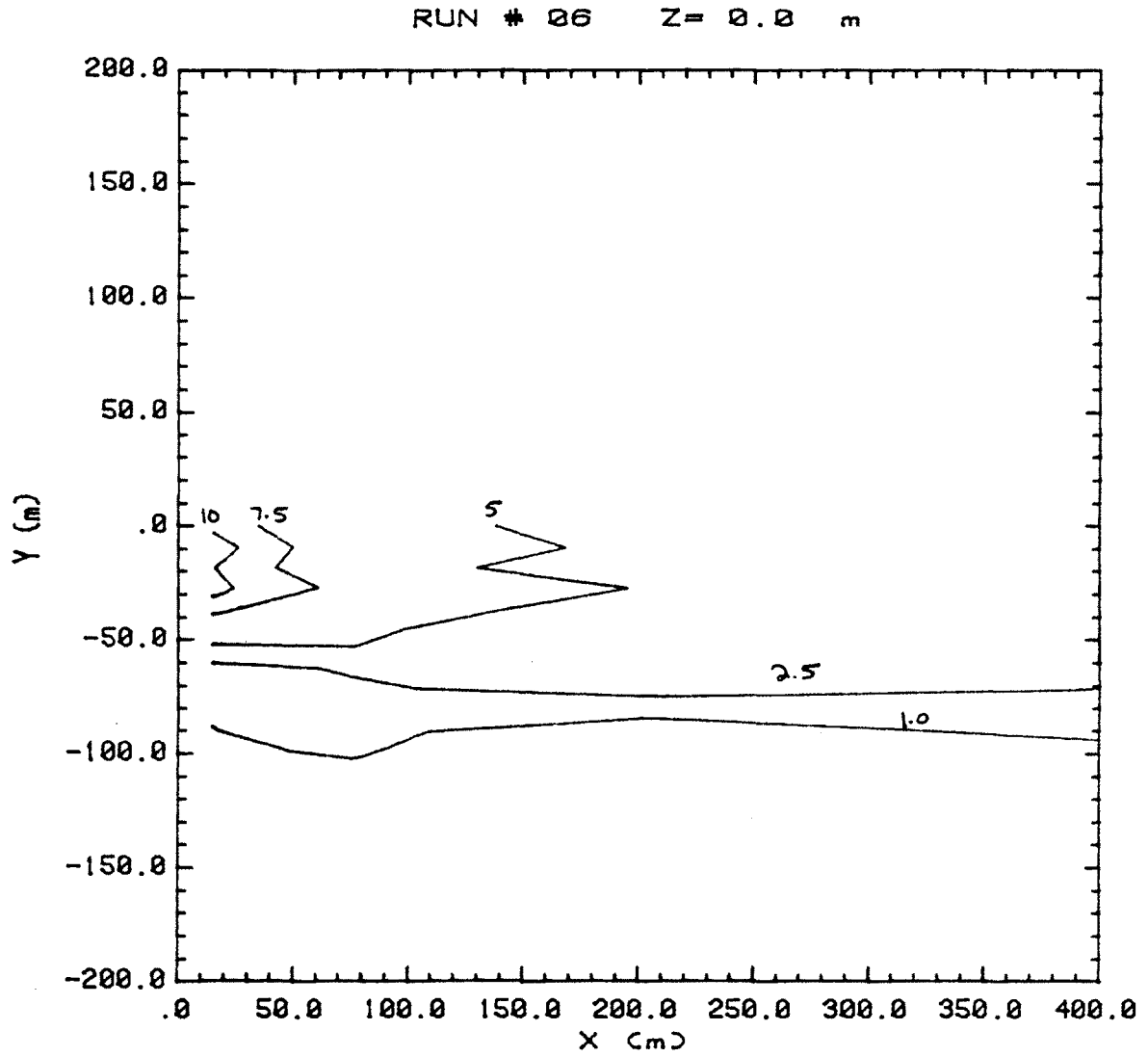


Figure 62. Concentration Contour Plot

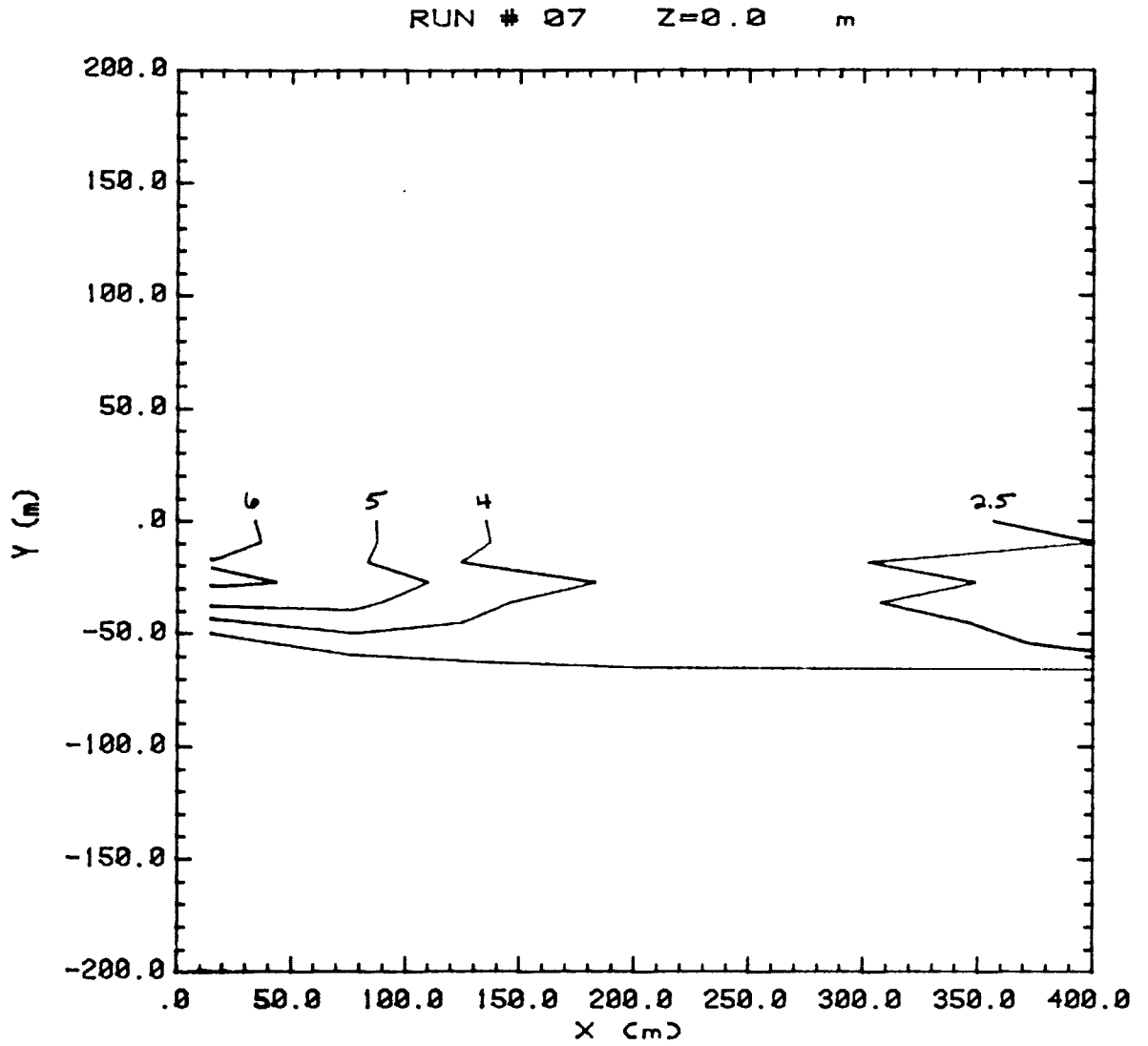


Figure 63. Concentration Contour Plot

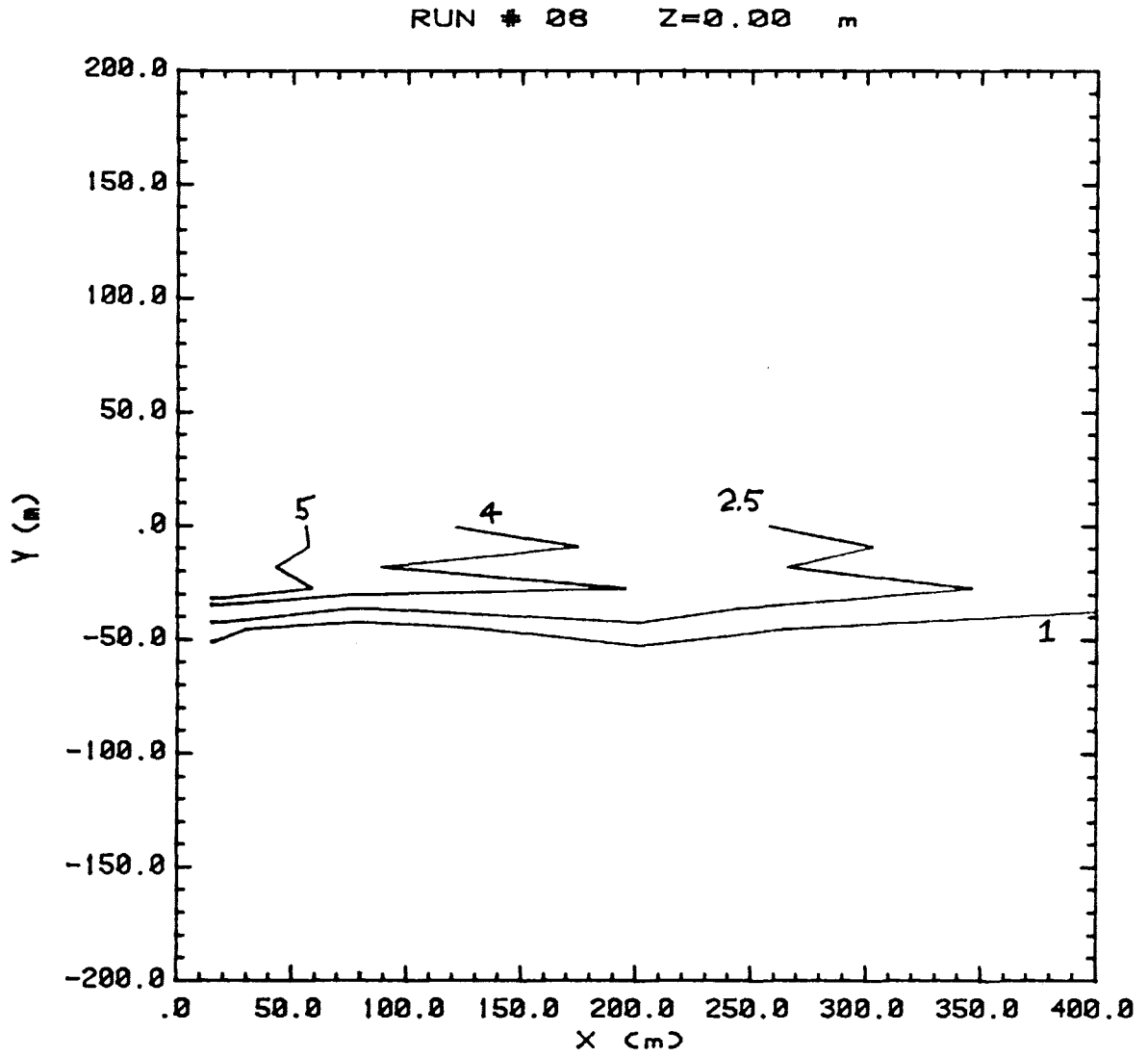


Figure 64. Concentration Contour Plot

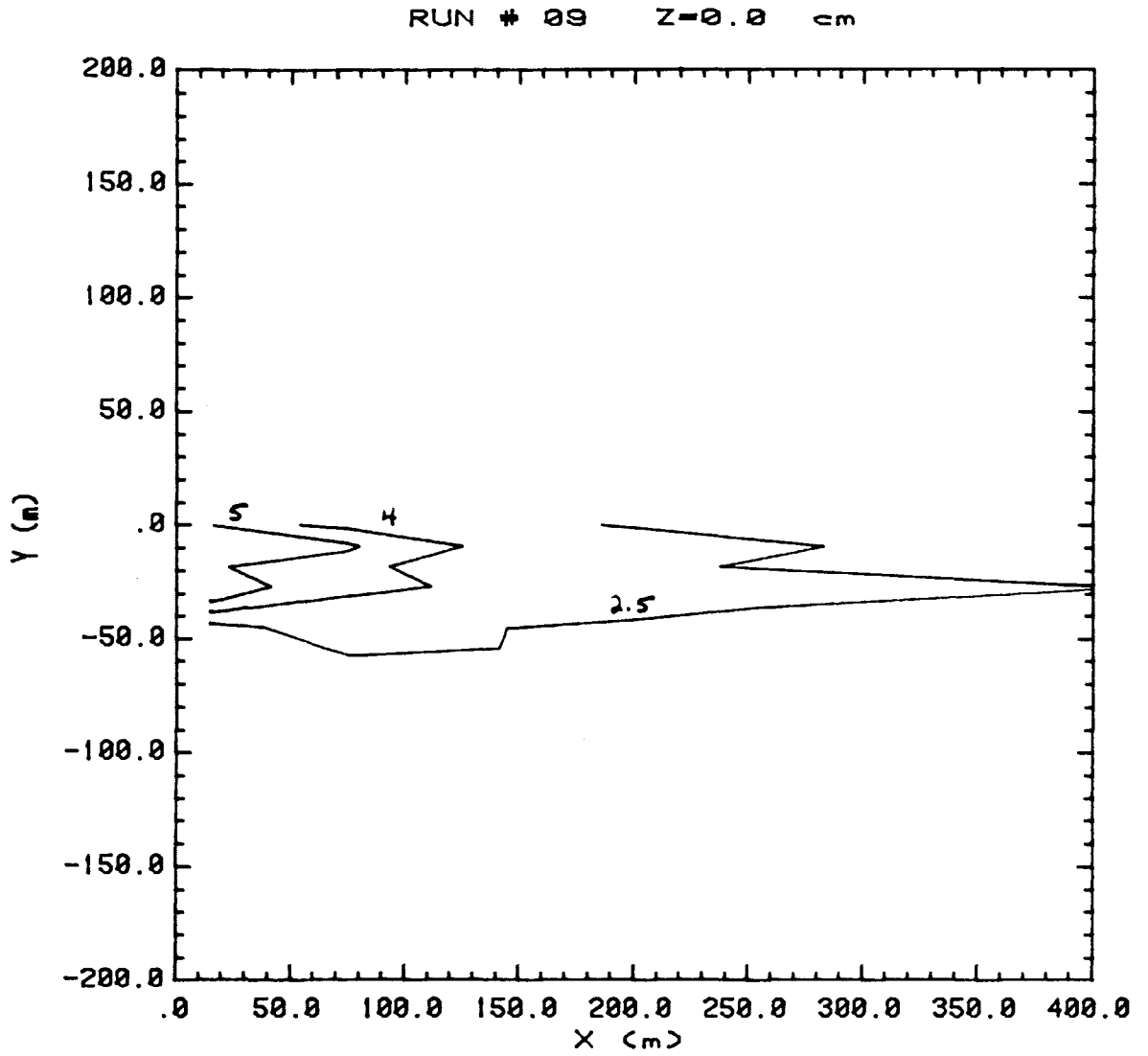


Figure 65. Concentration Contour Plot

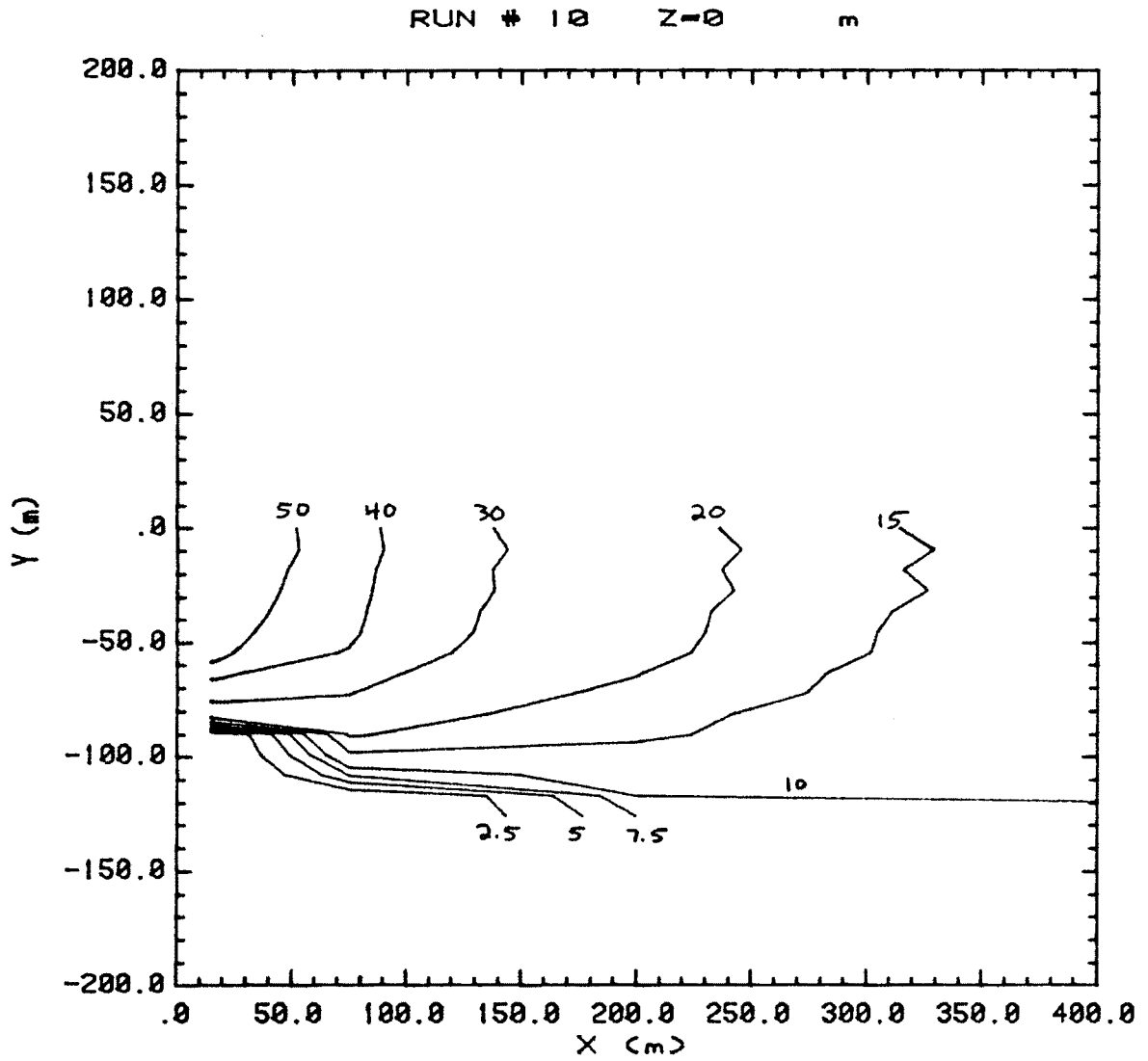


Figure 66. Concentration Contour Plot

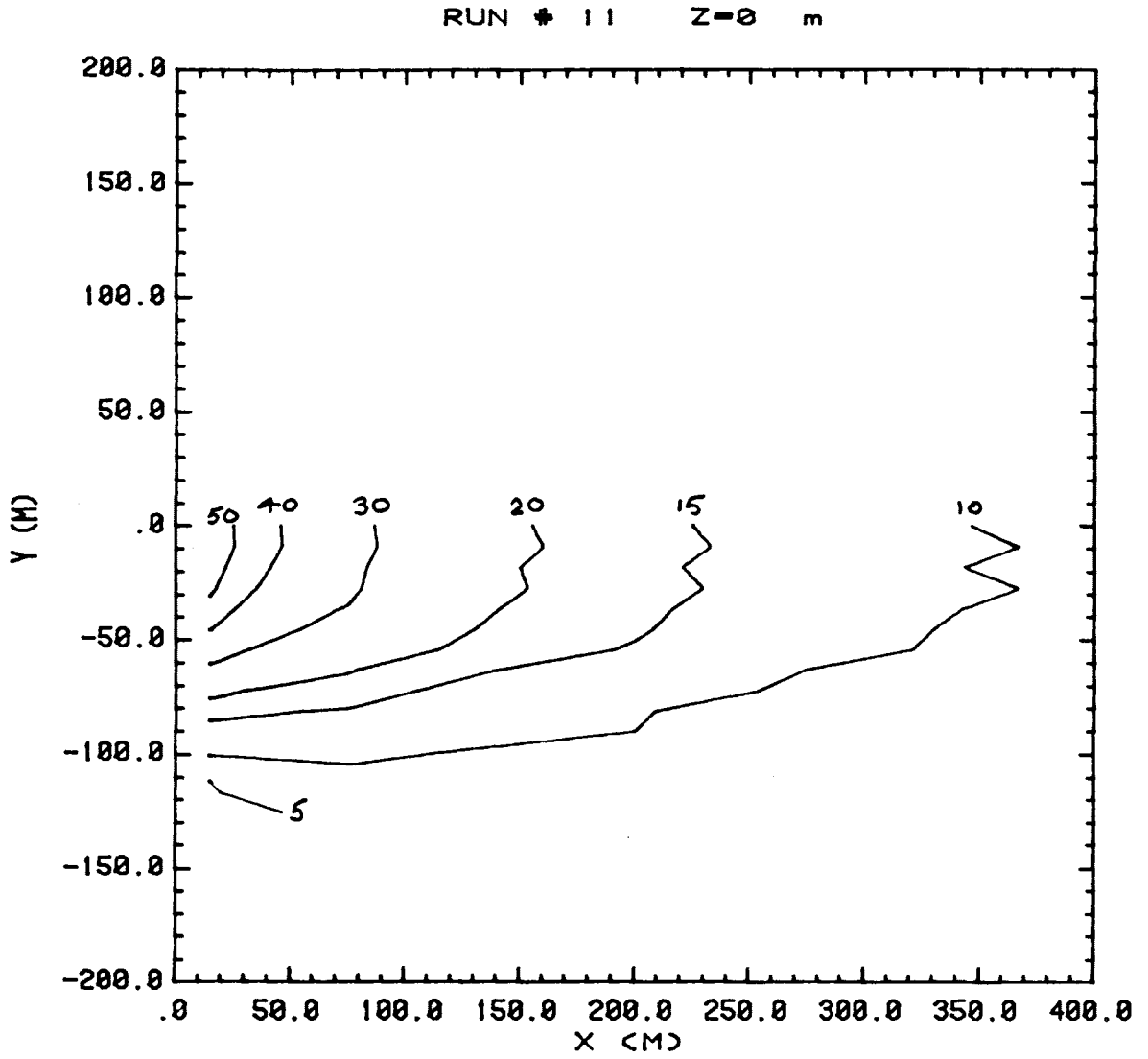


Figure 67. Concentration Contour Plot

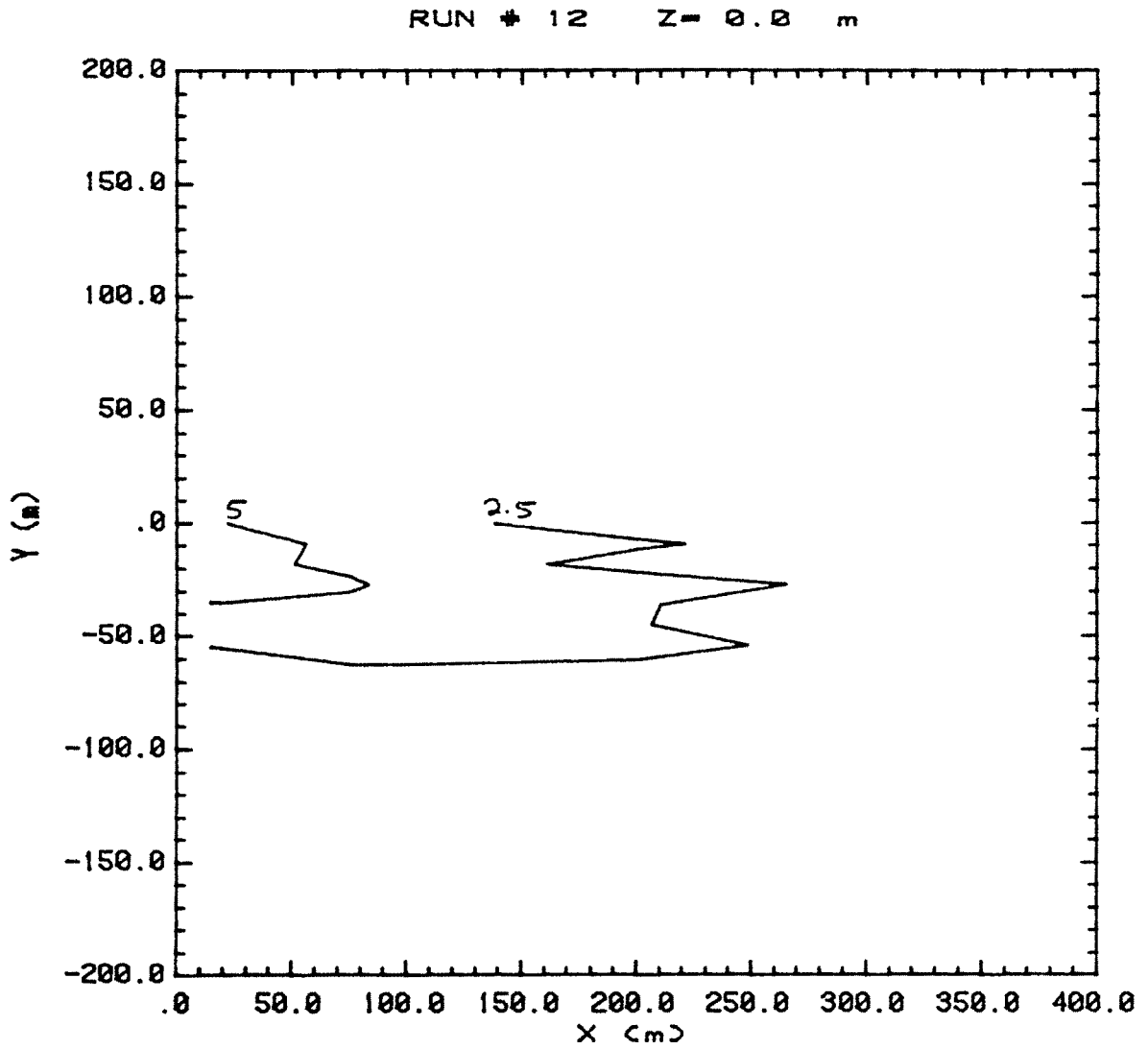


Figure 68. Concentration Contour Plot

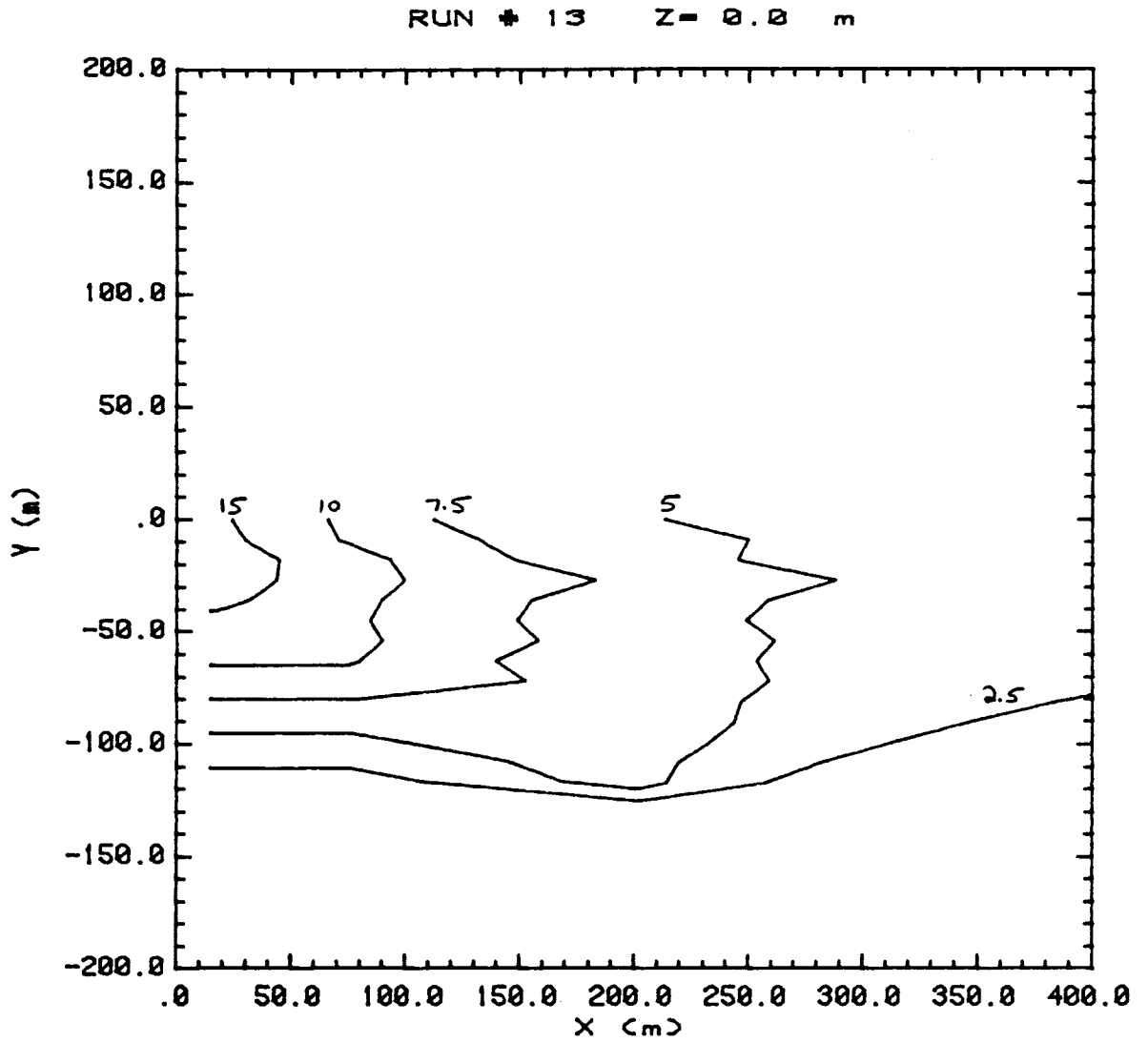


Figure 69. Concentration Contour Plot

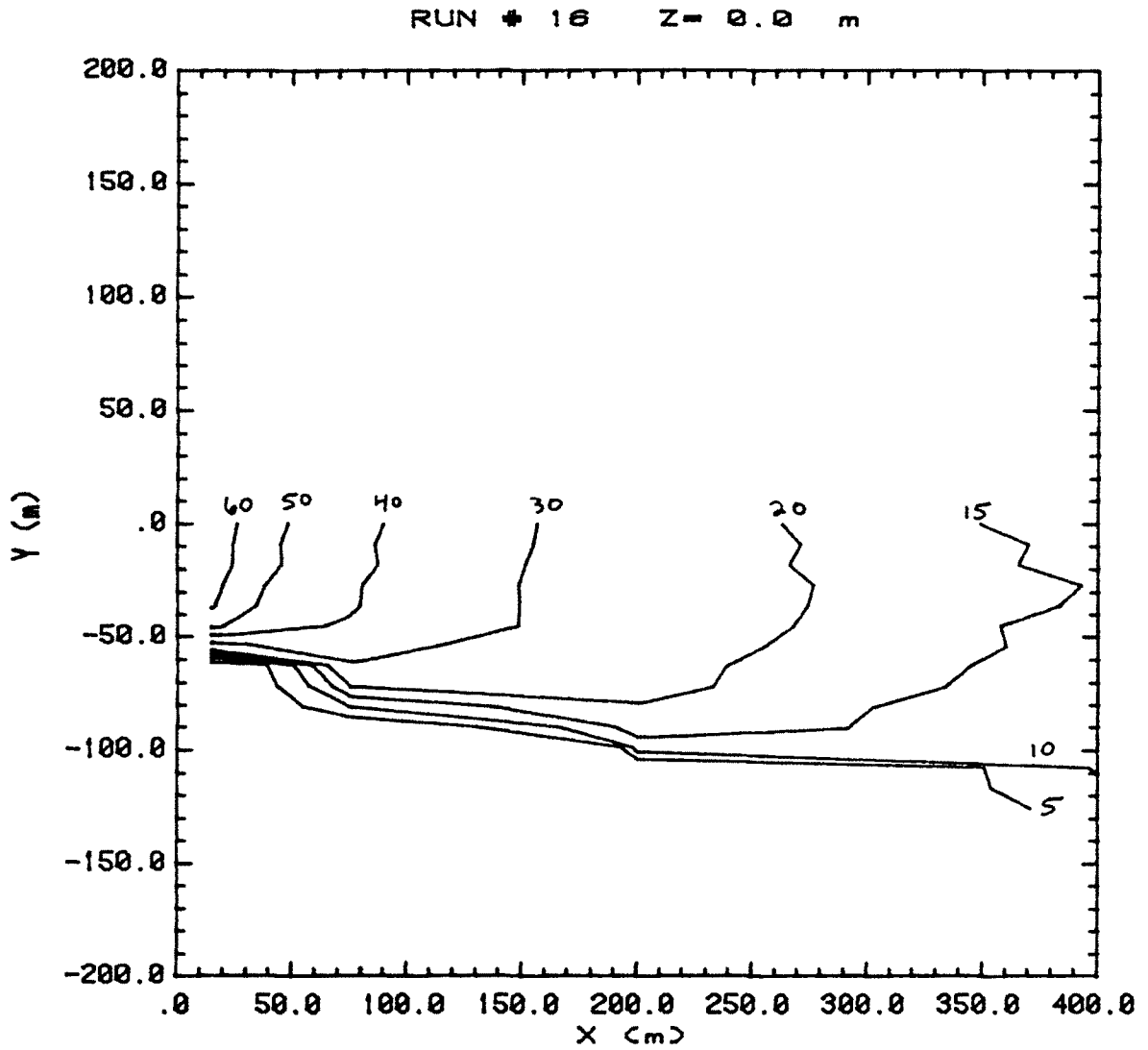


Figure 70. Concentration Contour Plot

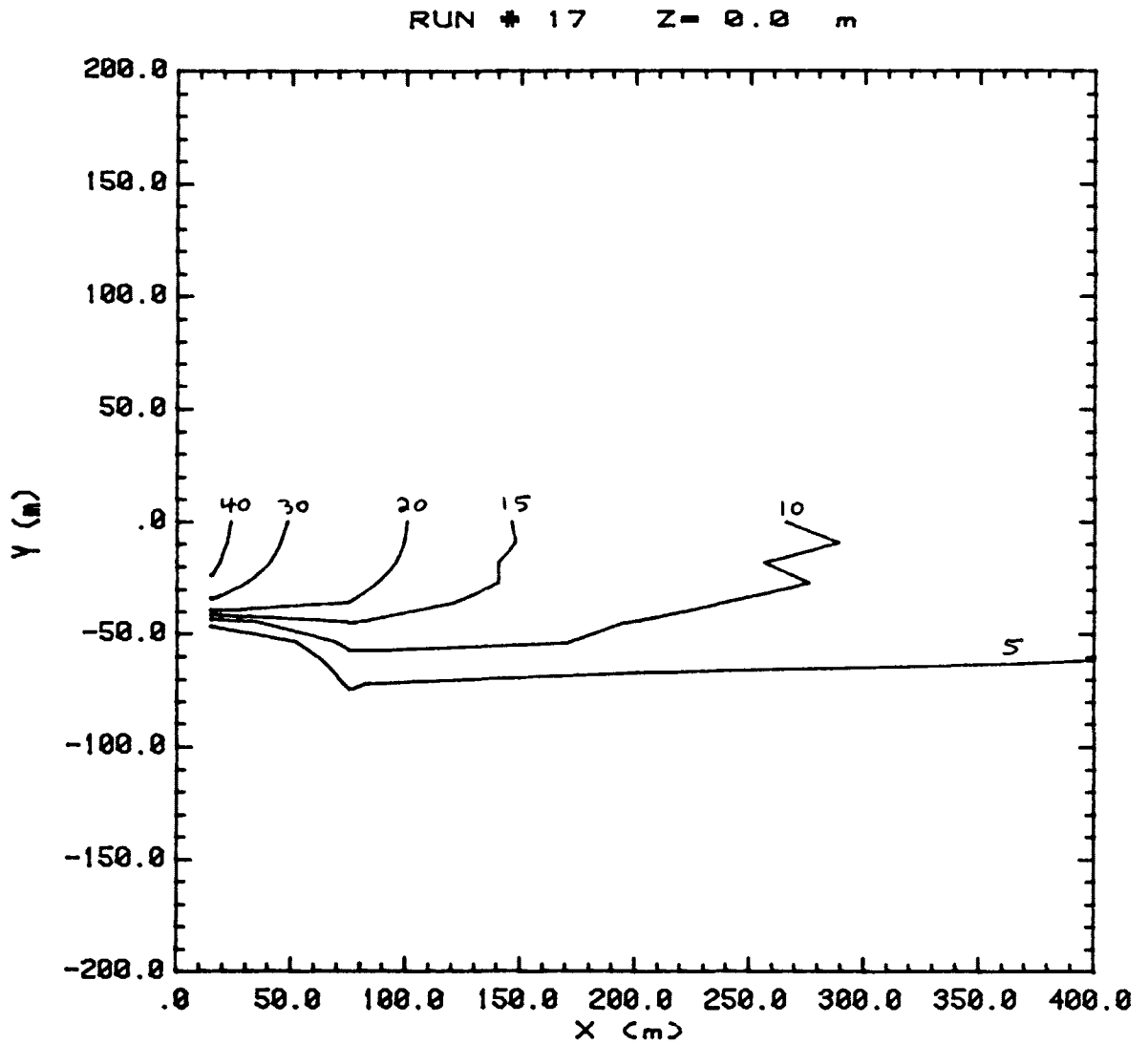


Figure 71. Concentration Contour Plot

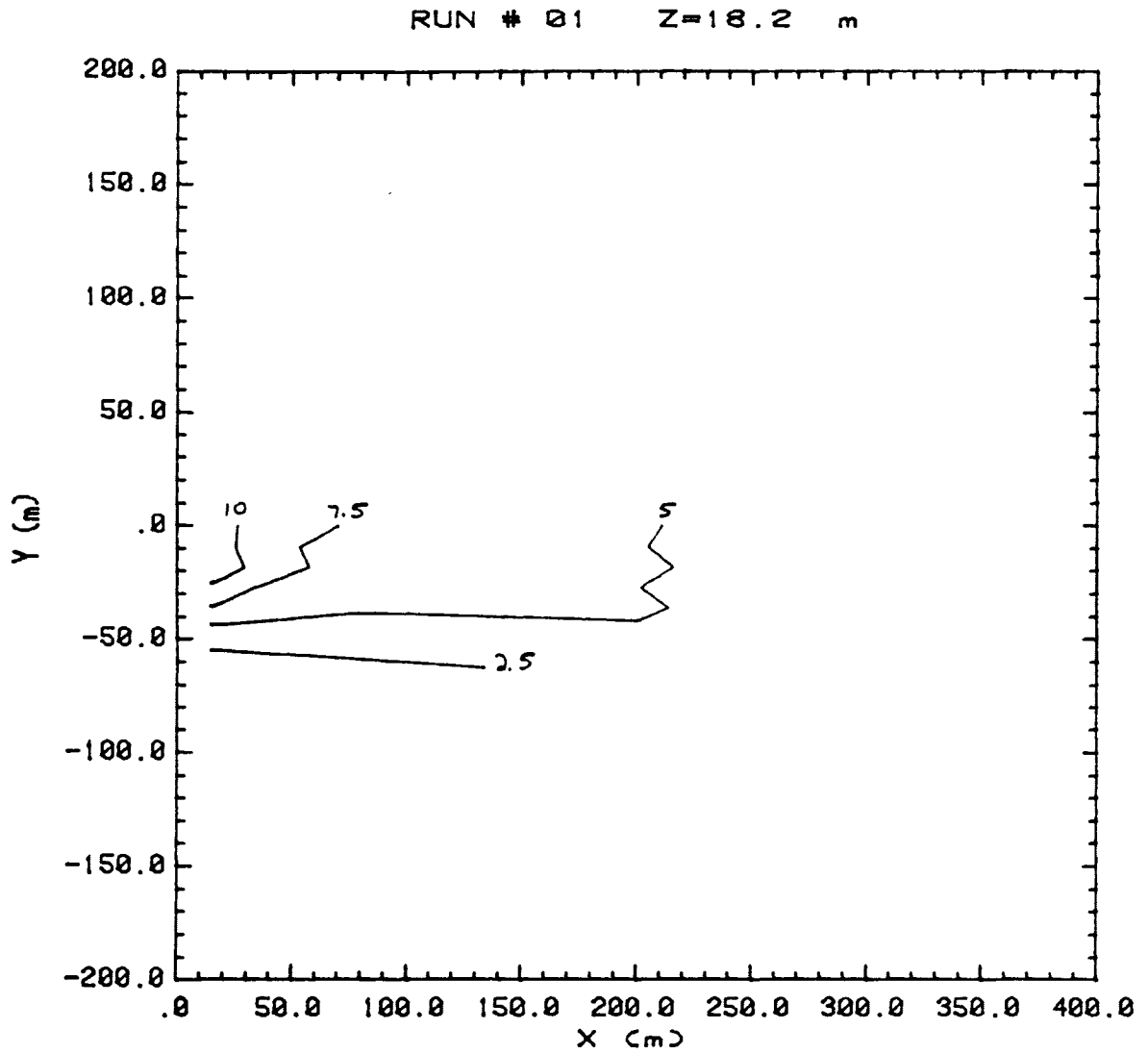


Figure 72. Concentration Contour Plot

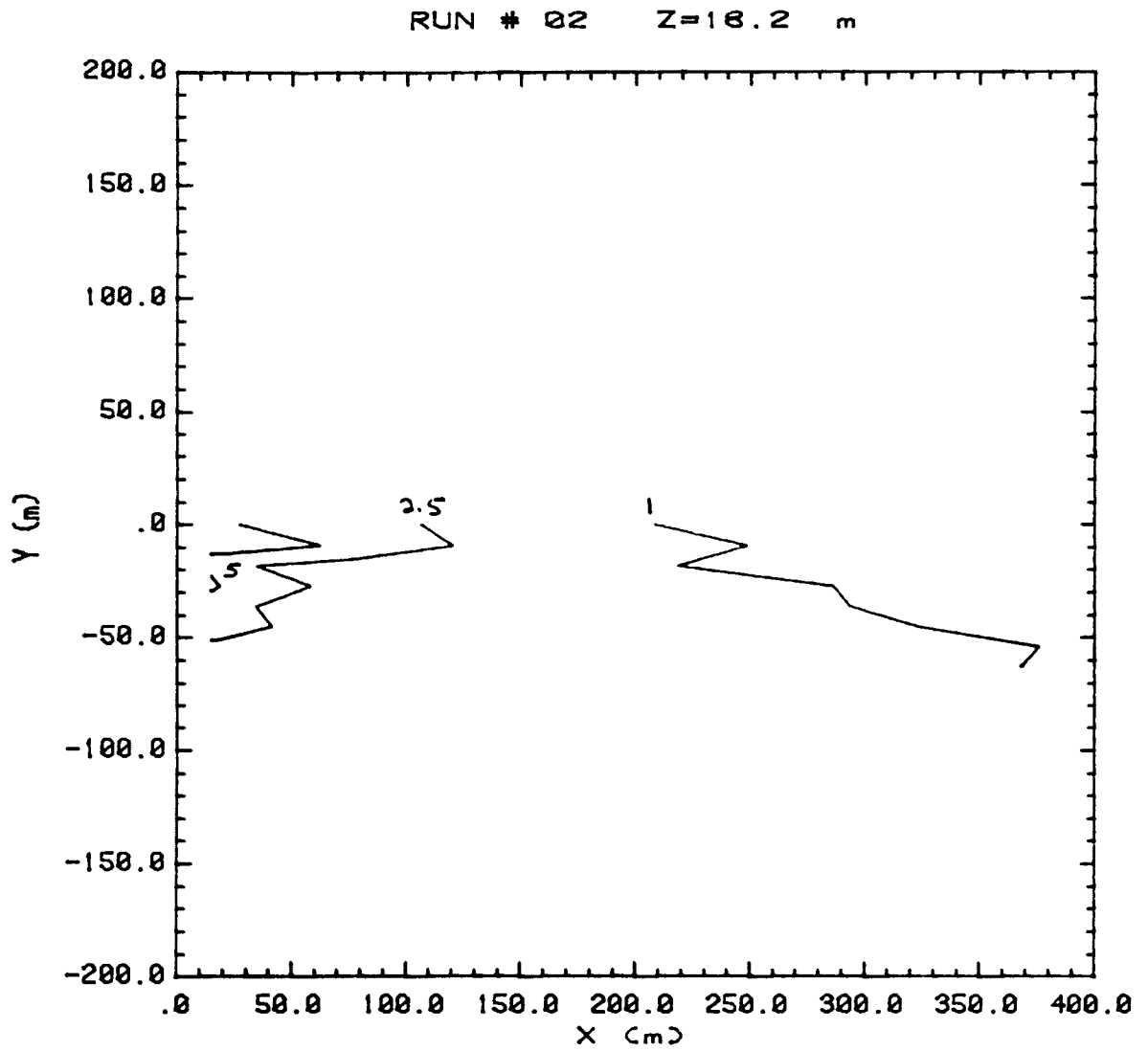


Figure 73. Concentration Contour Plot

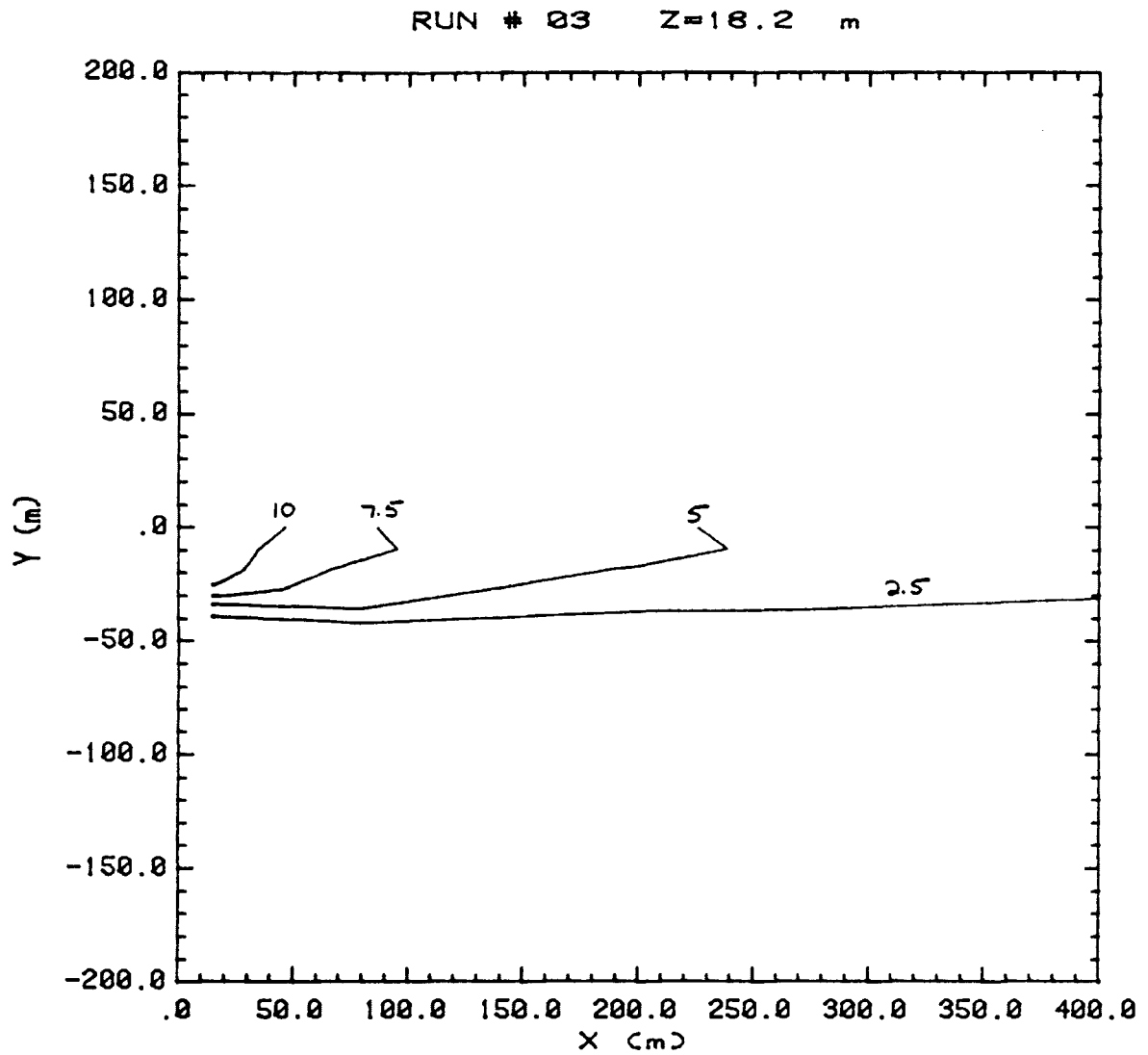


Figure 74. Concentration Contour Plot

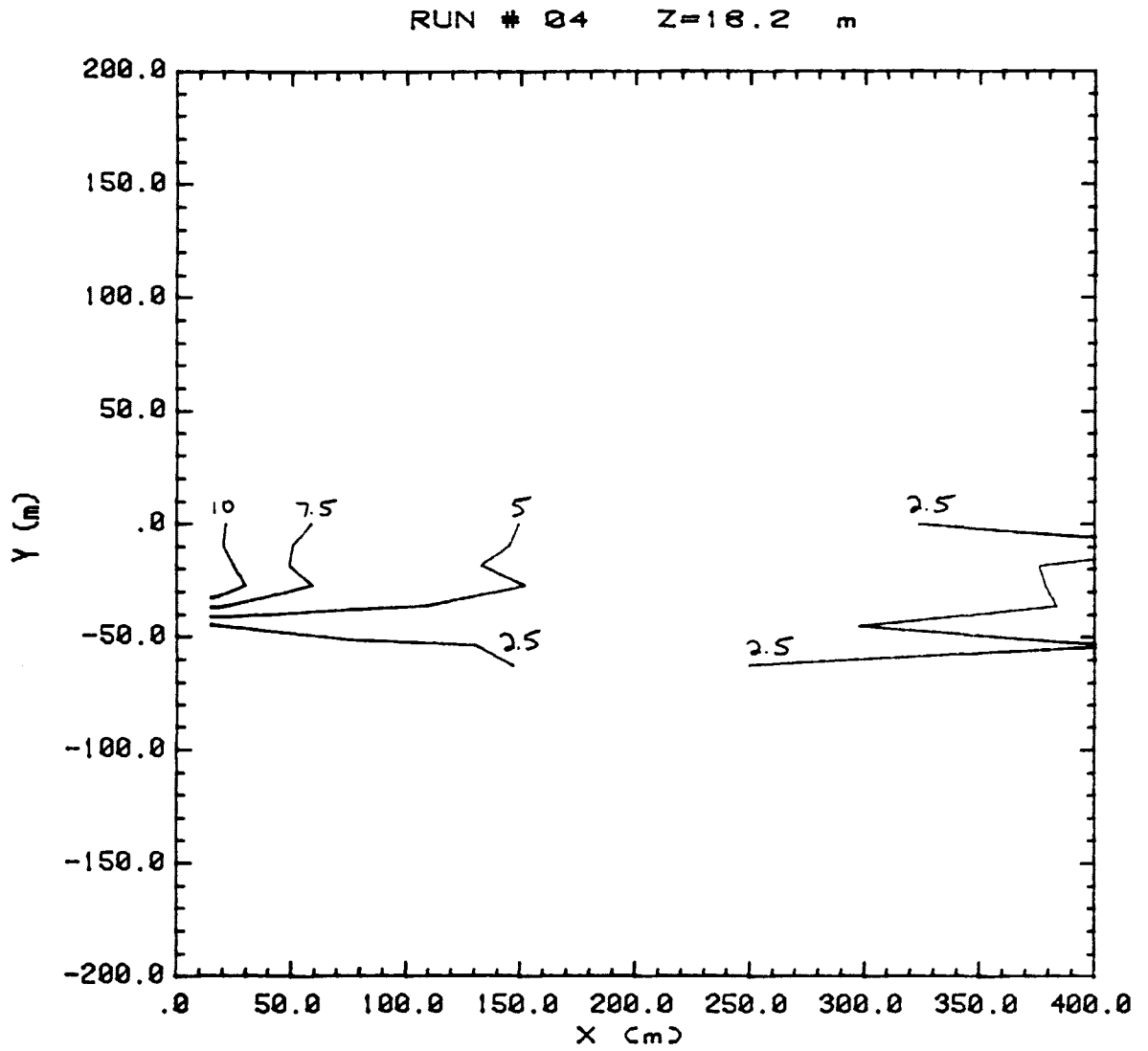


Figure 75. Concentration Contour Plot

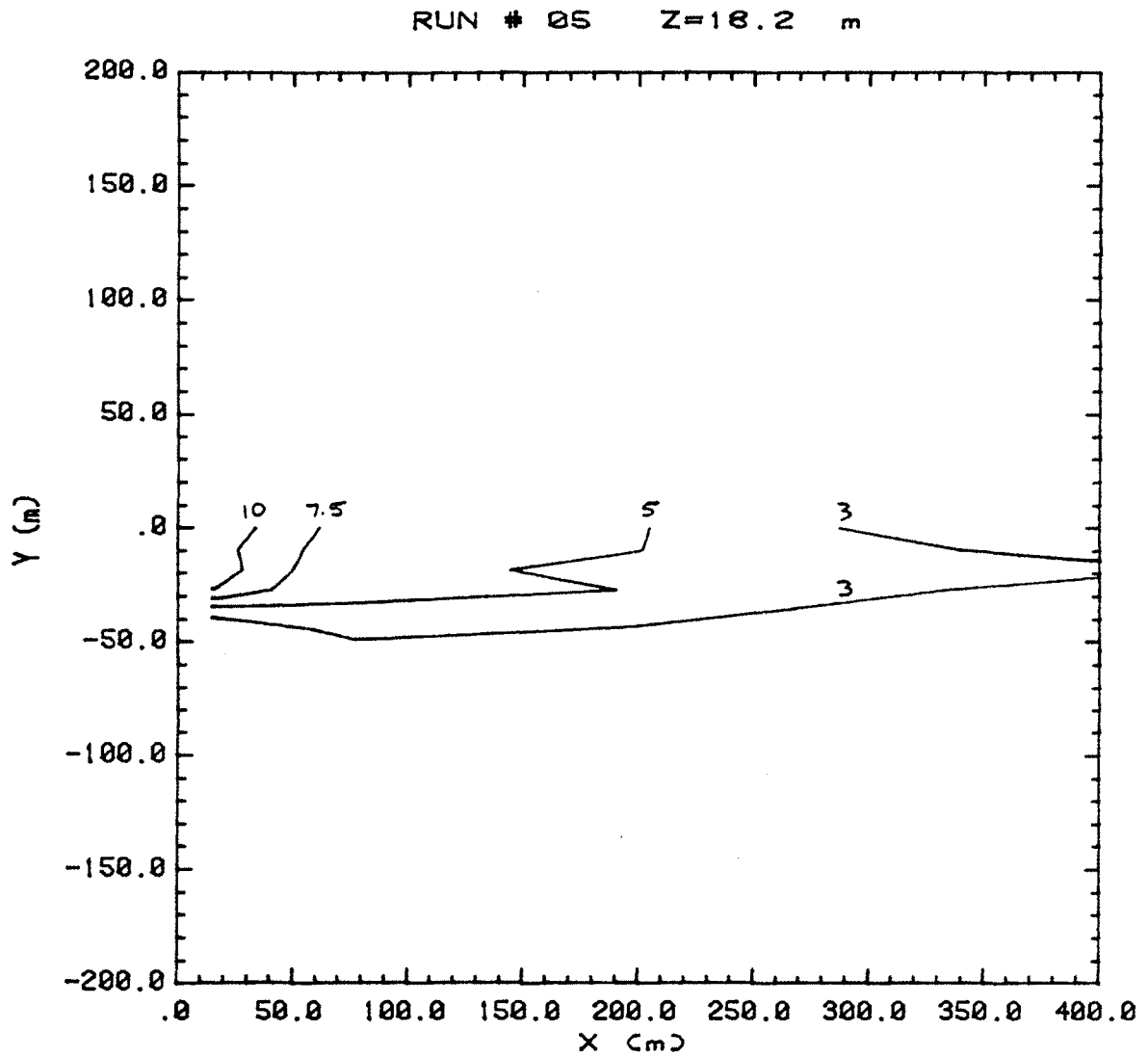


Figure 76. Concentration Contour Plot

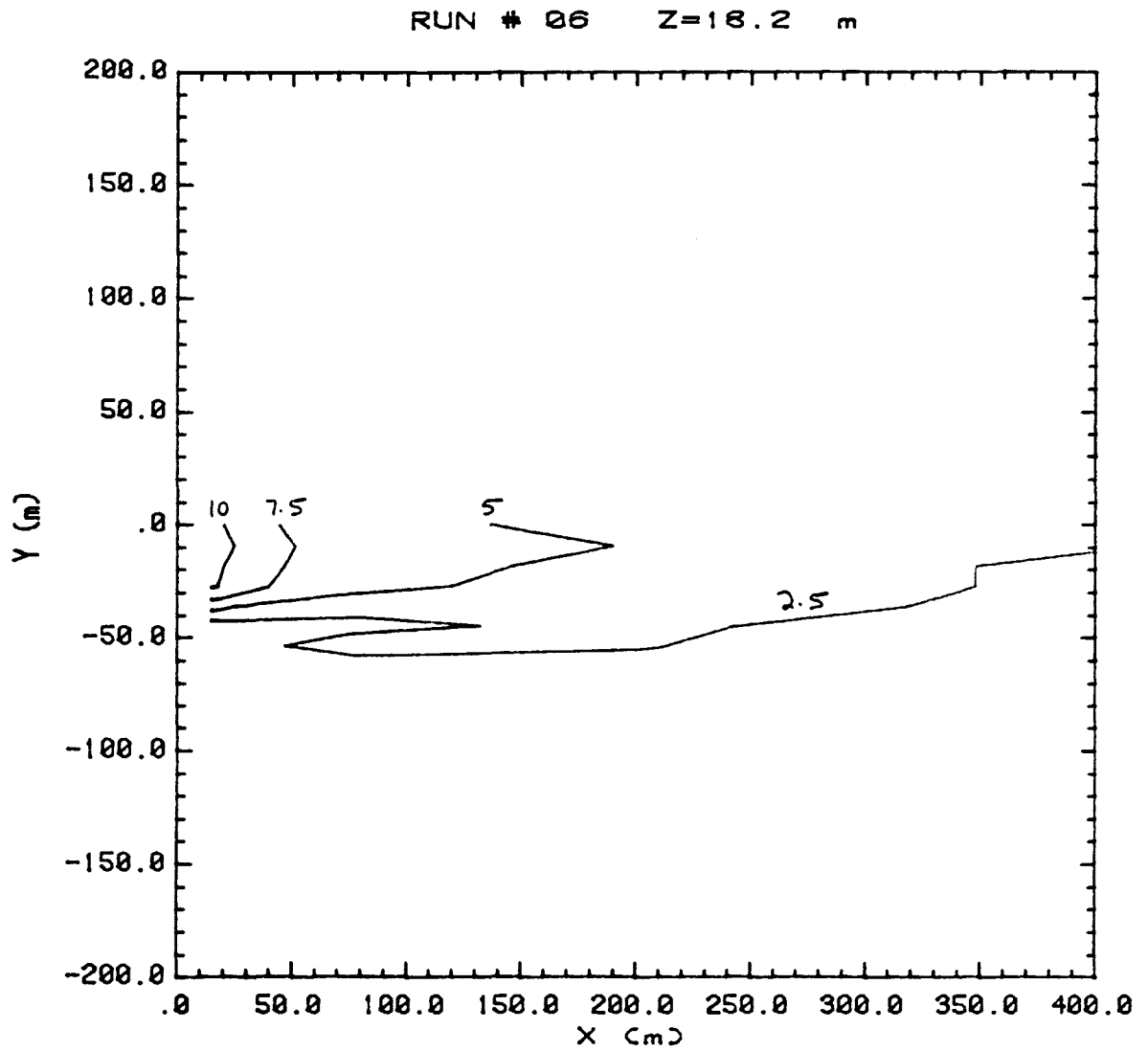


Figure 77. Concentration Contour Plot

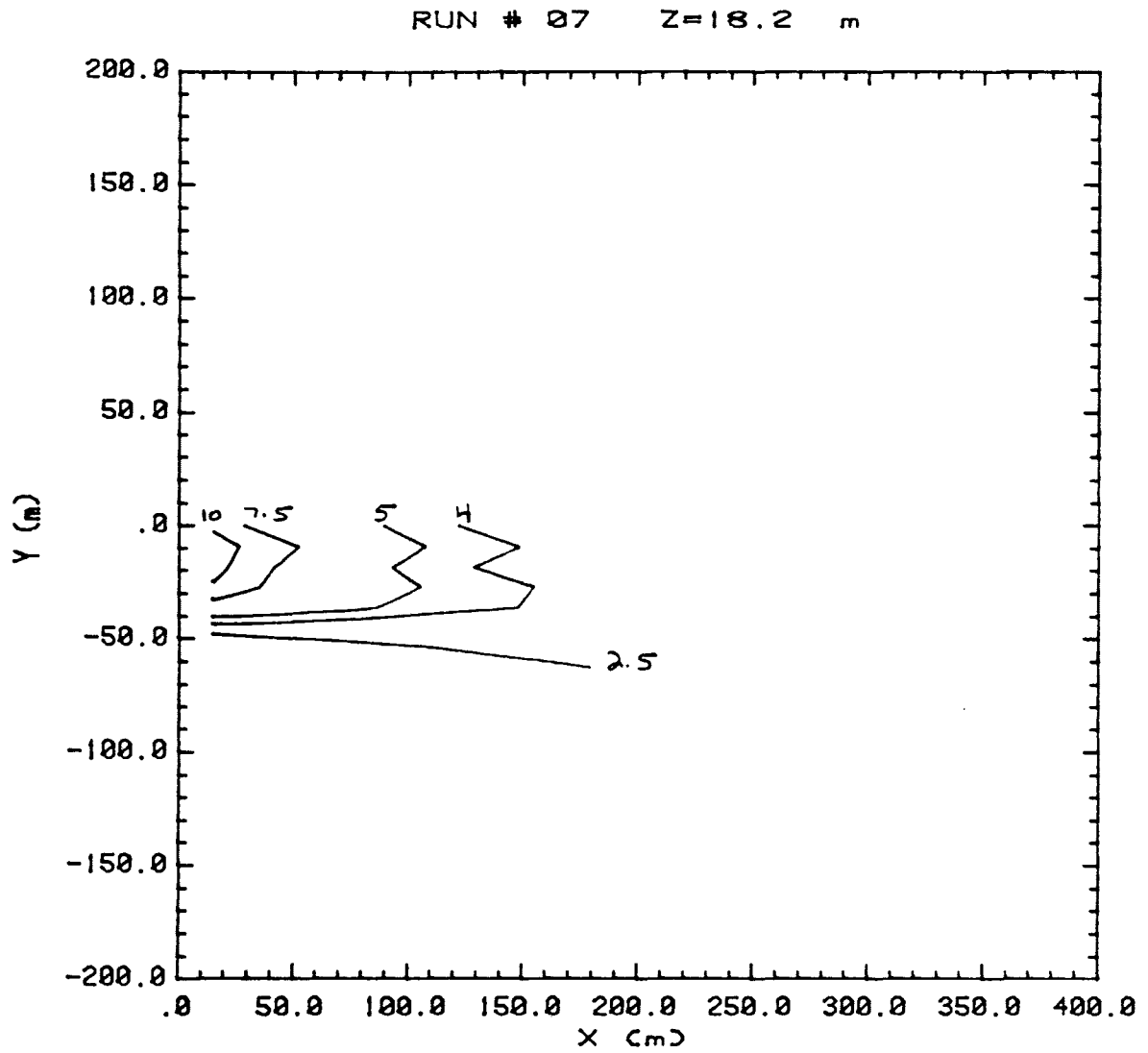


Figure 78. Concentration Contour Plot

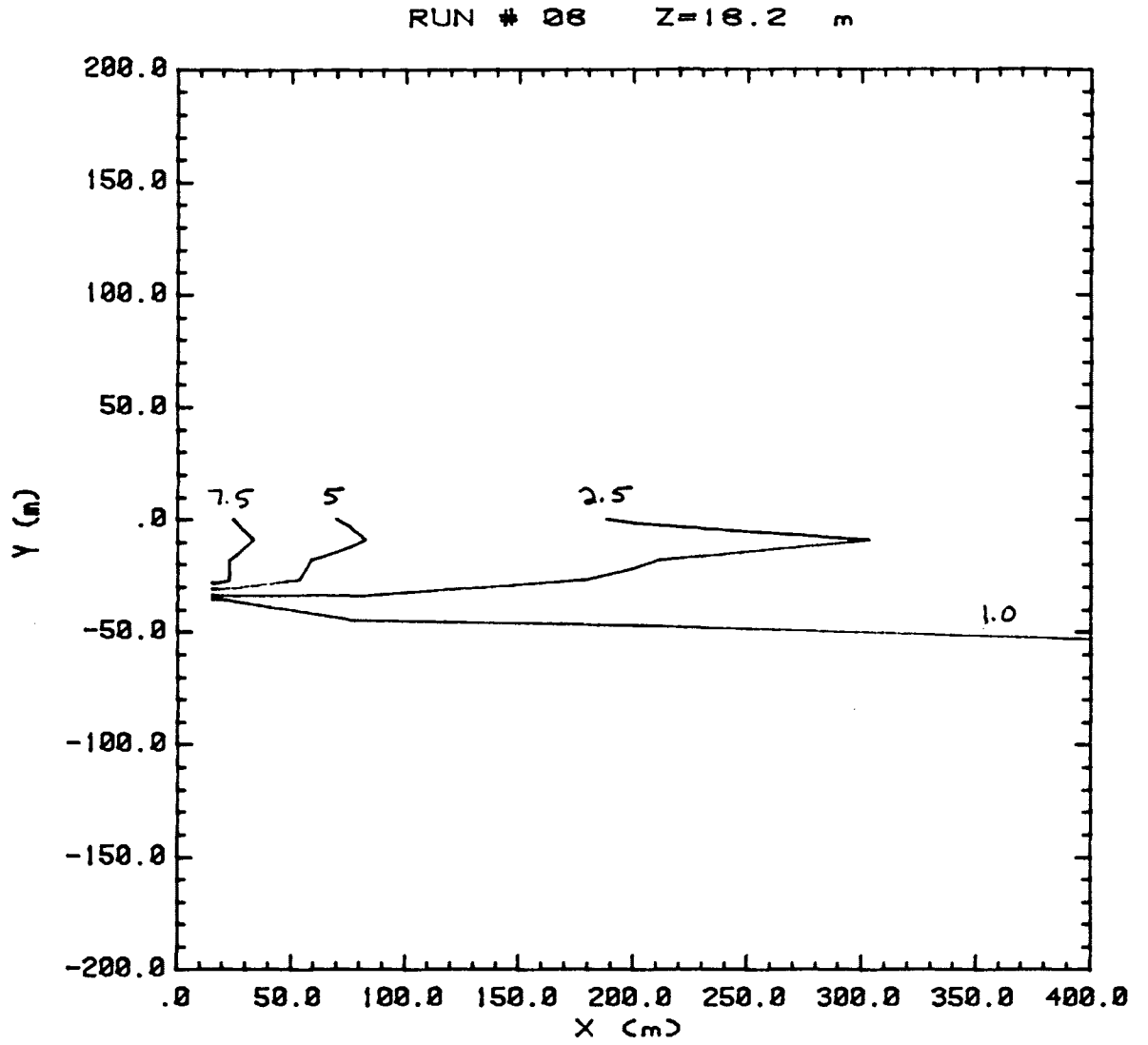


Figure 79. Concentration Contour Plot

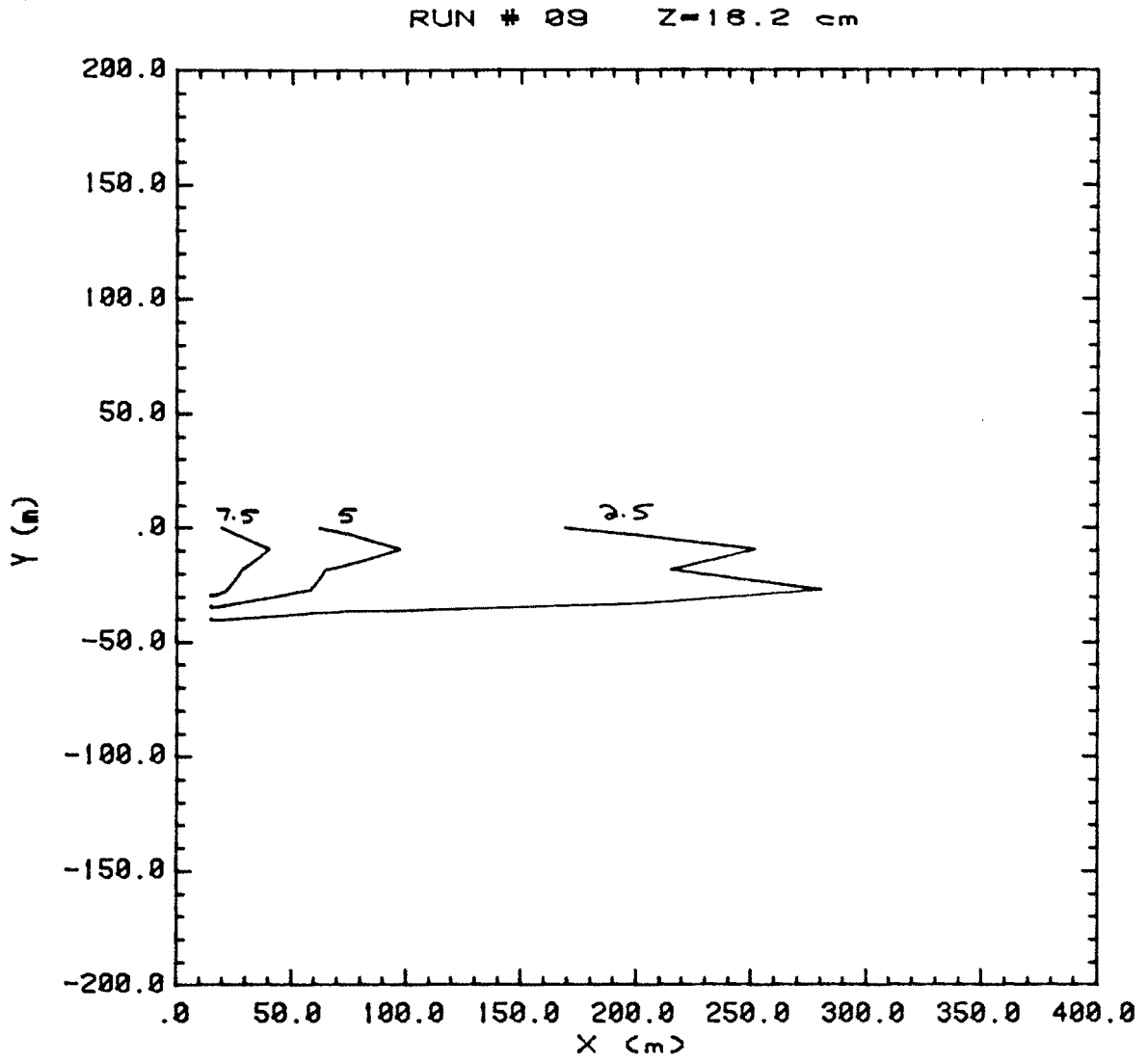


Figure 80. Concentration Contour Plot

APPENDIX

Reduced Concentration Data Listings

RUN NUMBER 01

MODEL CONDITIONS					PROTOTYPE CONDITIONS										
FILE NAME	FEAK CONC. (%)	1% ARR. TIME (SEC)	FEAK TIME (SEC)	1% END TIME (SEC)	SUM (X-S)	POSITION X (H)	Y (H)	Z (H)	FEAK CONC. (%)	5% ARR. TIME (SEC)	10% ARR. TIME (SEC)	FEAK TIME (SEC)	10% END TIME (SEC)	5% END TIME (SEC)	SUM (X-S)
AO11114	.2	0.0	51.0	0.0	-.01	13.6	-43.0	0.0	.5	0.0	0.0	444.0	0.0	0.0	-.26
BO11114	.1	0.0	119.7	0.0	-.03	13.6	-43.0	0.0	.4	0.0	0.0	1044.0	0.0	0.0	-.74
CO11114	.0	0.0	0.0	0.0	.01	13.6	-43.0	0.0	.5	0.0	0.0	7.0	0.0	0.0	.19
AO12114	.7	0.0	22.3	0.0	0.00	13.6	-43.0	4.6	1.9	0.0	0.0	203.0	0.0	0.0	-.09
BO12114	.7	0.0	22.3	0.0	-.03	13.6	-43.0	4.6	1.9	0.0	0.0	178.0	0.0	0.0	-.48
CO12114	.5	0.0	22.3	0.0	-.03	13.6	-43.0	4.6	1.3	0.0	0.0	199.0	0.0	0.0	-.80
AO13114	1.7	22.9	22.3	24.1	-.06	13.6	-43.0	9.1	4.6	0.0	0.0	227.0	0.0	0.0	-1.38
BO13114	.1	0.0	1.0	0.0	-.05	13.6	-43.0	9.1	.3	0.0	0.0	9.0	0.0	0.0	-1.22
AO14114	.1	0.0	135.1	0.0	-.04	13.6	-43.0	13.6	.3	0.0	0.0	1178.0	0.0	0.0	-.84
BO14114	.2	0.0	220.6	0.0	-.02	13.6	-43.0	13.6	.7	0.0	0.0	180.0	0.0	0.0	-.58
AO15114	.9	0.0	220.6	0.0	-.02	13.6	-43.0	13.6	2.4	0.0	0.0	237.0	0.0	0.0	-.44
BO15114	.3	0.0	18.5	0.0	0.00	13.6	-43.0	18.5	.8	0.0	0.0	162.0	0.0	0.0	-.02
AO16114	.3	0.0	20.4	0.0	-.03	13.6	-43.0	18.5	.8	0.0	0.0	178.0	0.0	0.0	-.79
BO16114	.3	0.0	44.0	0.0	-.02	13.6	-43.0	18.5	.9	0.0	0.0	384.0	0.0	0.0	-.81
AO17114	.1	0.0	9.9	0.0	-.02	13.6	-43.0	18.5	.3	0.0	0.0	257.0	0.0	0.0	-.38
BO17114	.1	0.0	22.3	0.0	0.04	13.6	-43.0	18.5	.4	0.0	0.0	7.0	0.0	0.0	.83
AO11113	1.4	22.2	22.3	23.7	0.00	13.6	-43.0	0.0	3.7	0.0	0.0	201.0	0.0	0.0	.08
BO11113	1.2	22.2	31.1	24.1	.03	13.6	-43.0	0.0	3.1	0.0	0.0	273.0	0.0	0.0	.80
CO11113	.9	22.2	22.7	28.8	.10	13.6	-43.0	0.0	2.7	0.0	0.0	247.0	0.0	24.3	2.42
AO12113	.2	16.6	22.4	43.7	.16	13.6	-43.0	4.6	2.0	0.0	0.0	204.0	0.0	374.0	33.65
BO12113	.1	15.0	19.6	65.9	.12	13.6	-43.0	4.6	1.1	0.0	0.0	171.0	0.0	217.0	2.77
CO12113	.4	15.0	22.2	31.4	.03	13.6	-43.0	4.6	1.8	0.0	0.0	185.0	0.0	274.0	.77
AO13113	.2	15.0	22.2	44.4	.03	13.6	-43.0	4.6	1.1	0.0	0.0	194.0	0.0	194.0	.79
BO13113	.5	22.0	22.3	44.4	-.16	13.6	-43.0	9.1	1.1	0.0	0.0	196.0	0.0	310.0	3.80
CO13113	.6	22.0	22.7	58.0	-.02	13.6	-43.0	9.1	1.7	0.0	0.0	235.0	0.0	0.0	.00
AO14113	.1	0.0	48.9	58.9	0.00	13.6	-43.0	0.0	2.0	0.0	0.0	311.0	0.0	0.0	-.06
BO14113	.1	0.0	48.9	58.9	0.00	13.6	-43.0	0.0	2.0	0.0	0.0	333.0	0.0	0.0	-.10
CO14113	.1	0.0	7.7	10.7	-.01	13.6	-43.0	0.0	1.4	0.0	0.0	25.0	0.0	253.0	1.57
AO15113	.6	0.0	20.7	20.8	-.01	13.6	-43.0	0.0	1.1	0.0	0.0	267.0	0.0	0.0	.00
BO15113	.6	0.0	20.7	20.8	-.01	13.6	-43.0	0.0	1.1	0.0	0.0	231.0	0.0	0.0	-1.80
CO15113	.6	0.0	20.7	20.8	-.01	13.6	-43.0	0.0	1.1	0.0	0.0	199.0	0.0	0.0	.00
AO16113	.3	0.0	51.0	51.0	0.00	13.6	-43.0	0.0	1.4	0.0	0.0	194.0	0.0	0.0	.00
BO16113	.3	18.0	22.3	51.0	.57	13.6	-43.0	0.0	1.4	0.0	0.0	174.0	0.0	0.0	.81
CO16113	.3	18.0	22.3	51.0	.57	13.6	-43.0	0.0	1.4	0.0	0.0	158.0	0.0	44.4	13.16
AO11112	.8	0.0	0.0	45.5	.43	13.6	-43.0	0.0	1.3	0.0	0.0	192.0	0.0	459.0	9.90
BO11112	.6	0.0	0.0	49.9	.48	13.6	-43.0	0.0	1.3	0.0	0.0	234.0	0.0	285.0	13.00
CO11112	.1	18.0	4.4	77.8	.38	13.6	-43.0	0.0	1.6	0.0	0.0	229.0	0.0	406.0	8.00
AO12112	.1	18.0	7.7	77.8	.30	13.6	-43.0	4.6	1.9	0.0	0.0	133.0	0.0	505.0	6.89
BO12112	.5	17.0	5.5	78.4	.36	13.6	-43.0	4.6	1.1	0.0	0.0	197.0	0.0	35.0	96.40
CO12112	.3	17.0	4.4	44.0	.07	13.6	-43.0	9.1	1.1	0.0	0.0	205.0	0.0	206.0	1.64
AO13112	.5	13.0	1.1	81.1	.12	13.6	-43.0	9.1	1.1	0.0	0.0	333.0	0.0	333.0	2.76
BO13112	.7	13.0	0.0	74.4	.10	13.6	-43.0	13.6	1.1	0.0	0.0	253.0	0.0	0.0	3.42
CO13112	.3	13.0	15.5	123.3	.05	13.6	-43.0	13.6	1.1	0.0	0.0	135.0	0.0	183.0	1.18
AO14112	.4	16.7	31.7	31.7	.10	13.6	-43.0	13.6	1.1	0.0	0.0	276.0	0.0	638.0	2.38
BO14112	.2	12.0	10.6	88.8	0.00	13.6	-43.0	13.6	1.1	0.0	0.0	110.0	0.0	0.0	-.12
CO14112	.0	12.0	74.4	74.4	.02	13.6	-43.0	13.6	1.1	0.0	0.0	650.0	0.0	650.0	.51
AO15112	.1	14.9	14.9	62.5	.03	13.6	-43.0	13.6	1.1	0.0	0.0	130.0	0.0	130.0	.78
BO15112	.1	0.0	70.5	0.0	.05	13.6	-43.0	13.6	.7	0.0	0.0	615.0	0.0	0.0	1.09

RUN NUMBER 01

MODEL CONDITIONS						POSITION			PROTOTYPE CONDITIONS						
FILE NAME	PEAK CONC. (%)	1% ARR. TIME (SEC)	PEAK TIME (SEC)	1% END TIME (SEC)	SUM (X-S)	X (M)	Y (M)	Z (M)	PEAK CONC. (%)	5% ARR. TIME (SEC)	10% ARR. TIME (SEC)	PEAK TIME (SEC)	10% END TIME (SEC)	5% END TIME (SEC)	SUM (X-S)
E01509	5.3	4.9	37.2	87.8	.82	15.0	-18.0	18.2	13.1	47.	182.	324.	417.	738.	18.72
C01509	5.9	5.7	25.3	94.6	.78	15.0	-18.0	18.2	14.5	72.	173.	221.	488.	738.	17.78
A01609	3.1	5.0	60.1	85.8	.22	15.0	-18.0	18.2	8.0	44.	0.	524.	0.	643.	4.94
A01709	2.9	12.1	40.8	76.7	.02	15.0	-18.0	18.2	2.6	188.	0.	356.	0.	520.	.42
E01108	3.7	8.8	21.6	93.2	1.98	15.0	-9.0	0.0	9.3	125.	0.	188.	0.	691.	44.99
A01108	3.2	12.6	23.2	86.3	1.62	15.0	-9.0	0.0	8.2	144.	0.	202.	0.	594.	36.78
C01108	4.1	10.2	24.5	94.7	1.88	15.0	-9.0	0.0	10.4	120.	212.	213.	215.	669.	42.78
A01208	5.8	9.9	23.6	87.2	1.97	15.0	-9.0	4.6	14.2	169.	112.	206.	441.	650.	44.40
E01208	4.9	6.3	17.3	95.2	1.98	15.0	-9.0	4.6	12.7	81.	149.	151.	405.	692.	44.79
A01208	7.4	5.1	19.6	87.9	1.58	15.0	-9.0	4.6	17.8	101.	159.	171.	499.	655.	44.63
C01308	7.8	4.4	22.4	82.0	1.78	15.0	-9.0	9.1	18.6	39.	127.	193.	423.	672.	40.19
A01308	7.0	6.7	18.2	92.0	2.04	15.0	-9.0	9.1	16.8	62.	78.	159.	475.	694.	46.02
E01308	9.0	6.1	24.8	86.9	1.89	15.0	-9.0	9.1	21.0	53.	187.	213.	421.	674.	42.73
A01408	7.6	3.9	228.4	91.9	1.62	15.0	-9.0	13.6	18.1	33.	91.	248.	442.	689.	36.71
C01408	9.9	4.6	229.9	94.3	1.51	15.0	-9.0	13.6	21.9	40.	135.	200.	489.	692.	34.24
E01408	7.8	4.9	15.5	85.6	1.50	15.0	-9.0	13.6	18.6	48.	67.	135.	488.	699.	34.15
A01508	5.7	4.3	24.6	85.1	.84	15.0	-9.0	19.9	14.1	38.	183.	215.	341.	670.	21.40
E01508	4.4	6.7	21.0	93.1	.94	15.0	-9.0	18.9	11.0	60.	183.	183.	416.	663.	19.30
A01508	4.6	7.0	55.2	93.8	.89	15.0	-9.0	19.9	11.6	61.	446.	482.	506.	723.	20.35
E01408	3.9	4.6	42.1	88.4	.34	15.0	-9.0	8.6	48.	0.	0.	367.	0.	657.	7.74
A01708	3.2	5.6	24.1	83.7	.07	15.0	-9.0	8.6	9.1	131.	0.	210.	0.	597.	1.54
E01107	5.8	9.3	37.4	87.9	1.75	15.0	-9.0	0.0	5.1	142.	0.	343.	0.	616.	40.62
A01107	9.4	9.4	39.4	87.9	1.09	15.0	-9.0	0.0	9.9	128.	0.	255.	0.	651.	47.39
C01167	8.7	8.4	26.6	94.5	1.91	15.0	-9.0	0.0	9.5	116.	0.	246.	0.	653.	43.90
A01207	4.7	9.7	24.7	87.8	1.99	15.0	-9.0	4.4	11.7	104.	151.	212.	304.	653.	44.90
E01307	5.0	8.5	33.4	87.9	1.63	15.0	-9.0	4.4	12.4	101.	205.	291.	347.	653.	43.71
A01207	4.6	9.9	33.3	91.3	1.95	15.0	-9.0	4.4	11.6	87.	146.	197.	263.	725.	44.51
E01307	5.8	4.4	35.6	85.1	1.77	15.0	-9.0	5.9	14.2	97.	177.	293.	394.	649.	40.12
A01307	5.1	4.2	17.9	82.3	1.73	15.0	-9.0	9.1	15.0	77.	117.	156.	392.	638.	39.09
E01407	7.9	4.3	31.0	90.8	1.87	15.0	-9.0	9.1	14.6	56.	116.	270.	311.	723.	42.92
A01407	7.1	4.6	31.9	92.8	1.33	15.0	-9.0	13.6	10.0	40.	114.	191.	358.	688.	30.99
E01407	6.5	4.1	31.4	86.8	1.29	15.0	-9.0	13.6	15.8	41.	168.	274.	341.	694.	29.46
A01407	6.8	5.8	15.0	97.4	1.46	15.0	-9.0	13.6	14.4	51.	124.	131.	540.	688.	33.24
E01507	5.2	7.9	9.5	89.2	.55	15.0	-9.0	18.2	12.9	82.	83.	83.	144.	729.	11.78
A01507	4.2	7.8	19.0	94.1	.67	15.0	-9.0	18.2	10.6	82.	144.	83.	144.	729.	11.78
E01507	4.8	5.0	39.6	88.4	.59	15.0	-9.0	18.2	11.9	70.	167.	345.	345.	641.	13.54
A01407	3.3	10.9	49.9	89.1	.22	15.0	-9.0	18.2	8.5	114.	0.	400.	0.	640.	4.98
E01707	2.6	5.6	63.6	87.1	.09	15.0	-9.0	18.2	6.7	130.	0.	554.	0.	680.	2.14
A01C14	.1	0.0	9.9	0.0	0.00	75.0	-126.0	0.0	.4	0.	0.	86.	0.	0.	.11
A01C13	.2	0.0	98.0	0.0	.05	75.0	-117.0	0.0	.5	0.	0.	854.	0.	0.	1.11
A01C12	.2	0.0	92.4	0.0	.06	75.0	-108.0	0.0	.4	0.	0.	805.	0.	0.	1.38
A01C11	.1	0.0	9.1	0.0	0.00	75.0	-99.0	0.0	.3	0.	0.	79.	0.	0.	.01
A01C10	.2	0.0	60.3	0.0	.06	75.0	-90.0	0.0	.6	0.	0.	526.	0.	0.	1.36
A01C09	.3	0.0	25.9	0.0	-.03	75.0	-81.0	0.0	.8	0.	0.	226.	0.	0.	.60
A01C08	.3	24.8	25.1	37.0	.10	75.0	-72.0	0.0	.9	0.	0.	219.	0.	0.	.21
E01814	2.3	20.1	234.8	61.1	.47	75.0	-63.0	0.0	6.0	185.	0.	217.	0.	235.	10.92
A01814	2.4	19.1	237.3	45.9	.50	75.0	-63.0	0.0	6.0	194.	0.	238.	0.	286.	11.46
C01814	2.3	18.2	237.8	56.5	.58	75.0	-63.0	0.0	6.0	202.	0.	242.	0.	340.	13.45

RUN NUMBER 01

MODEL CONDITIONS						PHOTOTYPE CONDITIONS									
FILE NAME	PEAK CONC. (%)	1% ARR. TIME (SEC)	PEAK TIME (SEC)	1% END TIME (SEC)	SUM (X-S)	X (H)	POSITION Y (H)	Z (H)	PEAK CONC. (%)	5% ARR. TIME (SEC)	10% ARR. TIME (SEC)	PEAK TIME (SEC)	10% END TIME (SEC)	5% END TIME (SEC)	SUM (X-S)
A01C07	0.8	19.7	44.3	48.7	.44	0.0	0.0	0.0	1.1	23.3	0.0	386.0	0.0	393.3	10.08
A01914	0.0	19.3	37.9	63.7	.13	0.0	0.0	0.0	0.0	39.3	0.0	386.0	0.0	393.3	10.08
F01914	0.0	21.0	44.6	49.7	.11	0.0	0.0	0.0	0.0	44.6	0.0	389.0	0.0	444.4	10.08
F01914	0.0	19.1	23.0	50.6	.15	0.0	0.0	0.0	0.0	23.0	0.0	200.0	0.0	204.4	5.39
A01A14	0.4	0.0	0.0	0.0	.03	0.0	0.0	0.0	0.0	0.0	0.0	181.0	0.0	0.0	7.71
F01A14	1.0	33.2	33.3	33.3	.01	0.0	0.0	0.0	0.0	33.2	0.0	389.0	0.0	0.0	7.24
C01A14	0.8	0.0	0.0	0.0	.05	0.0	0.0	0.0	0.0	0.0	0.0	330.0	0.0	0.0	1.20
A01B14	0.1	0.0	1231.9	0.0	-.01	0.0	0.0	0.0	0.0	0.0	0.0	1064.0	0.0	0.0	2.88
A01B13	0.6	16.0	34.5	68.9	.87	0.0	0.0	0.0	0.0	17.3	0.0	314.0	0.0	4.0	20.09
F01B13	0.6	16.0	35.5	71.8	.74	0.0	0.0	0.0	0.0	16.0	0.0	331.0	0.0	4.0	17.08
C01B13	0.7	17.3	35.8	58.3	.87	0.0	0.0	0.0	0.0	17.3	0.0	335.0	0.0	4.0	19.98
A01913	0.5	17.2	26.2	62.3	.27	0.0	0.0	0.0	0.0	17.2	0.0	339.0	0.0	4.0	6.39
F01913	0.5	20.3	39.7	63.3	.37	0.0	0.0	0.0	0.0	20.3	0.0	346.0	0.0	4.0	6.25
C01913	0.7	18.5	37.7	58.3	.35	0.0	0.0	0.0	0.0	18.5	0.0	340.0	0.0	4.0	5.75
F01A13	1.1	21.8	37.3	37.3	.03	0.0	0.0	0.0	0.0	21.8	0.0	335.0	0.0	0.0	6.69
F01A13	1.1	24.0	44.0	29.8	.03	0.0	0.0	0.0	0.0	24.0	0.0	309.0	0.0	0.0	6.69
A01A13	0.7	0.0	44.1	0.0	.03	0.0	0.0	0.0	0.0	0.0	0.0	385.0	0.0	0.0	8.81
A01B13	0.2	0.0	83.1	0.0	.03	0.0	0.0	0.0	0.0	0.0	0.0	725.0	0.0	0.0	6.62
A01B12	0.8	14.9	34.4	74.2	1.17	0.0	0.0	0.0	0.0	14.9	0.0	313.0	0.0	4.0	26.74
F01B12	0.8	14.9	35.7	75.3	1.15	0.0	0.0	0.0	0.0	14.9	0.0	333.0	0.0	4.0	26.24
A01B12	0.8	13.5	34.8	73.1	1.12	0.0	0.0	0.0	0.0	13.5	0.0	317.0	0.0	4.0	25.59
A01912	0.2	15.6	15.8	81.1	.37	0.0	0.0	0.0	0.0	15.6	0.0	138.0	0.0	0.0	8.72
F01912	0.8	15.3	16.9	80.8	.36	0.0	0.0	0.0	0.0	15.3	0.0	234.0	0.0	4.0	8.48
C01912	0.2	16.3	16.3	82.4	.36	0.0	0.0	0.0	0.0	16.3	0.0	439.0	0.0	5.0	8.28
F01A12	1.1	19.5	35.5	39.9	.66	0.0	0.0	0.0	0.0	19.5	0.0	357.0	0.0	0.0	1.40
A01A12	0.9	0.0	0.0	0.0	.64	0.0	0.0	0.0	0.0	0.0	0.0	192.0	0.0	0.0	1.95
A01B12	0.4	0.0	111.1	0.0	.01	0.0	0.0	0.0	0.0	0.0	0.0	110.0	0.0	0.0	7.21
A01B11	0.9	14.9	34.6	74.5	1.12	0.0	0.0	0.0	0.0	14.9	0.0	214.0	0.0	0.0	28.75
F01B11	0.8	14.0	34.4	75.5	1.12	0.0	0.0	0.0	0.0	14.0	0.0	191.0	0.0	0.0	28.47
F01B11	0.8	12.9	34.4	73.9	1.12	0.0	0.0	0.0	0.0	12.9	0.0	215.0	0.0	0.0	31.18
F01911	0.4	12.4	32.8	61.9	.49	0.0	0.0	0.0	0.0	12.4	0.0	233.0	0.0	1.0	11.38
C01911	0.4	13.2	32.8	73.8	.45	0.0	0.0	0.0	0.0	13.2	0.0	182.0	0.0	1.0	10.37
A01911	0.0	13.7	32.0	86.6	.50	0.0	0.0	0.0	0.0	13.7	0.0	218.0	0.0	1.0	12.97
A01A11	0.4	13.1	32.1	82.9	.51	0.0	0.0	0.0	0.0	13.1	0.0	250.0	0.0	1.0	12.12
C01A11	0.7	11.7	34.6	78.9	.61	0.0	0.0	0.0	0.0	11.7	0.0	338.0	0.0	2.0	2.47
F01A11	0.4	12.7	33.0	66.4	.60	0.0	0.0	0.0	0.0	12.7	0.0	375.0	0.0	3.0	1.25
A01B11	1.6	0.0	0.0	0.0	-.01	0.0	0.0	0.0	0.0	0.0	0.0	713.0	0.0	0.0	1.47
A01B10	0.9	15.5	35.3	83.4	1.12	0.0	0.0	0.0	0.0	15.5	0.0	197.0	0.0	0.0	31.91
F01B10	0.8	14.6	35.3	79.4	1.12	0.0	0.0	0.0	0.0	14.6	0.0	237.0	0.0	0.0	31.76
C01B10	0.8	13.0	34.1	79.1	1.12	0.0	0.0	0.0	0.0	13.0	0.0	210.0	0.0	0.0	33.25
C01910	0.0	11.1	33.3	79.9	.66	0.0	0.0	0.0	0.0	11.1	0.0	186.0	0.0	0.0	18.07
F01910	0.7	7.7	37.7	87.7	.79	0.0	0.0	0.0	0.0	7.7	0.0	217.0	0.0	0.0	21.17
F01A10	0.8	12.2	34.9	89.9	.88	0.0	0.0	0.0	0.0	12.2	0.0	233.0	0.0	1.0	17.48
A01A10	0.0	12.2	34.9	89.9	.88	0.0	0.0	0.0	0.0	12.2	0.0	334.0	0.0	0.0	17.48
F01A10	0.0	11.1	33.3	88.7	.81	0.0	0.0	0.0	0.0	11.1	0.0	357.0	0.0	0.0	4.13
F01A10	0.0	11.1	33.3	88.7	.81	0.0	0.0	0.0	0.0	11.1	0.0	357.0	0.0	0.0	3.74
A01B10	0.0	18.0	69.1	18.4	-.11	0.0	0.0	0.0	0.0	18.0	0.0	451.0	0.0	0.0	3.53
A01B09	0.0	14.7	33.8	85.8	1.42	0.0	0.0	0.0	0.0	14.7	0.0	196.0	0.0	0.0	32.51

RUN NUMBER 01

MODEL CONDITIONS						PROTOTYPE CONDITIONS									
FILE NAME	PEAK CONC. (%)	1% ARR. TIME (SEC)	PEAK TIME (SEC)	1% END TIME (SEC)	SUM (X-S)	X (M)	POSITION Y (M)	Z (M)	PEAK CONC. (%)	5% ARR. TIME (SEC)	10% ARR. TIME (SEC)	PEAK TIME (SEC)	10% END TIME (SEC)	5% END TIME (SEC)	SUM (X-S)
R01B09	2.9	14.6	26.9	82.6	1.46	75.0	-18.0	0.0	7.5	146.	0.	234.	0.	559.	33.26
C01B09	3.1	13.1	28.1	80.2	1.46	75.0	-18.0	0.0	7.9	157.	0.	245.	0.	525.	33.37
R01B09	3.6	11.6	25.8	70.2	.94	75.0	-18.0	9.1	9.1	120.	0.	225.	0.	516.	31.47
A01B09	3.7	7.5	24.5	82.2	1.03	75.0	-18.0	9.1	9.3	131.	0.	214.	0.	581.	23.72
C01B09	4.6	11.7	24.2	76.3	.93	75.0	-18.0	9.1	9.3	132.	0.	211.	0.	537.	21.36
R01A09	12.4	39.9	83.4	.25	.25	75.0	-18.0	18.2	7.2	130.	0.	348.	0.	558.	5.69
A01A09	6.7	43.1	86.4	.25	.25	75.0	-18.0	18.2	6.5	204.	0.	376.	0.	579.	5.64
R01A09	12.7	48.8	87.8	.24	.24	75.0	-18.0	18.2	6.4	180.	0.	425.	0.	536.	5.50
A01E09	13.0	18.0	79.2	-.03	-.03	75.0	-18.0	27.3	5.7	157.	0.	157.	0.	158.	-1.71
C01B08	13.8	28.3	74.6	1.31	1.31	75.0	-9.0	0.0	7.7	158.	0.	247.	0.	524.	29.87
R01B08	14.0	26.8	79.3	1.36	1.36	75.0	-9.0	0.0	7.2	146.	0.	233.	0.	558.	31.15
A01B08	14.4	22.9	84.8	1.41	1.41	75.0	-9.0	0.0	7.3	158.	0.	200.	0.	528.	32.34
R01B08	7.7	29.8	79.6	.85	.85	75.0	-9.0	9.1	8.4	129.	0.	260.	0.	494.	21.75
A01B08	11.9	23.1	69.9	.94	.94	75.0	-9.0	9.1	7.6	121.	0.	202.	0.	515.	21.52
C01B08	11.4	27.2	78.1	.89	.89	75.0	-9.0	9.1	7.8	138.	0.	237.	0.	478.	20.54
R01A08	12.4	30.1	77.2	.33	.33	75.0	-9.0	18.2	7.7	138.	0.	262.	0.	506.	7.60
C01A08	12.7	24.7	77.1	.28	.28	75.0	-9.0	18.2	6.4	148.	0.	216.	0.	522.	6.31
A01A08	10.8	23.0	83.0	.33	.33	75.0	-9.0	18.2	6.6	94.	0.	260.	0.	506.	7.50
A01E08	12.9	42.4	78.9	-.05	-.05	75.0	-9.0	27.3	5.3	34.	0.	370.	0.	577.	-1.21
R01B07	15.2	23.0	83.2	1.39	1.39	75.0	0.0	0.0	7.7	150.	0.	261.	0.	542.	31.83
C01B07	14.2	22.3	81.5	1.39	1.39	75.0	0.0	0.0	7.5	158.	0.	202.	0.	523.	31.72
R01B07	14.7	31.8	82.7	1.44	1.44	75.0	0.0	0.0	7.1	146.	0.	277.	0.	639.	32.86
R01B07	6.4	4.4	70.7	.99	.99	75.0	0.0	0.0	8.7	134.	0.	223.	0.	543.	22.62
A01B07	9.0	9.8	83.8	1.00	1.00	75.0	0.0	0.0	7.9	128.	0.	260.	0.	654.	22.94
C01B07	12.8	26.6	81.1	1.09	1.09	75.0	0.0	0.0	7.4	142.	0.	228.	0.	534.	24.97
R01A07	6.8	27.7	80.8	.37	.37	75.0	0.0	0.0	7.5	149.	0.	249.	0.	474.	8.60
A01A07	13.6	25.5	73.2	.33	.33	75.0	0.0	0.0	7.1	149.	0.	220.	0.	520.	7.59
C01A07	11.1	34.3	76.6	-.26	-.26	75.0	0.0	0.0	7.1	150.	0.	212.	0.	566.	-6.61
R01E07	16.1	34.4	78.1	-.08	-.08	75.0	0.0	0.0	6.0	204.	0.	204.	0.	578.	-1.55
A01H14	0.0	0.0	100.0	0.0	0.0	0.0	-12.0	0.0	7.7	0.	0.	0.	0.	0.	1.93
R01H13	0.0	40.9	0.0	0.0	0.0	0.0	-11.7	0.0	5.5	0.	0.	0.	0.	0.	1.37
A01H11	1.9	28.5	30.8	32.2	.11	0.0	-90.0	0.0	5.4	0.	0.	0.	0.	0.	2.68
A01H10	1.1	14.6	31.3	37.5	.43	0.0	-90.0	0.0	5.4	0.	0.	0.	0.	0.	15.01
A01H09	3.3	11.8	26.4	56.0	.66	0.0	-81.0	0.0	5.9	0.	0.	0.	0.	0.	33.77
A01H08	3.3	8.8	31.7	54.6	.74	0.0	-72.0	0.0	5.9	0.	0.	0.	0.	0.	17.04
A01H14	3.3	31.1	30.8	64.0	.91	0.0	-63.0	0.0	5.8	0.	0.	0.	0.	0.	20.97
R01B14	0.4	32.8	68.0	.90	.90	0.0	-63.0	0.0	5.8	0.	0.	0.	0.	0.	35.77
C01D14	3.1	2.2	31.6	65.7	.90	0.0	-63.0	0.0	5.4	0.	0.	0.	0.	0.	35.77
A01H07	3.1	1.0	31.6	64.7	.87	0.0	-63.0	0.0	6.4	0.	0.	0.	0.	0.	383.
A01E14	1.1	18.5	28.2	59.7	.23	0.0	-63.0	9.1	5.4	0.	0.	0.	0.	0.	399.
R01E14	3.3	20.5	40.3	62.0	.26	0.0	-63.0	9.1	6.0	0.	0.	0.	0.	0.	552.
A01F14	1.3	26.8	30.0	37.0	.06	0.0	-63.0	18.2	3.3	0.	0.	0.	0.	0.	1.32
R01F14	.9	0.0	60.6	0.0	.05	0.0	-63.0	0.0	1.5	0.	0.	0.	0.	0.	0.
A01G14	.7	0.0	55.7	0.0	.03	0.0	-63.0	27.3	1.8	0.	0.	0.	0.	0.	1.71
C01D13	2.3	20.2	30.4	69.5	1.00	0.0	-54.0	0.0	5.9	0.	0.	0.	0.	0.	22.93
A01D13	3.0	3.4	31.6	70.7	.99	0.0	-54.0	0.0	5.8	0.	0.	0.	0.	0.	21.85
R01D13	3.0	5.5	31.6	70.4	.94	0.0	-54.0	0.0	5.8	0.	0.	0.	0.	0.	21.52
A01E13	2.1	17.3	28.2	69.7	.28	0.0	-54.0	9.1	5.5	0.	0.	0.	0.	0.	6.52

RUN NUMBER 01

MODEL CONDITIONS						PROTOTYPE CONDITIONS									
FILE NAME	PEAK CONC. (%)	1% ARR. TIME (SEC)	PEAK TIME (SEC)	1% END TIME (SEC)	SUM (X-S)	X (M)	POSITION Y (M)	Z (M)	PEAK CONC. (%)	5% ARR. TIME (SEC)	10% ARR. TIME (SEC)	PEAK TIME (SEC)	10% END TIME (SEC)	5% END TIME (SEC)	SUM (X-S)
BO1E13	2.1	21.6	33.7	66.3	.31	200.0	-54.0	9.1	5.5	197.	0.	294.	0.	352.	7.32
AO1F13	1.1	29.7	29.7	39.1	.08	000.0	-54.0	18.0	0.0	0.	0.	258.	0.	0.	1.75
RO1F13	1.1	25.7	25.7	32.6	.06	000.0	-54.0	18.0	0.0	0.	0.	254.	0.	0.	1.34
AO1G13	0.6	0.0	23.9	0.0	.04	000.0	-54.0	27.3	0.0	0.	0.	208.	0.	0.	0.87
AO1D13	1.1	19.0	31.7	70.0	1.03	000.0	-44.0	0.0	0.0	0.0	0.0	277.	0.	373.	3.59
CO1B13	0.0	0.0	30.0	68.0	.99	000.0	-44.0	0.0	0.0	0.0	0.0	244.	0.	405.	2.65
AO1E13	1.1	17.3	39.7	57.1	.79	000.0	-44.0	0.0	0.0	0.0	0.0	248.	0.	324.	2.99
AO1E12	1.0	19.2	36.6	65.8	.40	000.0	-44.0	9.1	0.0	0.0	0.0	246.	0.	412.	2.25
AO1F12	1.0	21.3	33.3	69.0	.09	000.0	-44.0	18.0	0.0	0.0	0.0	319.	0.	0.	2.17
AO1E12	1.0	20.3	33.3	70.0	.13	000.0	-44.0	0.0	0.0	0.0	0.0	290.	0.	291.	3.11
AO1D12	0.5	0.0	70.0	0.0	.06	000.0	-45.0	0.0	0.0	0.0	0.0	213.	0.	0.	1.49
AO1D11	0.3	20.3	33.3	70.0	.99	000.0	-36.0	0.0	0.0	0.0	0.0	211.	0.	348.	2.91
CO1B11	0.3	19.7	32.6	71.3	.49	000.0	-36.0	0.0	0.0	0.0	0.0	264.	0.	361.	2.81
EO1D11	0.3	19.7	31.6	74.7	1.00	000.0	-36.0	0.0	0.0	0.0	0.0	276.	0.	370.	3.06
AO1E11	0.4	16.7	40.0	72.3	.58	000.0	-36.0	9.1	0.0	0.0	0.0	248.	0.	509.	1.53
EO1E11	0.4	17.6	30.7	71.0	.43	000.0	-36.0	9.1	0.0	0.0	0.0	268.	0.	302.	2.87
AO1F11	0.0	19.0	36.7	71.0	.20	000.0	-36.0	18.0	0.0	0.0	0.0	320.	0.	321.	4.64
EO1F11	0.0	19.9	22.2	73.7	.13	000.0	-36.0	18.0	0.0	0.0	0.0	194.	0.	334.	3.10
AO1G11	0.8	0.0	60.0	0.0	-.02	000.0	-36.0	27.3	0.0	0.0	0.0	223.	0.	0.	1.56
AO1D10	1.1	20.0	34.8	65.5	.68	000.0	-37.0	0.0	0.0	0.0	0.0	303.	0.	351.	2.93
CO1B10	0.3	20.0	31.8	64.8	.86	000.0	-37.0	0.0	0.0	0.0	0.0	277.	0.	356.	19.93
EO1H10	0.1	20.7	31.2	72.4	.89	000.0	-37.0	0.0	0.0	0.0	0.0	272.	0.	360.	20.55
EO1E10	0.4	18.8	35.0	72.5	.39	000.0	-37.0	9.1	0.0	0.0	0.0	305.	0.	383.	8.92
AO1E10	0.1	18.9	32.9	69.1	.47	000.0	-37.0	9.1	0.0	0.0	0.0	287.	0.	350.	10.92
AO1F10	0.7	19.0	36.8	70.9	.12	000.0	-37.0	18.0	0.0	0.0	0.0	321.	0.	321.	12.71
EO1F10	0.7	19.8	37.9	69.7	.06	000.0	-37.0	18.0	0.0	0.0	0.0	343.	0.	0.	1.43
AO1G10	1.5	53.0	64.7	64.9	-.01	000.0	-37.0	0.0	0.0	0.0	0.0	264.	0.	0.	1.33
AO1D09	0.1	19.1	33.8	72.0	.93	000.0	-18.0	0.0	0.0	0.0	0.0	325.	0.	354.	21.39
RO1D09	0.0	0.0	31.8	70.0	.89	000.0	-18.0	0.0	0.0	0.0	0.0	328.	0.	353.	20.44
CO1B09	0.1	11.1	31.6	68.0	.84	000.0	-18.0	0.0	0.0	0.0	0.0	350.	0.	338.	19.35
AO1E09	0.3	18.0	39.4	73.6	.47	000.0	-18.0	9.1	0.0	0.0	0.0	366.	0.	389.	10.79
EO1E09	0.3	16.9	35.3	72.6	.50	000.0	-18.0	9.1	0.0	0.0	0.0	307.	0.	385.	11.44
EO1F09	0.0	16.4	37.7	71.0	.06	000.0	-18.0	18.0	0.0	0.0	0.0	343.	0.	243.	1.32
AO1F09	0.1	18.0	37.7	70.2	.11	000.0	-18.0	18.0	0.0	0.0	0.0	177.	0.	506.	2.52
AO1G09	0.4	15.5	34.4	65.4	-.02	000.0	-18.0	27.3	0.0	0.0	0.0	266.	0.	0.	1.44
AO1H08	0.1	22.0	34.4	65.5	.76	000.0	-9.0	0.0	0.0	0.0	0.0	301.	0.	307.	17.93
CO1D08	0.1	22.0	32.9	73.0	.84	000.0	-9.0	0.0	0.0	0.0	0.0	250.	0.	351.	19.46
EO1H08	0.1	22.1	31.4	71.7	.91	000.0	-9.0	0.0	0.0	0.0	0.0	274.	0.	293.	21.00
AO1E08	0.5	18.0	40.6	68.6	.39	000.0	-9.0	9.1	0.0	0.0	0.0	344.	0.	465.	9.12
EO1E08	0.5	16.6	36.6	69.9	.44	000.0	-9.0	9.1	0.0	0.0	0.0	325.	0.	326.	10.16
EO1F08	0.1	19.9	36.6	62.9	.12	000.0	-9.0	18.0	0.0	0.0	0.0	377.	0.	0.	2.70
AO1F08	0.1	19.4	32.1	62.2	.09	000.0	-9.0	18.0	0.0	0.0	0.0	337.	0.	330.	2.08
AO1G08	0.1	0.0	39.4	59.9	-.03	000.0	-9.0	27.3	0.0	0.0	0.0	218.	0.	0.	1.64
CO1D07	0.2	21.1	32.1	69.9	.97	000.0	0.0	0.0	0.0	0.0	0.0	224.	0.	370.	22.41
AO1H07	0.0	21.0	34.6	74.0	.90	000.0	0.0	0.0	0.0	0.0	0.0	272.	0.	397.	20.82
EO1H07	0.0	21.1	31.0	71.8	.88	000.0	0.0	0.0	0.0	0.0	0.0	219.	0.	360.	20.22
RO1E07	0.3	16.7	27.9	72.0	.56	000.0	0.0	9.1	0.0	0.0	0.0	209.	0.	387.	13.02
AO1E07	0.2	18.7	29.3	67.9	.50	000.0	0.0	9.1	0.0	0.0	0.0	256.	0.	385.	11.63

RUN NUMBER 01

MODEL CONDITIONS						POSITION			PROTOTYPE CONDITIONS						
FILE NAME	PEAK CONC. (%)	1% ARR. TIME (SEC)	PEAK TIME (SEC)	1% END TIME (SEC)	SUM (X-S)	X (M)	Y (M)	Z (M)	PEAK CONC. (%)	5% ARR. TIME (SEC)	10% ARR. TIME (SEC)	PEAK TIME (SEC)	10% END TIME (SEC)	5% END TIME (SEC)	SUM (X-S)
B01F07	2.0	15.4	36.4	63.7	.13	200.0	0.0	18.0	5.1	270.0	0.0	317.0	0.0	317.0	3.05
A01F07	2.0	19.4	30.8	65.7	.13	200.0	0.0	18.0	5.1	241.0	0.0	288.0	0.0	331.0	2.94
A01G07	1.3	20.3	59.3	64.8	.02	200.0	0.0	18.0	5.1	0.0	0.0	517.0	0.0	0.0	1.36
A01K14	1.6	0.0	37.7	0.0	.06	400.0	-126.0	0.0	1.7	0.0	0.0	339.0	0.0	0.0	1.31
A01K13	1.1	36.1	36.8	37.7	-.06	400.0	-117.0	0.0	3.0	0.0	0.0	321.0	0.0	0.0	-1.45
A01K11	1.7	32.4	37.6	54.7	.49	400.0	-99.0	0.0	4.5	0.0	0.0	328.0	0.0	0.0	11.40
A01K10	1.7	32.5	47.1	53.4	.53	400.0	-90.0	0.0	4.4	0.0	0.0	410.0	0.0	0.0	12.33
A01K09	1.6	31.1	45.4	54.4	.61	400.0	-81.0	0.0	4.1	0.0	0.0	326.0	0.0	0.0	14.16
A01K08	1.5	31.6	43.3	70.1	.67	400.0	-72.0	0.0	4.0	0.0	0.0	377.0	0.0	0.0	15.50
A01I14	1.5	28.8	41.2	55.7	.61	400.0	-63.0	0.0	4.1	0.0	0.0	359.0	0.0	0.0	14.06
R01I14	1.6	30.1	37.7	69.4	.66	400.0	-53.0	0.0	4.3	0.0	0.0	328.0	0.0	0.0	15.39
C01I14	1.7	28.5	41.1	74.8	.75	400.0	-43.0	0.0	4.5	0.0	0.0	358.0	0.0	0.0	17.45
A01K07	1.6	30.7	43.1	59.4	.65	400.0	-43.0	0.0	4.2	0.0	0.0	374.0	0.0	0.0	15.18
A01J14	1.0	56.7	56.7	56.7	.19	400.0	-43.0	18.0	0.0	0.0	0.0	494.0	0.0	0.0	4.42
A01I13	1.4	29.2	35.5	63.7	.58	400.0	-43.0	0.0	4.2	0.0	0.0	318.0	0.0	0.0	13.58
R01I13	1.4	30.0	35.8	57.9	.60	400.0	-34.0	0.0	4.4	0.0	0.0	313.0	0.0	0.0	13.90
C01I13	1.5	30.4	40.4	62.9	.58	400.0	-24.0	0.0	4.1	0.0	0.0	353.0	0.0	0.0	15.76
A01J13	1.2	27.4	42.7	53.2	.17	400.0	-15.0	18.0	0.0	0.0	0.0	272.0	0.0	0.0	2.95
R01I12	1.2	29.9	30.5	65.2	.59	400.0	-15.0	0.0	4.2	0.0	0.0	266.0	0.0	0.0	13.63
A01I12	1.5	30.5	36.4	63.7	.56	400.0	-15.0	0.0	4.2	0.0	0.0	317.0	0.0	0.0	13.09
C01I12	1.4	31.2	41.7	55.7	.52	400.0	-15.0	0.0	4.3	0.0	0.0	344.0	0.0	0.0	11.94
A01J12	1.3	69.0	69.0	69.0	.07	400.0	-15.0	18.0	0.0	0.0	0.0	602.0	0.0	0.0	1.74
R01I11	1.2	35.1	36.6	56.1	.59	400.0	-15.0	0.0	4.5	0.0	0.0	319.0	0.0	0.0	13.75
C01I11	1.3	30.8	44.6	61.2	.60	400.0	-15.0	0.0	4.5	0.0	0.0	329.0	0.0	0.0	13.88
A01I11	1.5	30.7	35.3	63.5	.56	400.0	-15.0	0.0	4.1	0.0	0.0	316.0	0.0	0.0	12.88
A01J11	1.2	53.0	53.0	53.1	.16	400.0	-15.0	18.0	0.0	0.0	0.0	422.0	0.0	0.0	3.71
C01I10	1.3	33.9	45.0	55.1	.56	400.0	-15.0	0.0	4.5	0.0	0.0	323.0	0.0	0.0	12.84
A01I10	1.3	31.2	34.0	44.9	.56	400.0	-15.0	0.0	4.6	0.0	0.0	326.0	0.0	0.0	11.56
R01I10	1.2	31.2	35.4	42.2	.55	400.0	-15.0	0.0	4.7	0.0	0.0	329.0	0.0	0.0	12.82
A01J10	1.0	0.0	62.8	0.0	.01	400.0	-15.0	18.0	0.0	0.0	0.0	554.0	0.0	0.0	1.14
R01I09	1.1	33.3	33.3	42.2	.48	400.0	-18.0	0.0	4.8	0.0	0.0	291.0	0.0	0.0	11.21
A01I09	1.2	30.9	43.2	44.9	.53	400.0	-18.0	0.0	4.8	0.0	0.0	295.0	0.0	0.0	12.20
C01I09	1.3	30.8	45.0	55.0	.59	400.0	-18.0	0.0	4.9	0.0	0.0	323.0	0.0	0.0	13.67
A01J09	1.3	30.1	30.0	62.7	.51	400.0	-18.0	18.0	0.0	0.0	0.0	323.0	0.0	0.0	11.27
C01I08	1.3	33.2	35.5	55.5	.56	400.0	-19.0	0.0	5.0	0.0	0.0	317.0	0.0	0.0	13.02
R01I08	1.2	33.6	33.6	43.6	.57	400.0	-19.0	0.0	5.0	0.0	0.0	324.0	0.0	0.0	8.65
A01I08	1.3	30.6	33.3	44.7	.57	400.0	-19.0	0.0	5.0	0.0	0.0	324.0	0.0	0.0	13.25
A01J08	1.2	30.0	33.3	59.6	.52	400.0	-19.0	18.0	0.0	0.0	0.0	298.0	0.0	0.0	11.37
C01I07	1.2	32.4	35.5	49.8	.51	400.0	-19.0	0.0	5.1	0.0	0.0	326.0	0.0	0.0	11.90
R01I07	1.3	30.1	30.1	44.4	.58	400.0	-19.0	0.0	5.1	0.0	0.0	328.0	0.0	0.0	13.48
A01J07	1.4	30.0	44.5	45.9	.56	400.0	-19.0	18.0	0.0	0.0	0.0	320.0	0.0	0.0	11.12

RUN NUMBER 02

FILE NAME	MODEL CONDITIONS					POSITION			PROTOTYPE CONDITIONS						
	PEAK CONC. (%)	1% ARR. TIME (SEC)	PEAK TIME (SEC)	1% END TIME (SEC)	SUM (X-S)	X (M)	Y (M)	Z (M)	PEAK CONC. (%)	5% ARR. TIME (SEC)	10% ARR. TIME (SEC)	PEAK TIME (SEC)	10% END TIME (SEC)	5% END TIME (SEC)	SUM (X-S)
A02014	.3	0.0	45.9	0.0	0.00	15.0	-126.0	0.0	.8	0.	0.	400.	0.	0.	-2.54
A02013	.2	0.0	36.0	0.0	.07	15.0	-117.0	0.0	.6	0.	0.	314.	0.	0.	-1.12
A02012	.0	0.0	59.0	0.0	.03	15.0	-108.0	0.0	.4	0.	0.	514.	0.	0.	-1.92
A02009	.1	0.0	45.7	0.0	-0.03	15.0	-81.0	0.0	0.	0.	0.	2143.	0.	0.	-1.96
A02008	.0	0.0	48.0	0.0	.09	15.0	-82.0	0.0	0.	0.	0.	418.	0.	0.	-1.99
A02114	2	1.7	49.8	107.7	1.45	15.0	-83.0	0.0	5.4	426.	0.	434.	0.	532.	33.55
B02114	1	1.7	35.9	78.8	.44	15.0	-83.0	0.0	0.0	0.0	0.0	3113.	0.	0.	10.30
A02007	1	1.3	31.5	53.1	.45	15.0	-83.0	0.0	0.0	0.0	0.0	2733.	0.	0.	9.51
A02214	1	1.6	23.6	116.1	.56	15.0	-83.0	4.6	4.8	0.0	0.0	2233.	0.	0.	13.15
A02314	1	1.5	23.8	88.	.54	15.0	-83.0	9.1	3.9	0.0	0.0	3333.	0.	0.	5.54
F02314	1	1.1	39.3	57.7	.35	15.0	-83.0	0.0	0.0	0.0	0.0	3473.	0.	0.	8.21
A02314	1	1.1	30.8	0.0	.14	15.0	-83.0	0.0	0.0	0.0	0.0	443.	0.	0.	3.30
A022514	1	1.0	73.0	0.0	.07	15.0	-83.0	0.0	0.0	0.0	0.0	637.	0.	0.	1.69
F022514	1	1.4	66.4	0.0	.04	15.0	-83.0	0.0	0.0	0.0	0.0	579.	0.	0.	-1.46
A022614	1	1.3	49.7	0.0	.09	15.0	-83.0	0.0	1.1	0.0	0.0	347.	0.	0.	2.00
A022714	1	1.1	33.8	0.0	.06	15.0	-83.0	0.0	0.0	0.0	0.0	643.	0.	0.	-1.88
F0221113	1	1.1	33.3	122.	1.82	15.0	-83.0	0.0	0.0	221.	0.	0.	0.	429.	42.12
F0221113	1	1.1	34.3	140.	1.45	15.0	-83.0	0.0	0.0	0.	0.	3222.	0.	0.	34.51
F0221113	1	1.1	34.3	158.	1.36	15.0	-83.0	0.0	0.0	0.	0.	747.	0.	0.	30.22
F0221113	1	1.1	34.3	175.	1.25	15.0	-83.0	0.0	0.0	0.	0.	579.	0.	0.	12.23
F0221113	1	1.1	34.3	105.	1.15	15.0	-83.0	0.0	0.0	0.	0.	3333.	0.	0.	9.30
A022414	1	1.2	26.1	100.	.44	15.0	-83.0	0.0	0.0	226.	0.	0.	0.	228.	5.12
F022414	1	1.0	27.0	0.0	.20	15.0	-83.0	0.0	0.0	0.	0.	6225.	0.	0.	-1.65
F022414	1	1.0	27.0	0.0	.04	15.0	-83.0	0.0	0.0	0.	0.	714.	0.	0.	0.85
F022414	1	1.1	26.6	17.	.04	15.0	-83.0	0.0	0.0	0.	0.	211.	0.	0.	0.29
F022414	1	1.1	26.6	13.	.08	15.0	-83.0	0.0	0.0	0.	0.	114.	0.	0.	5.08
F022414	1	1.1	26.6	13.	.44	15.0	-83.0	0.0	0.0	208.	0.	0.	0.	111.	41.57
F022414	1	1.1	26.6	19.	.66	15.0	-83.0	0.0	0.0	0.	0.	0.	0.	0.	759.
F022414	1	1.1	26.6	18.	.66	15.0	-83.0	0.0	0.0	0.	0.	0.	0.	0.	249.
F022414	1	1.1	26.6	18.	.66	15.0	-83.0	0.0	0.0	0.	0.	0.	0.	0.	14.98
A023414	1	1.4	44.3	90.	.88	15.0	-83.0	0.0	0.0	0.	0.	382.	0.	0.	6.51
A023514	1	1.1	35.4	0.0	.07	15.0	-83.0	0.0	0.0	0.	0.	309.	0.	0.	5.56
A023111	4	4.4	33.6	16.	.44	15.0	-83.0	0.0	0.0	0.	0.	0.	0.	0.	5.98
F023111	4	4.4	33.6	180.	1.44	15.0	-83.0	0.0	10.	183.	208.	0.	208.	123.9.	55.98
F023111	4	4.4	33.6	180.	1.44	15.0	-83.0	0.0	10.	184.	208.	0.	208.	1384.	60.40
F023111	4	4.4	33.6	180.	1.44	15.0	-83.0	0.0	10.	184.	208.	0.	208.	1528.	39.09
A023111	4	4.4	33.6	180.	1.44	15.0	-83.0	0.0	10.	184.	208.	0.	208.	1177.	13.81
A023111	4	4.4	33.6	180.	1.44	15.0	-83.0	0.0	10.	184.	208.	0.	208.	791.	9.47
A024111	1	1.5	51.7	13.	.42	15.0	-83.0	0.0	0.0	0.	0.	450.	0.	0.	9.84
A023511	1	1.4	36.7	13.	.33	15.0	-83.0	0.0	0.0	0.	0.	1803.	0.	0.	2.49
F023511	1	1.0	0.0	0.0	.06	15.0	-83.0	0.0	0.0	0.	0.	1587.	0.	0.	-1.34
A023711	1	1.7	0.0	16.	.33	15.0	-83.0	0.0	0.0	0.	0.	1634.	0.	0.	4.32
A023711	1	1.7	0.0	16.	.33	15.0	-83.0	0.0	0.0	0.	0.	1994.	0.	0.	-1.32
A023711	1	1.7	0.0	16.	.33	15.0	-83.0	0.0	0.0	0.	0.	308.	0.	0.	7.01
A02110	5	5.4	16.8	1	1.1	15.0	-83.0	0.0	10.	140.	0.	0.	520.	140.9.	71.01
A02110	5	5.4	19.	1	0.7	15.0	-83.0	0.0	10.	149.	0.	0.	766.	165.1.	89.88
A02210	4	4.5	7.7	1	0.0	15.0	-83.0	0.0	11.	158.	0.	0.	194.	1658.	50.53
A02310	4	4.4	65.8	1	1.4	15.0	-83.0	9.1	11.	148.	573.	0.	573.	1703.	26.31
F02310	4	4.2	6.5	1	.80	15.0	-83.0	0.0	10.	139.	0.	0.	160.	1656.	18.40
A02410	5	5.1	83.0	1	1.3	15.0	-83.0	0.0	10.	139.	0.	0.	724.	1692.	7.45

RUN NUMBER 02

MODEL CONDITIONS						PROTOTYPE CONDITIONS									
FILE NAME	PEAK CONC. (%)	1% ARR. TIME (SEC)	PEAK TIME (SEC)	1% END TIME (SEC)	SUM (X-S)	X (M)	POSITION Y (M)	Z (M)	PEAK CONC. (%)	5% ARR. TIME (SEC)	10% ARR. TIME (SEC)	PEAK TIME (SEC)	10% END TIME (SEC)	5% END TIME (SEC)	SUM (X-S)
B02I07	.5	0.0	59.4	0.0	.46	400.0	0.0	0.0	1.3	0.	0.	518.	0.	0.	10.81
C02I07	.4	0.0	63.4	0.0	.37	400.0	0.0	0.0	1.1	0.	0.	553.	0.	0.	8.72
A02J07	.2	0.0	35.3	0.0	-.14	400.0	0.0	18.2	.4	0.	0.	308.	0.	0.	-3.21

RUN NUMBER 03

MODEL CONDITIONS						PROTOTYPE CONDITIONS									
FILE NAME	PEAK CONC. (%)	1% ARR. TIME (SEC)	PEAK TIME (SEC)	1% END TIME (SEC)	SUM (X-S)	X (H)	POSITION Y (H)	Z (H)	PEAK CONC. (%)	5% ARR. TIME (SEC)	10% ARR. TIME (SEC)	PEAK TIME (SEC)	10% END TIME (SEC)	5% END TIME (SEC)	SUM (X-S)
R03B08	1.6	17.3	30.0	37.0	10	200.0	-9.0	27.3	4.3	0.0	0.0	22.7	0.0	0.0	32
R03B07	1.0	16.1	30.3	44.6	10	200.0	0.0	0.0	1.1	0.0	0.0	22.7	0.0	0.0	34
R03E07	1.0	14.0	28.6	40.1	10	200.0	0.0	0.0	0.0	0.0	0.0	22.7	0.0	0.0	34
R03E07	1.0	14.1	28.9	44.0	10	200.0	0.0	0.0	0.0	0.0	0.0	22.7	0.0	0.0	34
R03F07	1.0	13.4	28.0	44.6	10	200.0	0.0	0.0	0.0	0.0	0.0	22.7	0.0	0.0	33
R03F07	1.1	13.1	28.0	42.0	10	200.0	0.0	0.0	0.0	0.0	0.0	22.7	0.0	0.0	34
R03G07	1.6	19.6	31.0	38.0	10	200.0	0.0	0.0	4.4	0.0	0.0	22.7	0.0	0.0	34
R03G07	1.9	19.6	31.0	45.5	10	200.0	0.0	0.0	3.1	0.0	0.0	22.7	0.0	0.0	34
R03I14	0.0	0.0	0.0	0.0	0.4	400.0	0.0	0.0	1.4	0.0	0.0	16.9	0.0	0.0	60
R03I14	0.0	0.0	0.0	0.0	0.7	400.0	0.0	0.0	1.8	0.0	0.0	16.9	0.0	0.0	64
R03I14	0.7	0.0	0.0	0.0	0.8	400.0	0.0	0.0	0.0	0.0	0.0	16.9	0.0	0.0	69
R03J14	0.6	0.0	0.0	0.0	0.1	400.0	0.0	0.0	1.5	0.0	0.0	16.9	0.0	0.0	64
R03I13	1.0	30.7	30.7	31.7	14	400.0	0.0	0.0	1.8	0.0	0.0	16.9	0.0	0.0	64
R03I13	1.0	0.0	0.0	0.0	14	400.0	0.0	0.0	0.0	0.0	0.0	16.9	0.0	0.0	68
R04I13	1.0	27.6	27.6	44.7	17	400.0	0.0	0.0	0.0	0.0	0.0	16.9	0.0	0.0	65
R03I13	1.7	0.0	0.0	0.0	0.1	400.0	0.0	0.0	1.9	0.0	0.0	16.9	0.0	0.0	69
R03I13	1.1	0.0	0.0	0.0	0.5	400.0	0.0	0.0	0.0	0.0	0.0	16.9	0.0	0.0	73
R03I13	1.1	0.0	0.0	0.0	0.4	400.0	0.0	0.0	0.0	0.0	0.0	16.9	0.0	0.0	73
R03I12	1.0	25.6	25.6	34.4	18	400.0	0.0	0.0	0.0	0.0	0.0	16.9	0.0	0.0	68
R03I12	1.8	0.0	0.0	0.0	0.6	400.0	0.0	0.0	0.0	0.0	0.0	16.9	0.0	0.0	74
R03I11	1.5	11.9	11.9	33.3	18	400.0	0.0	0.0	0.0	0.0	0.0	16.9	0.0	0.0	67
R03I11	1.4	0.0	0.0	0.0	0.3	400.0	0.0	0.0	0.0	0.0	0.0	16.9	0.0	0.0	65
R03I11	1.4	11.2	11.2	32.4	18	400.0	0.0	0.0	0.0	0.0	0.0	16.9	0.0	0.0	67
R03J11	0.9	0.0	0.0	0.0	0.5	400.0	0.0	0.0	0.0	0.0	0.0	16.9	0.0	0.0	69
R03I10	1.4	11.0	11.0	33.6	18	400.0	0.0	0.0	0.0	0.0	0.0	16.9	0.0	0.0	67
R03I10	1.7	0.0	0.0	0.0	0.6	400.0	0.0	0.0	0.0	0.0	0.0	16.9	0.0	0.0	74
R03I10	1.6	12.0	12.0	37.9	18	400.0	0.0	0.0	4.4	0.0	0.0	16.9	0.0	0.0	68
R03J10	1.0	0.0	0.0	0.0	0.3	400.0	0.0	0.0	0.0	0.0	0.0	16.9	0.0	0.0	69
R03I09	1.5	15.2	15.2	34.3	18	400.0	0.0	0.0	4.6	0.0	0.0	16.9	0.0	0.0	69
R03I09	1.3	0.0	0.0	0.0	0.6	400.0	0.0	0.0	0.0	0.0	0.0	16.9	0.0	0.0	74
R03I09	1.5	14.9	14.9	33.3	18	400.0	0.0	0.0	3.5	0.0	0.0	16.9	0.0	0.0	69
R03I08	1.5	17.4	17.4	34.4	18	400.0	0.0	0.0	3.4	0.0	0.0	16.9	0.0	0.0	67
R03I08	1.7	0.0	0.0	0.0	0.4	400.0	0.0	0.0	0.0	0.0	0.0	16.9	0.0	0.0	74
R03I08	1.6	22.0	22.0	38.8	18	400.0	0.0	0.0	4.0	0.0	0.0	16.9	0.0	0.0	68
R03I08	1.7	21.0	21.0	34.3	18	400.0	0.0	0.0	0.0	0.0	0.0	16.9	0.0	0.0	74
R03I08	1.6	21.1	21.1	38.8	18	400.0	0.0	0.0	4.4	0.0	0.0	16.9	0.0	0.0	68
R03J08	1.3	19.9	19.9	35.0	18	400.0	0.0	0.0	3.4	0.0	0.0	16.9	0.0	0.0	68
R03I07	1.1	11.3	11.3	33.7	18	400.0	0.0	0.0	0.0	0.0	0.0	16.9	0.0	0.0	67
R03I07	1.0	0.0	0.0	0.0	0.3	400.0	0.0	0.0	0.0	0.0	0.0	16.9	0.0	0.0	74
R03I07	1.1	10.1	10.1	33.7	18	400.0	0.0	0.0	0.0	0.0	0.0	16.9	0.0	0.0	67
R03I07	1.1	24.6	24.6	37.9	18	400.0	0.0	0.0	3.8	0.0	0.0	16.9	0.0	0.0	67
R03J07	1.2	18.7	18.7	44.9	10	400.0	0.0	0.0	3.1	0.0	0.0	16.9	0.0	0.0	64

RUN NUMBER 04

MODEL CONDITIONS						POSITION			PROTOTYPE CONDITIONS						
FILE NAME	PEAK CONC. (%)	1% ARR. TIME (SEC)	PEAK TIME (SEC)	1% END TIME (SEC)	SUM (X-S)	X (M)	Y (M)	Z (M)	PEAK CONC. (%)	5% ARR. TIME (SEC)	10% ARR. TIME (SEC)	PEAK TIME (SEC)	10% END TIME (SEC)	5% END TIME (SEC)	SUM (X-S)
A04114	.1	0.0	128.7	0.0	-.01	15.0	-63.0	0.0	.4	0.0	0.0	1122.	0.0	0.0	-.14
R04114	2.0	19.1	24.7	27.0	.14	15.0	-63.0	0.0	5.3	214.	0.0	216.	0.0	221.	3.31
C04114	.2	0.0	17.2	0.0	.02	15.0	-63.0	0.0	.4	0.0	0.0	150.	0.0	0.0	.57
A04214	2.6	21.9	22.0	22.2	.03	15.0	-63.0	4.6	6.6	191.	0.0	192.	0.0	192.	.64
R04314	1.3	19.4	19.4	19.5	.01	15.0	-63.0	9.1	3.6	0.0	0.0	170.	0.0	0.0	.17
R04314	.6	0.0	27.9	0.0	-.01	15.0	-63.0	9.1	1.2	0.0	0.0	243.	0.0	0.0	-.28
C04314	.9	0.0	22.0	0.0	-.01	15.0	-63.0	9.1	2.2	0.0	0.0	192.	0.0	0.0	-.28
A04414	.5	0.0	46.3	0.0	.03	15.0	-63.0	13.6	1.8	0.0	0.0	405.	0.0	0.0	.79
R04514	.5	0.0	23.1	0.0	.02	15.0	-63.0	18.2	.4	0.0	0.0	205.	0.0	0.0	.43
R04514	.5	0.0	71.1	0.0	.01	15.0	-63.0	18.2	.4	0.0	0.0	620.	0.0	0.0	.32
C04514	.2	0.0	65.3	0.0	-.02	15.0	-63.0	18.2	.5	0.0	0.0	537.	0.0	0.0	.44
A04614	.1	0.0	55.1	0.0	-.01	15.0	-63.0	22.7	.5	0.0	0.0	480.	0.0	0.0	-.13
A04714	.1	0.0	40.3	0.0	.01	15.0	-63.0	27.3	.2	0.0	0.0	351.	0.0	0.0	.27
R04113	2.3	17.9	22.0	29.0	.34	15.0	-54.0	0.0	6.0	0.0	0.0	192.	0.0	220.	7.96
C04113	1.4	21.4	25.5	37.4	.14	15.0	-54.0	0.0	3.6	166.	0.0	205.	0.0	0.0	3.19
A04113	1.3	19.9	38.0	38.4	.07	15.0	-54.0	0.0	3.4	0.0	0.0	331.	0.0	0.0	1.72
A04213	3.1	16.6	21.9	52.7	.23	15.0	-54.0	4.6	8.1	187.	0.0	191.	0.0	210.	5.34
R04313	1.8	17.4	32.8	33.2	.15	15.0	-54.0	9.1	4.6	0.0	0.0	284.	0.0	0.0	3.57
R04313	1.7	16.5	22.7	30.7	.13	15.0	-54.0	9.1	4.6	0.0	0.0	198.	0.0	0.0	3.03
C04313	2.0	19.6	24.6	51.2	.09	15.0	-54.0	9.1	5.2	214.	0.0	214.	0.0	216.	2.00
A04413	1.2	23.5	23.5	23.5	.03	15.0	-54.0	13.6	3.2	0.0	0.0	205.	0.0	0.0	.80
R04513	.4	0.0	22.4	0.0	0.00	15.0	-54.0	18.2	1.0	0.0	0.0	195.	0.0	0.0	-.04
R04513	.3	0.0	34.0	0.0	-.02	15.0	-54.0	18.2	.9	0.0	0.0	296.	0.0	0.0	-.41
C04513	.6	0.0	18.1	0.0	.01	15.0	-54.0	18.2	1.6	0.0	0.0	158.	0.0	0.0	.24
A04613	.1	0.0	71.0	0.0	0.00	15.0	-54.0	22.7	.2	0.0	0.0	3.	0.0	0.0	.08
A04713	.1	0.0	71.0	0.0	.02	15.0	-54.0	27.3	.4	0.0	0.0	619.	0.0	0.0	.51
A04112	1.8	19.7	20.0	56.2	.33	15.0	-45.0	0.0	4.6	0.0	0.0	174.	0.0	0.0	7.73
C04112	2.1	18.2	23.5	55.1	.37	15.0	-45.0	0.0	5.4	201.	0.0	205.	0.0	209.	8.56
R04112	3.6	13.3	24.1	49.4	.55	15.0	-45.0	0.0	9.1	155.	0.0	210.	0.0	419.	12.59
A04212	2.7	16.3	21.9	62.1	.28	15.0	-45.0	4.6	7.0	183.	0.0	191.	0.0	299.	6.45
R04312	2.0	15.8	21.3	35.0	.18	15.0	-45.0	9.1	5.3	186.	0.0	186.	0.0	187.	4.11
R04312	2.1	15.8	54.7	65.2	.12	15.0	-45.0	9.1	5.5	477.	0.0	477.	0.0	477.	2.92
C04312	1.8	18.0	42.4	51.9	.13	15.0	-45.0	9.1	4.8	0.0	0.0	370.	0.0	0.0	3.07
A04412	1.6	19.5	19.5	64.3	.07	15.0	-45.0	13.6	4.2	0.0	0.0	170.	0.0	0.0	1.56
A04512	.9	0.0	13.1	0.0	.02	15.0	-45.0	18.2	2.5	0.0	0.0	114.	0.0	0.0	.47
R04512	1.0	77.4	77.4	77.6	.02	15.0	-45.0	18.2	2.7	0.0	0.0	675.	0.0	0.0	.41
C04512	.9	0.0	42.0	0.0	.04	15.0	-45.0	18.2	2.4	0.0	0.0	366.	0.0	0.0	1.01
A04612	.6	0.0	90.4	0.0	.01	15.0	-45.0	22.7	1.6	0.0	0.0	788.	0.0	0.0	.24
A04712	.1	0.0	66.0	0.0	.02	15.0	-45.0	27.3	.4	0.0	0.0	575.	0.0	0.0	.56
A04111	3.3	14.0	17.9	57.6	.63	15.0	-36.0	0.0	8.4	130.	0.0	156.	0.0	490.	14.57
C04111	4.2	14.5	42.1	59.3	.61	15.0	-36.0	0.0	10.5	160.	367.	367.	368.	478.	14.15
R04111	4.1	13.0	31.7	70.3	.77	15.0	-36.0	0.0	10.4	113.	276.	277.	277.	419.	17.74
A04211	5.0	11.7	21.6	67.2	.40	15.0	-36.0	4.6	12.5	106.	188.	188.	429.	563.	9.14
R04311	7.9	6.0	30.1	80.8	.31	15.0	-36.0	9.1	18.8	102.	262.	263.	472.	575.	7.16
C04311	4.9	4.8	23.5	80.4	.28	15.0	-36.0	9.1	12.2	80.	205.	205.	330.	507.	6.45
A04311	4.0	9.1	19.3	78.0	.27	15.0	-36.0	9.1	10.1	79.	168.	168.	168.	639.	6.38
A04411	3.0	4.7	60.7	75.0	.17	15.0	-36.0	13.6	7.6	138.	0.0	529.	0.0	530.	4.03
A04511	2.8	9.6	45.6	77.6	.09	15.0	-36.0	18.2	7.3	282.	0.0	398.	0.0	615.	2.05

RUN NUMBER 04

MOREL CONDITIONS						POSITION			PROTOTYPE CONDITIONS						
FILE NAME	PEAK CONC. (%)	1% ARR. TIME (SEC)	PEAK TIME (SEC)	1% END TIME (SEC)	SUM (X-S)	X (M)	Y (M)	Z (M)	PEAK CONC. (%)	5% ARR. TIME (SEC)	10% ARR. TIME (SEC)	PEAK TIME (SEC)	10% END TIME (SEC)	5% END TIME (SEC)	SUM (X-S)
C04307	6.3	7.4	24.0	81.7	1.47	15.0	0.0	9.1	15.5	65.	185.	209.	344.	548.	33.41
R04307	6.3	9.1	36.4	85.9	1.52	15.0	0.0	9.1	15.4	113.	170.	317.	318.	601.	34.54
A04407	6.6	4.3	21.4	80.4	1.06	15.0	0.0	13.6	16.0	37.	108.	187.	404.	643.	24.21
A04507	4.1	8.3	45.9	81.6	.47	15.0	0.0	18.2	10.5	117.	145.	400.	400.	632.	10.88
R04507	4.6	4.4	55.7	89.6	.38	15.0	0.0	18.2	11.6	72.	486.	486.	486.	647.	8.77
C04507	4.4	3.4	42.1	90.1	.62	15.0	0.0	18.2	11.0	40.	222.	367.	522.	630.	14.18
A04607	3.0	5.2	61.2	94.0	.21	15.0	0.0	22.7	7.6	46.	0.	533.	0.	728.	4.93
A04707	2.7	16.9	17.8	82.5	-.02	15.0	0.0	27.3	7.1	147.	0.	155.	0.	632.	-3.88
R04814	1.1	25.3	25.5	25.4	.16	75.0	-63.0	0.0	2.8	0.	0.	220.	0.	0.	0.
R04814	1.0	19.7	26.4	31.4	.16	75.0	-63.0	0.0	3.2	228.	0.	230.	0.	247.	0.88
C04814	2.2	23.9	29.8	30.3	.13	75.0	-63.0	0.0	3.2	0.	0.	260.	0.	0.	0.
A04914	1.7	18.7	24.5	46.9	.10	75.0	-63.0	9.1	4.5	0.	0.	214.	0.	0.	3.45
R04914	1.9	19.6	20.2	34.1	.12	75.0	-63.0	9.1	5.0	176.	0.	176.	0.	177.	2.69
C04914	2.0	18.5	23.3	28.1	.12	75.0	-63.0	9.1	5.1	203.	0.	203.	0.	204.	2.82
A04A14	.5	0.0	25.4	0.0	.01	75.0	-63.0	18.2	1.3	0.	0.	221.	0.	0.	.26
R04A14	.8	0.0	22.2	0.0	-.02	75.0	-63.0	18.2	2.2	0.	0.	194.	0.	0.	-.44
C04A14	.8	0.0	24.9	0.0	0.00	75.0	-63.0	18.2	2.0	0.	0.	217.	0.	0.	-.01
A04B14	.1	0.0	0.0	0.0	-.02	75.0	-63.0	27.3	.2	0.	0.	1.	0.	0.	-.57
A04B13	1.9	22.6	34.1	52.5	.47	75.0	-54.0	0.0	4.9	0.	0.	297.	0.	0.	10.83
R04B13	2.8	16.0	25.8	52.9	.60	75.0	-54.0	0.0	7.3	218.	0.	225.	0.	308.	13.80
C04B13	2.3	18.1	29.6	45.9	.45	75.0	-54.0	0.0	6.0	185.	0.	238.	0.	243.	10.43
A04913	2.1	14.5	22.8	66.9	.17	75.0	-54.0	9.1	5.5	197.	0.	199.	0.	199.	4.03
R04913	1.8	11.4	40.6	45.6	.16	75.0	-54.0	9.1	4.8	0.	0.	354.	0.	0.	3.75
C04913	2.0	14.4	18.5	51.2	.15	75.0	-54.0	9.1	5.2	161.	0.	161.	0.	161.	3.62
R04A13	.8	0.0	24.7	0.0	.01	75.0	-54.0	18.2	2.0	0.	0.	215.	0.	0.	.17
C04A13	.8	0.0	23.5	0.0	.01	75.0	-54.0	18.2	2.0	0.	0.	205.	0.	0.	.13
A04A13	.9	0.0	50.6	0.0	.04	75.0	-54.0	18.2	2.3	0.	0.	442.	0.	0.	1.03
A04B13	.4	0.0	77.5	0.0	-.03	75.0	-54.0	27.3	1.1	0.	0.	676.	0.	0.	-.65
A04B12	2.5	17.8	35.3	55.8	.62	75.0	-45.0	0.0	6.4	210.	0.	308.	0.	319.	14.27
R04B12	3.2	15.9	25.6	60.9	.82	75.0	-45.0	0.0	8.1	142.	0.	223.	0.	361.	18.88
C04B12	2.4	16.8	26.7	48.2	.64	75.0	-45.0	0.0	6.3	177.	0.	233.	0.	391.	14.84
A04912	1.8	14.6	49.1	67.0	.17	75.0	-45.0	9.1	4.8	0.	0.	428.	0.	0.	4.03
R04912	2.7	19.1	40.5	61.3	.12	75.0	-45.0	9.1	7.0	202.	0.	353.	0.	398.	2.80
C04912	2.2	14.5	18.4	63.7	.24	75.0	-45.0	9.1	5.6	160.	0.	160.	0.	338.	5.70
C04A12	.9	0.0	69.6	0.0	.01	75.0	-45.0	18.2	2.5	0.	0.	607.	0.	0.	.20
A04A12	2.1	17.1	18.2	71.8	.21	75.0	-45.0	18.2	5.4	158.	0.	158.	0.	159.	4.95
R04A12	.8	0.0	22.2	0.0	0.00	75.0	-45.0	18.2	2.1	0.	0.	194.	0.	0.	-.02
A04B12	.6	0.0	68.5	0.0	.02	75.0	-45.0	27.3	1.7	0.	0.	597.	0.	0.	.55
A04B11	3.7	16.6	29.7	63.4	.89	75.0	-36.0	0.0	7.0	172.	0.	259.	0.	432.	20.52
R04B11	3.2	12.4	25.2	64.0	1.10	75.0	-36.0	0.0	8.2	146.	0.	220.	0.	461.	25.13
C04B11	3.0	16.7	30.2	66.2	.99	75.0	-36.0	0.0	7.7	170.	0.	263.	0.	512.	22.81
A04911	2.7	11.5	43.2	67.3	.34	75.0	-36.0	9.1	7.0	172.	0.	377.	0.	545.	7.97
R04911	2.9	11.2	21.3	65.4	.38	75.0	-36.0	9.1	7.4	98.	0.	186.	0.	534.	8.79
C04911	2.4	13.4	18.5	65.8	.32	75.0	-36.0	9.1	6.2	160.	0.	161.	0.	466.	7.35
R04A11	1.8	11.0	41.1	69.5	.06	75.0	-36.0	18.2	4.6	0.	0.	358.	0.	0.	1.47
C04A11	2.0	16.0	41.0	69.7	.06	75.0	-36.0	18.2	5.3	357.	0.	357.	0.	358.	1.29
A04A11	2.4	17.3	57.1	72.0	.08	75.0	-36.0	18.2	6.3	343.	0.	498.	0.	499.	1.96
A04R11	1.8	67.8	68.1	68.1	-.02	75.0	-36.0	27.3	4.7	0.	0.	594.	0.	0.	-.43

RUN NUMBER 04

MODEL CONDITIONS						POSITION			PROTOTYPE CONDITIONS					
FILE NAME	PEAK CONC. (%)	1% ARR. TIME (SEC)	PEAK TIME (SEC)	1% END TIME (SEC)	SUM (X-S)	X (M)	Z (M)	PEAK CONC. (%)	5% ARR. TIME (SEC)	10% ARR. TIME (SEC)	PEAK TIME (SEC)	10% END TIME (SEC)	5% END TIME (SEC)	SUM (X-S)
A04B10	3.0	15.5	29.9	64.3	1.07	75.0	-27.0	0.0	7.7	156.	0.	430.	24.58	
B04B10	3.2	11.5	26.5	68.7	1.22	75.0	-27.0	0.0	8.3	141.	0.	478.	28.89	
C04B10	3.3	15.6	29.7	71.1	1.17	75.0	-27.0	0.0	8.3	171.	0.	516.	26.67	
B04910	2.9	11.1	40.7	79.5	.66	75.0	-27.0	9.1	7.5	100.	0.	509.	15.10	
C04910	2.9	13.1	17.4	69.2	.58	75.0	-27.0	9.1	7.6	118.	0.	481.	13.30	
A04910	3.1	10.6	19.8	72.0	.63	75.0	-27.0	9.1	8.0	128.	0.	543.	14.60	
B04A10	2.3	11.1	41.1	75.8	.14	75.0	-27.0	18.2	6.1	176.	0.	526.	3.16	
A04A10	2.9	11.8	46.0	76.4	.17	75.0	-27.0	18.2	7.6	105.	0.	584.	4.00	
C04A10	2.6	11.8	27.3	69.8	.13	75.0	-27.0	18.2	6.7	165.	0.	487.	2.95	
A04R10	1.6	55.9	67.6	68.0	.02	75.0	-27.0	27.3	4.3	0.	0.	589.	0.	
A04B09	2.8	15.3	26.1	66.0	1.10	75.0	-18.0	0.0	7.2	165.	0.	439.	25.17	
B04B09	3.1	11.4	26.2	70.6	1.21	75.0	-18.0	0.0	8.0	158.	0.	436.	27.63	
C04B09	2.8	16.5	25.4	71.6	1.11	75.0	-18.0	0.0	7.2	173.	0.	520.	25.48	
C04909	3.2	12.0	28.7	65.3	.64	75.0	-18.0	9.1	8.2	152.	0.	412.	15.12	
A04909	3.3	11.9	32.2	62.5	.73	75.0	-18.0	9.1	8.5	166.	0.	461.	16.80	
B04909	3.0	9.4	23.1	73.0	.69	75.0	-18.0	9.1	7.6	105.	0.	563.	15.97	
A04A09	2.3	11.9	45.9	70.5	.19	75.0	-18.0	18.2	6.0	229.	0.	586.	4.35	
B04A09	2.4	12.9	28.7	75.1	.16	75.0	-18.0	18.2	6.2	144.	0.	456.	3.58	
C04A09	2.5	14.6	19.7	72.7	.19	75.0	-18.0	18.2	6.5	166.	0.	397.	4.40	
A04B09	1.9	23.3	23.4	69.7	.01	75.0	-18.0	27.3	5.0	204.	0.	204.	1.8	
B04B08	2.8	11.9	21.7	72.2	1.17	75.0	-9.0	0.0	7.2	163.	0.	497.	26.88	
A04B08	3.0	16.0	26.2	70.2	1.28	75.0	-9.0	0.0	7.6	150.	0.	479.	27.40	
C04B08	3.1	15.0	33.5	77.4	1.28	75.0	-9.0	0.0	8.1	150.	0.	292.	29.20	
A04908	2.9	12.1	25.6	71.9	.85	75.0	-9.0	9.1	7.4	159.	0.	539.	19.65	
B04908	2.6	19.1	30.9	76.1	.84	75.0	-9.0	9.1	9.1	140.	0.	445.	19.29	
C04908	2.3	12.9	25.1	66.8	.75	75.0	-9.0	9.1	8.4	147.	0.	476.	17.38	
A04A08	2.3	11.0	21.9	68.1	.23	75.0	-9.0	18.2	5.9	150.	0.	589.	4.99	
B04A08	2.1	11.3	31.2	75.5	.30	75.0	-9.0	18.2	7.9	144.	0.	457.	6.83	
C04A08	2.3	13.5	32.0	70.8	.32	75.0	-9.0	18.2	6.1	153.	0.	434.	5.62	
A04R08	2.1	16.5	23.5	66.0	.03	75.0	-9.0	27.3	5.4	205.	0.	205.	1.67	
B04B07	2.6	11.6	30.3	72.3	1.15	75.0	0.0	0.0	6.8	167.	0.	422.	26.75	
C04B07	3.1	14.5	26.5	72.6	1.15	75.0	0.0	0.0	7.9	185.	0.	525.	26.35	
A04B07	3.1	16.6	29.7	70.1	1.17	75.0	0.0	0.0	7.9	159.	0.	433.	26.73	
A04907	3.9	13.3	29.7	62.8	.85	75.0	0.0	9.1	7.6	159.	0.	504.	19.61	
C04907	3.0	12.9	27.2	66.9	.85	75.0	0.0	9.1	7.8	142.	0.	441.	19.63	
B04907	3.9	9.5	27.4	73.8	.89	75.0	0.0	9.1	7.6	100.	0.	448.	20.42	
B04A07	2.6	12.9	24.7	75.5	.30	75.0	0.0	18.2	6.6	196.	0.	456.	6.86	
C04A07	2.7	14.4	30.5	70.2	.28	75.0	0.0	18.2	7.0	200.	0.	391.	6.53	
A04A07	2.9	11.9	25.3	67.7	.33	75.0	0.0	18.2	7.4	151.	0.	504.	5.40	
A04R07	2.1	44.4	44.5	81.9	0.00	75.0	0.0	27.3	5.4	388.	0.	388.	-.07	
A04H13	.1	0.0	.5	0.0	-.01	200.0	-117.0	0.0	.4	0.	0.	5.	-.33	
A04H12	.1	0.0	76.8	0.0	-.02	200.0	-108.0	0.0	.2	0.	0.	669.	-.59	
A04H11	.2	0.0	101.8	0.0	-.01	200.0	-99.0	0.0	.5	0.	0.	888.	-.12	
A04H10	.9	0.0	27.8	0.0	.06	200.0	-90.0	0.0	2.4	0.	0.	342.	1.49	
A04H09	1.7	24.8	30.5	33.6	.24	200.0	-81.0	0.0	4.4	0.	0.	366.	5.54	
A04H08	1.8	23.6	31.5	62.5	.54	200.0	-72.0	0.0	4.8	0.	0.	375.	12.59	
A04H14	1.8	23.2	37.7	55.7	.65	200.0	-63.0	0.0	4.9	0.	0.	329.	14.94	
B04B14	2.1	23.1	30.7	60.6	.69	200.0	-63.0	0.0	5.5	262.	0.	368.	15.88	

RUN NUMBER 04

MODEL CONDITIONS						PROTOTYPE CONDITIONS									
FILE NAME	PEAK CONC. (Z)	1% ARR. TIME (SEC)	PEAK TIME (SEC)	1% END TIME (SEC)	SUM (X-S)	X (M)	POSITION Y (M)	Z (M)	PEAK CONC. (Z)	5% ARR. TIME (SEC)	10% ARR. TIME (SEC)	PEAK TIME (SEC)	10% END TIME (SEC)	5% END TIME (SEC)	SUM (X-S)
C04D08	1.8	23.6	38.2	66.3	.71	200.0	9.0	0.0	4.6	0.	0.	333.	0.	0.	16.45
R04D08	1.9	20.8	39.9	65.8	.82	200.0	-9.0	0.0	5.0	348.	0.	348.	0.	350.	18.93
A04E08	2.0	21.5	26.5	70.2	.46	200.0	9.0	9.1	5.1	231.	0.	231.	0.	231.	10.58
R04E08	2.1	22.0	42.4	65.0	.38	200.0	-9.0	9.1	5.4	369.	0.	370.	0.	370.	8.95
R04F08	1.6	17.6	40.7	61.0	.21	200.0	-9.0	18.2	4.3	0.	0.	355.	0.	0.	4.95
A04F08	1.7	23.5	28.5	60.6	.12	200.0	-9.0	18.2	4.4	0.	0.	248.	0.	0.	2.82
A04G08	1.5	21.4	39.7	51.5	0.00	200.0	-9.0	27.3	4.1	0.	0.	347.	0.	0.	-1.05
C04D07	1.8	22.5	35.9	68.9	.72	200.0	0.0	0.0	4.8	0.	0.	333.	0.	0.	16.78
A04D07	1.8	23.1	28.6	64.9	.73	200.0	0.0	0.0	4.6	0.	0.	250.	0.	0.	16.88
R04D07	1.8	21.6	27.7	66.7	.75	200.0	0.0	0.0	4.7	0.	0.	242.	0.	0.	17.29
R04E07	2.0	21.4	48.4	66.4	.38	200.0	0.0	9.1	5.1	422.	0.	422.	0.	422.	8.84
A04E07	2.0	22.3	30.3	64.7	.41	200.0	0.0	9.1	5.1	264.	0.	264.	0.	265.	9.64
R04F07	1.5	22.9	40.7	50.9	.11	200.0	0.0	0.0	4.1	0.	0.	355.	0.	0.	2.63
A04F07	1.8	23.3	38.6	60.4	.11	200.0	0.0	18.2	4.6	0.	0.	334.	0.	0.	2.53
A04G07	1.0	0.0	21.3	0.0	0.00	200.0	0.0	27.3	5.5	0.	0.	185.	0.	0.	6.11
A04K14	1.1	35.0	40.1	44.4	.29	400.0	-126.0	0.0	2.9	0.	0.	350.	0.	0.	6.71
R04K14	1.1	35.1	38.3	39.4	.31	400.0	-126.0	0.0	1.1	0.	0.	334.	0.	0.	7.17
A04K13	1.1	35.0	35.1	43.8	.32	400.0	-117.0	0.0	0.0	0.	0.	306.	0.	0.	7.34
R04K13	1.1	33.8	35.8	43.3	.43	400.0	-117.0	0.0	1.1	0.	0.	313.	0.	0.	9.99
A04K12	1.1	33.8	35.8	46.3	.40	400.0	-108.0	0.0	2.2	0.	0.	311.	0.	0.	9.25
R04K12	1.1	36.8	37.4	44.7	.41	400.0	-108.0	0.0	0.0	0.	0.	326.	0.	0.	9.56
A04K11	1.1	30.5	40.3	48.1	.49	400.0	-99.0	0.0	0.0	0.	0.	352.	0.	0.	11.31
R04K11	1.5	29.4	36.6	57.2	.49	400.0	-99.0	0.0	0.0	0.	0.	314.	0.	0.	11.43
A04K10	1.5	28.8	34.0	49.1	.51	400.0	-90.0	0.0	0.0	0.	0.	314.	0.	0.	11.94
R04K10	1.3	28.9	36.8	59.2	.53	400.0	-90.0	0.0	0.0	0.	0.	321.	0.	0.	12.27
A04K09	1.3	30.3	35.3	44.0	.44	400.0	-81.0	0.0	0.0	0.	0.	308.	0.	0.	10.34
R04K09	1.1	34.3	34.2	38.4	.45	400.0	-81.0	0.0	0.0	0.	0.	315.	0.	0.	10.56
A04K08	1.4	29.4	35.8	45.8	.50	400.0	-72.0	0.0	0.0	0.	0.	312.	0.	0.	11.59
R04K08	1.3	32.9	33.9	42.9	.48	400.0	-72.0	0.0	0.0	0.	0.	294.	0.	0.	11.16
A04I14	1.1	29.9	37.0	42.1	.44	400.0	-63.0	0.0	0.0	0.	0.	323.	0.	0.	10.16
R04I14	1.1	37.4	37.4	39.6	.40	400.0	-63.0	0.0	0.0	0.	0.	324.	0.	0.	9.42
C04I14	1.1	34.2	34.4	38.1	.40	400.0	-63.0	0.0	0.0	0.	0.	300.	0.	0.	9.31
A04K07	1.4	30.8	39.3	45.3	.51	400.0	-63.0	0.0	0.0	0.	0.	343.	0.	0.	11.78
R04K07	1.1	34.9	35.9	45.0	.49	400.0	-63.0	0.0	0.0	0.	0.	313.	0.	0.	11.31
A04J14	0.7	0.0	44.7	0.0	.02	400.0	-63.0	18.2	0.0	0.	0.	390.	0.	0.	9.35
R04I13	1.2	34.9	35.8	45.8	.40	400.0	-54.0	0.0	0.0	0.	0.	313.	0.	0.	9.38
A04I13	1.1	36.0	37.4	40.5	.43	400.0	-54.0	0.0	0.0	0.	0.	324.	0.	0.	10.03
C04I13	1.3	37.0	38.7	53.1	.43	400.0	-54.0	0.0	0.0	0.	0.	338.	0.	0.	10.07
A04J13	1.0	0.0	40.1	0.0	.04	400.0	-54.0	18.2	0.0	0.	0.	349.	0.	0.	8.85
C04I12	1.1	37.7	37.9	39.0	.42	400.0	-45.0	0.0	0.0	0.	0.	330.	0.	0.	9.89
R04I12	1.1	33.7	35.9	40.0	.43	400.0	-45.0	0.0	0.0	0.	0.	313.	0.	0.	9.92
A04I12	1.1	36.5	36.5	38.7	.37	400.0	-45.0	0.0	0.0	0.	0.	319.	0.	0.	8.54
A04J12	0.8	0.0	39.9	0.0	.04	400.0	-45.0	18.2	0.0	0.	0.	348.	0.	0.	8.84
C04I11	1.3	32.9	37.2	45.3	.41	400.0	-36.0	0.0	0.0	0.	0.	322.	0.	0.	9.51
R04I11	1.2	34.0	35.7	45.0	.40	400.0	-36.0	0.0	0.0	0.	0.	311.	0.	0.	9.39
A04I11	1.2	35.6	36.2	41.8	.36	400.0	-36.0	0.0	0.0	0.	0.	316.	0.	0.	8.41
A04J11	0.9	0.0	48.6	0.0	.05	400.0	-36.0	18.2	0.0	0.	0.	424.	0.	0.	1.26
A04I10	1.1	35.1	37.5	44.1	.44	400.0	-27.0	0.0	0.0	0.	0.	327.	0.	0.	10.24

RUN NUMBER 04

-----MODEL CONDITIONS-----						-----PROTOTYPE CONDITIONS-----									
FILE NAME	PEAK CONC. (%)	5% ARR. TIME (SEC)	PEAK TIME (SEC)	1% END TIME (SEC)	SUM (X-S)	X (M)	POSITION Y (M)	Z (M)	PEAK CONC. (%)	5% ARR. TIME (SEC)	10% ARR. TIME (SEC)	PEAK TIME (SEC)	10% END TIME (SEC)	5% END TIME (SEC)	SUM (X-S)
R04I10	1.2	33.2	35.9	40.9	.45	400.0	-27.0	0.0	3.3	0.	0.	313.	0.	0.	10.49
C04I10	1.3	30.7	35.7	47.9	.48	400.0	-27.0	0.0	3.3	0.	0.	312.	0.	0.	11.15
A04J10	.9	0.0	40.0	0.0	.06	400.0	-27.0	18.2	3.4	0.	0.	348.	0.	0.	1.39
R04I09	1.0	38.5	38.5	39.7	.35	400.0	-18.0	0.0	2.8	0.	0.	336.	0.	0.	8.37
C04I09	1.1	35.6	36.3	44.7	.36	400.0	-18.0	0.0	2.9	0.	0.	316.	0.	0.	8.37
A04I09	1.1	42.6	42.8	45.5	.40	400.0	-18.0	0.0	2.9	0.	0.	373.	0.	0.	9.23
A04J09	.9	0.0	44.0	0.0	.03	400.0	-18.0	18.2	2.4	0.	0.	384.	0.	0.	.71
C04I08	1.2	34.5	37.4	46.3	.44	400.0	-9.0	0.0	3.2	0.	0.	326.	0.	0.	10.21
R04I08	1.1	37.9	38.2	38.8	.41	400.0	-9.0	0.0	2.9	0.	0.	333.	0.	0.	9.53
A04I08	1.0	33.6	33.6	43.0	.40	400.0	-9.0	0.0	2.8	0.	0.	393.	0.	0.	9.30
A04J08	1.0	29.7	29.7	29.8	.07	400.0	-9.0	18.2	2.8	0.	0.	359.	0.	0.	1.53
C04I07	1.3	34.2	38.7	47.9	.44	400.0	0.0	0.0	3.4	0.	0.	337.	0.	0.	10.29
A04I07	1.2	32.6	42.6	45.8	.47	400.0	0.0	0.0	3.3	0.	0.	371.	0.	0.	10.91
R04I07	1.0	35.8	35.8	36.0	.37	400.0	0.0	0.0	2.7	0.	0.	312.	0.	0.	8.66
A04J07	.7	0.0	38.1	0.0	.02	400.0	0.0	18.2	2.0	0.	0.	332.	0.	0.	.54

RUN NUMBER 05

-----MOREL CONDITIONS-----						-----PROTOTYPE CONDITIONS-----										
FILE NAME	PEAK CONC. (%)	1% ARR. TIME (SEC)	PEAK TIME (SEC)	1% END TIME (SEC)	SUM (X-S)	X (M)	POSITION (M)			PEAK CONC. (%)	5% ARR. TIME (SEC)	10% ARR. TIME (SEC)	PEAK TIME (SEC)	10% END TIME (SEC)	5% END TIME (SEC)	SUM (X-S)
A05I08	1.4	33.1	35.9	46.6	.46	400.0	-9.0	0.0	0.0	3.6	0.	0.	313.	0.	0.	10.72
A05J08	1.0	0.0	52.1	0.0	.08	400.0	-9.0	18.2	0.0	2.5	0.	0.	454.	0.	0.	1.82
C05I07	1.1	41.4	41.4	43.7	.48	400.0	0.0	0.0	0.0	2.8	0.	0.	361.	0.	0.	11.26
B05I07	1.3	30.1	34.8	40.2	.48	400.0	0.0	0.0	0.0	3.4	0.	0.	303.	0.	0.	11.09
A05I07	1.4	31.3	37.2	47.2	.51	400.0	0.0	0.0	0.0	3.6	0.	0.	324.	0.	0.	11.78
A05J07	.7	0.0	39.9	0.0	.05	400.0	0.0	18.2	0.0	1.8	0.	0.	348.	0.	0.	1.17

RUN NUMBER 06

MODEL CONDITIONS						PROTOTYPE CONDITIONS									
FILE NAME	PEAK CONC. (%)	1% ARR. TIME (SEC)	PEAK TIME (SEC)	1% END TIME (SEC)	SUM (X-S)	X (M)	POSITION Y (M)	Z (M)	PEAK CONC. (%)	5% ARR. TIME (SEC)	10% ARR. TIME (SEC)	PEAK TIME (SEC)	10% END TIME (SEC)	5% END TIME (SEC)	SUM (X-S)
A06E07	1.7	24.6	42.1	67.3	.47	200.0	0.0	9.1	4.5	0.	0.	367.	0.	0.	11.02
R06F07	1.7	25.9	45.9	69.3	.24	200.0	0.0	18.2	4.6	0.	0.	322.	0.	0.	5.66
A06F07	1.6	31.7	47.7	68.6	.21	200.0	0.0	18.2	4.1	0.	0.	416.	0.	0.	4.94
A06G07	1.6	32.7	51.8	76.2	.10	200.0	0.0	27.3	4.3	0.	0.	451.	0.	0.	2.35
A06K14	.1	0.0	123.5	0.0	-.04	400.0	-12.0	0.0	4.3	0.	0.	1077.	0.	0.	1.85
A06K13	.2	0.0	47.2	0.0	-.03	400.0	-117.0	0.0	4.1	0.	0.	411.	0.	0.	1.52
A06K11	.2	0.0	47.1	0.0	-.01	400.0	-99.0	0.0	4.4	0.	0.	410.	0.	0.	1.50
A06K10	.5	0.0	47.3	0.0	.06	400.0	-90.0	0.0	1.3	0.	0.	412.	0.	0.	1.40
A06K09	.7	0.0	40.7	0.0	.17	400.0	-81.0	0.0	1.8	0.	0.	355.	0.	0.	3.99
A06K08	.9	0.0	53.6	0.0	.37	400.0	-72.0	0.0	2.5	0.	0.	468.	0.	0.	8.69
A06I14	1.0	51.0	51.0	53.3	.45	400.0	-63.0	0.0	2.7	0.	0.	445.	0.	0.	10.50
R06I14	1.0	55.7	55.7	55.8	.37	400.0	-63.0	0.0	2.8	0.	0.	486.	0.	0.	8.54
C06I14	1.1	46.2	47.6	53.9	.42	400.0	-63.0	0.0	3.0	0.	0.	415.	0.	0.	9.69
A06K07	.9	0.0	52.4	0.0	.43	400.0	-63.0	0.0	2.4	0.	0.	457.	0.	0.	10.12
A06J14	.7	0.0	55.7	0.0	.06	400.0	-63.0	18.2	3.0	0.	0.	486.	0.	0.	1.33
A06I13	1.0	54.6	56.1	67.3	.52	400.0	-54.0	0.0	2.7	0.	0.	489.	0.	0.	12.07
R06I13	1.2	47.9	53.5	59.5	.53	400.0	-54.0	0.0	2.2	0.	0.	467.	0.	0.	12.27
C06I13	1.1	47.1	47.3	56.9	.45	400.0	-54.0	0.0	2.9	0.	0.	412.	0.	0.	10.48
A06J13	.7	0.0	55.7	0.0	.02	400.0	-54.0	18.2	1.8	0.	0.	486.	0.	0.	1.53
A06I12	1.0	50.0	50.0	58.8	.52	400.0	-45.0	0.0	2.7	0.	0.	436.	0.	0.	12.04
C06I12	.9	0.0	53.8	0.0	.41	400.0	-45.0	0.0	2.5	0.	0.	469.	0.	0.	9.53
A06J12	.6	0.0	45.9	0.0	.01	400.0	-45.0	18.2	1.6	0.	0.	401.	0.	0.	1.22
R06I11	1.3	47.4	55.5	61.8	.56	400.0	-36.0	0.0	3.3	0.	0.	484.	0.	0.	13.51
C06I11	1.2	42.3	48.1	61.0	.56	400.0	-36.0	0.0	3.3	0.	0.	420.	0.	0.	13.14
A06I11	1.1	44.1	58.8	61.9	.54	400.0	-36.0	0.0	3.9	0.	0.	512.	0.	0.	12.65
A06J11	.7	0.0	55.3	0.0	.02	400.0	-36.0	18.2	1.9	0.	0.	657.	0.	0.	1.51
C06I10	1.3	42.0	53.8	67.8	.62	400.0	-27.0	0.0	3.4	0.	0.	469.	0.	0.	14.38
A06I10	1.2	40.4	48.3	62.0	.61	400.0	-27.0	0.0	3.1	0.	0.	421.	0.	0.	14.30
R06I10	1.2	38.7	49.4	64.3	.61	400.0	-27.0	0.0	3.2	0.	0.	431.	0.	0.	14.28
A06J10	.8	0.0	63.3	0.0	.05	400.0	-27.0	18.2	2.2	0.	0.	552.	0.	0.	1.19
R06I09	1.1	51.4	52.9	56.7	.53	400.0	-18.0	0.0	2.8	0.	0.	461.	0.	0.	12.20
A06I09	.9	0.0	41.8	0.0	.45	400.0	-18.0	0.0	2.4	0.	0.	365.	0.	0.	10.41
C06I09	1.1	52.2	52.6	54.4	.50	400.0	-18.0	0.0	2.8	0.	0.	458.	0.	0.	11.70
A06J09	.8	0.0	60.2	0.0	.06	400.0	-18.0	18.2	2.0	0.	0.	525.	0.	0.	1.36
C06I08	1.2	43.1	55.0	61.3	.59	400.0	-9.0	0.0	3.0	0.	0.	479.	0.	0.	13.62
R06I08	1.2	45.4	52.4	59.8	.64	400.0	-9.0	0.0	3.0	0.	0.	457.	0.	0.	14.98
A06I08	1.1	40.2	54.4	65.1	.59	400.0	-9.0	0.0	3.0	0.	0.	475.	0.	0.	13.62
A06J08	1.0	0.0	48.3	0.0	.11	400.0	-9.0	18.2	2.6	0.	0.	421.	0.	0.	2.51
C06I07	1.1	43.4	49.4	61.9	.59	400.0	0.0	0.0	3.0	0.	0.	431.	0.	0.	13.81
R06I07	1.1	48.6	51.8	58.8	.60	400.0	0.0	0.0	3.0	0.	0.	452.	0.	0.	13.85
A06I07	1.1	58.1	58.1	62.3	.60	400.0	0.0	0.0	3.0	0.	0.	506.	0.	0.	13.86
A06J07	1.1	45.3	45.5	45.6	.09	400.0	0.0	18.2	3.0	0.	0.	397.	0.	0.	2.01

RUN NUMBER 07

FILE NAME	MODEL CONDITIONS					POSITION			PROTOTYPE CONDITIONS						
	PEAK CONC. (%)	1% ARR. TIME (SEC)	PEAK TIME (SEC)	1% END TIME (SEC)	SUM (X-S)	X (M)	Y (M)	Z (M)	PEAK CONC. (%)	5% ARR. TIME (SEC)	10% ARR. TIME (SEC)	PEAK TIME (SEC)	10% END TIME (SEC)	5% END TIME (SEC)	SUM (X-S)
A07F08	1.3	46.1	79.6	79.6	.11	200.0	-9.0	18.2	3.4	0.	0.	694.	0.	0.	2.45
B07F08	1.2	47.3	89.1	91.7	.08	200.0	-9.0	18.2	3.1	0.	0.	777.	0.	0.	1.77
A07G08	1.0	0.0	75.6	0.0	-.03	200.0	-9.0	27.3	2.6	0.	0.	659.	0.	0.	-1.67
E07D07	1.2	62.1	79.3	101.6	.79	200.0	0.0	0.0	3.1	0.	0.	691.	0.	0.	18.32
C07D07	1.4	71.6	84.0	96.1	.77	200.0	0.0	0.0	3.7	0.	0.	733.	0.	0.	17.89
A07H07	1.1	47.8	67.9	97.1	.70	200.0	0.0	0.0	3.0	0.	0.	592.	0.	0.	16.30
R07E07	1.2	46.7	78.1	91.2	.51	200.0	0.0	0.0	9.1	0.	0.	681.	0.	0.	11.80
A07E07	1.3	46.7	69.4	100.1	.46	200.0	0.0	0.0	3.3	0.	0.	606.	0.	0.	10.84
R07F07	1.1	72.2	72.2	72.2	.11	200.0	0.0	18.2	3.3	0.	0.	630.	0.	0.	2.45
A07F07	1.0	90.4	90.4	90.5	.11	200.0	0.0	18.2	3.7	0.	0.	788.	0.	0.	2.54
A07G07	.8	0.0	31.1	0.0	-.02	200.0	0.0	27.3	2.2	0.	0.	271.	0.	0.	-1.39
A07I14	1.0	0.0	77.1	0.0	.67	400.0	-63.0	0.0	2.6	0.	0.	672.	0.	0.	15.52
A07I13	.9	0.0	93.9	0.0	.68	400.0	-54.0	0.0	2.4	0.	0.	818.	0.	0.	15.91
A07I12	.9	0.0	79.8	0.0	.57	400.0	-45.0	0.0	3.3	0.	0.	696.	0.	0.	13.21
A07I11	.8	0.0	95.6	0.0	.50	400.0	-36.0	0.0	3.1	0.	0.	834.	0.	0.	11.61
A07I10	.8	0.0	86.8	0.0	.45	400.0	-27.0	0.0	3.3	0.	0.	844.	0.	0.	10.61
A07I09	.8	0.0	95.8	0.0	.44	400.0	-18.0	0.0	3.5	0.	0.	835.	0.	0.	10.21
A07I08	.9	0.0	95.8	0.0	.55	400.0	-9.0	0.0	3.5	0.	0.	835.	0.	0.	12.94
A07I07	.9	0.0	95.8	0.0	.50	400.0	0.0	0.0	3.4	0.	0.	835.	0.	0.	11.75

RUN NUMBER 08

FILE NAME	MODEL CONDITIONS					PROTOTYPE CONDITIONS										
	PEAK CONC. (%)	1% ARR. TIME (SEC)	PEAK TIME (SEC)	1% END TIME (SEC)	SUM (X-S)	X (M)	POSITION Y (M)	Z (M)	PEAK CONC. (%)	5% ARR. TIME (SEC)	10% ARR. TIME (SEC)	PEAK TIME (SEC)	10% END TIME (SEC)	5% END TIME (SEC)	SUM (X-S)	
A08J14	.3	0.0	55.7	0.0	0.00	400.0	-63.0	18.2	.7	0.	0.	486.	0.	0.	.01	
A08I13	.1	0.0	.2	0.0	0.00	400.0	-54.0	0.0	.4	0.	0.	2.	0.	0.	-.10	
RO8I13	.1	0.0	104.8	0.0	-.07	400.0	-54.0	0.0	.4	0.	0.	914.	0.	0.	-1.54	
CO8I13	.2	0.0	60.5	0.0	.03	400.0	-54.0	0.0	.5	0.	0.	527.	0.	0.	.65	
A08J13	.4	0.0	31.1	0.0	.03	400.0	-54.0	18.2	1.0	0.	0.	271.	0.	0.	.70	
A08I12	.1	0.0	60.5	0.0	.04	400.0	-45.0	0.0	.3	0.	0.	527.	0.	0.	.89	
RO8I12	.1	0.0	87.1	0.0	.01	400.0	-45.0	0.0	.3	0.	0.	759.	0.	0.	.28	
CO8I12	.1	0.0	74.9	0.0	.02	400.0	-45.0	0.0	.3	0.	0.	654.	0.	0.	.46	
A08J12	.8	0.0	40.5	0.0	.10	400.0	-45.0	18.2	2.0	0.	0.	353.	0.	0.	2.35	
A08I11	.4	0.0	32.9	0.0	.06	400.0	-36.0	0.0	1.1	0.	0.	287.	0.	0.	1.35	
RO8I11	.3	0.0	47.8	0.0	-.01	400.0	-36.0	0.0	.7	0.	0.	417.	0.	0.	-.1	
CO8I11	.6	0.0	33.4	0.0	.14	400.0	-36.0	0.0	1.6	0.	0.	291.	0.	0.	3.25	
A08J11	.6	0.0	27.8	0.0	.10	400.0	-36.0	18.2	1.8	0.	0.	243.	0.	0.	2.25	
RO8I10	.7	0.0	36.8	0.0	.12	400.0	-27.0	0.0	1.8	0.	0.	321.	0.	0.	2.77	
A08I10	1.0	0.0	40.8	0.0	.30	400.0	-27.0	0.0	3.2	0.	0.	355.	0.	0.	7.00	
CO8I10	.8	0.0	31.5	0.0	.22	400.0	-27.0	0.0	2.2	0.	0.	273.	0.	0.	4.47	
A08J10	.8	0.0	48.3	0.0	.08	400.0	-27.0	18.2	2.2	0.	0.	421.	0.	0.	1.80	
RO8I09	.7	0.0	33.9	0.0	.20	400.0	-18.0	0.0	1.8	0.	0.	291.	0.	0.	4.68	
CO8I09	.5	0.0	28.1	0.0	.17	400.0	-18.0	0.0	1.4	0.	0.	245.	0.	0.	3.91	
A08I09	.7	0.0	40.3	0.0	.20	400.0	-18.0	0.0	1.8	0.	0.	351.	0.	0.	4.67	
RO8I09	.5	0.0	23.1	0.0	.04	400.0	-18.0	18.2	1.3	0.	0.	201.	0.	0.	.85	
CO8I08	.7	0.0	31.7	0.0	.25	400.0	-9.0	0.0	2.0	0.	0.	276.	0.	0.	5.90	
A08I08	.8	0.0	39.3	0.0	.24	400.0	-9.0	0.0	2.1	0.	0.	343.	0.	0.	5.63	
RO8I08	.6	0.0	46.0	0.0	.21	400.0	-9.0	0.0	1.6	0.	0.	401.	0.	0.	5.02	
A08J08	.8	0.0	29.3	0.0	.03	400.0	-9.0	18.2	2.2	0.	0.	255.	0.	0.	.80	
RO8I07	.6	0.0	39.1	0.0	.20	400.0	-9.0	0.0	1.7	0.	0.	341.	0.	0.	4.59	
CO8I07	.4	0.0	27.6	0.0	.15	400.0	-9.0	0.0	1.2	0.	0.	241.	0.	0.	3.42	
A08I09	.7	0.0	40.3	0.0	.20	400.0	-18.0	0.0	1.8	0.	0.	351.	0.	0.	4.67	
RO8I09	.5	0.0	23.1	0.0	.04	400.0	-18.0	18.2	1.3	0.	0.	201.	0.	0.	.85	
CO8I08	.7	0.0	31.7	0.0	.25	400.0	-9.0	0.0	2.0	0.	0.	276.	0.	0.	5.90	
A08I08	.8	0.0	39.3	0.0	.24	400.0	-9.0	0.0	2.1	0.	0.	343.	0.	0.	5.63	
RO8I08	.6	0.0	46.0	0.0	.21	400.0	-9.0	0.0	1.6	0.	0.	401.	0.	0.	5.02	
A08J08	.8	0.0	29.3	0.0	.03	400.0	-9.0	18.2	2.2	0.	0.	255.	0.	0.	.80	
RO8I07	.6	0.0	39.1	0.0	.20	400.0	-9.0	0.0	1.7	0.	0.	341.	0.	0.	4.59	
CO8I07	.4	0.0	27.6	0.0	.15	400.0	-9.0	0.0	1.2	0.	0.	241.	0.	0.	3.42	
RO8I07	.7	0.0	32.8	0.0	.22	400.0	-9.0	0.0	1.9	0.	0.	286.	0.	0.	5.20	
A08J07	.6	0.0	22.0	0.0	.07	400.0	-9.0	18.2	1.6	0.	0.	192.	0.	0.	1.66	

RUN NUMBER 09

FILE NAME	MODEL CONDITIONS					X (M)	POSITION			PROTOTYPE CONDITIONS					
	PEAK CONC. (%)	1% ARR. TIME (SEC)	PEAK TIME (SEC)	1% END TIME (SEC)	SUM (X-S)		Y (M)	Z (M)	PEAK CONC. (%)	5% ARR. TIME (SEC)	10% ARR. TIME (SEC)	PEAK TIME (SEC)	10% END TIME (SEC)	5% END TIME (SEC)	SUM (X-S)
B09D07	.9	0.0	25.9	0.0	.27	200.0	0.0	0.0	2.3	0.	0.	226.	0.	0.	6.22
C09D07	1.0	0.0	33.1	0.0	.30	200.0	0.0	0.0	2.6	0.	0.	289.	0.	0.	6.99
A09D07	.9	0.0	21.5	0.0	.29	200.0	0.0	0.0	2.3	0.	0.	188.	0.	0.	6.69
A09E07	1.0	23.6	23.6	23.7	.21	200.0	0.0	9.1	2.7	0.	0.	206.	0.	0.	4.83
R09E07	1.1	22.9	26.1	26.2	.21	200.0	0.0	9.1	3.0	0.	0.	228.	0.	0.	4.90
R09F07	.8	0.0	32.9	0.0	.10	200.0	0.0	18.2	2.1	0.	0.	287.	0.	0.	2.40
A09F07	.8	0.0	25.7	0.0	.11	200.0	0.0	18.2	2.2	0.	0.	224.	0.	0.	2.47
A09G07	.9	0.0	30.0	0.0	.04	200.0	0.0	27.3	2.5	0.	0.	261.	0.	0.	.83
A09K14	.2	0.0	16.0	0.0	.03	400.0	-126.0	0.0	.5	0.	0.	140.	0.	0.	.79
A09K13	.2	0.0	.1	0.0	.07	400.0	-117.0	0.0	.5	0.	0.	1.	0.	0.	1.61
A09K12	.1	0.0	79.8	0.0	.03	400.0	-108.0	0.0	.4	0.	0.	696.	0.	0.	.66
A09K11	.1	0.0	3.6	0.0	.03	400.0	-99.0	0.0	.3	0.	0.	32.	0.	0.	.76
A09K10	.2	0.0	35.4	0.0	.02	400.0	-90.0	0.0	.5	0.	0.	309.	0.	0.	.39
A09K09	.3	0.0	34.9	0.0	.03	400.0	-81.0	0.0	.8	0.	0.	305.	0.	0.	.67
A09K08	.6	0.0	35.8	0.0	.12	400.0	-72.0	0.0	1.5	0.	0.	312.	0.	0.	2.87
A09I14	.9	0.0	34.7	0.0	.18	400.0	-63.0	0.0	2.3	0.	0.	303.	0.	0.	4.13
R09I14	.9	0.0	37.8	0.0	.21	400.0	-63.0	0.0	2.3	0.	0.	329.	0.	0.	4.97
A09K07	.5	0.0	34.3	0.0	.11	400.0	-63.0	0.0	1.2	0.	0.	299.	0.	0.	2.50
A09J14	.4	0.0	29.9	0.0	.01	400.0	-63.0	18.2	1.0	0.	0.	261.	0.	0.	.19
A09I13	1.0	0.0	35.0	0.0	.23	400.0	-54.0	0.0	2.5	0.	0.	305.	0.	0.	5.43
R09I13	.9	0.0	40.6	0.0	.20	400.0	-54.0	0.0	3.3	0.	0.	354.	0.	0.	4.44
A09J13	.4	0.0	31.0	0.0	-.00	400.0	-54.0	18.2	1.0	0.	0.	370.	0.	0.	-1.07
R09I12	.8	0.0	37.1	0.0	.23	400.0	-45.0	0.0	2.0	0.	0.	323.	0.	0.	5.34
A09I12	.8	0.0	34.7	0.0	.24	400.0	-45.0	0.0	2.2	0.	0.	302.	0.	0.	5.58
A09J12	.4	0.0	28.5	0.0	.00	400.0	-45.0	18.2	1.2	0.	0.	249.	0.	0.	.09
R09I11	.8	0.0	31.6	0.0	.25	400.0	-36.0	0.0	2.1	0.	0.	276.	0.	0.	5.82
A09I11	.8	0.0	35.0	0.0	.24	400.0	-36.0	0.0	2.2	0.	0.	305.	0.	0.	5.69
A09J11	.6	0.0	47.8	0.0	.04	400.0	-36.0	18.2	1.5	0.	0.	417.	0.	0.	.88
A09I10	.9	0.0	35.5	0.0	.31	400.0	-27.0	0.0	2.5	0.	0.	309.	0.	0.	7.15
R09I10	1.0	0.0	37.3	0.0	.31	400.0	-27.0	0.0	2.6	0.	0.	325.	0.	0.	7.29
A09J10	.7	0.0	26.6	0.0	.05	400.0	-27.0	18.2	1.9	0.	0.	332.	0.	0.	1.18
A09I09	.7	0.0	30.5	0.0	.26	400.0	-18.0	0.0	1.9	0.	0.	266.	0.	0.	6.02
R09I09	.7	0.0	37.8	0.0	.24	400.0	-18.0	0.0	1.8	0.	0.	330.	0.	0.	5.59
A09J09	.6	0.0	26.8	0.0	.07	400.0	-18.0	18.2	1.7	0.	0.	234.	0.	0.	1.71
R09I08	.7	0.0	37.8	0.0	.22	400.0	-9.0	0.0	2.0	0.	0.	330.	0.	0.	5.04
A09I08	.7	0.0	30.6	0.0	.24	400.0	-9.0	0.0	2.0	0.	0.	267.	0.	0.	5.53
A09I07	.6	0.0	31.7	0.0	.20	400.0	0.0	0.0	1.6	0.	0.	277.	0.	0.	4.66
R09I07	.6	0.0	41.3	0.0	.17	400.0	0.0	0.0	1.6	0.	0.	360.	0.	0.	4.09
A09J07	.5	0.0	26.3	0.0	.07	400.0	0.0	18.2	1.4	0.	0.	229.	0.	0.	1.60

RUN NUMBER 10

FILE NAME	MODEL CONDITIONS					POSITION			PROTOTYPE CONDITIONS						
	PEAK CONC. (%)	1% ARR. TIME (SEC)	PEAK TIME (SEC)	1% END TIME (SEC)	SUM (X-S)	X (M)	Y (M)	Z (M)	PEAK CONC. (%)	5% ARR. TIME (SEC)	10% ARR. TIME (SEC)	PEAK TIME (SEC)	10% END TIME (SEC)	5% END TIME (SEC)	SUM (X-S)
A10S10	1.1	19.3	19.5	19.5	-0.01	400.0	-27.0	9.1	3.0	0.	0.	170.	0.	0.	-18
A10T10	1.5	0.0	22.0	0.0	-0.02	400.0	-27.0	13.6	0.	0.	192.	0.	0.	0.	-59
B10I09	4.9	18.6	35.7	54.9	1.38	400.0	-18.0	0.0	17.1	183.	247.	311.	385.	466.	30.70
A10I09	4.6	20.2	35.0	52.2	1.23	400.0	-18.0	0.0	11.5	184.	243.	306.	373.	428.	27.39
B10F09	2.4	17.9	25.5	50.2	.24	400.0	-18.0	4.6	6.1	178.	0.	222.	0.	271.	5.62
A10K09	2.4	18.3	21.6	50.1	.24	400.0	-18.0	4.6	6.3	188.	0.	188.	0.	286.	5.55
B10S09	1.1	18.6	18.6	18.6	.03	400.0	-18.0	9.1	2.9	0.	0.	162.	0.	0.	.70
A10S09	1.0	0.0	21.4	0.0	.01	400.0	-18.0	9.1	2.5	0.	0.	187.	0.	0.	.26
A10T09	1.4	0.0	18.4	0.0	0.00	400.0	-18.0	13.6	1.1	0.	0.	161.	0.	0.	-1.11
B10I08	5.2	18.9	31.9	55.3	1.42	400.0	-9.0	0.0	12.8	180.	230.	278.	389.	470.	31.42
A10I08	4.8	18.7	34.0	55.5	1.41	400.0	-9.0	0.0	11.9	183.	235.	297.	380.	463.	31.29
B10F08	3.3	16.3	23.5	50.6	.39	400.0	-9.0	4.6	8.4	160.	0.	205.	0.	440.	9.03
A10K08	2.5	17.2	31.0	47.9	.35	400.0	-9.0	4.6	6.5	163.	0.	271.	0.	411.	8.14
B10S08	1.4	19.6	19.7	19.7	.07	400.0	-9.0	9.1	3.8	0.	0.	172.	0.	0.	1.56
A10S08	1.0	0.0	18.0	0.0	.01	400.0	-9.0	9.1	2.6	0.	0.	157.	0.	0.	.25
A10I08	1.8	0.0	17.5	0.0	0.00	400.0	-9.0	13.6	2.2	0.	0.	151.	0.	0.	.05
A10I07	4.7	19.8	34.7	55.4	1.30	400.0	0.0	0.0	11.7	188.	240.	303.	376.	447.	29.00
B10I07	4.8	19.5	32.7	54.0	1.21	400.0	0.0	0.0	11.9	195.	237.	285.	376.	420.	26.42
B10F07	2.9	18.5	23.9	49.2	.32	400.0	0.0	4.6	7.6	185.	0.	208.	0.	310.	7.42
A10F07	2.3	17.6	22.4	49.4	.27	400.0	0.0	4.6	6.0	168.	0.	196.	0.	331.	6.34
A10S07	1.6	20.8	21.0	21.0	.03	400.0	0.0	9.1	4.2	0.	0.	183.	0.	0.	.70
B10S07	.9	0.0	22.2	0.0	.04	400.0	0.0	9.1	2.4	0.	0.	193.	0.	0.	.90
A10T07	.3	0.0	14.7	0.0	0.00	400.0	0.0	13.6	.8	0.	0.	129.	0.	0.	-1.10

RUN NUMBER 14

FILE NAME	MODEL CONDITIONS					PROTOTYPE CONDITIONS									
	PEAK CONC. (%)	1% ARR. TIME (SEC)	PEAK TIME (SEC)	1% END TIME (SEC)	SUM (X-S)	X (M)	POSITION Y (M)	Z (M)	PEAK CDNC. (%)	5% ARR. TIME (SEC)	10% ARR. TIME (SEC)	PEAK TIME (SEC)	10% END TIME (SEC)	5% END TIME (SEC)	SUM (X-S)
A16T14	.7	0.0	13.7	0.0	.02	400.0	-63.0	13.6	1.8	0.	0.	120.	0.	0.	.55
A16I13	5.5	11.7	26.8	35.4	.91	400.0	-54.0	0.0	13.7	114.	155.	234.	250.	297.	20.08
A16R13	1.8	9.9	16.7	33.8	.22	400.0	-54.0	4.6	8.1	104.	0.	146.	0.	291.	5.05
A16S13	1.8	12.5	15.5	32.1	.06	400.0	-54.0	9.1	4.6	0.	0.	135.	0.	0.	1.37
A16T13	1.0	0.0	27.7	0.0	.02	400.0	-54.0	13.6	2.7	0.	0.	242.	0.	0.	.55
A16I12	5.4	11.8	23.6	34.1	.87	400.0	-45.0	0.0	13.4	114.	151.	206.	251.	284.	19.18
A16R12	3.5	11.6	16.9	34.2	.12	400.0	-45.0	4.6	8.8	117.	0.	147.	0.	286.	2.79
A16S12	1.3	11.8	13.3	32.0	.04	400.0	-45.0	9.1	3.6	0.	0.	116.	0.	0.	.88
A16T12	.8	0.0	23.8	0.0	.02	400.0	-45.0	13.6	2.0	0.	0.	208.	0.	0.	.51
A16I11	5.9	11.4	27.2	34.4	.94	400.0	-46.0	0.0	14.5	114.	148.	237.	262.	289.	20.69
A16R11	4.3	10.3	24.6	33.4	.20	400.0	-46.0	4.6	10.8	111.	214.	214.	215.	276.	4.64
A16S11	1.7	12.3	32.8	33.2	.04	400.0	-46.0	9.1	4.4	0.	0.	286.	0.	0.	1.04
A16T11	.7	0.0	28.6	0.0	.01	400.0	-46.0	13.6	2.0	0.	0.	250.	0.	0.	.21
A16I10	6.0	11.1	25.1	34.3	.99	400.0	-27.0	0.0	14.8	113.	147.	219.	266.	290.	21.70
A16R10	3.3	10.3	15.3	33.0	.26	400.0	-27.0	4.6	8.3	107.	0.	133.	0.	281.	5.89
A16S10	2.0	10.0	32.7	33.1	.03	400.0	-27.0	9.1	5.1	285.	0.	285.	0.	285.	.75
A16T10	1.0	22.0	22.0	22.0	-.01	400.0	-27.0	13.6	2.8	0.	0.	192.	0.	0.	-.13
A16I09	5.6	12.4	25.1	33.7	.88	400.0	-18.0	0.0	13.8	115.	157.	219.	265.	279.	19.33
A16R09	3.2	10.5	29.6	32.7	.27	400.0	-18.0	4.6	8.3	110.	0.	258.	0.	276.	6.10
A16S09	1.7	11.3	33.3	33.3	.04	400.0	-18.0	9.1	4.4	0.	0.	291.	0.	0.	.85
A16T09	.6	0.0	26.0	0.0	0.00	400.0	-18.0	13.6	1.6	0.	0.	227.	0.	0.	-.04
A16I08	5.7	11.7	24.4	33.9	.93	400.0	-9.0	0.0	14.0	115.	161.	213.	270.	291.	20.46
A16R08	4.3	10.7	28.2	32.2	.30	400.0	-9.0	4.6	10.9	113.	246.	246.	247.	276.	6.89
A16S08	1.9	10.3	32.6	34.0	.01	400.0	-9.0	9.1	5.1	284.	0.	284.	0.	284.	-1.65
A16T08	1.2	11.2	21.5	21.7	0.00	400.0	-9.0	13.6	3.3	0.	0.	184.	0.	0.	.09
A16I07	5.3	12.8	25.9	33.4	.80	400.0	0.0	0.0	13.1	123.	166.	226.	266.	283.	17.64
A16R07	3.6	12.1	17.9	33.8	.22	400.0	0.0	4.6	9.2	121.	0.	156.	0.	264.	5.07
A16S07	2.0	12.1	22.2	30.4	.05	400.0	0.0	9.1	5.2	193.	0.	193.	0.	194.	1.05
A16T07	1.1	22.0	22.0	29.4	.02	400.0	0.0	13.6	2.8	0.	0.	192.	0.	0.	.51